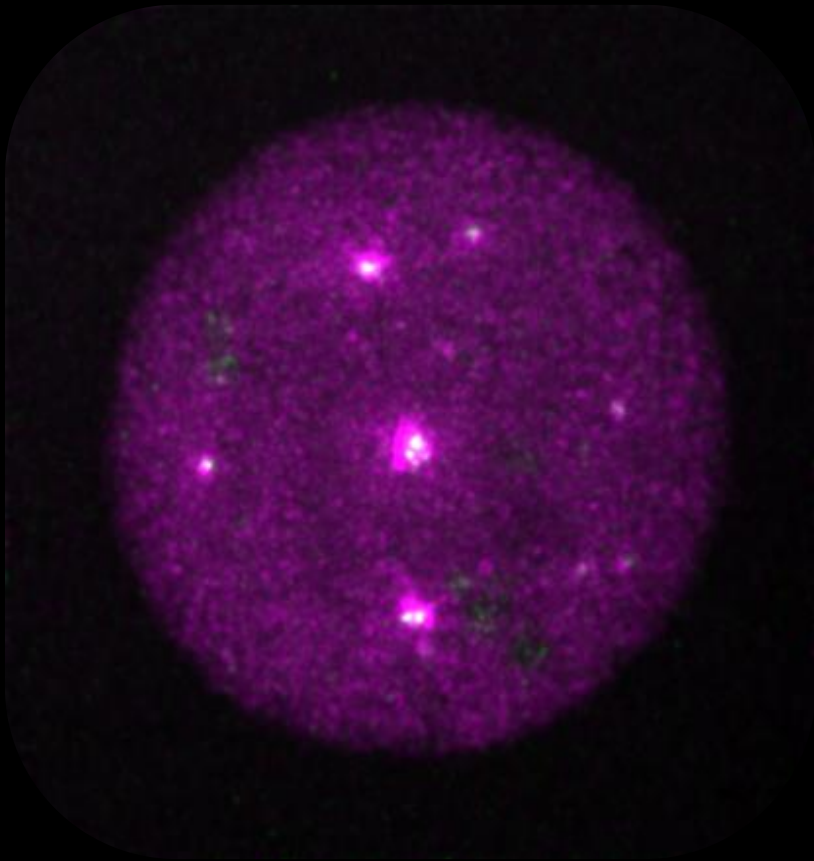


Dissecting the rules underlying de novo centrosome biogenesis

Catarina Antunes Angélico Pinto Nabais



Dissertation presented to obtain the Ph.D degree in Cellular Biology
Instituto de Tecnologia Química e Biológica António Xavier | Universidade Nova de Lisboa

Oeiras,
December, 2018



UNIVERSIDADE
NOVA
DE LISBOA

Dissecting the rules underlying de novo centrosome biogenesis

Catarina Antunes Angélico Pinto Nabais

Dissertation presented to obtain a Ph.D. degree in Cellular Biology

Instituto de Tecnologia Química e Biológica António Xavier | Universidade Nova de Lisboa

Research work coordinated by:



Oeiras, December, 2018



Declaration

I declare that this dissertation and the data herein presented are the result of my own work conducted from August 2014 to October 2018 in the laboratories of Dra. Mónica Bettencourt-Dias and Dr. Ivo Telley at the Instituto Gulbenkian de Ciência in Oeiras, Portugal.

Financial support was granted by a PhD Fellowship awarded to Catarina Nabais by Boehringer Ingelheim Fonds, an ERC-2010-StG-261344-CentriolStructure&Number and an ERC-2015-CoG-683258-Birth&Death.

All contributions have been acknowledged in the appropriate sections, under “Author Contribution” and/or in the “Acknowledgments”.

The Results presented in Chapters 2 and 4 are under preparation for a manuscript submission.

List of Publications:

Nabais C, Gomes Pereira S, Bettencourt-Dias M (2018) Noncanonical Biogenesis of Centrioles and Basal Bodies. Cold Spring Harbor Symposia on Quantitative Biology pii: 034694.

de-Carvalho J*, Deshpande O*, **Nabais C***, Telley IA* (2018) A cell-free system of *Drosophila* egg explants supporting native mitotic cycles. Methods in Cell Biology 144, 233-257 *All authors (in alphabetical order) contributed equally to this work.

Zitouni S, Francia ME, Leal F, Montenegro-Gouveia S, **Nabais C**, Duarte P, Gilberto S, Brito D, Kandels-Lewis S, Ohta M, Kitagawa D, Holland AJ, Karsenti E, Lorca T, Lince-Faria M, Bettencourt-Dias M (2016) CDK1/Cyclin B prevents unscheduled PLK4-STIL complex assembly restricting centriole biogenesis to one round per cell cycle. *Current Biology* 26(9):1127-37.

Zitouni S, **Nabais C**, Jana, SC, Guerrero A, Bettencourt-Dias M (2014) Polo-like kinases: structural variations lead to multiple functions. *Nature Reviews Molecular Cell Biology* 15(7): 433-52.

Acknowledgments/ Agradecimentos

Over these last five years, despite numerous “failures” and some less exciting results, I have learned immensely. It all could not have been possible without the support from a long list of people I admire, and to whom I am deeply thankful.

To Mónica Bettencourt-Dias, thank you for giving me limitless opportunities to learn and grow as a scientist. I am truly grateful for your patience, for encouraging me to explore my own ideas and for always being considerative towards my scientific opinions. You have been a role model of a successful scientist; pushing me to be persistent and to approach scientific problems in a mature way.

I thank my co-supervisor Ivo Telley for taking me in his lab and for teaching me several skills. In particular, I am most thankful for the knowledge in optics and microscopy you have given me. I am glad you fully encouraged me to attend multiple courses and workshops. Thank you for providing superb working conditions in the lab.

Delphine Pessoa, à parte da tua importante contribuição para o projecto, agradeço-te o teu entusiasmo e positivismo. Foi um prazer trabalhar contigo! Agradeço ao Jorge Carneiro por encorajar a nossa colaboração e pelas excelentes discussões que fomos tendo ao longo do projecto. Muito obrigada!

I thank Satyajit (Jitu) Mayor for kindly accepting me in his lab in India and for providing me excellent conditions to work and live at the NCBS. Thank you Thomas van Zanten for all your work and for teaching me most of what I know about FCS.

Ao Jorge Carvalho, obrigada pela tua ajuda, pelas críticas construtivas e por me ensinares inúmeras técnicas. Foi uma viagem divertida, por vezes exasperante mas, no geral, creio que tentámos

fazer boa ciência. Agradeço-te todos os momentos que estiveste ao meu lado e em que não me deixaste desistir.

I am thankful to all current and past CCR and PND lab members, it was a pleasure working with you. Paulo Duarte, pela tua disponibilidade, dedicação, encorajamento e pela tua valiosa ajuda! Gaëlle “Francisca” Marteil, I feel privileged to have shared so much with you. Thank you for your encouragement and guidance, you are a Fighter! À Mariana Faria pela paciência e ajuda. Por me teres ensinado muito e por teres lido a minha tese, muito obrigada! Sónia Pereira pela colaboração no artigo sobre criaturas estranhas que fazem CBBs de formas pouco convencionais. À Ana Rita Marques pelas preparações de ovários e ajuda nos Western Blots.

Thank you Boehringer Ingelheim Fonds Board and Staff for the substantial support during my PhD. Not only by granting me a generous stipend, but also for giving me the opportunity to travel to multiple places to attend courses and meetings.

I thank IGC and the IBB PhD Program 2014. I thank Élio, Ana Aranda and my batchmates – who would have guessed that, in the end, one might actually miss some of the time we spent together?!

To the staff of the IGC Light Microscopy Facility, in particular to Nuno Pimpão Martins and Gabriel Martins, thank you for your help and support, you guys are amazing! I am in debt to all members of the IGC Fly Facility for allowing my work to run so smoothly. I also thank the EM Facility led by Erin Tranfield for accepting my project. Sara Bonucci, foste incansável, muito obrigada pela tua dedicação! To Raquel Oliveira and Filipa Alves, my Thesis Committee, thank you for the scientific discussions.

I would also like to thank Cayetano González, Hélder Maiato, Edgar Gomes and Maria João Amorim, for promptly accepting to be part of my thesis defence jury.

I thank several scientists for sharing fly lines with us: Tomer Avidor-Reiss, Daniel St Johnston and Jordan Raff.

Aos meus amigos, perto ou longe, devo-vos um enorme agradecimento. Andreia Nunes, obrigada pelo teu companheirismo, apoio e por alinhares em todas as “maluqueiras”. Obrigada Joana Silva pela amizade e ajuda, pelos “chocolates misteriosos” e pelas conversas encorajadoras. À Margarida Bárbaro, Inês Albuquerque e Ricardo Leite, obrigada por me aturarem e ajudarem. À Joana Ribeiro, pelo teu apoio e por uma amizade absurdamente duradoura. À malta do “futebol das quartas”.

Aos meus pais, Jorge e Fátima, e à minha maninha Sofia, obrigada pela vossa ajuda e apoio incondicionais e por todos os sacrifícios que fizeram. A vossa ética de trabalho e resiliência são absolutamente fora de série e inspiram-me a tentar fazer mais e melhor. Aos meus avós, que sempre me fizeram sentir “a maior” e me motivaram com as suas conquistas e ensinamentos, não podia estar mais grata por vos ter conhecido. Tenho imenso orgulho em vocês.

Ao Eduardo Manuel, por me fazeres rir e por me apoiares ao longo destes anos intensos. Obrigada pela tua ajuda, carinho e paciência e por estares sempre ao meu lado.

Summary

The centrosome is the main microtubule organising centre (MTOC) in animal cells, regulating cell motility and polarity during interphase and organising the mitotic spindle in mitosis. Each centrosome has two centrioles, a mother and a daughter, which are surrounded by a multi-layered protein network called pericentriolar material (PCM) (Loncarek and Bettencourt-Dias, 2018; Nigg and Holland, 2018). The PCM contains critical components that anchor and nucleate microtubules (MTs). Centriole biogenesis is a highly regulated process that occurs only once per cell-cycle in proliferating cells (Breslow and Holland, 2019). De-regulation of centriole formation leads to defects in centriole number which cause cell-cycle arrest and mitotic defects (Ganem et al., 2009; Lambrus et al., 2015; Wong et al., 2015). Centrioles also form de novo in several eukaryotic cell-types, yet very little is known regarding the spatio-temporal and numerical regulation of this process.

Polo-like Kinase 4 (Plk4) is a master player in centriole biogenesis (Bettencourt-Dias et al., 2005; Habedanck et al., 2005; Kleylein-Sohn et al., 2007). Plk4 depletion causes a reduction in centriole number, while its overexpression leads to centriole amplification (Bettencourt-Dias et al., 2005; Habedanck et al., 2005; Kleylein-Sohn et al., 2007) or de novo centrosome formation in the absence of centrioles, in unfertilised *Drosophila melanogaster* eggs (Peel et al., 2007; Rodrigues-Martins et al., 2007). Therefore, Plk4 concentration and kinase activity must be tightly regulated to maintain a correct centrosome number in cells. Given its critical role in centriole formation, this thesis is focused on Plk4, aiming at providing quantitative assessments of its behaviour in live cells in order to determine how it regulates centriole duplication at its

endogenous levels and de novo centriole formation at high concentration.

In Chapter 2 we created fruit-flies that express endogenous Plk4 labelled with fluorescent reporters and characterised Plk4 localisation at the centrosome throughout the cell-cycle, in syncytial embryos. Plk4 levels oscillate at the centrosome during nuclear cycles 10 to 13, peaking in S-phase when centrioles duplicate, becoming almost undetectable throughout mitosis and increasing again in telophase. We then determined Plk4 properties in the cytosol by single-molecule quantification using Fluorescence correlation spectroscopy (FCS). Two different fractions of Plk4 with very different diffusion coefficients were identified: one moving rapidly and another very slowly, probably associating to quasi-immobile structures. Moreover, we determined Plk4 cytosolic concentration and provide evidences that it forms low-order oligomers, which possibly interact with cytoplasmic MTs. Our findings raise interesting hypotheses regarding Plk4 centrosomal localisation and activity, which are important for the spatio-temporal and numerical regulation of centriole duplication.

In Chapter 3 we established a cell-free assay which allows studying live de novo centrosome biogenesis in *Drosophila melanogaster*, at high spatio-temporal resolution. The assay relies on the production of cytoplasmic explants from single unfertilised eggs overexpressing Plk4. We chose the best fluorescent reporters available and optimised imaging conditions to accomplish a reliable centrosome detection in the cytoplasm. Finally, we validated the assay using other microscopy techniques and confirmed that the centrosomes that form in the explants contain centrioles and undergo canonical duplication in these explants.

In Chapter 4 we took advantage of the previously established assay to investigate the factors that regulate centriole de novo assembly and its spatial and temporal kinetics. We found that both canonical duplication and de novo pathways happen concomitantly within the same cytoplasmic explants suggesting that, under the conditions we tested, each process does not inhibit the other. We followed centriole de novo biogenesis over time and determined where and when they occurred in the explants. Comparing our observations to stochastic models, we demonstrated that recently formed centrioles do not impact the location where new centrioles assemble de novo, at high levels of Plk4 overexpression. Based on the time delay between centriole birth, Asterless (the main Plk4 recruiting molecule to the centrosome in *Drosophila*) incorporation and centriole duplication, the spatial independency may result from centrioles being immature and initially lacking the right amount of components. We observed that after an initial temporal delay, centrosomes assemble at a rapid rate that accelerates over time. This burst in biogenesis is not explained by a cell-cycle dependent mechanism but, instead, Plk4 concentration and probably its activation, seems to be the main driving force regulating the process. Diluting Plk4 concentration causes a longer delay in the birth of the first centrosomes indicating that the apparent acceleration in centriole assembly is likely a consequence of local Plk4 concentration and auto-activation, thus driving centriole biogenesis in several places independently. Altogether, these results show that Plk4 levels are critical in controlling the onset of centriole de novo formation and its temporal kinetics.

Sumário

Nas células animais, o centrossoma é o principal centro organizador de microtúbulos (MTOC), regulando o processo de mobilidade celular e polaridade durante interfase e participando na organização do fuso mitótico em mitose. Cada centrossoma possui dois centríolos, a mãe e o filho, que se encontram rodeados por uma complexa matriz proteica denominada material pericentriolar (PCM) (Nigg and Holland, 2018). A PCM contém componentes que são críticos para a ancoragem e nucleação de microtúbulos (MTs). A biogénese dos centríolos é um processo altamente regulado ocorrendo apenas uma única vez durante o ciclo-celular em células em proliferação (Breslow and Holland, 2019). A desregulação na formação dos centríolos conduz a alterações no número de centríolos na célula, causando um bloqueio do ciclo-celular e defeitos mitóticos (Ganem et al., 2009; Lambrus et al., 2015; Wong et al., 2015). Os centríolos também podem ser formados de novo em diversos tipos de células eucarióticas, no entanto, muito pouco se sabe relativamente a como este processo é regulado do ponto de vista espacial, temporal e numérico.

A cinase Plk4 é uma proteína central para a biogénese dos centríolos (Bettencourt-Dias et al., 2005; Habedanck et al., 2005; Kleylein-Sohn et al., 2007). A sua ausência causa uma redução no número de centríolos, enquanto a sua sobre-expressão leva à amplificação do número de centríolos (Bettencourt-Dias et al., 2005; Habedanck et al., 2005; Kleylein-Sohn et al., 2007) ou à formação de centrossomas de novo em ovos não fertilizados de *Drosophila melanogaster*, inicialmente desprovidos centríolos (Peel et al., 2007; Rodrigues-martins et al., 2007). Assim sendo, a concentração e actividade cinática da Plk4 nas células deve ser devidamente

regulada de modo a manter um número correcto de centrossomas. Tendo em conta o papel tão importante desempenhado pela Plk4, nesta tese procurámos quantificar a sua dinâmica em células vivas de modo a compreender melhor como os níveis endógenos de Plk4 regulam a duplicação dos centríolos e promovem a formação de centríolos de novo quando em concentrações elevadas.

No Capítulo 2, criámos moscas da fruta que expressam Plk4 endógena associada a marcadores fluorescentes e caracterizámos a localização da Plk4 no centrossoma ao longo do ciclo celular nos embriões. Observámos que os níveis de Plk4 no centrossoma oscilam durante os ciclos nucleares 10 a 13, sendo máximos durante a fase S quando os centríolos duplicam, quase indetectáveis durante mitose e aumentando novamente em telófase. De seguida, determinámos as propriedades da Plk4 no citosol por Espectroscopia de Correlação de Fluorescência (FCS) através de detecção de moléculas individuais. Identificámos duas fracções de Plk4 com diferentes coeficientes de difusão: uma primeira fracção que se desloca mais depressa e outra, muito mais lenta, que provavelmente se associa a estruturas quase imóveis. Para além disso, determinámos a concentração citoplasmática da Plk4 e demonstrámos que forma oligómeros compostos por um número reduzido de monómeros, e que possivelmente interagem com os microtúbulos citoplasmáticos. Este estudo levanta hipóteses interessantes relativamente à forma como a Plk4 localiza e é activada no centrossoma, tratando-se de mecanismos importantes para a regulação espacial, temporal e numérica da duplicação dos centríolos.

No Capítulo 3, estabelecemos um ensaio experimental desprovido de membrana celular que permite estudar ao vivo a biogénese de centríolos de novo em *Drosophila melanogaster*,

beneficiando de elevada resolução espacial e temporal. Este sistema baseia-se na produção de explantes citoplasmáticos extraídos de ovos não fertilizados que sobre-expressam Plk4. Testámos e escolhemos os melhores marcadores fluorescentes actualmente disponíveis e optimizámos as condições de visualização ao microscópio de modo a conseguirmos detectar inequivocamente os centrossomas formados no citoplasma. Por fim, validámos o ensaio utilizando outras técnicas de microscopia, confirmando assim que os centrossomas formados nos explantes contêm centríolos e que estes são capazes de duplicar.

No Capítulo 4, utilizámos o ensaio estabelecido previamente para investigar quais os factores que regulam a formação de centríolos de novo e determinar a sua dinâmica espacial e cinética temporal. Apurámos que as duas vias de biogénese de centríolos, a duplicação e a de novo, co-ocorrem nos explantes citoplasmáticos e exibem a sua própria cinética temporal sugerindo que, nestas condições experimentais, essas mesmas vias não se inibem mutuamente. Seguimos a formação dos centríolos de novo ao longo do tempo e determinámos onde e quando os eventos de biogénese ocorrem nos explantes. Comparando as nossas observações com modelos estocásticos conseguimos demonstrar que, na presença de níveis elevados de Plk4, os centríolos recém-formados não influenciam o local onde novos centríolos se formam. Com base no atraso temporal entre a formação de um centríolo, o seu enriquecimento em Asterless (a principal proteína que recruta a Plk4 para o centrossoma em *Drosophila*) e a sua duplicação, colocamos a hipótese de que a independência espacial entre os centrossomas recém-formados poderá resultar do facto destes serem imaturos e inicialmente desprovidos dos componentes necessários. Observámos ainda que, após um atraso inicial, os centrossomas

formam a uma taxa mais rápida, que acelera ao longo do tempo. Este aumento súbito na taxa de biogénese não pode ser explicada por uma regulação por parte do ciclo celular mas sim pela concentração e activação da Plk4. Suportando esta hipótese, a diluição da concentração de Plk4 nos explantes causa um atraso mais prolongado na biogénese dos primeiros centrossomas, sugerindo que a aceleração aparente da taxa de biogénese resulta provavelmente da concentração e auto-activação local da Plk4 que, deste modo, gera independentemente centríolos em múltiplos sítios. Concluimos, desta forma, que os níveis de Plk4 controlam o início da formação de centríolos de novo e a sua cinética temporal.

List of Abbreviations

3D - Tri-dimensional, XYZ

4D - Four-dimensional, XYZT

A.U. - Arbitrary units

ACF - Autocorrelation function

AKAP450 - A-kinase anchoring protein 450

Ana - Anastral

APC/C - Anaphase promoting complex/Cyclosome

Apo – Apochromatic correction

Asl – Asterless

Asp - Abnormal spindle

ATP - Adenosine triphosphate

AurA – Aurora A

Bld10 – Bald 10

BRCA1 - Breast cancer 1

CAMSAP - Calmodulin-regulated spectrin-associated protein

Cas9 - CRISPR associated protein 9

CBBs - Centrioles and basal bodies

CCD - Charge-coupled device

Cdc14 - Cell division cycle 14 homolog B

Ccdc78 - Coiled-Coil Domain-Containing Protein 78

Cdc6 - Cell division cycle 6 homolog

CDF - Cumulative distribution function

Cdk - Cyclin-dependent kinase

Cdk5rap2 - CDK5 Regulatory subunit-associated protein 2

Cdt1 - Chromatin licensing and DNA replication factor

Cep - Centrosomal protein

Chk1 - Checkpoint kinase 1

CHO - Chinese hamster ovary

CM1 motif - Centrosomin motif 1
Cnn – Centrosomin
Cpap - Centrosomal P4.1-associated protein
CPM - Counts per molecule
CRE - cAMP response elements
CRISPR - Clustered Regularly Interspaced Short Palindromic Repeats
CSF - Cytostatic factor
CSU – Confocal Scanner Unit
DDK - Dbf4-Dependent Kinase
Deup1 - Deuterosome Assembly Protein 1
DNA - Deoxyribonucleic Acid
D-Pip - *Drosophila* Pericentrin-Like Protein
EM - Electron Microscopy
EMT - Epithelial-to-mesenchymal transition
ER - Endoplasmic reticulum
FBXW - F-box and WD repeat domain containing
FCS - Fluorescence Correlation Spectroscopy
FRAP - Fluorescence recovery after photobleaching
FRET - Fluorescence Resonance Energy Transfer
Gal - DNA-binding transcription activating GALactose metabolism genes
GC - Giant centriole
GCP - Gamma-tubulin complex component
GDP - Guanosine-5'-diphosphate
Grip – Gamma-tubulin ring proteins
gRNA – guide RNA
GTP - Guanosine-5'-triphosphate
HCT116 - Human colorectal carcinoma cell line
HeLa - Henrietta Lacks Cervical Cancer cell line

HR – Homologous recombination
KASH - Klarsicht/ANC-1/Syne-1 homology
Kbp – Kilo base pairs
Klp - Kinesin-like protein
LECA - Last Eukaryotic Common Ancestor
LINC - Linker of nucleoskeleton and cytoskeleton complexes
MAP – Microtubule-Associate Protein
MCC - Multiciliated cells
MCM - Minichromosome maintenance helicase complex
mEGFP – Monomeric Enhanced Green Fluorescent Protein
MEM - Maximum Entropy Method
MII - Meiosis II
MIP - Maximum intensity projection
ML - Maximum Likelihood
MLS - Multi-layered structure
mRNA - Messenger RNA
Mto1 - Mitochondrial Translation Optimisation 1
MTOC – Microtubule Organising Centre
MTs – Microtubules
Mud - Mushroom body defect
NA - Numerical Aperture
NAB - Nuclear-Associated Body
Ncd - Non-claret disjunctional
ncMTOC - non-centrosomal Microtubule Organising Centre
NEDD1 - Neural Precursor Cell Expressed, Developmentally Down-Regulated 1
Nek2 - NIMA (never in mitosis gene a)-related kinase 2
NG – mNeonGreen
nos – *nanos* promoter
NRF1 - Nuclear respiratory factor 1

OE – Overexpression

ORC - Origin recognition complex

p16 - Cyclin-dependent kinase inhibitor 2A

p21 – Cyclin-dependent kinase inhibitor 1A

p27 - Cyclin-dependent kinase inhibitor 1B

p53 – Tumour suppressor protein 53

PACT - Pericentrin-AKAP-450 centrosomal targeting domain

PB - Polo boxes

PBD - Polo box domain

PCL - Proximal centriole-like

PCM - Pericentriolar material

Pcp1 - Processing of cytochrome c peroxidase 1

PCR - Polymerase Chain Reaction

PEST - Proline (P), glutamate (E), serine (S) and threonine (T) – rich residues

PF - Protofilament

Plan - Flat-field correction

Plk – Polo-like kinase

PLL - Poly-L-lysine

PNG - Pan Gu kinase complex

Poc - Proteome of the centriole

PP2A - Protein phosphatase 2A

PSF - Point Spread Function

pTEN - Phosphatase and tensin homolog

pUbq – Polyubiquitin

Rb - Retinoblastoma protein

RC - Replication complexes

RFP - Red Fluorescent Protein

RICS - Raster Image Correlation Spectroscopy

RNA - Ribonucleic Acid

RNAi – RNA interference
ROI - Region of Interest
RPE-1 - Retinal pigment epithelium 1 cell line
SAC - Spindle Assembly Checkpoint
Sak – Snk/Plk-akin kinase
SAPs - Sas6/Ana2 particles
Sas - Spindle assembly
SCF - SKP1-CUL1-F-Box
SD – Standard deviation
SEM - Standard error of mean
Sfi - Stimulatory factor I
Shot - Short stop
SIM - Structured Illumination Microscopy
siRNA – small interfering RNA
Slimb/Slmb – Supernumerary limbs
SPB - Spindle-Pole Body
Spc - Spindle pole component
Spd - Spindle defective
STAN - STil/ANa2
Stil - SCL/TAL1-interrupting locus protein
SUN - Sad1p, UNC-84 domain
Tacc - Transforming acidic coiled coil
TTL - Tubulin tyrosine ligase
U2OS - Human bone osteosarcoma epithelial cell line
UAS - Upstream Activating Sequence
UTR - Untranslated Region
WT – Wild-type
XMAP215 – *Xenopus* MAP 215
Zyg - Zygote defective
γ-TuRC - γ-Tubulin Ring Complexes

γ -TuSC - γ -Tubulin Small Complexes

β TrCP - beta-transducin repeat containing protein

Table of Contents

| | |
|---|------------|
| Declaration | i |
| Acknowledgments/Agradecimentos | iii |
| Summary | vii |
| Sumário | xi |
| List of Abbreviations | xv |
| Chapter 1: General Introduction | 1 |
| 1.1 Spatial and Temporal Intracellular Organisation | 3 |
| 1.1.1 The Eukaryotic cytoskeleton | 3 |
| 1.1.1.1 MT function and dynamic instability | 5 |
| 1.1.1.2 MT nucleation | 12 |
| 1.1.2 The Cell-cycle | 15 |
| 1.1.2.1 The cell-cycle phases | 16 |
| 1.1.2.2 Cell-cycle regulation | 19 |
| 1.1.2.3 The cell-cycle in early development | 28 |
| 1.2 Microtubule Organising Centres (MTOCs) in eukaryotes ... | 33 |
| 1.2.1 MTOCs structure and function | 33 |
| 1.2.1.1 The centrosome..... | 34 |
| 1.2.1.2 The spindle-pole body | 39 |
| 1.2.1.3 The nucleus-associated body | 41 |
| 1.2.1.4 Non-centrosomal MTOCs (ncMTOCs) | 42 |
| 1.2.2 Canonical centriole biogenesis (duplication) | 49 |
| 1.2.3 Molecular players in centriole biogenesis..... | 52 |
| 1.2.3.1 Procentriole assembly | 52 |
| 1.2.3.2 Centriole elongation | 54 |
| 1.2.3.3 Centriole maturation | 55 |
| 1.2.3.4 PCM role in centriole biogenesis | 58 |
| 1.2.3.5 Licensing and cell-cycle coordination | 60 |

| | | |
|--|--|------------|
| 1.2.4 | Centrosome reduction in animal gametogenesis and its inheritance in embryos | 65 |
| 1.3 | Polo-like kinase 4 (Plk4) is a master regulator of centriole biogenesis | 69 |
| 1.3.1 | Plk4, the odd one out in the Plk family | 69 |
| 1.3.2 | Plk4 structure | 70 |
| 1.3.3 | Plk4 regulation | 74 |
| 1.3.4 | Plk4 centrosomal recruitment | 78 |
| 1.3.5 | Plk4 substrates and downstream effectors | 79 |
| 1.4 | Non-canonical pathways of centriole biogenesis | 82 |
| 1.4.1 | Diversity in modes of centriole biogenesis across eukaryotes | 83 |
| 1.4.1.1 | Deuterosome-mediated biogenesis | 83 |
| 1.4.1.2 | De novo centriole biogenesis | 86 |
| 1.4.2 | Mechanisms and their regulation | 94 |
| 1.4.3 | Experimental systems to study de novo MTOC biogenesis..... | 68 |
| 1.4.4 | Framework of the thesis | 100 |
| Chapter 2: Determination of endogenous Plk4 properties in the early <i>Drosophila melanogaster</i> embryo | | 103 |
| 2.1 | Author Contribution | 105 |
| 2.2 | Summary | 105 |
| 2.3 | Introduction | 106 |
| 2.4 | Material and Methods | 112 |
| 2.4.1 | Fly strains and fly husbandry | 112 |
| 2.4.2 | Glass coverslips preparation | 112 |
| 2.4.3 | Embryo collection and sample preparation | 113 |
| 2.4.4 | Time-lapse imaging on a spinning disk confocal microscope and image data analysis of whole embryos | 113 |

| | | |
|---|--|------------|
| 2.4.5 | Fluorescence Correlation Spectroscopy acquisition and data analysis | 115 |
| 2.4.6 | mNeonGreen and mEGFP protein purification | 120 |
| 2.5 | Results | 121 |
| 2.5.1 | Targeting the endogenous <i>Drosophila melanogaster</i> Plk4 locus..... | 121 |
| 2.5.2 | Plk4 levels at the centrosome fluctuate in sync with the cell-cycle in early fly development | 127 |
| 2.5.3 | Plk4 single-molecule quantification and cytoplasmic diffusion in syncytial embryos | 130 |
| 2.6 | Discussion and Conclusions | 144 |
| 2.7 | Acknowledgements..... | 151 |
| Chapter 3: An <i>ex vivo</i> system to study de novo centriole biogenesis in <i>Drosophila melanogaster</i> eggs | | |
| 3.1 | Author Contribution | 155 |
| 3.2 | Summary | 155 |
| 3.3 | Introduction | 156 |
| 3.4 | Materials | 159 |
| 3.4.1 | Fly strains and fly husbandry | 159 |
| 3.4.2 | Glass coverslips and capillaries preparation | 160 |
| 3.4.3 | Embryo collection and sample preparation | 161 |
| 3.5 | Methodology | 161 |
| 3.5.1 | Extract preparation | 161 |
| 3.5.2 | Time-lapse explant imaging in the spinning disk confocal microscope..... | 162 |
| 3.5.3 | 3D-Structured Illumination Microscopy | 164 |
| 3.5.4 | Correlative Light Electron Microscopy | 164 |
| 3.6 | Results and Discussion | 166 |
| 3.7 | Acknowledgements | 176 |

| | |
|--|------------|
| Chapter 4: Spatial and Temporal kinetics of de novo centriole assembly in unfertilised eggs | 179 |
| 4.1 Author Contribution | 181 |
| 4.2 Summary | 181 |
| 4.3 Introduction | 182 |
| 4.4 Material and Methods | 188 |
| 4.4.1 Fly strains and fly husbandry | 188 |
| 4.4.2 Sample preparation and extraction | 189 |
| 4.4.3 Time-lapse explant imaging in the spinning disk confocal microscope | 189 |
| 4.4.4 Biochemical perturbations | 190 |
| 4.4.5 Data analysis | 190 |
| 4.4.6 Statistics and modelling | 192 |
| 4.5 Results | 194 |
| 4.5.1 Centrosomes assembled de novo recruit centriolar and centrosomal components | 194 |
| 4.5.2 Spatial organization of centriole de novo assembly | 197 |
| 4.5.3 Temporal kinetics of centriole de novo biogenesis | 200 |
| 4.5.4 Centriole maturation and duplication | 209 |
| 4.6 Discussion and Conclusions | 212 |
| 4.7 Acknowledgements | 220 |
| Chapter 5: General Discussion | 222 |
| References | 238 |

Chapter 1

General Introduction

1.1 Spatial and Temporal Intracellular Organisation

Spatial organisation or modularity is found at every scale of metazoan complexity, from the whole organism to its organs and tissues, to cells and their components and molecular interactions. Cellular compartmentalisation allows spatial confinement of biochemical reactions and confers structural organisation, contributing to the cell architecture and mechanical properties. Eukaryotic cells have evolved biochemically distinct compartments called organelles, which organise their internal environment and play specialised functions. Regulating organelle biogenesis is essential, as to ensure cells maintain a homeostatic organelle copy number, perfectly capable of performing its function at the right place and time, under each physiological condition. The eukaryotic cytoskeleton plays a dominant role in organelle positioning by transporting and/or anchoring them at specific subcellular locations. Organelle positioning has functional consequences, from orchestrating local signalling to promoting cell growth and polarisation, and it is usually coordinated with the cell-cycle, a series of irreversible transitions regulated by a timing mechanism, which allows for a cell to divide and originate two identical daughter cells.

1.1.1 The Eukaryotic cytoskeleton

The cytoskeleton is an intricate intracellular scaffold composed of different interconnected polymers. This network is critical for cellular structural and functional organisation, regulating cell morphology (shape and size) and its mechanical properties, and

generating forces necessary for cell division and migration (reviewed in (Huber et al., 2013)). In addition, the cytoskeleton also mediates cellular responses to external signals, integrating environmental cues and modulating gene expression (Rosette and Karin, 1995). The term cytoskeleton, derived from the greek word *skeletos* (= the group of rigid bones of an animal body), is however misleading, since these polymers are in fact bendable and highly dynamic, oscillating between polymerisation (growing) and depolymerisation (shrinking) states. Although the fundamental building blocks are similar within all animal cells, the cytoskeleton architecture varies substantially from different tissues to single cells; organising intracellular compartments differently and conferring distinct mechanical characteristics. Three different functional modules compose the cytoskeleton of animal cells: the actin filaments, microtubules (MTs) and intermediate filaments, all of which assemble micrometre long fibres or filaments. These differ in size, mechanical stiffness, stability and protein composition, allowing them to perform different functions (Fletcher and Mullins, 2010; Huber et al., 2013). Despite their specific properties, they often cooperate; during cell polarisation, directed migration and asymmetric cell division (reviewed in Rodriguez et al., 2003; Salmon et al., 2002; Waterman-storer et al., 2000). This mechanical coupling is achieved via molecular cross-linkers acting as physical bridges, capable of binding different polymers simultaneously.

Most of those molecules are actin-microtubule cross-linkers which participate in a plethora of functions during development and tissue maintenance. In *Drosophila*, one of the best studied cross-linkers is Short stop (Shot), which has a paradigmatic role in the cortical MT anchoring and nucleation in the fly oocyte, via the microtubule-associated protein (MAP) Patronin (Nashchekin et al.,

2016a; Voelzmann et al., 2017). Deregulation of the cytoskeleton network and defects in its regulators contributes to numerous human diseases. For instance, misfolding and accumulation of isoforms of the MAP Tau are a hallmark of Alzheimer's disease (Fontela et al., 2017), while cancer progression is typically accompanied by extensive cytoskeleton remodelling and loss of polarity and cell junctions upon epithelial-to-mesenchymal transition (EMT) (reviewed in Zhang et al., 2017).

In spite of the intimate association between the different cytoskeletal elements, my Introduction will be mostly focused on MT dynamics and MT-based organelles, since these were the main scope of my PhD project.

1.1.1.1 MT function and dynamic instability

MT function and composition

MTs are present in all extant eukaryotes characterised to date. The last eukaryotic common ancestor (LECA) most likely had not only MTs but also several genes coding for dynein and kinesin motor proteins, which navigate along the MT lattice (Pollard and Goldman, 2017). Their conservation over evolutionary time and in highly divergent lineages indicates that MTs and their associated proteins (MAPs) have a fundamental role within eukaryotic cells. One of their main functions is establishing the mitotic spindle, a highly dynamic force-generating machine that separates the chromosomes during mitosis (McIntosh and Hays, 2016). Moreover, MTs provide intracellular tracks for motors that transport organelles, vesicles and other structures (Gao et al., 2018; Salogiannis and Reck-Peterson, 2017). Consequently, the MT network is important for intracellular organisation, and specifically, for organelle positioning and

establishing cell polarity. Additionally, MTs assemble specialized organelles, called centrosomes and cilia, the latter being involved in motility or signalling (Loncarek and Bettencourt-Dias, 2018).

MTs are composed of α - and β -tubulin heterodimers, highly conserved across eukaryotes (Carvalho-Santos et al., 2011). These dimers assemble head-to-tail into linear protofilaments which associate laterally into the hollow MT cylinder, composed of 13 protofilaments, in most cases (Figure 1.1).

Although spontaneous MT polymerisation occurs *in vitro* at high tubulin concentration, this process is very slow, hindered by an initial, energetically unfavourable, lag phase and strongly dependent on tubulin concentration (Caudron et al., 2002; Desai and Mitchison, 1997; Hyman and Karsenti, 1998; Mitchison and Kirschner, 1984). *In vivo*, tubulin is present below its critical concentration and cells have evolved specialised structures, generically called Microtubule Organising Centres (MTOCs) (Pickett Heaps, 1969), which concentrate critical components that promote rapid growth of cytoplasmic MTs (reviewed in Wu and Akhmanova, 2017). In proliferating animal cells, the centrosome is the main MTOC and it is composed of two MT-based cylinders called centrioles. However, several other organelles such as the Golgi, the nuclear envelope, the cell cortex and mitochondria are also capable of nucleating MTs.

MT organisation and dynamics are regulated by a complex interplay between proteins that bind MTs and can: *i*) nucleate or stabilise their growth; *ii*) sever or destabilise the MT lattice; *iv*) bundle or anchor MTs; *iv*) drive selective transport along them (reviewed in Goodson and Jonasson, 2018). Polymerisation is initiated within nucleating seeds, usually containing γ -tubulin and associated proteins, where MTs are anchored and grow by the incorporation of tubulin subunits. The rate of elongation and MT size is regulated by

MAPs with antagonist function, giving rise to longer-lived or short-lived MTs. Motor proteins bind to and transport cargo along mature MTs and generate mechanical forces together with non-motor MAPs with capacity of bundling or gliding apart overlapping filaments (Goodson and Jonasson, 2018; Monroy et al., 2018).

MT dynamic instability

MTs are the stiffest and widest cytoskeleton polymers and, similarly to actin, they are polarised, containing a fast-growing plus tip and a less dynamic minus end tip (Figure 1.1) (Fletcher and Mullins, 2010; Huber et al., 2013). MTs undergo stochastic transitions between long growing phases (“rescue”) and abrupt shortening (“catastrophe”), a process called “dynamic instability” (Figure 1.1) (Mitchison and Kirschner, 1984; Schulze and Kirschner, 1986). This “dynamic instability” drives fast MT cytoskeleton reorganisation, facilitating intracellular spatial prospection thus reducing the time to encounter specific targets, which is particularly important for chromosome search-and-capture in mitosis (Blackwell et al., 2017; Holy and Leibler, 1994).

MTs grow by the incorporation of tubulin dimers, preferentially at their plus-end tips. The α - and β -tubulin subunits are structurally similar, containing a GTP-binding N-terminal domain facing the faster growing plus tip, an intermediate domain directed towards the minus tip and a C-terminal domain protruding from the MT wall (Manka and Moores, 2018; Nogales et al., 1998). Upon dimer incorporation, the GTP-binding site of α -tubulin is buried within the dimer and remains bound to GTP, while the β -tubulin GTP is exposed and can be hydrolysed to GDP. When β -tubulin is GTP-bound it can associate head-to-tail with α -tubulin from free tubulin dimers, driving MT polymerisation. Moreover, the lateral association

between the tubulin protofilaments gives rise to mature polymers with straight conformation, where longitudinal and lateral lattice contacts are temporarily stabilised (Figure 1.1) (Driver et al., 2017; Rice et al., 2008).

MT depolymerisation is triggered by the hydrolysis of the β -tubulin-bound GTP upon its association with α -tubulin from the incoming dimer; therefore MT growth and GTP hydrolysis are coupled and responsible for the polymer instability. Cryo-Electron Microscopy reconstructions have shown that the hydrolysis of the GTP- β -tubulin causes uneven force distribution introducing strain into the MT lattice; first by compressing tubulin dimers and tightening their longitudinal contacts and secondly, driving conformational changes in α -tubulin and weakening lateral lattice contacts (Alushin et al., 2014; Brouhard and Rice, 2018; Manka and Moores, 2018). The strain causes inside-out bending of the protofilaments by force-release, eventually breaking up the lateral contacts between the dimers and promoting depolymerisation (Figure 1.1) (Alushin et al., 2014; Hyman et al., 1995; Manka and Moores, 2018; Tran et al., 1997). According to the 'GTP-cap' model, the MT plus end grows as long as it contains GTP-tubulin subunits, but when the GTP cap is lost MTs undergo rapid tubulin depolymerisation (Desai and Mitchison, 1997; Howard and Hyman, 2009; Mitchison and Kirschner, 1984). The latest studies propose that MTs grow until the lateral contacts between tubulin dimers can no longer counteract the uneven forces generated in the lattice upon GTP hydrolysis and therefore MT catastrophe releases the accumulated strain energy (Alushin et al., 2014; Brouhard and Rice, 2018; Manka and Moores, 2018).

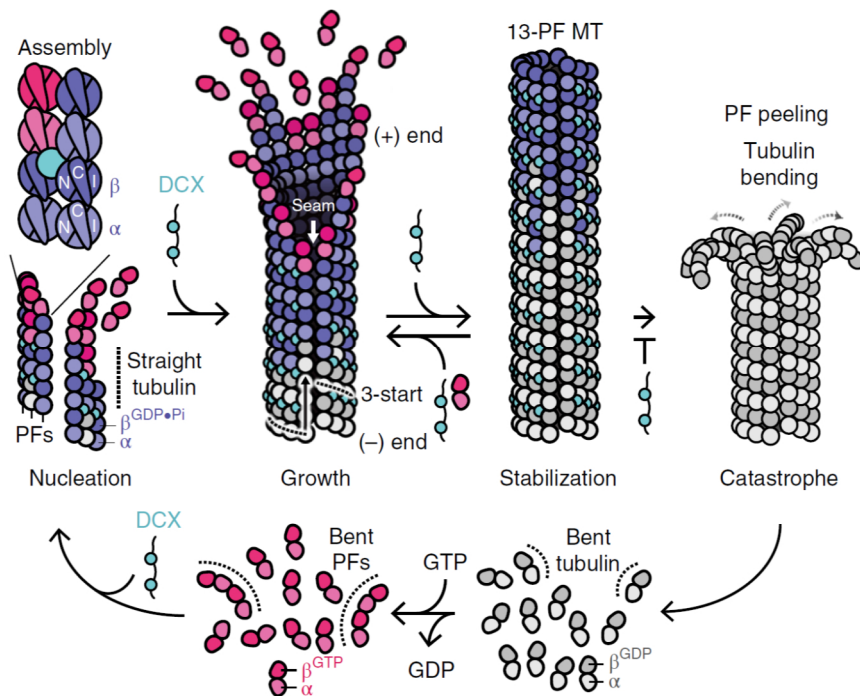


Figure 1.1 – The tubulin assembly–disassembly cycle and MT stabilisation by a MT-associated protein called DCX. The cycle of tubulin polymerisation and depolymerisation is driven by the hydrolysis of GTP bound to β -tubulin. MTs grow by incorporation of tubulin heterodimers composed of α - and β -tubulin bound to GTP (in pink). GTP hydrolysis occurs with a delay, after the dimer is incorporated into the growing MT plus tip. MTs grow while maintaining a GTP cap, stabilising the MT lattice and adopting a closed polymer conformation, composed of 13 protofilaments (PF). MAPs such as doublecortin (DCX, in light blue) bind tubulin dimers in the MT lattice helping stabilising its straight conformation. Loss of the GTP cap and unbinding of stabilising MAPs, leads to MT catastrophe whereby GDP-bound tubulin bends inside-out causing the PF to peel off and leading to rapid MT depolymerisation (catastrophe). Adapted from (Manka and Moores, 2018).

Regulation of MT dynamic instability

Overall, MT organisation can vary depending on the cell-type, cell-cycle or differentiation stage. For instance, stable and long-lived microtubules present in interphase are replaced by short-sized and highly dynamic microtubules in mitosis (Goodson and Jonasson, 2018). MT dynamic instability is spatially and temporally modulated by the localisation and activity of motor and non-motor MAPs and by tubulin post-translational modifications (Brouhard and Rice, 2018; Goodson and Jonasson, 2018; Monroy et al., 2018; Wloga et al., 2017).

Most MAPs promote MT growth or catastrophe at their plus end (Ayaz et al., 2014). Stabilising MAPs can either promote MT polymerisation and/or suppress depolymerisation, but these activities are difficult to distinguish apart. It is still not clear how most MT stabilisers work, but the fact that several of them contain multiple MT-binding domains suggest that they may cross-link protofilaments, hence stabilising the MT lattice (Peet et al., 2018; Shigematsu et al., 2018). Other proteins, such as the highly conserved XMAP215, promote MT polymerization by increasing the rate of tubulin incorporation (Ayaz et al., 2014; Brouhard and Rice, 2018). This can be achieved by binding free tubulin subunits and depositing them at the tip, as in the case of XMAP215 (Ayaz et al., 2014; Brouhard and Rice, 2018; Nithianantham et al., 2018), or by cross-linking the MT tip and catalyse the incorporation of incoming tubulin into the lattice (Gardner et al., 2011).

Destabilising MAPs promote the transition from dynamic MTs towards free tubulin subunits. This can be achieved either by severing the MTs, by inducing their depolymerisation at the MT tip, by accelerating the hydrolysis of tubulin-bound GTP or by sequestering free tubulin dimers preventing them from polymerising

(Maurer et al., 2012; Sharp and Ross, 2012). For instance, depolymerising kinesins retrieve energy from ATP hydrolysis to actively remove tubulin subunits from the MT tip (Benoit et al., 2018; Hunter et al., 2003; Wang et al., 2016). On the other hand, MT severing proteins such as Katanin, Spastin and Fidgetin ATPases, remove tubulin dimers from the GDP lattice. This process destabilises the polymer and unless GTP-bound tubulin is newly incorporated, the exposed MT ends suffer rapid depolymerisation (Vemu et al., 2018).

Numerous studies have revealed that cells possess MT subpopulations with different stability, and while most cytoplasmic MTs rapidly depolymerise upon treatment with cold or MT-depolymerising agents, others can resist these perturbations. Free tubulin dimers and polymerised MTs accumulate a variety of post-translational modifications, known as “tubulin code”, which alter the MT surface and modulate their stability and regulation *in vivo*. Some tubulin modifications, such as polyamination, acetylation and detyrosination typically render MTs more stable and resistant to cold and some MT-depolymerising agents (Janke and Montagnac, 2017). This is important in cells like the neurons, which require long-lived stable MTs to perform their functions (Yuyu Song et al., 2013). Long-lived cellular structures, such as cilia and centrioles, also undergo vast tubulin modifications. High levels of polyglutamylation are present on mammalian centrioles and are important for ciliary function, contributing for the stabilisation of these structures and regulating the binding of molecules such as kinesin motors (Bobinnec et al., 1998; Grau et al., 2013; Ikegami et al., 2010; Lessard et al., 2018; Sirajuddin et al., 2014; Wloga et al., 2016).

On the other hand, tubulin tyrosination and phosphorylation are associated to dynamic MTs. Tyrosine is usually the last amino

acid residue composing α -tubulin and, after MT polymerisation, it can be removed and bound to free tubulin by tubulin tyrosine ligases (TTLs), therefore detyrosination is associated with less recent MTs (Raybin and Flavin, 1975; Szyk et al., 2011). The phosphorylation of specific residues within α -tubulin blocks tubulin incorporation into MTs potentially by destabilising the interactions between α - and β -tubulin of subsequence heterodimers (Lin et al., 2015).

Nevertheless, the same type of tubulin modification can lead to different outcomes in distinct cell-types and even within the same MT there can be different patterns of tubulin modifications. This is important during cell-cycle progression and cell-differentiation and it has been shown to be altered in tumorigenesis (Magiera et al., 2018) and neurodegeneration (Chakraborti et al., 2016) and to impair proper chromosome segregation during mitosis (Barisic and Maiato, 2015). The extent of tubulin modifications is regulated by the levels and activity of each modifying enzyme and, if present, their counteracting enzyme and by their localisation within the cell.

1.1.1.2 MT nucleation

γ -TuSC and γ -TuRC nucleating complexes

In most cells, MT nucleation occurs at the MTOCs and relies on ring-shaped protein complexes containing γ -tubulin and several associated proteins (Farache et al., 2018; Moritz et al., 1995; Stearns et al., 1991). γ -tubulin is a highly conserved member of the tubulin superfamily, though it is not incorporated into the MT lattice (Findeisen et al., 2014; Joshi, 1993; Lin et al., 2015).

Plants and animals contain large γ -tubulin ring complexes (γ -TuRC) composed of several copies of γ -tubulin and a smaller number of the γ -tubulin binding proteins GCP2-6 (Luders and

Stearns, 2007), which are recruited to the MTOC as pre-formed complexes (Teixido-Travesa et al., 2012). Budding yeast only possesses homologues of GCP2 and GCP3 (Spc97p and Spc98p, respectively) and γ -tubulin (Tub4p), which assemble the γ -tubulin small complexes (γ -TuSC) (Brilot and Agard, 2018; Vinh et al., 2002). All GCPs contain an N-terminal grip1 domain which mediates their lateral association, whereas at their C-terminal region a grip2 domain binds to γ -tubulin (Farache et al., 2018).

Both the γ -TuSC and γ -TuRC complexes cap the minus end of MT filaments preventing its growth and depolymerisation and provide stable sites for tubulin heterodimers to bind and initiate MT nucleation. Interaction with specific adaptors and activator proteins at the MTOCs regulates MT nucleation from these complexes, limiting their activity to specific sub-cellular locations (Sulimenko et al., 2017). Most of those adaptor proteins comprise a conserved N-terminus CM1 motif (Centrosomin motif 1), which strongly interacts with the N-terminal region of yeast GCP3 and they anchor the γ -tubulin complexes to their respective MTOC via specific motifs in their carboxy-terminal region (Farache et al., 2018; Lin et al., 2014; Lyon et al., 2016). In yeast, those proteins include Spc110p and Spc72 in *S. cerevisiae*, and Pcp1 and Mto1 in *S. pombe* (Lin et al., 2015), whereas in animals several proteins contain the CM1 motifs among which the *Drosophila* Centrosomin (Cnn) and vertebrate CDK5RAP2, Myomegalin and Pericentrin (Fong et al., 2008; Wang et al., 2014a; Zimmerman et al., 2004).

Nucleation of MTs by the γ -Tubulin complexes

Cryo-EM structural studies in yeast, have provided a significant understanding on how γ -tubulin complexes nucleate MTs. While γ -TuSC are only composed of GCP2 and GCP3, they are

sufficient to assemble helical rings with similar geometry to that of a single MT filament (Brilot and Agard, 2018; Farache et al., 2018; Kollman et al., 2015). These helical structures are established by lateral GCP2 and GCP3 interaction, whereby each subunit binds longitudinally one molecule of γ -tubulin, and together with Spc110p they self-assemble into oligomeric γ -TuSC, exposing 13 γ -tubulin molecules, capable of nucleating MT with 13 protofilaments (PFs) (Brilot and Agard, 2018; Farache et al., 2018; Kollman et al., 2015). Moreover, *in vivo*, γ -TuSC complexes adopt a closed conformation when bound to MTs, then perfectly matching the MT architecture (Kollman et al., 2015). In its closed conformation, γ -TuSC becomes a stronger MT nucleator, suggesting that γ -TuSC closure is one mechanism that regulates γ -TuSC activity (Kollman et al., 2015). Additionally, studies demonstrated that Spc110p oligomerisation is essential for the assembly of γ -tubulin complexes (Kollman et al., 2015; Lyon et al., 2016) and that γ -tubulin is activated by conformational changes upon its assembly into the γ -TuSC structure (Brilot and Agard, 2018).

Based on studies in yeast, a revised “template model” has been proposed for MT nucleation from the larger γ -TuRC complex, whereby the γ -TuRC-specific GCPs (GCP4, GCP5 and GCP6) may establish hybrid structures with γ -TuSCs proteins GCP2 or GCP3, assembling a ring of alternate γ TuRC/ γ TuSC molecules. In this conformation, MT nucleation takes place by longitudinal interaction between γ -tubulin and the α/β -tubulin dimers, forming a direct template for tubulin incorporation and MT polymerisation (Farache et al., 2018; Kollman et al., 2015; Oakley et al., 2015).

MT nucleation in cells involves several steps: γ -tubulin complexes form templates resembling MT geometry, these templates are subsequently recruited to the MTOCs and

independently activated by other proteins (and very likely by conformational changes) and finally, early nucleation is stabilised by MAPs, which facilitate the incorporation of tubulin dimers at the plus tip and stabilise lateral interactions between protofilaments, closing the MT cylinder.

1.1.2 The cell-cycle

The cell-cycle is a sequence of events that allow a single cell to divide and give rise to two genetically identical daughter cells. This process entails that cells need to duplicate their DNA and cellular organelles and, in most cases, equally segregate their duplicated content to their daughters. This fundamental process is repeated billions of times during metazoan development and growth, ensuring the succession of living organisms.

In the early 17th century, the development of microscopy techniques allowed the first observations of cells and their microstructures. In 1665, Robert Hooke published *Micrographia*, a compilation of his miscellaneous microscopical observations. His descriptions of the cork structure coined the term *cells*, which later inspired the “cell theory”. Antony van Leeuwenhoek, well-known for his outstanding contribution to the microscopy field, published his observations on single-cell organisms in the following year. Together, these studies provided some of the first evidences of structural organisation within living organisms. Nonetheless, it was only more than one century later that the “cell theory” was officially formulated, driven by significant technical improvements in microscopy and the contributions of many scientists, among which Matthias Jakob Schleiden, Theodor Schwann and Jan Purkyňe. Between 1837 and 1839, Schleiden, Schwann and Purkyňe explicitly

postulated that both plants and animals were composed of a same structural element, the cell, which is governed by similar fundamental principles. At the time, the mechanisms underlying cell reproduction were unknown and largely controversial. In the 1850s, Carl Nägeli and Robert Remak correctly described cell division in plants and animals, and together with Rudolf Virchow and Albert Kölliker, they finally demonstrated that cells form through scission of existing cells, formulating the basic principle of cell inheritance (reviewed Mazzarello, 1999). Towards the end of the nineteenth century, the main cellular organelles had been identified. In 1882, Walther Flemming first described in detail the behaviour of salamander chromosomes inside the cell nucleus, during the cell-cycle. He observed the chromosomes condensing into shorter and thicker structures before their separation into two opposite cell poles, coining the term 'mitosis' (from the greek *mitos* = "warp thread" and the latin word *osis* = "act, process") (Flemming, 1965). The remaining, seemingly "inactive" phase of the cell-cycle, was called interphase (Pollard, 2017).

1.1.2.1 The cell-cycle phases

Chromosome duplication and partitioning is common to all cell-cycles, since most cells need to inherit a complete genome set to survive and function properly. The hallmark discovery of the DNA double helix structure by Rosalind Franklin, James Watson, Francis Crick and Maurice Wilkins provided the conceptual framework to understand how the genetic material is replicated (Nurse, 2000; Watson and Crick, 1953). In the same decade, it was also shown that DNA replication is restricted to a short interphase period called Synthesis or S-phase (Nurse, 2000; Swift, 1950). Together, these

two studies contributed to the classification of the eukaryotic cell-cycle into four phases: G1 (Gap 1), S, G2 (Gap 2) and M (Mitosis) phases (Figure 1.2) (Pollard, 2017).

Contrary to the initial premise proposing that interphase corresponded to an inactive stage without conspicuous morphological changes, G1, S and G2 are, in fact, highly metabolically active phases. In G1, cells increase gene transcription and protein synthesis, undergoing rapid growth and volume expansion. Then, they can either become committed to undergo division or they exit the cycle, entering a G0 (Gap 0) phase, whereby they usually differentiate. Most somatic cells in the adult body are in a non-dividing, “terminally differentiated” G0 state, becoming very unlikely for them to re-enter the cell-cycle. When a cell commits to continue dividing past G1, it will start S-phase, duplicating its DNA. After DNA replication, cells increase their size and boost protein biosynthesis during G2, in preparation for mitosis. M phase is composed of two processes: nuclear division (mitosis) and cell division (cytokinesis), the later usually happening already in G1 of the next cell-cycle. In mitosis, the duplicated chromosomes are equally segregated into two daughter cells. In cytokinesis, the cytoplasm (and its organelles) from the parental cell is physically split into two individual daughter cells (Pollard, 2017).

Mitosis is categorised into discrete stages according to chromosome morphology and localisation: prophase, metaphase, anaphase and telophase (Figure 1.2). During prophase, the chromosomes start to condense and the nuclear envelope breaks down. In most animal and plant species the nuclear envelope is almost entirely disassembled, whereas in other organisms it is partly retained or remains completely intact, like in fission yeast, which undergoes “closed mitosis”. During this phase, MT nucleation

increases at the MTOCs which are positioned at opposite poles. Then, while chromosomes keep condensing, MT fibres attach to their kinetochores. By metaphase, chromosomes are lined up at the equatorial region, forming the metaphase plate, and each sister chromatid is attached to the MT spindle connected to one of the MTOCs. At anaphase, the sister chromatids are pulled apart towards opposite poles and by telophase the two chromosome sets reach maximum separation. At this point, the daughter chromosomes begin to decondense, the nuclear envelope reassembles around them and the mitotic spindle depolymerises (Pollard, 2017).

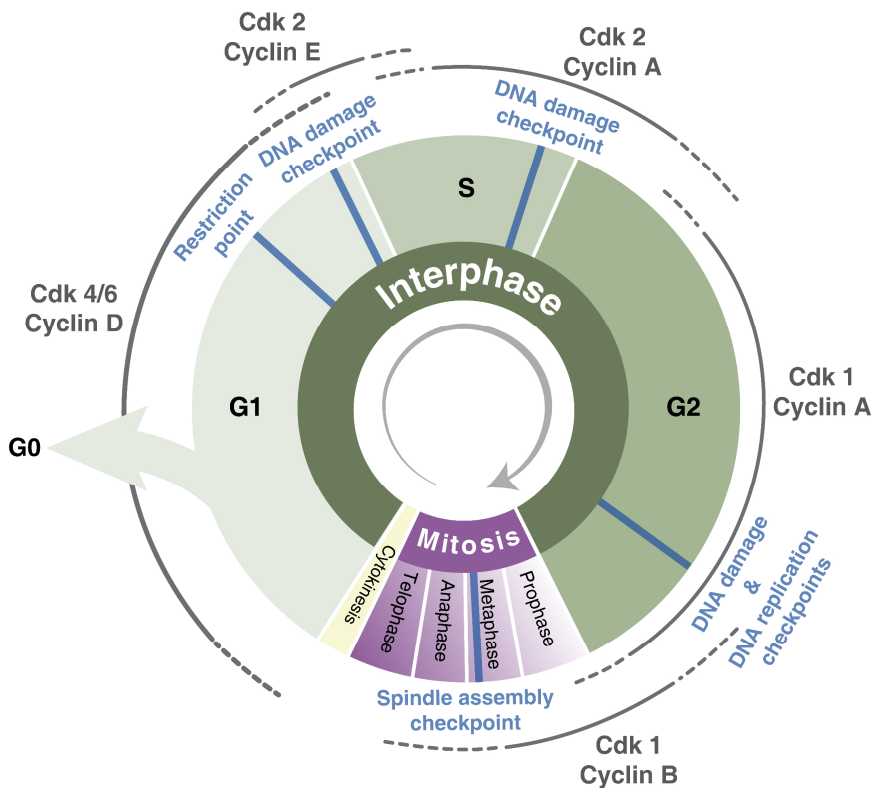


Figure 1.2 - Main cell-cycle phases and changes in Cdk activity in proliferating animal somatic cells. In G1-phase, cells either commit to undergo cell-cycle progression or exit the cycle going into G0 (usually

differentiating). Cells that continue cycling, duplicate their chromosomes and centrosomes during S-phase. In G₂, cells prepare for mitosis, when they finally segregate their duplicated DNA and cytosolic content into two daughter cells that become physically separated upon cytokinesis. Multiple checkpoints monitor different physiological conditions and ensure proper cell-cycle progression. Cdk activity changes as cells progress through the cell-cycle. Cyclin D binds and activates Cdk4 and Cdk6, promoting G₁ progression. Cdk2-Cyclin E activity increases during G₁, concomitantly with a decrease in the APC/C activity, driving entry into S-phase. Cyclin A and B levels increase in G₂ forming a complex with Cdk1. High activity of Cdk1-Cyclin B triggers mitotic progression and, finally, Cyclin B degradation by the APC/C promotes mitotic exit.

1.1.2.2 Cell-cycle regulation

Cyclin-dependent kinases

The Cyclin-dependent kinases (Cdk) are the main regulators of cell-cycle progression. Cdks are serine/threonine protein kinases that phosphorylate multiple substrates required for the major cell-cycle events, such as DNA synthesis and mitotic progression. The genes encoding Cdks were first identified in yeast from genetic studies characterising mutations that cause cell-cycle arrest (Hartwell et al., 1974; Moir and Botstein, 1982; Nurse and Thuriaux, 1980). Cyclins, on the other hand, named after their oscillatory levels throughout the cell-cycle, were first described in fertilised sea urchin eggs (Evans et al., 1983).

Progression through each cell-cycle phase relies on the association between different Cdk-Cyclin complexes. Since the kinases are mostly inactive without their Cyclin partners, phase-specific, Cyclin expression and degradation, controls timely Cdks activation. In addition to Cyclin binding, Cdks activity is also

regulated by phosphorylation by other kinases and dephosphorylation events operated by phosphatases, triggering positive and negative feedback loops. Once activated, Cdk-Cyclin complexes phosphorylate other cell-cycle proteins which in turn drive the physiological changes needed to go into, through, or out of a particular cell-cycle phase. Before their inactivation, the activity of each Cdk-Cyclin complex sequentially activates the next one. This ensures that the cell-cycle is a temporally ordered and unidirectional pathway (Pollard, 2017).

Cell-cycle checkpoints

Each cell-cycle phase and their transitions are highly regulated events, with multiple checkpoints, that prevent deleterious mistakes from propagating during cell proliferation. The checkpoints monitor proper cell-cycle progression, ensuring that each process is correctly completed before proceeding to the next phase (Figure 1.2) (Barnum and O'Connell, 2014; Hartwell and Weinert, 1989). Checkpoints act directly or indirectly upon the Cdks, for instance by inhibiting their activity (e.g. in the case DNA damage and the S to G2 transition) (Saldivar and Cimprich, 2018) or by preventing timely Cyclin degradation, for example by delaying anaphase onset until all chromosomes are properly aligned at the metaphase plate. Despite the underlying mechanism, the outcome of checkpoint activity is halting progression through the cell-cycle.

Checkpoints behave like surveillance systems; they are constitutively active and require the satisfaction of different requisites in order to allow cells to go into the next phase. Otherwise, a series of transduction cascades are initiated that delay or block cell-cycle progression until the checkpoint is satisfied or until it finally

relaxes (Mirkovic et al., 2015; Musacchio and Salmon, 2007; Pollard, 2017; Sansregret et al., 2014; Sullivan and Morgan, 2007). Many of the components involved in these transduction cascades are conserved across eukaryotes, and include known tumour suppressors such as p16, p53, BRCA1 and pTEN, which are activated upon deregulation and lead to cell-cycle arrest (Lai et al., 2012; Minami et al., 2017; Velez et al., 2015).

Although the following classification is highly debatable, it has been proposed that the cell-cycle checkpoints monitor: i) cell-cycle entry, also known as Restriction Point (in G₀/G₁); ii) cell size (in G₁ and G₂ phases); iii) DNA damage (in G₁, G₂, S and G₂/M) and iv) bipolar chromosomal attachment, ensuring proper chromosome segregation, known as the Spindle Assembly Checkpoint (SAC) (in mitosis) (Figure 1.2) (Barnum and O'Connell, 2014; Pollard, 2017).

Cell-cycle progression

In non-proliferating animal cells, the activity of Cdks is very low and the retinoblastoma protein (Rb), a key regulator of cell-cycle entry, is non-phosphorylated and bound to E2F transcription factors. In animal somatic cells, mitogenic signals upregulate several transcription factors and drive the expression of Cyclin D, which binds and activates Cdk4 and Cdk6, promoting G₁ progression (Figure 1.2). Throughout G₁, all the other Cdk-Cyclin complexes are inhibited by multiple repressors, among which, the Anaphase Promoting Complex/Cyclosome (APC/C). Activation of the Cdk4/6-Cyclin D complexes leads to partial Rb inactivation by phosphorylation. When phosphorylated, Rb releases transcription factors from the E2F family, driving the expression of Cyclin E (Massagué, 2004). Cyclin E up-regulation assembles the Cdk2-Cyclin E complex at the G₁/S transition. Cdk2-Cyclin E further

phosphorylates Rb causing its full inactivation. It also drives APC/C inhibition and, most importantly, it phosphorylates proteins needed for DNA replication. Cdk2 is then activated by Cyclin A expression at late stages of DNA replication, driving the transition from S to G2 phase (Figure 1.2). Cyclin A and B levels increase in G2 forming a complex with Cdk1. These Cdks are repressed by Wee1 phosphorylation throughout G2 and until mitotic onset. Cdk1-CyclinA/B activation is mediated by Cdc25 phosphatases, promoting entry into mitosis through a positive feedback loop. After nuclear envelope breakdown, Cyclin A is degraded and mitosis is driven by Cdk1–Cyclin B. Finally, Cdk1-Cyclin B starts to be degraded at the metaphase-to-anaphase transition, an event triggered by the APC/C, promoting mitotic exit. At the end of mitosis all Cdks are inactive (Figure 1.2) (Malumbres and Barbacid, 2009; Pollard, 2017).

Cell-cycle progression, a current view

Over recent years, the classical view of Cdk-Cyclin activity and cell-cycle progression has been increasingly challenged. Genetic studies in mice have shown that Cdk2, Cdk4 and Cdk6 are not essential for somatic cell-cycle progression (Malumbres and Barbacid, 2005). Instead, these Cdks are only important in specific cell types, and Cdk1 activity alone has been proposed to be enough for driving the entire cell-cycle. Cdk1 can be activated by both interphasic (D, E and A) and mitotic (B-type) Cyclins and shares over 60% amino-acid sequence homology with Cdk2, likely explaining its compensatory activity over the latter. Based on Cdks and Cyclin knock-out studies, Stern and Nurse (1996) proposed a threshold-driven Cdk activity model, for cell-cycle progression in fission yeast, according to which Cyclin B bound to either Cdk1 or Cdk2 is enough to regulate the entire cell-cycle.

The cell-cycle starts in G1 when Cdk, initially inactive, is slowly activated by binding to newly synthesized Cyclin. Low Cdk1-Cyclin B levels in interphase can drive S-phase onset and G2 progression, whereas high Cdk1-Cyclin B levels trigger mitotic entry. The difference between interphasic and mitotic Cdks probably relies more on their levels and phosphorylation activity required to activate their substrates and drive each cell-cycle transition (Gutierrez-Escribano and Nurse, 2015).

In agreement, recent studies have provided evidences on how substrates respond to Cdk-mediated phosphorylation thresholds and how these impact the order of cell-cycle events. These studies, conducted in yeast, demonstrated that substrates that are highly phosphorylated by Cdk1/Cdc2 and particularly rich in serine residues, tend to be phosphorylated earlier in the cell-cycle, at lower Cdk activity. On the other hand, Cdk substrates rich in threonine residues, which are also good targets of counteracting phosphatases, generally undergo slower phosphorylation and need higher Cdk levels to become active, which occurs later in the cell-cycle (Godfrey et al., 2017; Swaffer et al., 2016).

In animal cells, Cyclins have different sub-cellular localisations throughout the cell-cycle. Cyclin A and E are nuclear whereas Cyclin B is cytoplasmic, only entering the nucleus upon nuclear envelope breakdown in mitosis. In animal cells, the threshold model requires further complexity; any combination between nuclear Cyclin A or E with Cdk1 or Cdk2 might drive S-phase, whereas Cdk1-Cyclin B is needed for mitosis (Hochegger et al., 2008; Malumbres and Barbacid, 2009). While further studies are required to fully understand the role of each Cdk complex and its requirement in different cell-types and organisms, from an evolutionary point of view, one can speculate that having multiple Cdk complexes may be

advantageous in multicellular organisms. Redundant effectors provide robustness to the cell-cycle, while allowing the sub-functionalisation of individual Cdk-Cyclin combinations, so that each complex can develop specialised substrate interactions. Specific interactions can regulate their sub-cellular localisation and temporal activity, providing cell-type specific regulation of cell proliferation.

DNA replication and licensing

Every organelle in a particular cell-type has a specific copy number, size and position, which is important for cellular function. Yet, a longstanding question in the field is how precisely, and at which levels, does a cell control the number of copies of a given organelle. Biological systems are, in many aspects, quite stochastic and several processes contribute to organelle abundance. One of such processes is biogenesis, which can occur either *de novo*, or by fission or duplication of an already existing organelle.

Most organelles are synthesized throughout the cell-cycle. Small membrane-bound cytoplasmic organelles, like the mitochondria and the lysosomes, reproduce by growth and fission of existing organelles and are equally segregated to daughter cells, except during intrinsically asymmetric cell division. Larger organelles, like the Golgi and in some cases the Endoplasmic Reticulum (ER), fragment into smaller structures which are then distributed in mitosis (Pollard, 2017). Conversely, DNA and centrosomes duplicate once, and only once, per cycle.

The initiation of DNA replication is thought to be regulated by licensing mechanisms, which also prevent re-replication of DNA. The DNA licensing model, first formulated by Blow and Laskey (Blow, 1993; Blow and Laskey, 1986), postulates the requirement for an active licensing factor for DNA replication to start *in vivo*.

Nowadays, it is known that there are two distinct regulatory phases in DNA licensing: a licensed state at mitotic exit/G1, when cells re-enter the cell-cycle and become primed for DNA replication; and a second unlicensed state, after DNA replication has started in S-phase, when the initial priming events can no longer happen, but DNA undergoes replication and the cell-cycle continues. These temporally detached states, timely regulate DNA replication and prevent its reduplication.

Licensing starts with the assembly of the pre-replication complexes (pre-RCs) at the origins of replication by the Origin recognition complex (ORC), as cells exit mitosis. Pre-RC mark all potential origins, providing a positional cue for downstream replication factors. Pre-RC assembly proceeds throughout G1, with the enrichment of multiple licensing factors at the DNA origins of replication, culminating in chromosomes becoming poised/licensed to replicate by the end of G1.

At a (highly simplified) molecular level, the Cdk4/6-Cyclin D complexes regulate the transcription of genes needed for pre-RC assembly in G1 (Nishitani and Lygerou, 2004; Symeonidou et al., 2012). The ORC1-6 complex binds to the replication origins and recruits the Cdc6 ATPase and the cell division protein Cdt1. Both Cdc6 and Cdt1 are necessary for the loading of the minichromosome maintenance (MCM) helicase complex at the pre-RCs (Figure 1.3). Once the MCM2-7 are loaded, the origins become licensed and can start replication in S-phase. High Cdk2-Cyclin E and Dbf4-Dependent Kinase (DDK) (which comprises the serine/threonine kinase Cdc7 and its regulatory subunit Dbf4) kinase activity, activate the MCM2-7 helicase in early S-phase, triggering the initiation of DNA replication from the licensed origins (Figure 1.3) (Nishitani and Lygerou, 2004; Symeonidou et al., 2012; Tsaniras et al., 2014).

Then, replication factors convert the pre-RC to a replisome, which is required for the recruitment of DNA polymerase.

Throughout S/G2 phase and mitosis, re-licensing of origins is prevented by high Cdk2 and Cdk1 activity respectively, blocking pre-RC assembly at origins that have already fired. Cdt1 becomes inactive early in S-phase due to inhibition by Geminin and interaction with S-phase Cdk2-Cyclin A complex, resulting in Cdt1 phosphorylation and degradation (Li et al., 2004; Symeonidou et al., 2012). The MCM proteins move away from the origins with the replication fork, also preventing de novo licensing.

Other phosphorylation events modulate the ability of licensing factors to bind chromatin after DNA replication. Both ORCs and MCMs are phosphorylated by Cdks, and in *Xenopus* extracts Cdk2-Cyclin A dependent phosphorylation perturbs ORC, Cdc6 and MCM chromatin binding (Findeisen et al., 1999).

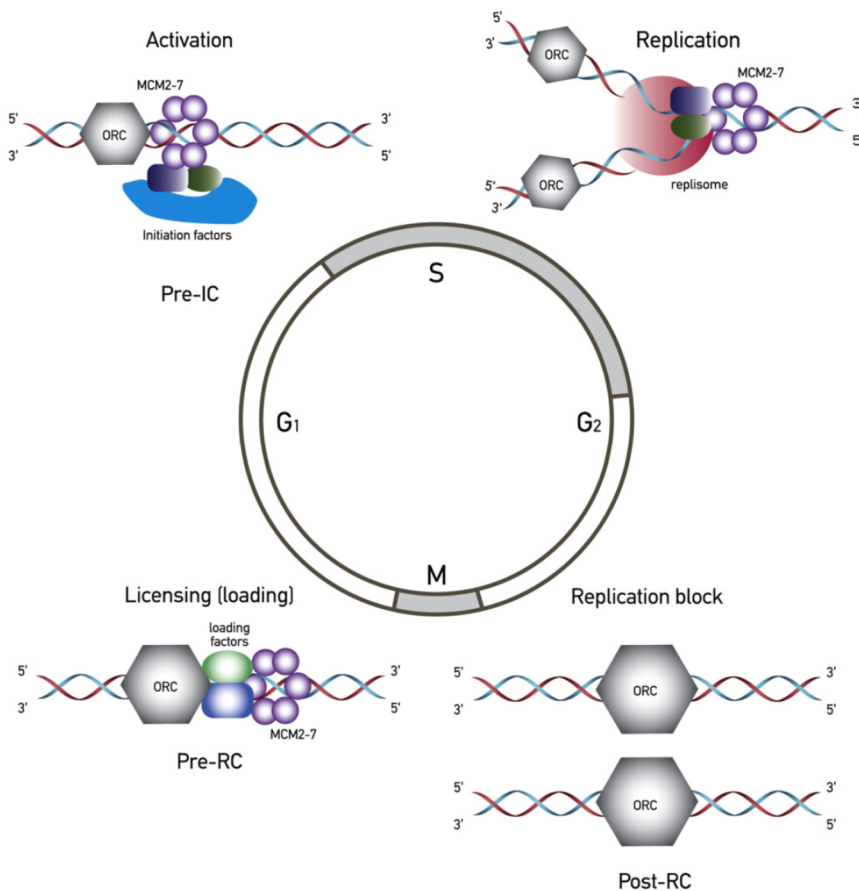


Figure 1.3 – The assembly of protein complexes onto replication origin regulates the timing of DNA replication. In eukaryotes, DNA replication is initiated at multiple sites in the genome called origins of replication. The origin recognition complexes (ORC) recognise and bind onto these sites, initiating the assembly of pre-replication complexes (pre-RC) in early G1. Once the ORC1-6 complexes bind to the replicating origins, they recruit Cdc6 and Cdt1 (in green and blue). These proteins promote the loading of the minichromosome maintenance (MCM) helicase complex at the pre-RCs. Once the MCM2-7 are loaded, the origins become licensed for replication. At the onset of S-phase, multiple initiation factors bind to the pre-RC, converting them into pre-initiation complex (pre-IC). Then, replication factors are loaded to the pre-IC driving the assembly of

the replisome and the initiation of DNA replication. After the origins have fired, Cdc6, Cdt1 and MCM proteins unbind the DNA and de novo licensing of the origins is prevented from S-phase onwards. From (Symeonidou et al., 2012).

1.1.2.3 The cell-cycle in early development

In most animals, early embryonic development is characterised by a modified and extremely fast cell-cycle. Early embryonic cells have no nutrient uptake from external sources and rapidly proliferate thanks to a generous supply of maternally deposited components. This modified cell-cycle is characterised by: i) absence of cell growth; ii) rapid DNA replication and iii) minimal or absent gap phase between S-phase and mitosis (Figure 1.4) (Farrell and O'Farrell, 2014; Morgan, 2007; Siefert et al., 2015).

In *Xenopus* and *Drosophila melanogaster* embryos, cells proceed directly from S-phase to M and then directly on to the next S-phase, without gap phases (Farrell and O'Farrell, 2014; Masui and Wang, 1998). In the sea urchin embryo, cells undergo G2 phase, but they lack G1 and duplicate their DNA while still in M phase (Figure 1.4). In most somatic cells, mitosis and cytokinesis are completed at G1 entry. In the early sea urchin embryo, cytokinesis overlaps entirely with S-phase and it is only completed after DNA replication. In early *Drosophila* embryos, the cell division and nuclear division are dissociated (Figure 1.4). Fly development takes place in a syncytium, where nuclei divide without cytokinesis, within a common cytoplasm. Only after 13 rounds of nuclear division the embryo undergoes cellularisation and a plasma membrane forms around each individual nucleus (Farrell and O'Farrell, 2014; Siefert et al., 2015).

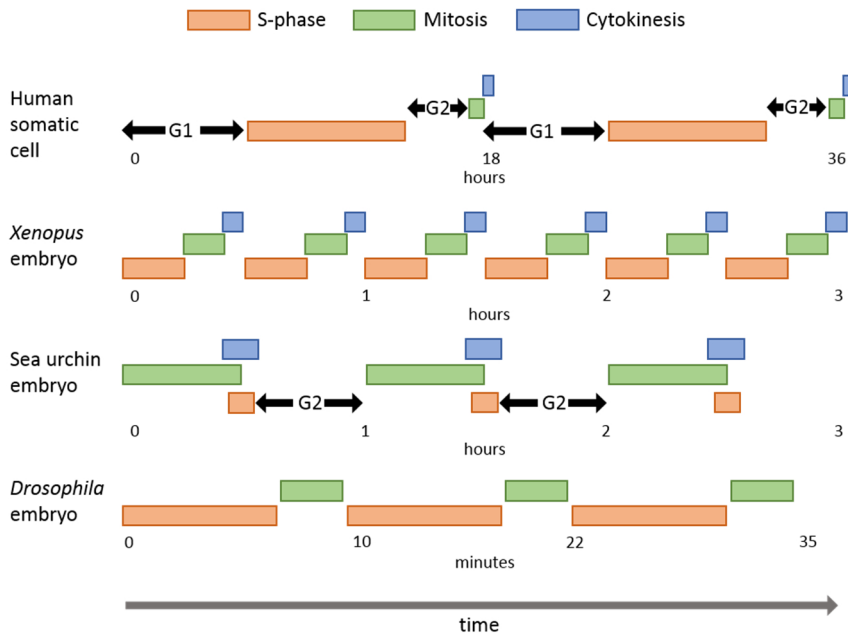


Figure 1.4 – Diversity in cell-cycle progression in different cell-types.

A schematic representation of the configuration of each specific cell-cycle is depicted with a time scale beneath each diagram. Gap phases are shown whenever present. Gap phases are missing during early *Xenopus* and *Drosophila* embryogenesis. Additionally, cytokinesis is also absent in fly embryos, as the early nuclear divisions occur within a multinucleated syncytium. Adapted from (Morgan, 2007).

***Drosophila melanogaster* embryogenesis**

As in other animal oocytes, the fly egg is filled with maternally deposited proteins and RNAs needed for rapid cell division and development. After fertilisation, the embryo undergoes rapid and synchronous nuclear divisions, spatially confined deep inside the egg – pre-blastoderm stage. The cell-cycle takes around 8 minutes and zygotic transcription is almost inexistent. During nuclear cycles 7 to 9, the nuclei migrate towards the cortex, and by cycle 10 they

dock to the cellular membrane forming the blastoderm (Foe and Alberts, 1983).

Once at the cortex, the nuclei divide another 4 rounds before cellularisation takes place. The cell-cycle slows down, zygotic expression slowly increases and S-phase progressively lengthens with every consecutive cycle, taking around 21 minutes to undergo nuclear cycle 13. After cellularisation, zygotic expression is fully activated, yet some maternal components are still present (reviewed in Farrell and O'Farrell, 2014; Morgan, 2007).

Blastoderm cellularisation is followed by gastrulation, a massive reorganisation of the embryo into a multilayered structure, the gastrula. After nuclear cycle 14 the cell-cycle is deeply remodelled, acquiring a long G2. In cycles 14-16 the cell-cycle duration is variable across different embryonic regions. Cells undergo division in a programmed spatial and temporal pattern according to complex morphogenetic cues. From cycle 17 onwards, cells acquire a G1 phase and rely mostly on the zygotic-specific gene expression (Morgan, 2007).

Maternal contribution hinders the analysis of mutant phenotypes in early embryos. Mutations in zygotic genes often do not produce any visible phenotype until the maternal gene product is no longer present. Maternal components are depleted at different timepoints; while some proteins are fully depleted by cycle 13, others can remain for longer, until mid to late larval development. Consequently, studying a gene's function in early development requires working with genetically mutant mothers that lay deficient eggs or driving RNAi expression specifically in the mother germline. On the other hand, zygotic expression is gradually initiated throughout early development. Different zygotic genes start being expressed at different cycles indicating that zygotic transcriptional

activation is a continuous process rather than a discrete transition in development (Edgar and Schubiger, 1986; Lott et al., 2011).

Cell-cycle regulation in the early *Drosophila melanogaster* embryo

In flies, early embryonic cell-cycles are mostly regulated by Cdk1 activity. During pre-blastoderm cycles, both Cyclin bulk levels and Cdk1 kinase activity do not oscillate. Since Cyclin destruction and Cdk1 inactivation are required to exit mitosis, the widely accepted explanation is that Cyclin destruction at these early stages occurs only locally, around the nuclei (Su et al., 1998). During blastoderm, Cyclin degradation and Cdk1-Cyclin activity become more evident, presenting a clear oscillatory behaviour (Deneke et al., 2016; Edgar et al., 1994). With this conspicuous oscillatory Cyclin degradation, Cdk1 becomes inactive for increasingly longer periods at the beginning of each blastoderm cycle. Additionally, the DNA replication checkpoint becomes activated, most likely as a consequence of increased DNA content in the embryo (Deneke et al., 2016). In S-phase, the DNA replication checkpoint depends on the activity of the Chk1/grapes signal transducing kinase. Chk1 regulates cell-cycle progression by inhibiting Cdk1 (Yuan et al., 2016). A decrease in Cdk1 activity can cause lengthening of S-phase and delay mitotic onset, so the progressively slower cell-cycles observed in blastoderm embryos may result from a Cdk1/Chk1 double negative feedback mechanism, causing longer Cdk1 inactivity in S-phase (Deneke et al., 2016).

The appearance of G2 in cell-cycle 14 coincides with inhibitory phosphorylation of all the Cdk1-Cyclins complexes. Although a widespread inhibitory phosphorylation does not occur in the early cycles, it has been proposed that Wee1 kinase, via Chk1 activation,

modulates Cdk1 activity locally via inhibitory phosphorylation (Farrell and O'Farrell, 2014).

Until recently, the mechanisms by which the cell-cycle remains synchronised throughout early embryonic divisions, across the whole syncytium, remained elusive. Deneke and colleagues (2016) used a Cdk1 Fluorescence Resonance Energy Transfer (FRET)-sensor activity reporter, a Chk1 localisation sensor and mathematical modelling to understand how the oscillatory Cdk1 chemical waves propagates in the embryo in different cell-cycle stages. They demonstrated that a double negative feedback mechanism between Cdk1 and Chk1 in S-phase generates an active chemical wave of Cdk1 activity that propagates across the embryo, faster than diffusion and synchronises the cell-cycle. On the other hand, the Cdk1 mitotic wave propagates as a passive, kinematic wave, only reflecting a predefined temporal delay. In this case, the mitotic wave of Cdk1 inactivation results from the Cdk1 oscillations occurring in the previous S-phase, and therefore the travelling velocity of one and the other are strongly correlated. These observations demonstrated that the cell-cycle slowdown in blastoderm stages results specifically from the activation of the S-phase DNA replication checkpoint and the resulting Cdk1 regulation by Chk1/Wee1 pathway but not by a slower activation of the mitotic switch (Deneke et al., 2016).

It is evident that the spatiotemporal control of cell-cycle progression relies on a complex interplay between kinases and phosphatases responsible for creating feedback and feed-forward loops. Timely protein synthesis and degradation allows fine tuning of the processes and ensuring some transitions are irreversible.

1.2 Microtubule Organising Centres (MTOCs) in eukaryotes

1.2.1 MTOCs structure and diversity

MTs assemble into radial asters and parallel or antiparallel bundles (Sanchez and Feldman, 2017; Surrey et al., 2001). These configurations, resulting primarily from MT intrinsic polarity, are amplified by the binding specificity of different MAPs, and largely determined by MT association with their MTOCs, giving rise to different MT networks in distinct cell-types. Even though MTOC morphology and composition is highly variable across eukaryotic organisms, cell-types and differentiation stages, they generally contain γ -tubulin nucleating complexes. Nonetheless a few cell-types, specifically *Drosophila* S2 (Rogers et al., 2008) cells and *C. elegans* embryos (Hannak et al., 2002), seem to be able to maintain cytoplasmic MT nucleation in interphase upon depletion of γ -tubulin.

The centrosome is the dominant MTOC in most animal cells, from which MTs, anchored through their minus end, are radially nucleated (Wu and Akhmanova, 2017). Yeasts organise linear MT arrays from the Spindle-Pole Body (SPB) (Cavanaugh and Jaspersen, 2017; Ito and Bettencourt-Dias, 2018; R uthnick and Schiebel, 2016), whereas some species of Amoebozoa possess Nuclear-Associated Bodies (NAB) (Azimzadeh, 2014; Gr af et al., 2015). Flowering plants do not have centrosomes, but have evolved alternative strategies to organise their cytoplasmic MT arrays by relying on the cell cortex, the nuclear envelope and activity of motor proteins (Hamada, 2014; Hodges et al., 2012). In many differentiated animal cells, the MTOC function is taken upon by non-centrosomal sites (ncMTOCs) thereby generating non-radial MT arrays more

adequate to the new cellular functions (Sanchez and Feldman, 2017).

The activity of MTOCs allows sorting of proteins, positioning of organelles such as the cell nucleus, the Golgi and endosomes, and overall establishment of cellular polarity (Bornens, 2008). For instance, MT-dependent nuclear positioning is crucial after fertilisation to guide the male and female pronuclear apposition in the large ctenophore egg (Rouviere et al., 1994). In *Drosophila*, this process was shown to depend on a plus-end directed microtubule motor called Klp3A/Kinesin-4, whose main activity is the depolymerisation of MTs at their plus-end tip (Williams et al., 1997).

1.2.1.1 The centrosome

The centrosome is composed of two centrioles, surrounded by a dynamic proteinaceous compartment called pericentriolar material (PCM) that is important for centriole biogenesis and centrosome maintenance (Dammermann et al., 2004; Pimenta-Marques et al., 2016). γ -tubulin is amongst the numerous proteins that compose the PCM and it is one of the most abundant components of the centrosome (Bauer et al., 2016)), playing a dominant role in MT anchoring and nucleation.

Centrioles can also dock to the cell membrane, becoming basal bodies, and template the growth of cilia. In animals, most cells form only one cilium (the primary cilium) but others can form hundreds (multiciliogenesis). Cilia can be motile, functioning in cell movement or flow motility, or immotile for sensing environmental cues (Mirvis et al., 2018).

Centrioles and basal bodies (CBBs) are well-conserved structures, present across the eukaryotic tree of life and probably derived from a basal body-like organelle, already present in the last eukaryotic ancestor (LECA) (Cavalier-Smith, 2002; Hodges et al., 2010). The canonical CBB is a 250 nm wide and 200 to 500 nm long (depending on the cell-type) barrel-shaped structure, often made of nine MT triplets (Figure 1.5). Each triplet is composed of a complete A-tubule made of 13 PFs, adjoined by partial B- and C-tubules (reviewed in (Winey and Toole, 2014)). Centrioles in *Drosophila* and *C. elegans* have a variable structure containing, for instance, doublet and singlet MTs (González et al., 1998; Greenan et al., 2018; Jana et al., 2018; Pelletier et al., 2006).

Light microscopy has been widely used to determine the approximate localisation of centrosomal components, but since centriole size is so close to the diffraction-limited optical resolution, their ultrastructural characterisation strongly relies on Electron Microscopy (EM) and, more recently, on advanced super-resolution fluorescence microscopy techniques (Sonnen et al., 2012; Sydor et al., 2015). EM studies have revealed that centrioles are polarised along their proximal-distal end and usually arranged in an orthogonal configuration within the centrosome (Figure 1.5). At their proximal lumen, immature centrioles and in some species matured ones, have a ninefold-symmetrical cartwheel structure. The cartwheel is composed of a central ring (hub) connected by filaments (spokes) to the inner part of the A-tubule of the triplet MT. Centrioles typically possess the cartwheel organised in multiple stacks within their lumen (reviewed in (Hirono, 2014)). In some species, the older (mature) centriole possesses subdistal and distal appendages that anchor cytoplasmic MTs and dock centrioles to the cell membrane,

respectively (Figure 1.5) (Bornens, 2002; Paintrand et al., 1992; Rattner and Phillips, 1973).

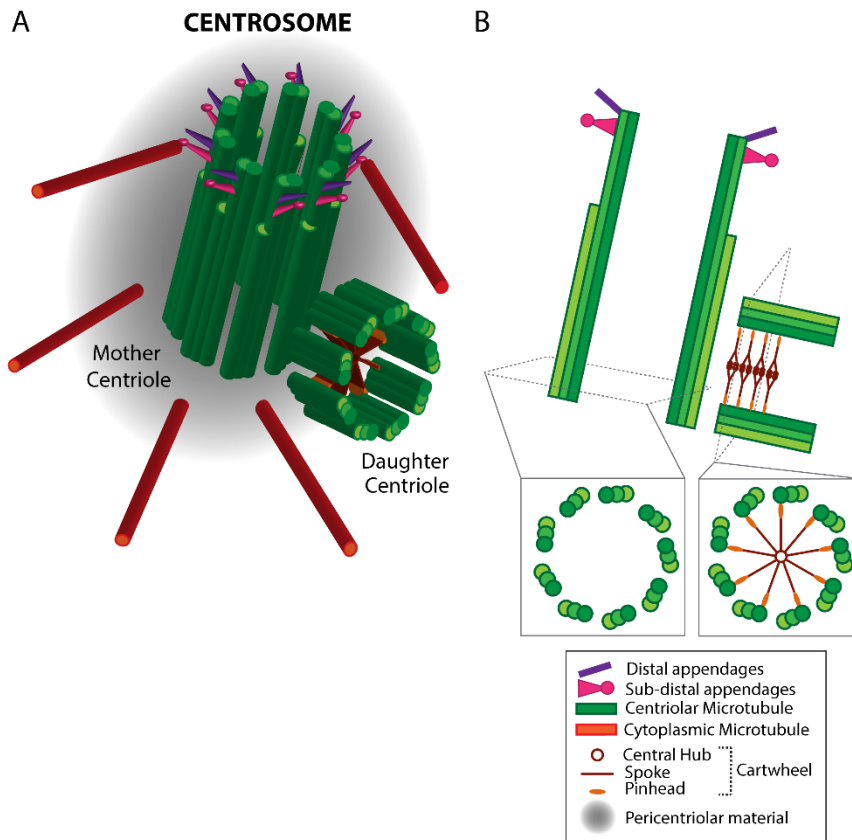


Figure 1.5 – Centrosome organisation and structure. A) Representation of the “canonical” centriole pair, found in most animal cells. Centrioles are barrel-shaped structures composed of nine MT triplets. Each centrosome has one mother (older) with subdistal (pink) and distal appendages (purple) and one, newly assembled, daughter centriole. The pericentriolar material (PCM, in grey) is nucleated by the mother centriole. **B)** Schematic representations of longitudinal and cross sections of the two centrioles. In vertebrate cells, the cartwheel is only present in daughter centrioles. The cartwheel is comprised of a central hub from which nine spokes emanate and connect to the MT wall via the pinheads. Adapted from (Marteil and Bettencourt-Dias, 2017).

Centriole diversity in Drosophila melanogaster

The diversity in centrosome composition and centriole architecture in *D. melanogaster* exhibits, like in other metazoans, cell-type specificity (González et al., 1998; Gottardo et al., 2015; Jana et al., 2018). Therefore, centrioles have different protein composition and number of MTs around the cartwheel, variable length and different MT nucleation capacity in different fly tissues (González et al., 1998; Jana et al., 2018).

In embryos and cultured cells, centrioles are very short, about 200 nm long and 200 nm wide and composed of MT doublets. In addition, they have a cartwheel along their entire length, contrary to what is observed in other cell-types (Callaini et al., 1997). Centrioles with MT singlets have also been detected in embryos, although it is unclear if these are intermediate stages preceding the formation of complete doublets (Gottardo et al., 2015). In a few somatic tissues, specifically in cells from the wing epidermis and in interommatidia sensory bristles, centrioles have been reported to present triplets of MTs and lack a cartwheel. Additionally, in the female germ cells, centrioles from early oocytes are also composed of MT triplets (Mahowald and Strassheim, 1970). In the male spermatocytes, centrioles display MTs triplets around the cartwheel, which only extends less than half the length of these exceptionally long centrioles that reach 1 μm in size (Gottardo et al., 2015).

Numerical centrosome abnormalities

Centrosome depletion, by genetic or chemical perturbation, has shown that centrosomes are not strictly required for cell survival. However, in untransformed vertebrate cells, centrosomes are important for rapid and faithful chromosome segregation, for the

formation of astral microtubules and for proliferation (Lambrus et al., 2015; Wong et al., 2015). Centrosome depletion by degradation or inhibition of the kinase activity of Polo-like kinase 4 (Plk4), a major regulator of centriole biogenesis, causes a progressive loss in centriole number in cycling human cultured cells. Untransformed cells become arrested in G1 phase with a single centriole whereas cancer cells continue to proliferate even in the absence of centrosomes (Bazzi and Anderson, 2014; Lambrus et al., 2015; Meitinger et al., 2016; Wong et al., 2015). Interestingly, p53 inhibition allows Plk4-depleted normal cells to continue proliferating without centrioles. Therefore failure in centriole duplication causes p-53 dependent cell-cycle arrest in untransformed vertebrate cells leading to cell senescence or apoptosis, which does not always occur in cancer cells since these often have p53 mutated or suppressed (Lambrus et al., 2015; Wong et al., 2015).

In flies, centriole loss does not cause cell-cycle arrest in S2 cultured cells (Bettencourt-Dias et al., 2005; Rogers et al., 2008), but centrosomes are essential for early embryonic cycles, for male meiotic divisions and for cilia assembly in sensory neurons and sperm (Chen et al., 2015; Megraw et al., 1999; Riparbelli et al., 2013; Rodrigues-Martins et al., 2008). Fly embryos derived from Plk4 or Asterless (Asl) mutant mothers have low centrosome number, which result in mitotic abnormalities that cause early embryonic lethality (Rodrigues-Martins et al., 2008; Varmark et al., 2007a).

On the other hand, centrosome amplification is also deleterious for cell division, triggers a p53-dependent arrest in vertebrate cells and is correlated to several human diseases (Denu et al., 2018; Godinho and Pellman, 2014; Godinho et al., 2014; Levine et al., 2018; Lopes et al., 2018; Marteil et al., 2018). Cells

with more than two centrosomes generally struggle to establish a bipolar spindle and undergo multipolar mitosis, segregating their genome unevenly. Aneuploid progeny from normal cells that divided in a multipolar fashion are frequently unviable and undergo apoptosis (Ganem et al., 2009), whereas altered cells cope better with these alterations, often by clustering supernumerary centrosomes. In fact, several human tumours display abnormally high centriole number and the level of amplification can change throughout cancer progression (Denu et al., 2018; Lingle et al., 2002; Lopes et al., 2018; Marteil et al., 2018). Interestingly, in different types of cancer, centriole amplification and bad prognosis have been correlated with upregulation of Plk4 levels (Kazazian et al., 2017; Ko et al., 2005; Liao et al., 2019; Marina and Saavedra, 2014). In *Drosophila*, there is no p53-dependent cell-cycle arrest in the presence of supernumerary centrosomes and different cell-types, such as neuroblasts and embryos, frequently cluster excess centrosomes (Basto et al., 2008).

1.2.1.2 The spindle-pole body

Evolutionary studies comparing multiple centrosomal components across eukaryotes suggest that fungi derive from an ancestor containing centrioles but, throughout evolution, yeasts lost centrosomes and developed a functionally equivalent structure called Spindle Pole Body (SPB). The SPB is a multi-layered organelle that is embedded in the nuclear membrane throughout the cell-cycle. In *Saccharomyces cerevisiae*, it is composed of an outer and inner plaques on the cytoplasmic and nuclear sides, respectively, allowing the scSPB to organise both cytoplasmic and

nuclear MTs (Figure 1.6). These two plaques are connected to a central layer via two internal layers. The ScSPB also contains an electron dense structure called half bridge which is involved in MT nucleation in G1 and it establishes the site of ScSPB duplication.

In *Schizosaccharomyces pombe* the SpSPB is less layered, consisting of a bulky cytoplasmic structure docked to the inner nuclear membrane through an unknown tether. Due to this conformation, throughout interphase, the SpSPB only organises cytoplasmic MTs. In mitosis, a process of invagination allows the SpSPB to nucleate both spindle and astral microtubules in a similar way as in *S. cerevisiae* (Figure 1.6). The SpSPB also possesses a half bridge which connects duplicated SPBs (reviewed in (Cavanaugh and Jaspersen, 2017; Ito and Bettencourt-Dias, 2018)). The SPBs duplicate only once per cell-cycle.

In the process of SPB duplication, the daughter SPB precursor (generically called satellite), assembles at the distal end of the half bridge. The precursor develops into a SPB which, in *S. cerevisiae*, is inserted at the nuclear envelope at G1/S, continuing to mature by recruiting nuclear SPB components. In *S. pombe*, both old and new SPBs remain cytoplasmic throughout duplication, which is only completed in G2. Mother and daughter SpSPB are embedded in the nuclear envelope by late G2/mitotic onset. The key known molecules involved in SPB duplication are Centrin and Sfi1. Sfi1 is cell-cycle regulated by the kinase and phosphatase activities of Cdk1 and Cdc14, respectively. During G2 and early mitosis, Cdk1 phosphorylates Sfi1, blocking SPB duplication. At anaphase onset, Cdc14 dephosphorylates Sfi1 allowing its incorporation at the half-bridge and promoting SBP duplication (Cavanaugh and Jaspersen, 2017; Rüttnick and Schiebel, 2016). These mechanisms regulate Sfi1-Centrin interaction, timely controlling SPB duplication.

1.2.1.3 The nucleus-associated body

The nucleus-associated body (NAB) is an electron dense, three-layered structure best characterised in the *Dictyostelium discoideum* amoeba. The NAB is surrounded by the corona, an electron dense matrix functionally equivalent to the PCM. In interphase, the NAB is localised in the cytosol and it only associates with the nuclear envelope upon its duplication in mitosis, when it organises the mitotic spindle (Figure 1.6) (reviewed in (Gräf et al., 2015; Ito and Bettencourt-Dias, 2018)). Most amoeba, like yeasts, do not assemble or require cilia throughout their life cycles, perhaps explaining the extremely derived morphology of their MTOCs. It is believed that the requirement for ciliary motility, and not the MT organisation activity, imposed a functional constraint on the CBB architecture throughout evolution (Azimzadeh, 2014; Hodges et al., 2010).

Amoebozoa share with animals a limited set of centrosomal proteins. They have γ -tubulin and some of its interacting molecules, Centrin, Cep192/Spd2, Centrosomin (Cnn) and members of the Cdk family (Carvalho-Santos et al., 2011). These components were likely part of an ancestral centrosomal protein set.

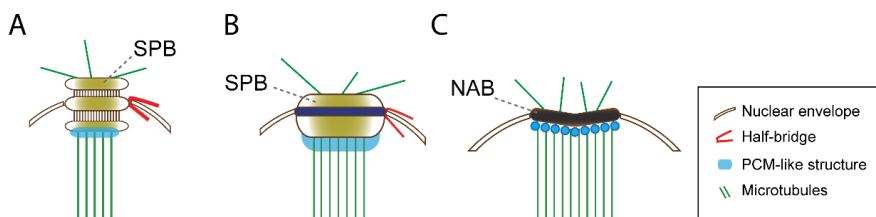


Figure 1.6 – Structure of the Spindle-Pole Body (SPB) and Nucleus-Associated Body (NAB) in yeasts and amoebzoa, respectively.

Yeasts such as *S. cerevisiae* and *S. pombe* contain a centriole-less MTOC called SPB, which presents a tripartite structure in *S. cerevisiae* (A) and bulky conformation in *S. pombe* (B). Some amoebzoa, such as *Dictyostelium discoideum*, have a centriole-less MTOC called NAB (C) that only associates with the nuclear envelope during mitosis. Adapted from (Ito and Bettencourt-Dias, 2018).

1.2.1.4 Non-centrosomal MTOCs (ncMTOCs)

Numerous sub-cellular structures can acquire, in different stages of cell differentiation or under certain conditions, MT organising capacity. Unlike the centrosomes, these ncMTOCs do not focus the MT minus ends into asters, but instead assemble parallel bundles (Figure 1.7). The establishment of new ncMTOCs generally requires the attenuation of MTOC activity at the centrosome and the localisation of MTOC components to the newly designated location and ensuing activation of its MTOC function. ncMTOC formation may involve different mechanisms, depending on whether the ncMTOC only anchors MTs or if it acquires the capacity of both anchoring and nucleating MTs. Accordingly, either the centrosomes nucleate and release MTs that are captured and bound through specific adaptor proteins at non-centrosomal sites; or MTs are nucleated, stabilised and anchored at the centrosome and directly transported along MTs to dock at ncMTOCs, otherwise, ncMTOC localise all the components needed for autonomous MT nucleation, stabilisation and anchoring and do not require any MT nucleation from the centrosomes (Sanchez and Feldman, 2017).

The process of switching off centrosomes and switching on other ncMTOCs usually involves γ -tubulin nucleating complexes to be displaced from the centrosomes and their localisation at the ncMTOCs, in the cases when these acquire MT nucleation capacity (Feldman and Priess, 2012; Muroyama and Lechler, 2017; Muroyama et al., 2016). Activation of MTOC function at non-centrosomal sites must be coupled to a change in cell state, either a cell-cycle transition or, more often, cell differentiation, whereby cells stop dividing and their MTOCs are not primarily involved in spindle assembly but rather in other functions such as establishing cell shape and polarity (Sanchez and Feldman, 2017). This timely regulation of the localisation and activity of these ncMTOCs capable of nucleating, stabilising and anchoring MTs is important for the diversity of functions MTs play within cells (Wu and Akhmanova, 2017). Future work might disclose how cells switch between these different MTOCs, tailoring them for different, cell-type specific functions.

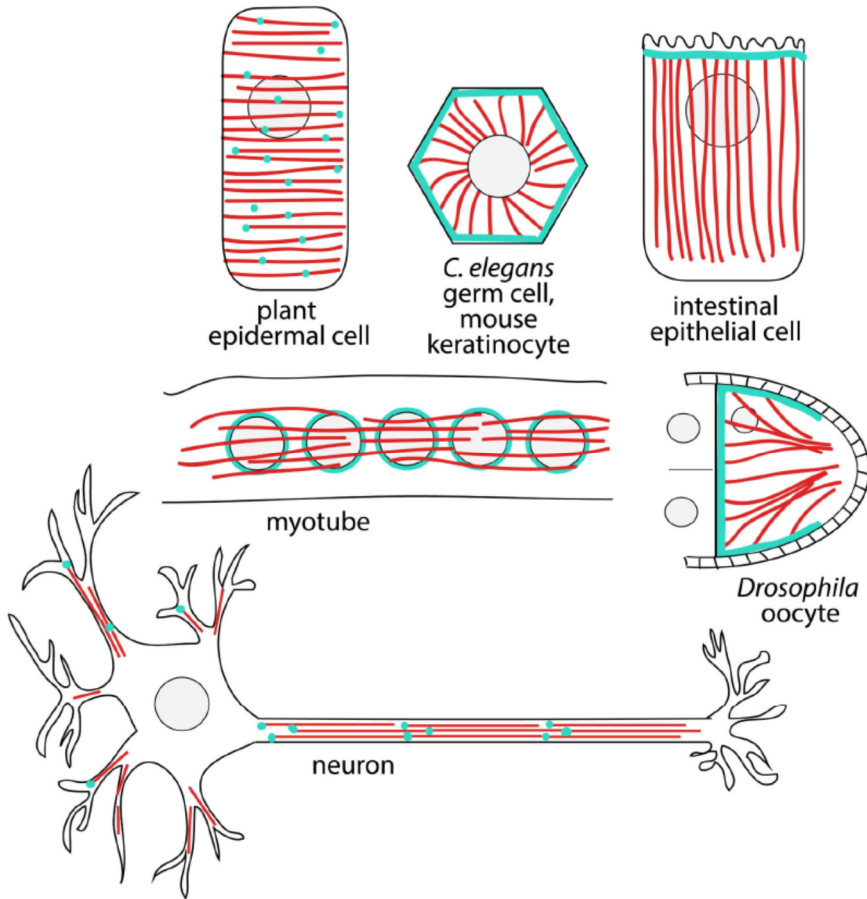


Figure 1.7 – Diversity in non-centrosomal MTOCs assembled in different cell-types. Distinct ncMTOCs (blue) organise cytoplasmic MTs (red), giving rise to different MT architectures depending on the cell-type and its function. Adapted from (Sanchez and Feldman, 2017).

MT nucleation from the Golgi

After the centrosome, the Golgi is the second major MTOC in animal cells. MT nucleation from the Golgi requires the large A-Kinase Anchoring Protein AKAP450, a γ -TURC interacting protein that binds the *cis*-side of the Golgi apparatus. Although AKAP450 has a similar centrosomal targeting domain (PACT) as the PCM

protein Pericentrin, it seems dispensable for centrosomal activity, however its depletion completely abolishes MT nucleation at the Golgi (Rivero et al., 2009). AKAP450 recruits γ -tubulin directly through its C-terminal region or indirectly, through the γ -TuRC-binding protein CDK5RAP2. Other molecules are then recruited to anchor and stabilise MT growth (reviewed in (Wu and Akhmanova, 2017)). In flies, the MTOC activity at the Golgi is not so well-established. It has been proposed that the ncMTOCs assembled in neuronal dendritic branches, containing Cnn, γ -tubulin and D-Plp, also coincide with Golgi foci (Ori-McKenney et al., 2012). Further investigation is necessary to characterise the role of Golgi MT activity in *Drosophila* neurons.

MT nucleation at the nuclear envelope

In some plant cells, differentiated muscle cells and in the *Drosophila* oocyte, MTs are organised at the nuclear envelope. In all these cases, γ -tubulin is directly involved. However, plants lack most homologues of PCM and γ -TuRC regulators, such as CDK5RAP2/Cnn, Plk1 and Pericentrin, indicating that they possibly evolved plant-specific γ -TuRC activators (Yamada and Goshima, 2017).

During myoblast to myotube differentiation, centrosomes are inactivated and several PCM components are recruited to the nuclear envelope, which then becomes the major MTOC in mammalian muscle cells (Figure 1.7). Linker of nucleoskeleton and cytoskeleton (LINC) complexes, composed of SUN domain proteins in the inner side of the nuclear membrane and KASH domain-containing proteins (among which Nesprin, in mammals) in the outer

nuclear membrane, recruit AKAP450 to the nuclear envelope, promoting MT nucleation via γ -tubulin nucleating complex (Gimpel et al., 2017). Knocking-down Nesprin1 or AKAP450 by siRNA affects nuclear distribution within differentiated myotubes. MT nucleation from the nucleus and kinesin-1 activity are critical for proper nuclear positioning and for muscle function (Gimpel et al., 2017; Metzger et al., 2012).

Oocyte specification in *Drosophila* is accompanied by the migration of all centrioles from the nurse cells into the oocyte. The centrioles then cluster on the posterior side of the oocyte, in-between the nucleus and the posterior follicle cells, forming a large MTOC, during stages 1-6 of oocyte development. A ncMTOC also forms on the posterior hemisphere of the oocyte nucleus, and in stages 6-7, the nucleus migrates from the posterior to the anterior end of the oocyte, through the combined activity of nuclear and centrosomal MTs (Figure 1.7) (Tillery et al., 2018; Tissot et al., 2017). Nuclear repositioning, together with Gurken protein localisation at the anterior-dorsal site, establishes the anterior-dorsal axis of the future embryo (González-Reyes et al., 1995; Guichet et al., 2001; Tillery et al., 2018; Tissot et al., 2017; Zhao et al., 2012).

MT nucleation at the cell cortex

The cell cortex is the major MTOC in plants, playing a fundamental role in plant cell division. The mechanisms underlying cortex nucleation in plants are not fully understood.

The MTOC activity of the cell cortex is important for apico-basal polarity in animal epithelial cells. While the MT minus ends are anchored at the ncMTOC on the apical side, the MT plus ends

interact with the basal side of the cell, thereby establishing cell polarity by differential plus end- or minus end-directed transport of structural and signalling components (Sanchez and Feldman, 2017). Overall, cortical MT nucleation in epithelial ncMTOCs is mediated by MT minus end regulators such as Patronin/CAMSAP, γ -tubulin, and Ninein. While the role of Ninein in cortical MT nucleation in flies is still unclear, the Patronin-dependent pathway seems to be essential in several cell-types. For instance, membrane-anchored ncMTOC formation in the *Drosophila* ovarian follicle cells and in the oocyte requires the function of Patronin, Short stop and β H2-spectrin (Khanal et al., 2016; Nashchekin et al., 2016b; Voelzmann et al., 2017).

Mitochondrial MT nucleation in sperm

During *Drosophila* spermiogenesis, the mitochondria fuse giving rise to two giant mitochondria that acquire MT nucleation capacity and participate in the important step of sperm elongation. This process is mediated by the expression of a non-centrosomal Cnn splice variant in the testes (CnnT), which lacks the centrosome targeting domain but contains instead a mitochondrial-targeting region at its C-terminus. CnnT also retains its conserved N-terminus CM1 motif (Centrosomin motif 1), mediating the recruitment of γ -tubulin and γ -TURC associated proteins and converting the mitochondria into a ncMTOC (Chen et al., 2017).

Acentriolar female meiosis

In flies and many other animals, the female meiotic spindles are acentriolar. Spindle assembly in *Drosophila* meiosis I requires γ -

tubulin 37C and cooperation between several motor proteins such as the Non-claret disjunctional (Ncd) minus-end directed kinesin 14, Klp61F that slides antiparallel MTs, Klp54D and spindle pole Abnormal spindle (Asp) to bundle MTs and establish a bipolar spindle (Radford et al., 2017; Tavosanis et al., 1997). In meiosis II, a specialised disk-shaped ncMTOC is formed within the central spindle, between two adjoining spindles. This central ncMTOC nucleates astral MTs and it is enriched with several PCM proteins such as γ -tubulin, Cnn, CP190, Mud, Asp and Kinesin-6 motor Pavarotti. Mutations in Polo, Cnn or γ -TURC, impair central aster assembly resulting in problems in spindle organisation and in meiotic resumption (Riparbelli and Callaini, 2005; Riparbelli et al., 2002; Tillery et al., 2018; Vogt et al., 2006).

MT nucleation from the augmin complex

In animal and plant cells, the evolutionary conserved augmin complex is a γ -TURC regulator that promotes MT nucleation from existing MTs. The augmin complex binds to spindle MTs and recruits γ -tubulin, increasing the density of the mitotic spindle in *Drosophila* S2 cells (Goshima et al., 2008). In plant cells and in neurons the augmin complex is important for the organisation of the interphasic MT network (Figure 1.7) (Lawo et al., 2009; Liu et al., 2014; Sánchez-Huertas et al., 2016; Uehara et al., 2009).

In vitro MT nucleation without γ -tubulin

It was recently shown *in vitro* that MTs can be polymerised below critical tubulin concentration and without γ -tubulin, from a

supramolecular scaffold formed by Spindle-defective protein 5 (Spd5), a master PCM recruiter in *C. elegans*, likely the ortholog of Cnn in flies. At high concentration, Spd5 forms condensates that can recruit MAPs such as TPX2 and ChTOG/XMAP215. These are capable of concentrating α - and β -tubulin and organise MT asters (Woodruff et al., 2017).

1.2.2 Canonical centriole biogenesis (duplication)

In proliferating cells, centriole biogenesis follows the canonical pathway by which two daughter centrioles form adjacent to two existing mothers. In early G1, cells enter the cell-cycle with one centrosome composed of two centrioles (mother and daughter) orthogonally oriented. Before duplication, the two centrioles disengage, losing their orthogonal configuration, and both become mother centrioles (Agircan et al., 2014; Robbins et al., 1968). From G1 to S-phase, one procentriole assembles orthogonally to each mother. The procentrioles elongate along S and G2 phases and each centrosome starts recruiting PCM components, a process known as centrosome maturation (Banterle and Gönczy, 2017; Kuriyama and Borisy, 1981; Robbins et al., 1968). From G2 to mitosis, the two centrosomes separate and migrate toward opposite poles of the cell. Mitotic centrosomes recruit more PCM, which increases their MT nucleation activity, important for organising the mitotic spindle (Figure 1.8). During mitosis, daughter centrioles undergo centriole-to-centrosome conversion by which they lose the cartwheel (in vertebrate cells) and incorporate a series of proteins required for PCM organisation and centriole biogenesis in the following cell-cycle (Fu et al., 2016; Izquierdo et al., 2014; Wang et

al., 2011). This process renders daughter centrioles competent or “licensed” for motherhood (Fu et al., 2016). Upon mitotic completion, each daughter cell inherits exactly one pair of centrioles. At the beginning of each G1 phase, the oldest centriole acquires both distal and subdistal appendages (Figure 1.8) (Kong et al., 2014; Rattner and Phillips, 1973). In *Drosophila*, both appendages are seemingly absent from the mother centriole (Callaini et al., 1997).

The synchronisation between centriole duplication (only once per cell-cycle) and segregation with the DNA cycle, as well as the spatial bias imposed by the mother centriole on the location of procentriole assembly, ensures cells maintain a correct centriole number over generations. Although canonical biogenesis (duplication) is the most prevalent, and likely the ancestral pathway of MTOC formation in eukaryotes, centrioles can also assemble via non-canonical mechanisms, which often give rise to the formation of an exceptionally large centriole number. These mechanisms and the diverse centriole number they generate, seem more confined to specific cell types during differentiation or life-cycle stages, and are discussed in detail in Section 1.4.

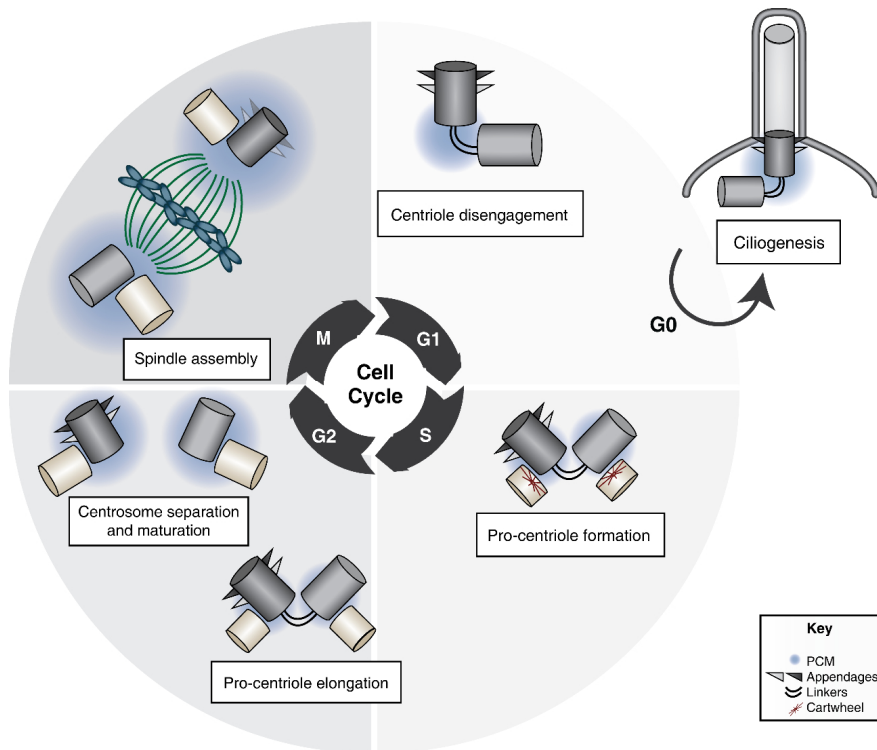


Figure 1.8 - Canonical Biogenesis in cycling cells. In early G1, cells have one centrosome with two centrioles (mother and daughter) orthogonally oriented. Before duplication, the two centrioles disengage (G1), losing their orthogonal configuration and both become mother centrioles. From G1 to S-phase, one pro-centriole forms orthogonally to each mother. From G2 to mitosis, the pro-centrioles elongate, each centrosome recruits PCM and the two centrosomes separate, migrating towards opposite poles of the cell. Mitotic centrosomes are highly enriched in PCM components, allowing them to organise the mitotic spindle. Upon mitotic completion, each daughter inherits exactly one pair of centrioles. At the beginning of each G1 phase, the oldest centriole acquires both distal and sub-distal appendages in vertebrate cells. When cells exit the cell-cycle (going into G0), the mother centriole can dock to the cell membrane via its distal appendages and nucleate the formation of a primary cilium. From (Nabais et al., 2018).

1.2.3 Molecular players in centriole biogenesis

1.2.3.1 Procentriole assembly

Procentriole assembly relies on the sequential interaction between a conserved set of proteins. In animals, the serine/threonine Polo-like kinase 4 (Plk4 or Sak in *Drosophila*, Zyg-1 in *C. elegans* (O'Connell et al., 2001)) is the master driver of centriole biogenesis (Bettencourt-Dias et al., 2005; Habedanck et al., 2005; Kleylein-Sohn et al., 2007). Together with SCL/TAL1-interrupting locus protein Stil (Anastral-spindle 2, Ana-2 in *Drosophila* and Sas-5 in *C. elegans*), and Sas-6, they initiate procentriole formation (Arquint and Nigg, 2016) (Figure 1.9 and 1.10).

In human cells, Plk4 recruitment and binding to the centrioles is mediated by Cep63, Cep192 and Cep152 (Figure 1.10) (Brown et al., 2013; Hatch et al., 2010; Kim et al., 2013; Sonnen et al., 2013). In flies, Plk4 is recruited by Asl/Cep152 (Dzhindzhev et al., 2010; Klebba et al., 2015a), whereas in worms Zyg1 recruitment to the centrosomes relies on Spindle-defective protein 2 Spd2/Cep192 (Delattre et al., 2006; Pelletier et al., 2006). Plk4 phosphorylates Stil on multiple residues, promoting its binding to Sas-6, the main structural component of the cartwheel (Cottee et al., 2015; Dzhindzhev et al., 2014; Kratz et al., 2015; Moyer et al., 2015). Sas-6 and Cep135/Bld10 associate and assemble the cartwheel, which confers the centriole its ninefold symmetry. Recently, it was shown *in vitro*, that *Chlamydomonas* Sas-6 and Bld10 are able to self-organise into a *bona fide* cartwheel, composed of multiple stacks similarly to what is observed in cells, thus recapitulating the structure of the centriolar core (Guichard et al., 2017). Cep152/Asl also binds

centrosomal P4.1-associated protein Cpap (Sas-4 in *Drosophila* and in *C. elegans*) which interacts with the centriolar MT wall and promotes the incorporation of PCM components (Figure 1.9 and 1.10) (Kohlmaier et al., 2009; Lin et al., 2013a; Pelletier et al., 2006; Schmidt et al., 2009; Tang et al., 2009).

In some species, the MT triplet wall is formed sequentially. The A-tubules are first assembled, attaching to the cartwheel pinheads, followed by the sequential formation of the incomplete B- and C-tubules (Greenan et al., 2018; Guichard et al., 2010). The stabilisation of the centriole MT wall depends on Sas-4, γ -tubulin and Bld10 (Basto et al., 2006; Carvalho-Santos et al., 2012; Dammermann et al., 2008; Gonczy et al., 2000; Raynaud-Messina et al., 2004).

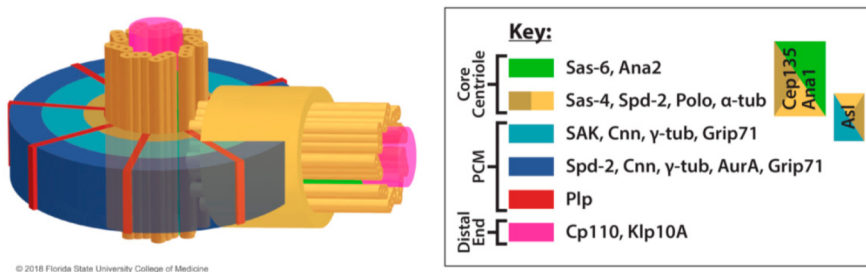


Figure 1.9 – Molecular organisation of the *Drosophila* centrosome. Localisation of some centriolar and pericentriolar material (PCM) proteins at the centrosome during interphase. The mother centriole organises the PCM, which adopts a specific sub-structure that has recently been revealed by super-resolution microscopy. The PCM is sub-divided into different zones: one closer the centriole barrel, where components such as Sak/Plk4, Cnn and γ -tubulin are localised, an intermediate region where some of the main PCM recruiters bind and an outer zone. From (Tillery et al., 2018).

1.2.3.2 Centriole elongation

Centriole length varies depending on the species and cell-types in an organism. Centriole elongation is regulated by molecules with antagonistic activity. In mammalian cells, Cpap, Cep120, Poc5, Cep295 and Centrobin promote centriole elongation (Azimzadeh et al., 2009; Chang et al., 2016; Gudi et al., 2015; Lin et al., 2013b; Schmidt et al., 2009; Tang et al., 2009). In *Drosophila*, Asl plays a positive role in regulating centriole length (Galletta et al., 2016). On the other hand, other proteins, such as CP110 and Cep97, form a cap at the distal centriole end, preventing centriole overelongation in human cells (Franz et al., 2013; Schmidt et al., 2009). In *Drosophila* S2 cells, CP110 depletion has an opposite effect than in mammalian cells, whereas the microtubule-depolymerizing kinesin-13/Klp10A, restricts centriole size via its MT depolymerisation activity (Delgehyr et al., 2012). In fly spermatocytes, Bld10, Sas4, D-Plp and Poc1 mutants have shorter basal bodies than wildtype. Anastral-spindle 1 (Ana1), recruited to the daughter centrioles by Bld10, promotes centriole elongation in a dose-dependent manner in spermatocytes and wing disc cells (Saurya et al., 2016). Recently, it was proposed that Plk4 regulates the rate and period of centriole elongation during S-phase in fly embryos (Aydogan et al., 2018). Altogether, it is not well-understood how centriole length is controlled in different cell-types and what is the interplay between centrosomal components and MAPs in regulating this process.

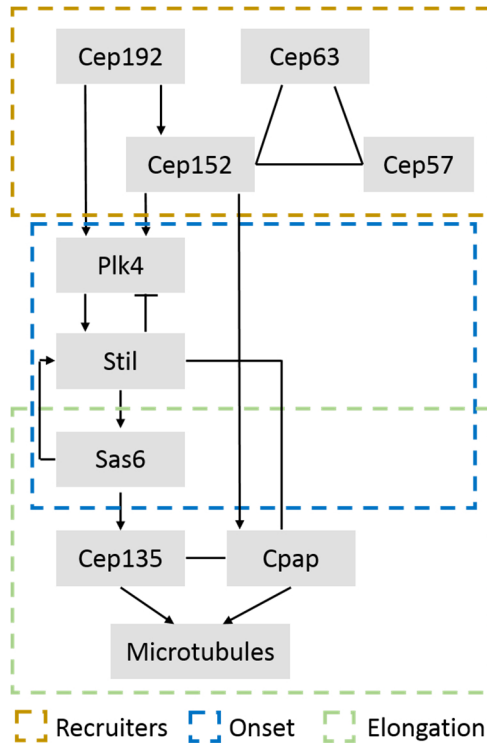


Figure 1.10 - Simplified molecular cascade driving centriole assembly in human cells. Lines indicate physical interaction between the components while the arrows depict recruitment of the downstream element to the centrosome. Three functional modules have been highlighted. The first module includes the Plk4 ‘recruiters’ Cep192, Cep152, Cep63 and Cep57. The second group comprises the core conserved molecules needed to drive the ‘onset’ of pro-centriole assembly, Plk4, Stil and Sas6. The third module includes Sas6, Cep135 and Cpap, and participates in centriole ‘elongation’, promoting cartwheel growth and elongation of the MT-wall of nascent centrioles. Adapted from (Banterle and Gönczy, 2017).

1.2.3.3 Centriole maturation

From G2-phase to mitosis, centrosomes are drastically enriched with PCM components, therefore increasing their MT

anchoring and nucleation capacities at the onset of mitosis (Conduit et al., 2010; Woodruff et al., 2014). This process, called centrosome maturation, occurs by PCM expansion around the centrioles, and it is important for chromosome capture, bipolar spindle formation and correct chromosome segregation (Woodruff et al., 2014).

Centrosome maturation entails distinct processes for the mother and the daughter centrioles: while the mother centrioles undergo PCM enrichment their daughters go through 'centriole-to-centrosome' conversion, whereby they become competent for duplication and PCM recruitment in the following cell-cycle.

Mother centriole maturation depends on the activity of multiple mitotic kinases, including Cdk1, Plk1 (Polo in flies) and Aurora A (AurA) (Wang et al., 2014b). In human cells, centrosome maturation is initiated by Pericentrin phosphorylation by Plk1 at mitotic onset, which is necessary for the recruitment of γ -tubulin, Aurora A and Plk1-specific substrates Cep192, Cep215 (Cnn in *Drosophila*) and NEDD1 to the centrosomes (Lee and Rhee, 2011). AurA directly phosphorylates and activates Plk1 upon mitotic entry (Macûrek et al., 2008) and regulates the recruitment of γ -tubulin complexes and MAPs (Hannak et al., 2001). AurA centrosomal localisation during mitosis depends on Plk1, so these two proteins interact by a mutual positive feedback mechanisms, important for centrosome maturation and mitotic progression (Bruinsma et al., 2014; Lee and Rhee, 2011). Cdk1 and Plk1 sequentially phosphorylate NEDD1, promoting its interaction with γ -tubulin and targeting γ -TURC to the centrosomes (Burkard et al., 2009).

In flies, Spd2 recruits Cnn (Dix and Raff, 2007; Giansanti et al., 2008), which in turn is phosphorylated by Polo/Plk1 at mitotic onset

(Conduit et al., 2014b). Cnn phosphorylation promotes its oligomerisation, assembling a scaffold around centrioles that spreads outwards, as Cnn molecules are newly incorporated closer to the centrioles (Conduit et al., 2014b). Recently, it has been shown that Polo also phosphorylates and contributes to Sas4 expansion in mitosis in *Drosophila* spermatocytes, brain cells and embryos (Ramani et al., 2018). This phosphorylation is likely a very early event in PCM maturation as it is important for the recruitment of other key PCM components such as Cnn and γ -tubulin (Ramani et al., 2018). Polo, Cnn and Spd2 establish a positive regulatory network, promoting PCM expansion at the mother centriole (Alvarez-Rodrigo et al., 2018; Conduit et al., 2014a). Cnn phosphorylation by Polo is important for Cnn enrichment and Spd2 maintenance at the centrosome. Spd2 and Cnn interaction promotes Cnn recruitment and finally, Spd2-mediated Polo recruitment, closes the autocatalytic loop (Alvarez-Rodrigo et al., 2018; Conduit et al., 2010; Conduit et al., 2014a). Since Cnn does not recruit Spd2 or Polo, the previously mentioned molecular loop depends on other molecules such as Asl (Blachon et al., 2008; Novak et al., 2014) and Sas4 (Ramani et al., 2018) for the centrosomal recruitment of Cnn and Spd2. The Spd2–Cnn scaffold forms the main anchor for γ -tubulin within the PCM region adjacent to the centriole wall.

Besides directly recruiting PCM proteins to the mother centrioles, Plk1/Polo is also involved in daughter cell modification into a mature centrosome. Daughter centriole-to-centrosome conversion is dependent on Cep295 (*Drosophila* Ana1) and governed by Plk1/Polo and Cdk1, “licensing” daughter centrioles for motherhood (Fu et al., 2016; Izquierdo et al., 2014; Novak et al., 2016; Wang et al., 2011). In flies, Cdk1 phosphorylation on Sas4

Thr200 during mitosis, creates a docking site for Polo, somehow recruiting Asl to the daughter centriole (Novak et al., 2016). Then the sequential loading of Bld10/Cep135, Ana1/Cep295 and Asl/Cep152 onto daughter centrioles and the interaction between these components, promotes daughter maturation. Asl/Cep152 loading is critical, since this protein has a dual role; both in PCM recruitment and in Plk4 recruitment and centriole duplication in the next cell-cycle (Conduit et al., 2014b; Fu et al., 2016; Izquierdo et al., 2014; Loncarek, J; Hergert, P; Khodjakov, 2010; Novak et al., 2014; Wang et al., 2011).

1.2.3.4 PCM role in centriole biogenesis

Recent super-resolution microscopy studies have shown that the PCM in human and fly centrosomes is not an amorphous material, as previously thought. Instead, it is a well-organised molecular scaffold, where proteins occupy defined localisations (Fu and Glover, 2012; Lawo et al., 2012; Mennella et al., 2012; Sonnen et al., 2012). Alterations in PCM size and organisation are regulated during cell-cycle progression and differentiation (reviewed in (Fry et al., 2017)). During interphase, many PCM proteins form concentric ring-shaped structures or toroids around the centriole wall. This conformation is altered in mitosis when the drastically expanded PCM is visualised as a protein meshwork (Fu and Glover, 2012; Lawo et al., 2012; Sonnen et al., 2012).

Several PCM components are implicated in the spatial and numerical control of centriole formation. One of such components is the core PCM protein γ -tubulin. In *C. elegans* embryos and in human cells, PCM recruitment and centriole duplication are impaired by γ -

tubulin depletion (Dammermann et al., 2004; Kleylein-Sohn et al., 2007). Depletion of the centrosomal proteins Spd2 and Spd5 causes the same effect in *C. elegans* (Dammermann et al., 2004; Delattre et al., 2006; Kemp et al., 2004; Pelletier et al., 2004). The Spd2 mutant produces the most severe phenotype probably due to its role in recruiting Zyg1, the orthologue of Plk4, the master kinase driving centriole biogenesis in the worm (Delattre et al., 2006). However, Spd2/Cep192 and Spd5/Cnn knockdowns do not seem to affect centriole duplication in *Drosophila* or in human cells (Dix and Raff, 2007; Gomez-Ferreria et al., 2007; Zhu et al., 2008). Surprisingly, despite having a direct role in Plk4 recruitment to the centrosomes, Cep192 depletion does not cause defects in centriole duplication in human cells, possibly because Cep152 and Cep63 compensate for its loss.

Multiple studies have demonstrated Asl/Cep152 requirement for centriole duplication in flies, human cells, zebrafish and *Xenopus* (Blachon et al., 2008; Goshima et al., 2007; Hatch et al., 2010; Varmark et al., 2007). Asl/Cep152 recruits and interacts with Plk4 in flies and in humans. In human cells, Cep152 also has an effect on Cpap localisation at the centrosome, suggesting that the Cep152-Plk4 interaction plays a role in Cpap recruitment and regulation of centrosome duplication (Cizmecioglu et al., 2010; Hatch et al., 2010). On the other hand, Asl is also very important for the recruitment and organisation of PCM components. In flies, Asl is a major recruiter of Spd2 and Cnn to the centrosomes (Blachon et al., 2008; Conduit et al., 2014a; Dobbelaere et al., 2008; Giansanti et al., 2008).

Sas4/Cpap, another conserved player in centriole biogenesis, plays distinct structural roles in different subcellular compartments. On one hand, it interacts with MTs contributing for the assembly of

the centriolar MT walls (at the centrosome), on the other hand, it has been suggested by Gopalakrishnan and colleagues that Sas4/Cpap promotes the pre-assembly of PCM cytoplasmic complexes (composed of Cnn, Asl and Plp) that are later tethered to the centrosome and drive PCM accumulation (Conduit et al., 2015; Gopalakrishnan et al., 2011). While in flies Sas4 depletion renders pro-centrioles unstable, in human cells, centriole biogenesis is suppressed when Cpap is depleted (Gopalakrishnan et al., 2011; Kohlmaier et al., 2009).

It is complex to disentangle the function of PCM components in PCM organisation and their role in centriole assembly, since these two are intimately associated. PCM enrichment at the centrosomes promotes MTOC activity which, either directly or indirectly, can recruit centriolar proteins to the centrosome. Additionally, the localisation of PCM proteins is regulated by the cell-cycle, allowing them to play different functions at different timepoints. In *Drosophila* culture cells, it was demonstrated that Cnn, Spd2 and γ -tubulin change their spatial localisation at the centrosome between G2 and mitosis (Fu and Glover, 2012).

1.2.3.5 Licensing and cell-cycle coordination

Centriole disengagement and Plk1

Similarly to chromosomes, centrosomes have to be correctly duplicated and distributed to daughter cells each cell-cycle. Centrosome biogenesis is usually coordinated with the DNA cycle, sharing regulatory features: there seems to be an early priming event for duplication and, after one daughter structure forms, re-duplication should be prevented. Several mechanisms have been proposed to

couple the centriole and the cell-cycles (reviewed in (Loncarek and Bettencourt-Dias, 2018)).

The physical separation (disengagement) between mother and daughter has been described as a licensing step that enables centrioles to duplicate, while their association from S-phase to mitosis is thought to block overduplication. Fusion of cells in different cell-cycle stages has shown that unduplicated G1 centrosomes can duplicate in non-permissive G2 cell-cycle stage whereas mother centrioles that have duplicated (G2 centrosomes), do not re-duplicate when fused to cytoplasm permissive for duplication (G1/S cytoplasm) (Wong and Stearns, 2003). Similarly, purified centrioles from S-phase arrested HeLa cells only duplicate in interphasic cycling *Xenopus* extract when they become disengaged (Tsou and Stearns, 2006). These experiments suggest that the licensing and block to re-duplication is centrosome intrinsic and imposed by daughter centrioles on their mothers. More recently, it was proposed that distancing of the daughter centriole from the mother enables reduplication in human cells, even if the original daughter centriole retains its orthogonal configuration (Shukla et al., 2015). Centriole disengagement in late mitosis requires Plk1 activity. Some studies propose that separase, the protease that cleaves sister chromatids during mitosis, also cleaves a physical linker between mother and daughter centrioles at anaphase onset. However, loss of separase in human HCT116 cells slows down but does not prevent centriole disengagement, while double inhibition of Separase and Plk1 completely blocks centriole disengagement and centriole duplication in the following interphase (Tsou et al., 2009). In *C. elegans* embryos, separase depletion impairs separation and duplication of the sperm centrioles at the meiosis to mitosis transition, but it does not affect the centriole cycle in the following mitotic divisions,

indicating that different centriole separation mechanism might be present in different cell-types and developmental stages (Cabral et al., 2013). In human cells, the expression of constitutively active Plk1 causes premature centriole disengagement and centriole-reduplication (Shukla et al., 2015). Plk1 inhibition in *Xenopus* CSF extract blocks centriole disengagement (Schöckel et al., 2011). Further investigation is needed to determine if Plk1-mediated centriole disengagement is, in fact, an universal mechanism and identify the substrates it acts upon.

Cyclin-dependent kinases

Cdks regulate both DNA and centrosome cycles. Uncoupling between these cycles allows testing the function of Cdks in just one of these processes. For e.g., inhibition of DNA polymerisation in *Drosophila* embryos or *Xenopus* eggs leads to multiple rounds of centrosome assembly (Hinchcliffe et al., 1999; Raff and Glover, 1988). In *Xenopus* eggs, these repeated centrosome duplications are abrogated by blocking Cdk2-Cyclin E activity. Similarly, Cdk2-Cyclin E inhibition blocks centrosome duplication in sea urchin zygotes and in the early *Xenopus* embryo (Lacey et al., 1999; Schnackenberg et al., 2008). Altogether, these studies indicate that Cdk2-Cyclin E activity is needed for centrosome duplication in embryonic systems.

Cdk2 activity also regulates the centriole cycle in some mammalian somatic cells. Inhibition of p21, one of the major p53 targets, increases Cdk2 activity and causes centrosome amplification in human hematopoietic cells (Mantel et al., 1999). Similarly, Cdk2 activity is required for centriole reduplication in S-phase arrested Chinese hamster ovary (CHO) cells and in mouse fibroblasts (Duensing et al., 2006; Kuriyama et al., 2007; Meraldi et

al., 1999). However, Cdk2 is not strictly needed for cell-cycle progression in somatic cells nor for normal centriole duplication (Duensing et al., 2006). In Cdk2 null mouse cells, centrioles duplicate normally suggesting that other Cdk-Cyclin have redundant functions in this process. One study proposes that Cdk4 participates with Cdk2 in the regulation of the centrosome cycle. Cdk2 and Cdk4 double knockout in mouse fibroblasts display a stronger reduction in centriole number than the single mutants. In the p53 knock-out background, permissive to centriole amplification, Cdk2 and/or Cdk4 depletion prevents centriole re-duplication. This study proposed that Cdk2 and Cdk4 drive centriole reduplication by hyperphosphorylating a common site in nucleophosmin, a putative licensing factor of centrosome duplication (Adon et al., 2010). Cdk1-Cyclin B prevents centriole re-duplication in mitosis by binding and phosphorylating Stil (Zitouni et al., 2016), promoting its degradation by the APC/C pathway (Arquint and Nigg, 2014). The interaction between Cdk1-Cyclin B and Stil also outcompetes the formation of the Plk4-Stil complex required for procentriole assembly. After Cdk1 inactivation upon mitotic exit, Plk4 can bind and phosphorylate Stil, recruiting Sas6 and driving pro-centriole assembly in S-phase (Zitouni et al., 2016).

Recently, the DNA replication licensing factor Cdc6 has been shown to negatively regulate centriole duplication (Xu et al., 2017) and centrosomal MTOC activity, in human cultured cells (Lee et al., 2017a). Cyclin A mediates Cdc6 centrosomal recruitment during S and G2 phases, where it localises as two dots on the proximal side of the parental centrioles. Cdc6 negatively regulates centriole amplification by binding and inhibiting Sas6-Stil interaction. Conversely, Plk4 binds and phosphorylates Cdc6 during S phase, likely suppressing the inhibitory activity of Cdc6 on Sas6. Cdc6

depletion induces centrosome over-duplication, whereas overexpression of wild-type Cdc6 or Cdc6 mutant resistant to Plk4 phosphorylation decreases centrosome overduplication in the context of Plk4 co-overexpression. This study suggests Cdc6 and Plk4 have antagonistic roles in centriole duplication and provides an interesting mechanism for the coupling between the centrosome and the cell-cycles (Xu et al., 2017).

Centriole-to-centrosome conversion

It has been proposed that Asl recruitment onto daughter centrioles licenses centriole duplication in *Drosophila* embryos (Novak et al., 2014). During mitosis, Cdk1 phosphorylates Sas4 on a single docking site, which drives Polo (Plk1) recruitment to daughter centrioles (Novak et al., 2016). In both *D. melanogaster* and human cells, centrosomal Polo/Plk1 triggers the assembly of Bld10/Cep135, Ana1/Cep295 and Asl/Cep152 (Fu et al., 2016; Izquierdo et al., 2014; Saurya et al., 2016). Interestingly, Asl incorporation at the daughter centriole only occurs at the end of mitosis, once it disengages from its mother. Asl enrichment confers the daughter centriole the ability to recruit PCM, becoming a mature centrosome, competent for duplication in the next cycle (Novak et al., 2014; Novak et al., 2016). In mammalian cells, Cep295 seems to be important for stabilising young centrioles and contribute to daughter-to-mother centriole conversion in late mitosis through the recruitment of Cep192 (Tsuchiya et al., 2016). Although *C. elegans* lacks a clear Cep295 homologue, a recently described centriolar component called Spindle-assembly abnormal 7 (Sas7) might play analogue functions. Sas7 binds Spd2, regulating its recruitment to

the centrosome, and is required for procentriole assembly and PCM formation (Sugioka et al., 2017).

More comprehensive studies are required to understand exactly how the activity of different Cdk-Cyclin complexes regulate each phase on the centriole cycle and characterise the molecular events responsible for licensing centriole duplication and preventing its reduplication in S and G2 phases.

1.2.4 Centrosome reduction in animal gametogenesis and its inheritance in embryos

Theodor Boveri first proposed in the 1890's, based on his observations of the centrosome cycle in fertilised eggs of sea urchins and nematodes, that only the paternal (sperm) centrosome gives rise to a functional MTOC in animal embryos. This uniparental centrosome inheritance requires centrioles to be maintained during spermatogenesis and their elimination from the maternal oocyte before the first embryonic division (Hoyer-fender, 2012; Manandhar et al., 2005; Pimenta-Marques et al., 2016).

In most animal species, the sperm retains some kind of centriolar structure which, after fertilisation, recruits PCM from the female oocyte, restoring its MTOC activity. This hybrid centrosome can then enter the canonical duplication cycle, giving rise to two centrosomes and forming a bipolar spindle (Manandhar et al., 2005). Such complementation strategy ensures the proper number of centrosomes at the time of the first embryonic division, since the excess or limited centrosome number causes fertilisation failures or developmental abnormalities (Kemp et al., 2004; Pimenta-Marques et al., 2016; Terada et al., 2010). Moreover, this process also

reinforces sexual reproduction, so that fertilisation occurs every generation, thereby creating random combinations from genetically diverse sperm and eggs, increasing species' genetic variation and their chances of survival.

In animals that naturally develop by parthenogenesis, without sperm contribution, centrosomes are lost during oogenesis but are assembled *de novo* in the embryo. This is also the case in mice, where both female and male germ cells lack centrioles (Courtois et al., 2012; Gueth-Hallonet et al., 1993; Schatten et al., 1985).

Centrosome reduction in the sperm

During male and female gametogenesis, centrioles undergo partial or complete degeneration, respectively. Centrosome inactivation during spermiogenesis consist on the attenuation of its MT nucleation function by the loss of pericentriolar material and some centriolar components (Avidor-Reiss, 2018; Khire et al., 2015; Khire et al., 2016; Schatten and Stearns, 2015). Therefore, each post-meiotic sperm-cell has only a minimum set of centrosomal proteins and two more-or-less structurally normal centrioles, the proximal and the distal, needed to accomplish fertilisation. The extent at which the centrosomal components are reduced and centrioles themselves degenerate in the sperm varies depending on the species (Avidor-reiss, 2018; Hoyer-Fender, 2012). In several mammalian species and in insects, one centriole presents a typical morphology while the other degenerates, forming an atypical centriole with modified ultrastructure. However, despite their differences, after fertilisation both typical and atypical centrioles recruit maternal PCM and form functional zygotic centrosomes that establish the first bipolar spindle (Avidor-Reiss, 2018; Hoyer-Fender, 2012).

While in most mammals, the atypical centriole is the distal one, in insects it is the opposite, therefore the *Drosophila* sperm contains a morphologically normal, distal centriole (named the giant centriole – GC) and, a highly altered, proximal centriole-like (PCL) structure (Blachon et al., 2009; Khire et al., 2016). During fly spermatogenesis, most PCM components are lost from the spermatozoa, among which γ -tubulin, Cnn, Spd2 and Asl, but the sperm retains Ana1, Poc1, Sas6 and Bld10 (Blachon et al., 2009; Khire et al., 2016; Riparbelli et al., 1997). Some stick insect species (Baccetyi and Dallai, 1978) and rodents (Manandhar et al., 1998; Woolley and Fawcett, 1973) lose both centrioles during spermatogenesis and the zygotic centrosomes are established from maternal components.

Centriole elimination in the oocyte

During female oogenesis, the centrioles completely degenerate and the PCM components become dispersed. Centrosome elimination takes place at different stages in oogenesis in different organisms. In *M. musculus*, *D. melanogaster*, *Xenopus*, humans and *C. elegans*, centrosomes are eliminated before the first meiosis and, consequently, the spindle poles during meiotic I and II divisions are acentriolar and anastral (Hertig and Adams, 1967; Manandhar et al., 2005; Mikeladze-Dvali et al., 2012; Sköld et al., 2015; Theurkauf et al., 1993). On the other hand, in some echinoderm and mollusc species, centriole elimination happens during or after meiotic divisions. In the star fish oocyte, centriole elimination occurs throughout meiotic divisions, by selective extrusion of the two mother centrioles in the first and in the second polar bodies (Borrego-Pinto et al., 2016).

Recently, a study by Pimenta-Marques et al. (2016) has revealed the molecular program underlying centrosome elimination in *D. melanogaster* and shown the biological consequences of retaining centrioles in the eggs. In wild-type female flies, Polo/Plk1 is downregulated and displaced from the oocyte centrosomes during oogenesis. This Polo de-localisation, causes a timely decay of PCM components at the centrosomes and, in the absence of these components, the centrioles become unstable and are eliminated before meiosis. Ectopic Polo expression and anchoring to the centrioles retains the PCM components at the centrioles and stabilises them during oogenesis. The ectopic presence of active centrosomes causes abnormal meiotic divisions in the egg, mitotic defects after fertilisation and embryonic lethality (Pimenta-Marques et al., 2016).

In *C. elegans*, germline centrosomes also undergo a similar degeneration process, whereby they progressively lose PCM, centriolar proteins and consequently MTOC activity. Interestingly, MTOC capacity is lost even before all PCM components are delocalised. Centrioles are eliminated during prophase of meiosis I (Mikeladze-Dvali et al., 2012).

These studies in *Drosophila* and *C. elegans* indicate that one possible pathway through which centrioles are eliminated during animal oogenesis is by shutting down MTOC activity by first delocalising some PCM components from the centrosomes causing the centrioles to be less stable and to degenerate, possibly going through intermediate centriolar structures without MTOC capacity, until they are finally eliminated.

1.3 Polo-like kinase 4 (Plk4) is a master regulator of centriole biogenesis

1.3.1 Plk4, the odd one out in the Plk family

Polo-like kinase 4 (Plk4) or Sak (from Snk-akin kinase) was first identified in mouse cells as a serine/threonine kinase, sharing homology with the *Drosophila* Polo, the *S. cerevisiae* Cdc5 and mouse Snk/Plk2, a group of proteins with a role in cell-cycle progression (Fode et al., 1994). Plk4 is the most divergent member of the Plk family and probably resulted from gene duplication and subsequent sub-functionalization from an ancestral Plk1-like gene, before the divergence of fungi and animals. Plk4 has direct homologues in most animals studied so far, except in *C. elegans*, where centriole biogenesis is regulated by the functional homologue Zyg1 (Delattre et al., 2006; O'Connell et al., 2001; Pelletier et al., 2006).

Plk4 is the master regulator of centriole duplication in *Drosophila* and vertebrate cells (Bettencourt-Dias et al., 2005; Habedanck et al., 2005; Kleylein-Sohn et al., 2007). Plk4 depletion prevents centriole formation whereas its overexpression triggers centriole amplification or *de novo* centrosome formation in the absence of centrioles, in unfertilised fly eggs (Rodrigues-Martins et al., 2007). In activated *Xenopus* eggs, Plk4 upregulation drives the assembly of acentriolar MTOCs (Eckerdt et al., 2011; Montenegro Gouveia et al., 2018). In mice, Plk4 is required for acentriolar MTOC formation, both in oocytes (together with AurA) and during early embryonic divisions, but it does not drive *de novo* centriole formation in eggs or in early embryos (Bury et al., 2017; Coelho et al., 2013). Increased levels of Plk4 have been detected in several human cancers and are related

with poor prognosis, stimulating interest in Plk4 both as a tumour prognosis marker and therapeutic target (Denu et al., 2016; Kazazian et al., 2017; Ko et al., 2005; Liao et al., 2019; Maniswami et al., 2018; Marina and Saavedra, 2014). Therefore, the regulation of active Plk4 levels in cells is critical to preserve a correct centriole number and, consequently, a normal cell-cycle and cell function.

1.3.2 Plk4 structure

All members of the Polo-like kinase family (Plk1-5, in humans) have a similar architecture: they possess an N-terminal serine/threonine catalytic domain and a C-terminal Polo box domain (PBD) composed of two or three Polo boxes (PB) (Jana et al., 2012; Park et al., 2010; Zitouni et al., 2014). Except for Plk5 that contains a truncated pseudokinase domain (de Cárcer et al., 2011), Plk1-4 share a Glycine-rich ATP-binding domain, consisting of a GxGxFA motif, within the catalytic region (Fode et al., 1994; Yamashita et al., 2001). Pairwise sequence analysis of the catalytic domain from the human Plk1-4, clusters Plk2 and 3 together and these with Plk1, whereas Plk4 has the lowest sequence homology (Johnson et al., 2007).

The PBD mediates substrate interaction and kinase targeting to specific subcellular locations (Archambault and Glover, 2009; Lee et al., 1998; Lee et al., 2008; Park et al., 2010; Swallow et al., 2005). Functional studies replacing Plk1-PBD with the PBD from Plk2,3 and 4, partially rescued Plk1 functions in bipolar spindle formation, centrosome maturation and substrate binding, in Plk1-depleted human cells. However, from all hybrid proteins, the PBD from Plk2 provided the most effective rescue, whereas complementation was least efficient with the Plk4 PBD domains (van de Weerd et al.,

2008). Plk1,2,3 and 5 have two structurally similar PB domains called PB1 and PB2, which in Plk1-3 recognize phosphorylated substrates (Elia et al., 2003b). In Plk1, the two PBs also promote homodimerisation (Elia et al., 2003b), which is important for the regulation of its kinase activity (Elia et al., 2003a; Elia et al., 2003b).

Plk4 has three Polo-Box (PB) domains: PB1 and PB2 are organised in tandem forming the previously known 'cryptic' PB (CPB) and PB3 is located at C-terminus and exhibits low homology with PB1 or PB2 (Figure 1.11A) (Leung et al., 2002; Sillibourne and Bornens, 2010; Slevin et al., 2012). The crystal structure of the *Drosophila* CPB revealed that the PB1 and PB2 individually resemble Plk1 PBs but lack a flexible linker between them. As a consequence, the CPB cannot fold within itself, adopting a more rigid conformation. The CPB forms stable homodimers in solution and one conformation adopted is an intermolecular dimer where PB1 and PB2 interact side-by-side (Figure 1.11 B and C) (Slevin et al., 2012).

More recently, a new dimerisation model was proposed for Plk4, whereby the two PBs in the CPB orient end-to-end, interacting by their PB2 domains. The two PB1 do not directly interact with each other but instead, they face opposite sides of the dimer (Figure 1.11 D and E) (Shimanovskaya et al., 2014). This X-shape conformation is also adopted by *C. elegans* Zyg1 CPB, but structural changes in the CPB between flies and worms, confers Plk4 and Zyg1 proteins different substrate specificity. Whereas the *Drosophila* Plk4 CPB can bind both Asl and Spd2 with similar affinity, the Zyg1 CPB is very specific in binding Spd2. Such protein conformation likely explains the differential mode of recruitment and docking to the centrosomes between Plk4 and Zyg1 (Shimanovskaya et al., 2014). The PB1-PB2 cassette is required for robust centriole targeting (via Asl/Cep152

binding in flies), homodimerisation and substrate interaction through phospho-independent binding (Shimanovskaya et al., 2014; Slevin et al., 2012).

The PB3 also promotes Plk4 dimerisation independently of the CPB domain and potentially mediates inter-dimer association, forming higher order molecular scaffolds (Jana et al., 2012). Even though the PB3 is not critical for centrosome targeting, it plays an important role in regulating Plk4 activity. Similarly to other Plks, Plk4 possesses an autoinhibitory mechanism mediated by its *cis*-acting L1 linker. Plk4 autoinhibition is relieved after PB3 homodimerisation and autophosphorylation of residues within L1 (Klebba et al., 2015b). According to the model, newly synthesized Plk4 is autoinhibited by L1 interaction with the activation loop (T-Loop), located in the kinase domain. Plk4 first dimerises through its PB1-PB2 cassette. Next, the PB3 relieves the kinase autoinhibition by interfering with the L1-kinase positioning. This releases the kinase domain, allowing Plk4 to phosphorylate domains important for its full activation and for substrate interaction. This autoinhibition and relief mechanism provide a temporal regulation of Plk4 oligomerisation, activity and, ultimately, its stability. Plk4 stability is governed by PEST sequences, rich in proline (P), aspartate (D), glutamate (E), serine (S) and threonine (T) residues. The first PEST sequence is located at N-terminus, right after the catalytic domain and it is conserved in many species. Human and mouse Plk4 have two additional PEST sequences at C-terminus, but these are less important for protein turn-over (Sillibourne and Bornens, 2010; Yamashita et al., 2001).

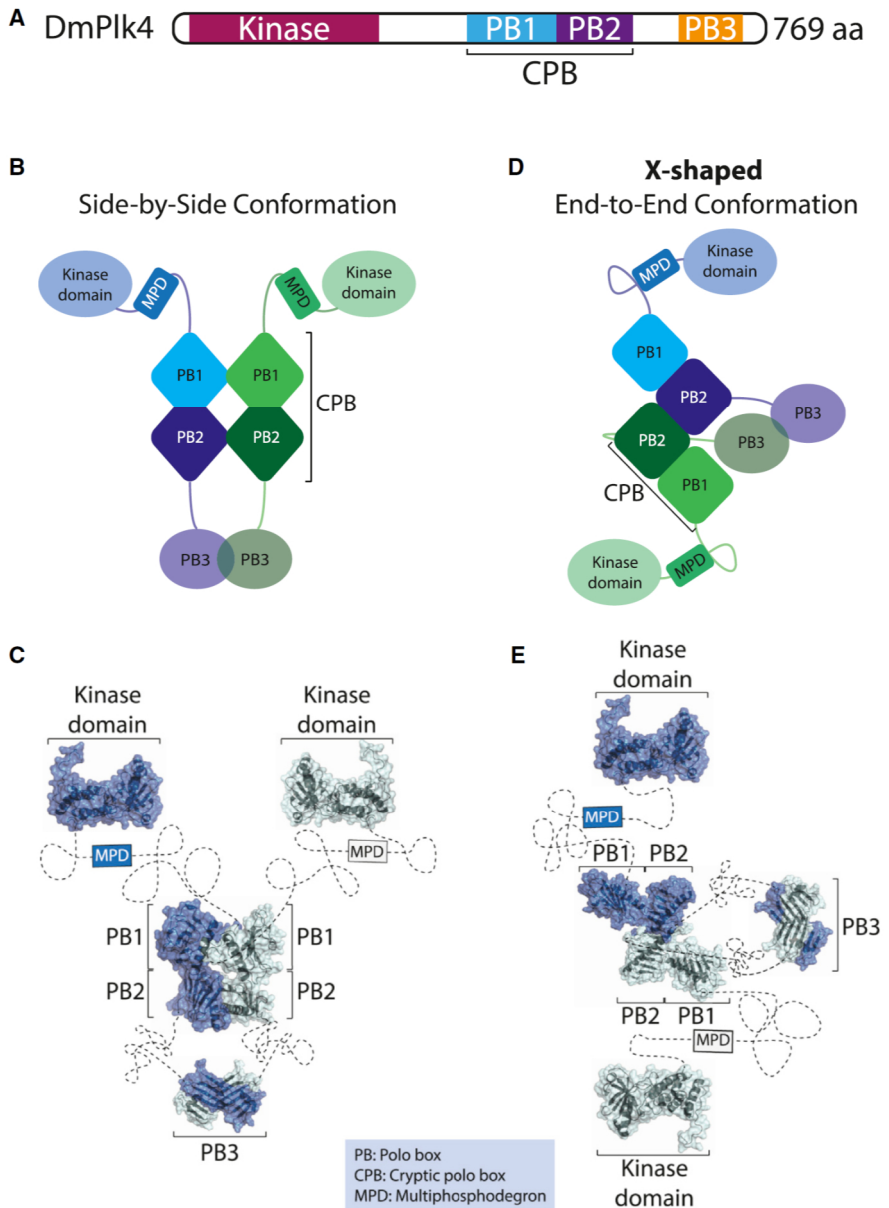


Figure 1.11 – Structure of the *Drosophila* Plk4 (dmPlk4) and two different models proposing its dimerisation. A) Schematic representation of the structural domains composing *Drosophila* Plk4. The kinase domain is located at its N-terminus while the Cryptic polo box (CPB), including Polo-box (PB) 1 and 2 in tandem, followed by the Polo-box 3 domain are present at C-terminus. **B and C)** Schematic representations

and respective crystal structures (**C and E**) of dmPlk4 dimerisation mediated by the CPB domains. **B and C**) Proposes a side-by-side Plk4 interaction mediated by both the PB1 and PB2 within the CPB domains (Slevin et al. 2012). **D and E**) Proposes the assembly of homodimers in an X-shaped configuration, whereby the two Plk4 molecules interact only through their PB2 domains (Shimanovskaya et al. 2014). Adapted from (Levine and Holland, 2014).

1.3.3 Plk4 regulation

Plk4 transcription and translation

Most aspects of Plk4 stability and activity rely on its autoregulation. The coupling between these self-regulatory mechanisms and the cell-cycle are not yet fully understood.

PLK4 is expressed and localised at the centrosomes in a cell-cycle-dependent manner. In murine and *Drosophila* S2 cells, Plk4 is expressed at low levels in the beginning of the cell-cycle and peaks during mitosis (Cunha-Ferreira et al., 2009; Fode et al., 1996; Rogers et al., 2009; Winkles and Alberts, 2005). Similarly, active Plk4 first localises at the mother centriole in early S-phase and increases through interphase, reaching a maximum during mitosis in human cells (Sillibourne et al., 2010). In mouse cells, *Plk4* transcription is positively regulated by NRF1 and CRE sites in the gene promoter region. Plk4 expression is downregulated by binding of the p53-DREAM (DB, Rb-like, E2F4 and MuvB) complex to the gene promoter in G0 and G1 phases. In G2 and mitosis, Plk4 downregulation is achieved by the MMB (Myb-MuvB) complex. Cell-cycle and p53-dependent Plk4 repression is abolished by the human papillomavirus (HPV) E7 oncoprotein, which disrupts the binding of those inhibitory complexes to the Plk4 promoter (Fischer et al.,

2014). Recently, it was shown that the 5'UTR plays an important role in regulating Plk4 transcriptional levels by giving rise to differently stable transcripts (Holland 2017, personal communication).

Plk4 activation

Plk4 full activation is accomplished by *trans*-autophosphorylation of a critical threonine residue within the T-loop in the catalytic domain (Lopes et al., 2015). Mutants where the threonine residue is replaced by a non-phosphorylated alanine residue have very low catalytic activity compared to the wild-type protein. This Plk4 mutant is incapable of driving centriole biogenesis even though it is recruited to the centrosomes, demonstrating that full kinase activity is required for centriole assembly. Since autophosphorylation takes place in *trans*, Plk4 activation depends on its local concentration and oligomerisation. The centrosome provides the primary platform for Plk4 concentration and activation in cells. When centrosomes are depleted from *Drosophila* S2 cells, auto-phosphorylation of wild-type Plk4 on its T-loop is undetectable. Ectopic targeting of the protein to a different organelle is enough to concentrate Plk4 and activate it in a concentration-dependent manner. Finally, this study also shows that the expression of high Plk4 levels drives both centriolar and acentriolar (cytoplasmic) biogenesis within the same cell, but these dynamics were not characterised, therefore it was not possible to conclude about the interplay between these biogenesis pathways (Lopes et al., 2015). It is unclear what regulates Plk4 basal activity, before its T-loop dependent full activation. Possibly, other centrosomal components, acting upstream of Plk4, play a role in that process.

The cell-cycle dependent, Plk4-Stil binding, promotes Plk4 self-phosphorylation in the activation loop, contributing to the

temporal regulation of Plk4 activation (Moyer et al., 2015; Zitouni et al., 2016). Recently, a study identified Cep85 as a centriole duplication factor that directly interacts with the N-terminal domain of Stil. This interaction is not only important for Stil centrosomal localisation but also impacts Plk4 activity. Cep85 mutants that do not bind Stil, fail to localise it at the centrosome and show altered Plk4 phosphorylation. This study proposes that Cep85-mediated Stil recruitment to the centrosome facilitates Plk4 activation and centriole duplication (Liu et al., 2018).

Plk4 degradation

Spatial and temporal regulation of Plk4 kinase activity is critical for limiting centrosome duplication to once per cell-cycle and controlling centriole number in cells. In mouse cells, Plk4 half-life was determined to be around 2-3 hours and the protein was found to be multi-ubiquitinated, suggesting that it could be targeted for rapid degradation by the 26S proteasome (Fode et al., 1996). Numerous studies have demonstrated that, indeed, the SKP1-CUL1-F-Box (SCF) Slimb/ β TrCP-E3 ubiquitin ligase complex regulates Plk4 levels and centriole number in cells (Cunha-Ferreira et al., 2009; Guderian et al., 2010; Holland et al., 2010; Holland et al., 2012; Rogers et al., 2009). In *D. melanogaster*, the SCF-E3 ubiquitin-ligase complex physically interacts with Plk4 through the F-box protein Slimb (Cunha-Ferreira et al., 2009; Rogers et al., 2009). This interaction mediates Plk4 ubiquitination by the E3 ubiquitin-ligase and promotes proteolytic degradation. Slimb RNAi-mediated depletion or mutations in the consensus Slimb recognition degron on Plk4 render this kinase non-degradable, leading to Plk4 accumulation at the centrosome and causing centriole

overduplication (Cunha-Ferreira et al., 2009; Cunha-Ferreira et al., 2013; Rogers et al., 2009).

The regulatory function of the SCF-E3 ubiquitin ligase complex is conserved in vertebrates and in *C. elegans*. In mice and human cells, the Slimb homologue β TrCP also regulates Plk4 levels and centriole number (Guardavaccaro et al., 2003; Guderian et al., 2010; Holland et al., 2010). However, contrary to flies, mutations in the Plk4 β TrCP destruction motif cause a minor effect on the stability of the mouse Plk4. Instead, the phosphorylation of multiple sites around the N-terminal PEST domain, are required to efficiently drive Plk4 destruction and regulate its stability in these cells (Holland et al., 2010). In *C. elegans*, Zyg1 levels are regulated by the Slimb/ β TrCP-E3 homolog LIN-23. In addition, a second F-box protein called SEL-10 also cooperates with LIN-23 to promote Zyg1 proteasomal degradation (Peel et al., 2012). Plk4 catalytic activity is required to trigger its own SCF Slimb/ β TrCP-E3 –mediated degradation (Guderian et al., 2010; Holland et al., 2010). Plk4 kinase-dead (KD) mutants are more stable than the wild-type protein, since their interaction with the SCF Slimb/ β TrCP-E3 is compromised (Guderian et al., 2010; Holland et al., 2010). Remarkably, overexpression of Plk4-KD in cells causes centriole overduplication only in the presence of the endogenous wild-type copies. This indicates that Plk4 oligomerises and self-phosphorylates in *trans* (Cunha-Ferreira et al., 2013; Guderian et al., 2010; Holland et al., 2010; Klebba et al., 2013). Timely, multi-site Plk4 trans-autophosphorylation within the phosphodegron and in a second phospho-cluster outside the degron, ensure that only after a certain threshold of Plk4 activity, the protein is targeted for proteasomal degradation. This feedback loop, self-orchestrated by Plk4 without any additional kinase, is fundamental to limit its own activity and prevent centriole overduplication (Cunha-

Ferreira et al., 2013; Guderian et al., 2010; Holland et al., 2012; Klebba et al., 2013).

Even though Slimb plays a major role in Plk4 stability, it localises at the centrosome throughout the entire cell-cycle, potentially driving continuous Plk4 degradation (Rogers et al., 2009). This suggests that another regulatory network is important for the cell-cycle control of Plk4 activity and stability. In *Drosophila* and *C. elegans*, it has been shown that the phosphatase PP2A stabilises Plk4/Zyg1, protecting it from degradation (Brownlee et al., 2011; Song et al., 2011). In flies, Twins, a PP2A regulatory subunit, associates with PP2A in a cell-cycle dependent manner, counteracting Plk4 autophosphorylation. This process leads to the stabilisation of Plk4 levels in late mitosis, when the kinase presumably exerts its priming role in centriole biogenesis (Brownlee et al., 2011), via its interaction with Stil. In *C. elegans* embryos, PP2A binding to its regulatory subunit SUR-6 regulates Zyg1 and Sas5 levels, positively regulating centriole biogenesis (Song et al., 2011).

1.3.4 Plk4 centrosomal recruitment

As previously mentioned, Plk4 recruitment to the centrosome relies on Cep152, Cep192 and Cep63 in human cells (Brown et al., 2013; Sonnen et al., 2013), whereas in flies and in the worm it is mostly recruited by Asl or Spd2, respectively (Cizmecioglu et al., 2010; Dzhindzhev et al., 2010; Pelletier et al., 2006). Depletion of those proteins prevents normal centriole duplication and centrosomal localisation of pro-centriole components. In humans, the N-terminal regions of Cep192 and Cep152 interact with the PB1-PB2 cassette (or 'crypto'-Polo-box) of Plk4 (Hatch et al., 2010; Sonnen et al., 2013). In addition, Cep192 and Cep152 also interact

with each other through a centriolar binding region, cooperating in the same redundant pathway where Cep192 plays the strongest role (Sonnen et al., 2013). Cep152 interacts with Cep63 independently of centrosomal localisation, but they both rely on each other for their centrosomal recruitment. In *Drosophila*, Asl/Cep152 also interacts through its N-terminus with the Plk4 CPB domain (Cizmecioglu et al., 2010; Dzhindzhev et al., 2010). Asl depletion prevents centriole duplication while its overexpression causes centriole overduplication in cells and embryos and *de novo* centriole formation in unfertilised eggs (Dzhindzhev et al., 2010).

1.3.5 Plk4 substrates and downstream effectors

Plk4 has been reported to phosphorylate several centrosomal proteins. Yet, in most cases, the functional consequences of those phosphorylations are still poorly understood. On the contrary, Stil/Ana2 is one of the best-studied Plk4 substrates, and its interaction is critical for recruiting Sas6 and initiating procentriole assembly (Cottee et al., 2015; Dzhindzhev et al., 2014; Dzhindzhev et al., 2017; Kratz et al., 2015; Mclamarrah et al., 2018; Moyer et al., 2015). Plk4 binds Stil/Ana2 and phosphorylates conserved residues within its STil/ANa2 (STAN) motif. This phosphorylation allows Ana2 to bind and recruit Sas6 to the centrosomes where it assembles the cartwheel. Mutations in Ana2 STAN motif abolish its interaction with Sas6 and, as a result, centriole biogenesis is impaired. Ana2 centriolar localisation is independent of Plk4 phosphorylation and of Sas6 (Arquint and Nigg, 2016; Arquint et al., 2015; Dzhindzhev et al., 2014; Kratz et al., 2015; Moyer et al., 2015; Ohta et al., 2014; Zitouni et al., 2016). Stil/Ana2 interacts via its central coiled coil domain (CC) with Plk4 PB3 and L1 linker (Arquint et al., 2015;

Mclamarrah et al., 2018). This interaction possibly relieves Plk4 autoinhibition by promoting a conformational change that drives the L1 linker and the activation T-loop apart (Klebba et al., 2015b). According to this elegant model, Stil-Plk4 interaction provides a spatial and temporal regulation of Plk4 basal activation. Additionally, Stil/Ana2/Sas5 oligomerises through its CC domain, therefore its removal disrupts Stil centriolar localisation and centriole duplication.

Recent studies have uncovered fine aspects behind the Stil-Plk4 interaction, whereby a two-step Plk4 phosphorylation of Stil locally restricts Plk4 activity at the mother centriole and triggers sequential recruitment of Stil/Ana2 and Sas6. In early G1 before procentriole assembly, Plk4 localises to the mother centriole in a ring-shape manner. At G1/S, the Plk4 ring converts into a single spot where the new procentriole forms (Kim et al., 2013; Ohta et al., 2014; Ohta et al., 2018). This transition is presumably driven by transient Stil/Ana2 binding to Plk4 on a different site than the CC, which promotes Plk4 'hyperactivation' causing extensive autophosphorylation and degradation. Plk4 is removed from the centrosome except at the site where Stil/Ana2 stabilises Plk4 through its CC binding (Ohta et al., 2018). Plk4 first phosphorylates Stil/Ana2 at its N-terminus in a conserved region, promoting Stil/Ana2 recruitment. Then, the second phosphorylation in the STAN motif enables stable Stil/Ana2 to recruit Sas6 onto the single Plk4 location dot (Dzhindzhev et al., 2017; Mclamarrah et al., 2018). The transition in Plk4 centriolar localisation from a ring to a single dot is involved in controlling the number of procentrioles that form per mother each cell-cycle, since disruption of Plk4 degradation gives rise to stable Plk4 rings that recruit multiple Stil foci. In *C elegans*, the Plk4/Zyg1-Sas5-Sas6 core module is differently regulated. Zyg1 interacts directly and phosphorylates Sas6 and the

formation of the Sas5-Sas6 complex is Zyg1-independent (Kitagawa et al., 2009; Leidel et al., 2005).

Plk4 binds to and phosphorylates Bld10/Cep135 (Galletta et al., 2016). This phosphorylation likely causes a conformational change in Bld10 that exposes its N-terminal region, allowing it to interact with Asl C-terminus. Bld10-Asl interaction is important for Asl centriolar localisation in *Drosophila* spermatocytes. Plk4 also binds and phosphorylates Asl, establishing a feedback-loop whereby Asl regulates Plk4 activity at the centrosome according to its phosphorylation state (Boese et al., 2018). Non-phosphorylated Asl binds Plk4 and stimulates its kinase activity, relieving Plk4 autoinhibition. Active Plk4 phosphorylates Asl, generating a negative-feedback whereby the hyperphosphorylated Asl inhibits Plk4 catalytic activity, temporally limiting centriole biogenesis (Boese et al., 2018).

Plk4 phosphorylates additional substrates in specific organisms. In mammalian cells, Plk4 phosphorylates CP110, a known regulator of centriole length. Plk4-mediated CP110 phosphorylation is important for centriole assembly, but the mechanism is still unknown (Lee et al., 2017b). Human Plk4 phosphorylates GCP6, one of the γ -TuRC components. This interaction impacts mitotic spindle formation and Plk4-induced centriole overduplication (Bahtz et al., 2012). SCF-FBXW5, an E3 ubiquitin ligase, degrades Sas6 in a cell-cycle dependent way, preventing centriole reduplication. Human Plk4 phosphorylates SCF-FBXW5, negatively regulating its activity, thus abolishing Sas6 ubiquitination in defined cell-cycle stages (Puklowski et al., 2011).

1.4 Non-canonical pathways of centriole biogenesis

This Chapter is adapted from:

Nabais C, Gomes Pereira S, Bettencourt-Dias M (2018) Noncanonical Biogenesis of Centrioles and Basal Bodies. *Cold Spring Harbor Symposia on Quantitative Biology* pii: 034694.

Cells can assemble CBBs via non-canonical pathways. These are widespread in nature but little is known in terms of their regulation and origin. They can be classified into two categories: deuterosome-mediated biogenesis, when centrioles form in bulk in the presence of resident centrioles, and *de novo*, strictly referring to biogenesis without any previously existing centrioles in the cell/organism. There are multiple *de novo* strategies, depending on the organism, cell-type and number of centrioles that are formed.

CBBs have been lost within plant, fungi and amoebae lineages or reduced to particular tissues or life-cycle stages in other eukaryotic lineages, in some cases even acquiring new morphologies. For instance, in plants, CBBs are only present in species that form motile sperm and somehow depend on a moist environment for fertilisation to take place. Some gymnosperms (Pinaceae and Gnetales) and all angiosperms (Magnoliophyta) no longer have motile cilia and fertilisation depends on a pollen tube with immotile sperm cells. Even in plants that form cilia, the CBB is restricted to sperm cells, forming *de novo* during spermatogenesis and giving rise to either biflagellated or multiflagellated sperm.

1.4.1 Diversity in modes of centriole biogenesis across eukaryotes

1.4.1.1 Deuterosome-mediated centriole biogenesis

Post-mitotic cells containing two resident centrioles can differentiate into multiciliated cells (MCCs), assembling numerous CBBs through the deuterosome-mediated pathway (Meunier and Azimzadeh, 2016). Vertebrates have many multiciliated tissues - the respiratory tract, the oviduct, skin, efferent ducts and the brain ependymal – which are all composed of MCCs. Over recent years, the molecular characterisation of multiciliogenesis in vertebrate MCCs has demonstrated that deuterosome-mediated and canonical biogenesis share part of their molecular cascade (Azimzadeh et al., 2012; Klos Dehring et al., 2013; Mori et al., 2017; Vladar and Stearns, 2007; Zhao et al., 2013). A similar biogenesis pathway might also contribute to the formation of multiciliated sperm in some invertebrates, such as in molluscs (*C. malleata* [Gall 1961]) and the insect *M. termites* (Baccetyi and Dallai, 1978; Riparbelli et al., 2009), but so far there are no molecular evidences supporting that.

In MCCs, centriole biogenesis takes place around pre-existing centrioles but it also requires specialised structures (deuterosomes) to efficiently assemble a large number of CBBs. Several EM studies have described the formation of electron-dense granules ('fibrogranular material') in the cytosol; usually in the apical cell region and in the vicinity of resident centrioles, as early CBBs precursors (Figure 1.12 A and E) (Dirksen, 1971; Hagiwara et al., 2004; Kalnins and Porter, 1969; Sorokin, 1968; Steinman, 1968; Vladar and Stearns, 2007) . Over time, these granules increase their size and condense into deuterosomes, large electron dense bodies without a discernible structure, suggesting they consist of highly

concentrated proteins (Figure 1.12 B, C and F). Frequently, Golgi cisternae, small vesicles and microtubules are detected in the vicinity of the deuterosomes (Dirksen, 1971; Kalnins and Porter, 1969; Sorokin, 1968; Vladar and Stearns, 2007), raising the possibility that these organelles might contribute to deuterosome formation and pro-centriole biogenesis. The Golgi has MTOC capacity, while vesicle transport along MTs, possibly supplies the deuterosome with centrosomal precursors. Resident centrioles may contribute with activating enzymes, including Plk4, which catalyse centriole biogenesis from the centriolar precursors. Multiple pro-centrioles assemble simultaneously from each deuterosome. In most tissues, pro-centrioles form both around the amorphous deuterosome (acentriolar-mediated) and the pre-existing centrioles (centriolar-mediated) (Figure 1.12 C, F and G) (Al Jord et al., 2014; Anderson and Brenner, 1971; Hagiwara et al., 2004; Sorokin, 1968). During ependymal MCC differentiation, deuterosomes arise at the wall of the (pre-existing) daughter centriole (Al Jord et al., 2014). Nonetheless, in all tissues, most of the centrioles (70-90%) are generated via deuterosomes rather than directly from centrosomal centrioles. The specific centriole amplification mechanism used by different MCCs, may depend on the number of cilia they produce (Meunier and Azimzadeh, 2016).

Downregulation of the Notch signaling pathway initiates the multiciliogenesis program in vertebrate MCCs precursor cells. Then, MCCs activate a molecular cascade, mediated by the Geminin C1-Multicilin-E2f4/5 complex which triggers cell-cycle exit, cytoskeleton remodeling and upregulation of several centriole biogenesis components, including Cep152, Plk4, Cpap, Sas6, Stil and Centrin (Arbi et al., 2017; Hoh et al., 2012; Mori et al., 2017; Vladar and

Stearns, 2007; Zhao et al., 2013). These proteins are usually at very low abundance in cycling cells, limiting the number of centrioles that can form. MCCs also express deuterosome-specific components; Deup1 (a paralog of Cep63) and Ccdc78, which localise at the centre of the deuterosome (Klos Dehring et al., 2013; Zhao et al., 2013). Deup1 binds Cep152, recruiting Plk4 (Al Jord et al., 2014; Mori et al., 2017; Zhao et al., 2013). As MCCs start differentiating, E2f4 moves from the nucleus to the cytosol, where it interacts with Deup1 (Mori et al., 2017). Cep152, Plk4 and Centrin are subsequently enriched at the deuterosome and at the resident centrioles, seeding the biogenesis of multiple CBBs.

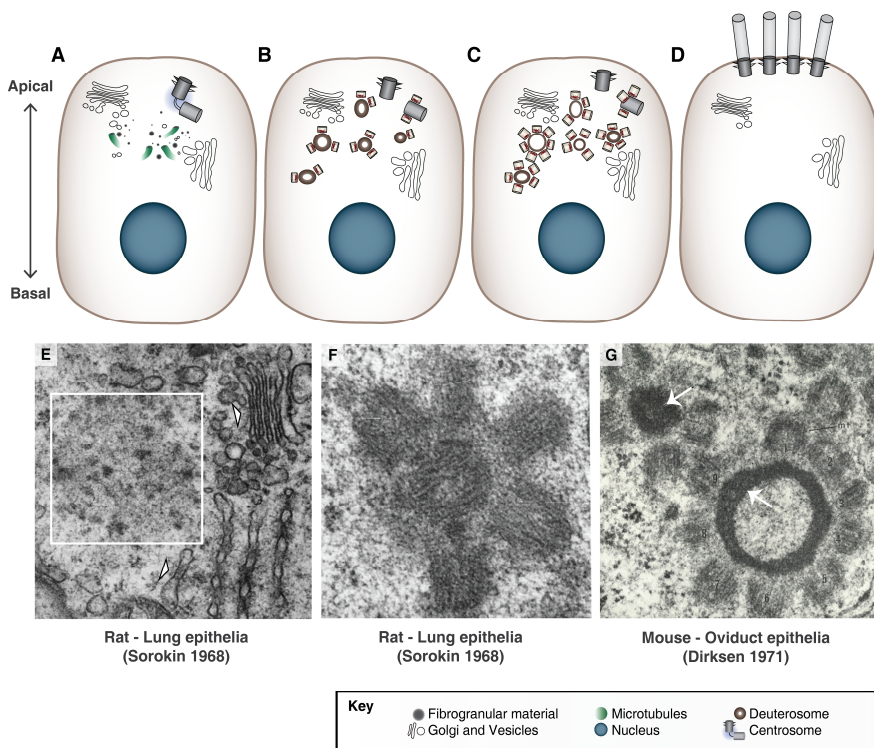


Figure 1.12 – Deuterosome-mediated biogenesis in vertebrate multiciliated cells (MCCs). Multiciliogenesis starts with the formation of electron-dense ‘fibrogranular material’ ((A) and depicted within the white

square in the EM micrograph (**E**) in the cytosol, close to pre-existing centrioles. This dense material is usually enriched with microtubules (MTs), Golgi cisternae and vesicles (**A**, **E** - arrowheads). The 'fibrogranular material' condenses and deuterosomes – electron-dense hollow spheres– are formed (**B**, **G** – arrows). A recent study in ependymal cells demonstrated that the resident daughter centriole is capable of generating multiple deuterosomes, which detach from its wall and give rise to many pro-centrioles (**B**, **C** and **G**) (Al Jord et al. 2014). Additionally, pro-centrioles assemble directly around the resident centrioles (**C**), as shown in the EM micrograph (**F**). Hundreds of CBBs are formed in the cytosol, which then migrate and dock to the cell membrane assembling hundreds of cilia (**D**). Figures E and F - Adapted from Sorokin 1968, Figure G - Adapted from Dirksen 1971. General figure from (Nabais et al., 2018).

1.4.1.2 De novo centriole biogenesis

Several eukaryotic species assemble centrioles *de novo*, i.e. without centriolar structures present in the cell. However, in most naturally occurring cases, the mechanisms remain poorly understood. Centrioles may arise as single units, as two centrioles coaxially oriented (Bicentriole) or within electron-dense spheres (Blepharoplasts) forming a massive number of CBBs (Miki-Noumura, 1977; Renzaglia and Garbary, 2001; Riparbelli et al., 1998).

De novo via unknown mechanisms

Amoebae to flagellate transition in *Naegleria gruberi* is accompanied by the biogenesis of two centrioles. Since amoebae lack centrosomes and a cytoplasmic MT cytoskeleton, and so far no

basal body precursor was found, it has been proposed that centrioles assemble *de novo* (Dingle and Fulton 1966; Fulton and Dingle 1971). By studying the localisation of Centrin and γ -tubulin during the transition, Fritz-Laylin and colleagues (2016) have shown that only the first centriole assembles *de novo* while the second one appears to duplicate from the first. There is no EM support for the underlying pathway and despite some molecular insights from recent studies (Fritz-Laylin and Fulton, 2016; Fritz-Laylin et al., 2010; Kim et al., 2005; Lee et al., 2015; Suh et al., 2002), the exact cascade is still unknown.

Most cases of *de novo* biogenesis of single centrioles are known to take place in the female germline: in parthenogenetic insect eggs (in *Muscidifurax uniraptor* [Riparbelli et al. 1998], and *Drosophila mercatorum* [Riparbelli and Callaini 2003]) and artificially activated eggs of sea urchin (Dirksen, 1961; Miki-Noumura, 1977) and *Spisula solidissima* (Kuriyama et al., 1986; Palazzo et al., 1992). When development in the oocyte is artificially induced, single centrioles that nucleate tubulin monoasters form *de novo* in the cytoplasm (Figure 1.13) (Miki-Noumura 1977; Palazzo et al. 1992; Riparbelli et al. 1998; Riparbelli and Callaini 2003). In parthenogenetic hemynopteran eggs, multiple MTOCs form along the cortex during meiosis II (Figure 1.13 B). These MTOCs migrate towards the centre of egg, and two of them are captured by the female pronuclei, forming the first mitotic spindle and initiating development (Figure 1.13 C) (Riparbelli et al., 1998; Tram and Sullivan, 2000).

The mouse sperm does not carry any centrioles and it is unable to nucleate MTs after fertilisation (Gueth-Hallonet et al., 1993; Schatten et al., 1985), therefore the first embryonic divisions are acentrosomal (Courtois et al., 2012; Gueth-Hallonet et al., 1993).

Centrioles are only detected by EM from 64-cell stage onwards (Gueth-Hallonet et al., 1993). Throughout the first mitotic divisions, the spindles become progressively more focused and enriched with PCM and centriolar components, such as Centrin, Pericentrin and CP110. Nevertheless, the exact mechanism underlying centriole assembly is still unclear. The most favourable hypothesis is that the gradual concentration of PCM and centriolar components throughout the mitotic cycles surpasses a molecular threshold that enables centriole formation, perhaps based on a phase-transition process, which has been proposed to promote the assembly of diverse non-membrane-bound compartments in cells (Courtois et al., 2012; Hyman et al., 2014).

Though centrioles do not assemble spontaneously in most animal eggs, overexpression of Plk4 is sufficient to drive *de novo* formation of multiple centrioles in the cytoplasm (Peel et al., 2007; Rodrigues-Martins et al., 2007). Centrioles assembled *de novo* seem to be able to replicate through the canonical pathway (Fritz-Laylin et al., 2016; Palazzo et al., 1992; Rodrigues-Martins et al., 2007). Not surprisingly, in *Naegleria*, both CBBs form cilia, highlighting that centrioles formed *de novo* and canonically are equally capable of nucleating cilia without the need to undergo a full cell-cycle to mature.

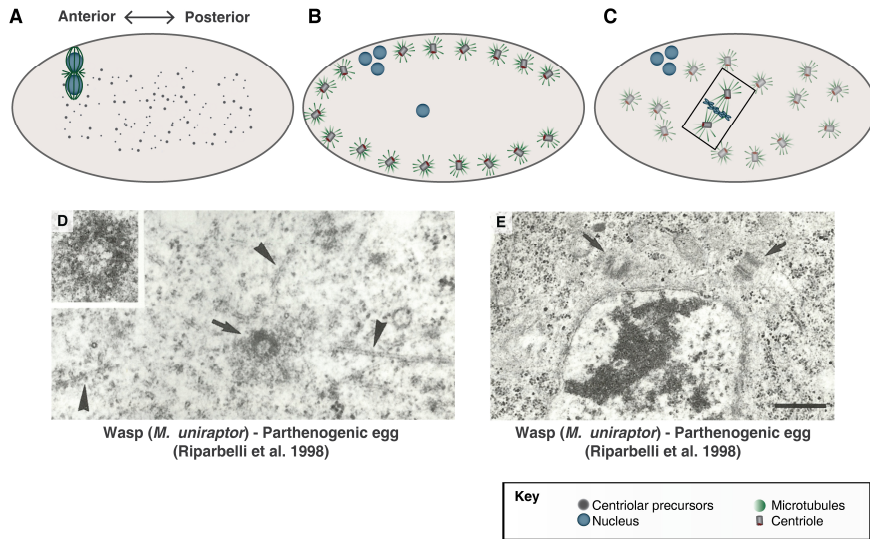


Figure 1.13 - *De novo* centriole biogenesis in parthenogenetic insect eggs. Unfertilized eggs do not have centrioles but contain high levels of centriolar precursors (**A**). Upon egg activation and meiotic resumption, centrioles are formed *de novo* along the cell cortex (**B**). These single centrioles nucleate MT asters. Meiosis is completed and the free centrosomes migrate towards the egg centre (**C**). Two asters interact with the female pro-nucleus, assembling the first mitotic division and triggering embryonic development (C – black rectangle). The remaining centrosomes degenerate (Riparbelli et al. 1998). **D and E**) EM micrographs depict single centrioles (dark arrows) surrounded by microtubules (dark arrowheads) formed *de novo* in the *M. uniraptor* parthenogenetic wasp – adapted from Riparbelli et al. 1998. General figure adapted from (Nabais et al., 2018).

De novo via bicentriole formation

In plants, such as bryophytes, that produce biflagellated sperm and, surprisingly, in the unrelated protist *Labyrinthula spp.*, centrioles form *de novo* through a structure called bicentriole (Moser and Kreitner, 1970; Perkins, 1970; Robbins, 1984). A bicentriole is composed of two centrioles oriented tail-to-tail, aligned along the

same axis and connected by a continuous cartwheel hub, whereas the MT walls between the two centrioles are discontinuous (Figure 1.14 C and F) (Moser and Kreitner, 1970; Robbins, 1984). In land plants, two bicentrioles form simultaneously in the sperm mother-cell. First, an electron-dense body without any recognisable structure is detected close to the outer surface of the nucleus (Figure 1.14 A and B). Very often, microtubules emanate from this structure, suggesting that it has MTOC activity. Next, it separates into two different lobes (pro-bicentrioles) with a lighter central core surrounded by a darker matrix (Figure 1.14 B and F) (Robbins, 1984). Before mitosis, the two pro-bicentrioles separate, migrate towards the poles of the cell and mature into bicentrioles, assembling MT-triplets (Figure 1.14 C and D) (Renzaglia and Duckett, 1987; Robbins, 1984).

To date, there is no molecular information available on bicentriole assembly, except these structures appear to contain γ -tubulin (Shimamura et al., 2004). Only one study, focusing on spermatogenesis in the bryophyte *Riella Americana*, reports the initial stages preceding bicentriole assembly. Early land plants, such as *Marchantia polymorpha*, *Physcomitrella patens* and *Selaginella moellendorffii*, assemble CBBs through the bicentriole pathway and, therefore, are good models to understand this pathway and its regulatory mechanism.

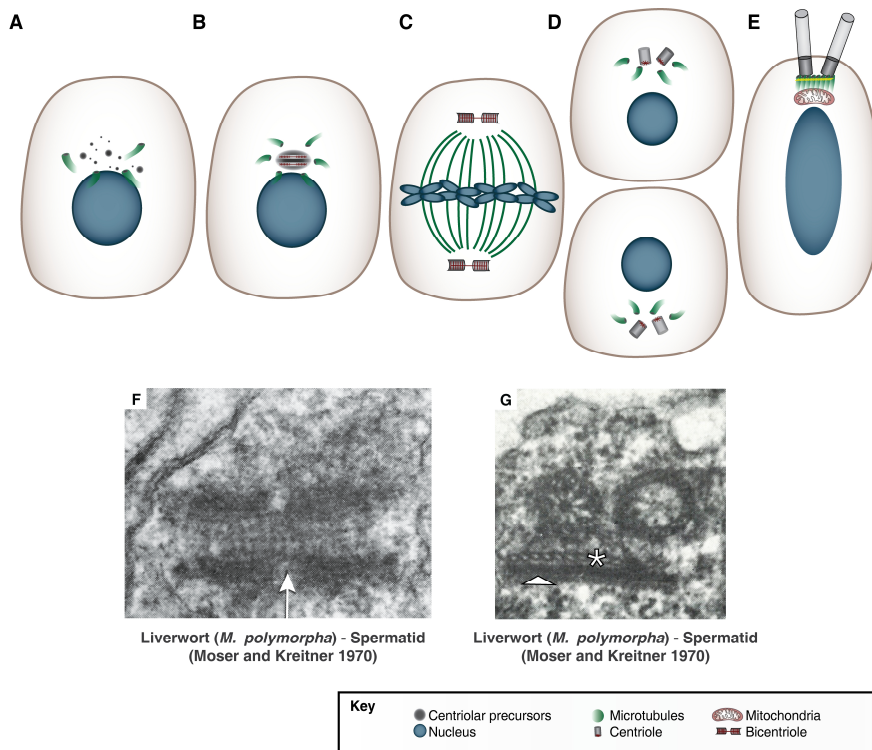


Figure 1.14 – Bicentriole-mediated biogenesis in land plants with biciliated sperm. During spermatogenesis, electron-dense material enriched in microtubules (MTs) is found near the nuclear envelope (**A**). This material assembles into two light lobes, surrounded by a darker matrix (**B**). As mitosis begins, the two lobes separate and migrate towards the poles of the spindle and mature into bicentrioles (**C**). Bicentrioles are composed of two coaxial centrioles connected by their central hub and with discontinuous MT triplets (**F** – white arrow). Each daughter cell (spermatid) inherits one bicentriole that breaks in half and separates into two centrioles (**D**) that will migrate to the edge of the cell and anchor to the multi-layered structure (MLS), serving as basal bodies during ciliogenesis (**E and G**). The MLS is composed of a bundle of parallel MTs – the spline (**G** – asterisk) – and layers of electron-dense material – the lamellar strip (**G** – arrowhead). F and G - Adapted from Moser and Kreitner 1970. General figure from (Nabais et al., 2018).

De novo via blepharoplast formation

In land plants that produce multiciliated sperm such as ferns, cycads and *Ginkgo biloba*, CBBs are formed through blepharoplasts. The blepharoplast arises *de novo* as a spherical electron-dense organelle initially amorphous and, during maturation, it assembles lighter cylinders embedded in an electron-opaque matrix. These cylinders mature into centrioles that later give rise to the basal bodies of numerous cilia (Figure 1.15) (Gifford and Larson, 1980; Hepler, 1976).

In the very early steps of blepharoplast biogenesis two hemispherical, densely stained structures, form near the cell nucleus (Figure 1.15 B and F). Next, cylinders organise within the electron-dense matrix, and MTs emanate from the blepharoplast. The large structures grow and become spherical, giving rise to two blepharoplasts (Figure 1.15 G) (Hepler, 1976; Hoffman and Vaughn, 1995; Mizukami and Gall, 1966). The two blepharoplasts separate and migrate to the spindle poles of the mitotic cell, where they probably act as MTOCs (Figure 1.15 C and H) (Hepler 1976; Gifford and Larson 1980; Doonan et al. 1986). In the metaphase-anaphase transition of the last mitosis, the blepharoplast becomes more diffuse and loses its MT-nucleating ability. The cylinders acquire a nine-fold symmetry and a hub-and-spokes configuration similar to a cartwheel. The blepharoplast eventually collapses, giving rise to individualised centrioles (Figure 1.15 D) (Doonan et al., 1986; Mizukami and Gall, 1966; Norstog, 1986). Centrioles form alongside sperm formation, so some of the transcriptional factors that initiate sperm formation are possibly also involved in centriole *de novo* assembly (Hepler, 1976; Renzaglia and Maden, 2000).

Molecular characterisation of blepharoplast assembly is still scarce. However, a few studies have reported the localisation of Centrin, acetylated, tyrosinated and β -tubulins at the blepharoplast (Doonan et al., 1986; Klink and Wolniak, 2001; Vaughn and Renzaglia, 2006). Centrin's function was studied in *M. vestita*, where RNAi experiments highlighted its requirement for proper blepharoplast and centriole biogenesis (Klink and Wolniak, 2001).

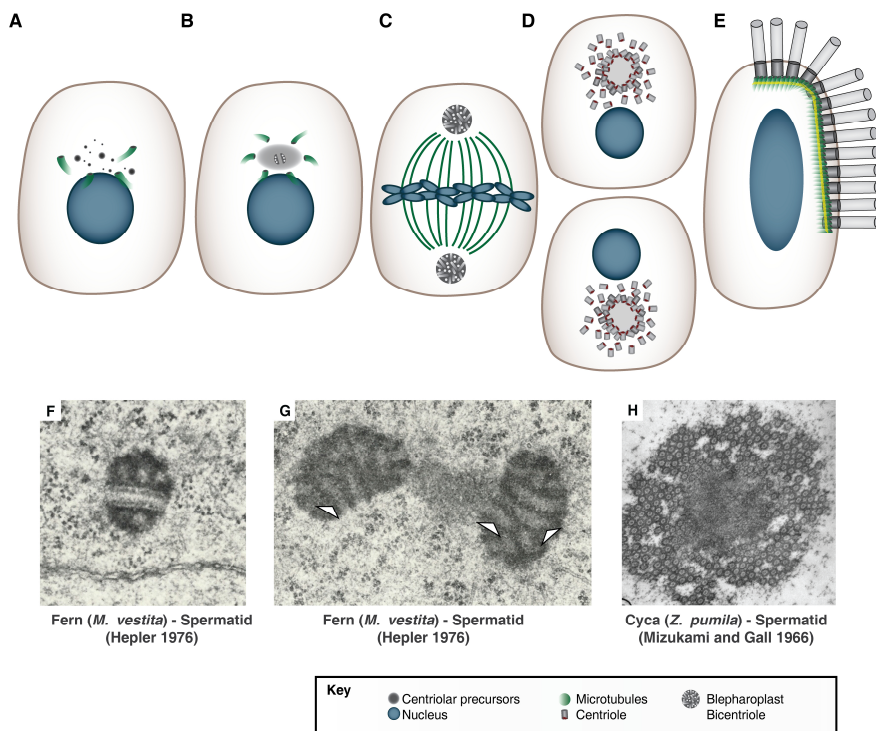


Figure 1.15 – Blepharoplast-mediated biogenesis in land plants with multiciliated sperm. In plants with multiciliated sperm, an electron-dense agglomerate of material and microtubules (MTs) is first detected near the nuclear envelope of the sperm mother-cell (**A**). This material develops into two darker hemispherical lobes, intercalated by lighter cylinders (**B**, **F** and **G** - arrowheads). As the cell approaches mitosis, the lobes keep developing

and separate **(G)**. Each lobe migrates to a pole of the mitotic spindle and assembles a blepharoplast **(C)**. Each spermatid inherits one blepharoplast, where many centrioles are assembled. The blepharoplast eventually collapses releasing the individual centrioles **(D and H)** that will migrate and anchor into the MLS, giving rise to the basal bodies of the several cilia **(E)**. F and G – Adapted from Hepler 1976; H - Adapted from Mizukami and Gall 1966. General figure from (Nabais et al., 2018).

1.4.2 Mechanisms and their regulation

The regulation of centriole number in cells is still not fully understood. While in the canonical pathway the coupling between the centriole and cell-cycles helps maintaining the correct centrosome number, this cannot be the case in non-canonical modes, since cells are usually not cycling. One possibility is that the number of centrioles assembled strongly depends on the amount of building blocks available in the cell, therefore as centrioles are formed, the components are depleted and biogenesis halts. Under this hypothesis, regulation takes place at the levels of transcription and translation. A different strategy consists on the activation of a negative feedback mechanism once the right amount of centrioles are assembled, driving proteolysis of centrosomal components and further inhibiting biogenesis. Interestingly, even non-canonical pathways appear to follow some kind of centriole number regulation since, in most cell-types studied so far, a consistent number of centrioles is assembled.

In spite of the diversity in pathways, their outcome is similar: the generation of CBBs with a conserved ultrastructure and function. The strategy employed by each cell-type or organism seems to depend on the number of CBBs they have to begin with and how many more will be generated. Building a centriole requires the

concentration and assembly of conserved components that serve as building blocks. Some molecules with self-assembling capacity may establish primary scaffolds to which other building blocks can associate to. MTs might transport critical components, including stabilising factors such as MAPs and enzymes with catalysing activity and together drive the assembly of centrioles with structural integrity.

Conservation of critical components

Nevertheless, canonical and non-canonical pathways share several features. Two centriolar proteins - Sas6 and Centrin - and pericentriolar components γ -tubulin and Pericentrin have been detected in CBBs or in its precursors, formed by both canonical and non-canonical pathways, in multiple species. Sas6, the major cartwheel component, is the most conserved centriolar protein, and it is essential for centriole and basal body assembly (Kitagawa et al., 2011; Nakazawa et al., 2007; van Breugel et al., 2011). In plants, Centrin and γ -tubulin are enriched in the blepharoplast of *Ceratopteris richardii* (Hoffman et al., 1994) and functional studies demonstrated that Centrin is needed to form the blepharoplast and the ciliary apparatus in *Marsilea vestita* sperm (Klink and Wolniak, 2001). *De novo* CBB formation in *Naegleria gruberi* is preceded by the formation of a γ -tubulin, Pericentrin and myosin II complex, at the site where Sas6 and Centrin-positive centrioles later localise (Fritz-Laylin and Fulton, 2016; Fritz-Laylin et al., 2010; Lee et al., 2015). In vertebrates, all of the previously mentioned components plus others, localise to centrioles generated *de novo* in mammalian cultured cells (Khodjakov et al., 2002; La Terra et al., 2005; Uetake et al., 2007)

and are upregulated upon multiciliogenesis (Klos Dehring et al., 2013; Mori et al., 2017; Vladar and Stearns, 2007; Zhao et al., 2013). Though the molecules are the same, differential regulation of their concentration might provide the trigger that overcomes the number limitation imposed by canonical biogenesis.

The importance of a concentrator and MT nucleation

The location where pro-centrioles assemble is determined by the site where its precursors concentrate, hereafter called “concentrator”. Even though the “concentrator” may look morphologically different between centriolar and acentriolar pathways, the critical components must first accumulate in a defined location in the cytosol to seed the growth of CBBs. In the canonical pathway the mother centriole acts as a concentrator, whereas in the non-canonical pathways organisms evolved multiple structures where centriolar components are specifically enriched – the blepharoplast, the deuterosome and other electron-dense structures. In this way, the concentrator regulates the location and number of CBBs assembled.

The MT cytoskeleton provides a targeted way of transporting components to the concentrator. CHO cells, upon centriolar removal form centrioles *de novo*. However, if treated with nocodazole, they are no longer capable of assembling centrioles *de novo* (Khodjakov et al., 2002). Multiciliogenesis is accompanied by cytoskeleton remodelling that promotes assembly of stable cytoplasmic microtubules that are more resistant to depolymerisation (Vladar and Stearns, 2007). Microtubule enrichment is also detected close to the fibrogranular material preceding deuterosome formation (Dirksen,

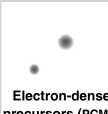





1971; Steinman, 1968) and microtubules regrow from the blepharoplast, upon depolymerisation treatment (Vaughn and Bowling, 2008). Overall, multiple observations hint that microtubules are important for CBBs assembly, however it is still left to determine when exactly they are critical; if at the very early stages of precursor concentration or if they can only recruit components once a primitive MTOC is established from PCM proteins. Some MAPs and motor proteins with MT affinity concentrate at the MTOCs and may facilitate the process. Proteins like chTOG/XMAP215, members of the Tacc family, Cpap/Sas4 and γ -tubulin are important for PCM assembly and microtubule organisation and are present in many eukaryotes (Dammermann et al., 2004; Hodges et al., 2010; Peset and Vernos, 2008). Since PCM components also have a role in centriole duplication and stabilisation, they might be important in promoting the concentration of centriolar proteins within a suitable environment for biogenesis (Dzhinzhev et al., 2010; Varmark et al., 2007).

Self-assembling properties are important for centriole formation



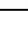
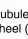
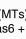
Self-assembly along with the catalytic activity of some centrosomal components are determinant in driving CBBs biogenesis. Plk4 self-organises into scaffolds that recruit tubulin (Montenegro Gouveia et al., 2018). When oligomerised, Plk4 autocatalytic activity establishes a positive feedback loop, important for the phosphorylation of downstream targets (Arquint and Nigg, 2016; Arquint et al., 2015; Dzhinzhev et al., 2014; Kratz et al., 2015; Lopes et al., 2015; Moyer et al., 2015; Ohta et al., 2014). Other components have self-assembling properties *in vitro*: the centriolar

protein Sas6 forms homodimers that subsequently assemble higher order oligomers through interactions via their N-terminal region (Kitagawa et al., 2011); and the centrosomal proteins Spd5 forms supramolecular scaffolds with MT affinity (Woodruff et al., 2017). Future work should assess *in vivo* the contribution of self-assembling properties in driving centriole formation.

Table 1 – Common principles underlying centriole biogenesis among known pathways. From (Nabais et al., 2018).

| PATHWAYS |  Electron-dense precursors (PCM?) |  Microtubule enrichment |  "Concentrator" |  PCM enrichment |  Pro-CBB assembly |  CBB |
|-----------------------|--|--|--|--|--|---|
| Canonical | 1 per Mother Centriole | Yes | Mother Centriole | Yes | Yes | Yes |
| Deuterosome | Many | Yes | Deuterosomes and Resident Centrioles | Yes | Yes | Yes |
| <i>de novo</i> | Not clear | Yes | Not clear | Yes | Yes | Yes |
| Bicentriole | 1 | Not clear | 2 Pro-bicentrioles | Yes | Yes | Yes |
| Blepharoplast | 1 | Yes | 2 Blepharoplasts | Yes | Yes | Yes |

Key

-  Microtubules (MTs)
-  PCM (γ-tubulin)
-  Cartwheel (Sas6 + Cep135/Bld10)
-  MTs-wall (MTs triplet)
-  Sas4/Cpap + Centrin + ?

1.4.3 Experimental systems to study *de novo* MTOC biogenesis

Centriole elimination in oogenesis renders female eggs the most established system to study *de novo* centriole biogenesis in animals. Cellular extracts, in particular, have been used for over 30 years to dissect many cellular and biochemical processes. The absence of a cellular membrane facilitates the physical manipulation of intracellular components or organelles and performing

biochemical perturbations, by protein addition or depletion, chemical inhibition and addition of labelled molecules.

Large volume, cell extracts prepared from frog eggs recapitulate the early embryonic cell-cycle in a test tube. Since their discovery in 1983 (Lohka and Masui, 1983), they have been widely used to study cell-cycle progression and regulation, chromatin dynamics (DNA replication, chromosome condensation and decondensation), meiotic spindle assembly and MT dynamics (Guse et al., 2012; Heald et al., 1996; Lohka and Masui, 1983; Lohka and Masui, 1984; Maddox et al., 2003; Murray et al., 1996; Shintomi et al., 2017; Stearns and Kirschner, 1994)). Different kinds of egg extracts can be produced from *Xenopus laevis*. If eggs are kept in their inactive state, the cytoplasm is arrested in metaphase II, in a state known as CSF (from cytostatic factor preventing egg maturation). It is also possible to prepare extract from metaphase I oocytes to study meiotic progression (Siefert et al., 2015). Finally, eggs can be activated, either by the addition of calcium or electrical or mechanical stimulation prior to the preparation of the extract. The cytoplasm prepared from activated eggs is released from meiosis II and enters interphase (cycling extract) (Siefert et al., 2015). The ability to undergo multiple S-M/M-S transitions *in vitro* is limited and variable.

Recently, *Xenopus* egg extracts allowed identifying a mechanism preventing centriole biogenesis during M-phase, whereby Cdk1-Cyclin B binds Stil, preventing the Plk4-Stil interaction (Zitouni et al., 2016). As a consequence, Plk4 is only capable of triggering MTOC formation in interphase, when Cdk1 activity is low (Zitouni et al., 2016). However, the major caveat of this experimental system is that the Plk4-induced MTOCs do not contain centrioles. In contrast, Plk4 overexpression in *D. melanogaster* eggs

drives the formation of centriolar MTOCs (Rodrigues-Martins et al., 2007). Compared to other laboratory animal species, *Drosophila* is a great genetic model, with a vast library of characterised genetic mutants and transgenic lines, allowing ectopic expression of genes and reporters in specific tissues or under the control of inducible promoters. Additionally, fruit flies have a short generation time, produce a large number of progeny and are easily reared in the laboratory (Hales et al., 2015).

Cell-free extracts from multiple *Drosophila* eggs have been used to study mRNA degradation by double-stranded RNA, mRNA translational control and DNA replication (Jeske et al., 2006; Svitin and Chesnokov, 2010; Tuschl et al., 1999), but only recently, a single embryo or egg extract assay was developed (Telley et al., 2013). This reductionist approach circumvents the problem of stochastic inter-egg variation and more importantly, it allows high-resolution time-lapse imaging of nuclear cycles and other cellular processes occurring deep inside the *D. melanogaster* egg/embryo, otherwise invisible by conventional optical microscopy *in vivo*. This protocol was optimised in this thesis to perform time-lapse imaging of *de novo* centriole biogenesis in *D. melanogaster* eggs allowing, for the first time, tri-dimensional (3D) μm -scale centrosome detection and sub-minute characterisation of centrosome formation, MTOC dynamics and centriole duplication.

1.4.4 Framework of the thesis

Centriole *de novo* biogenesis is a poorly characterised process from the spatial, temporal and numerical standpoints. Very little is known in terms of how this process is regulated *in vivo* and how Plk4 levels modulate its kinetics, partly due to the lack of a suitable

experimental system to approach this problem. Understanding how Plk4 levels influence the parameters of centriole biogenesis is also very challenging due to Plk4 physiological properties: its endogenous levels are very low in cells and unknown in flies and it is hard to detect and quantify by conventional imaging techniques or by Western Blot.

The main aims of this thesis are to provide a quantitative assessment of Plk4 in flies and dissect the rules underlying Plk4-induced *de novo* centriole assembly. My first goal was to quantify, for the first time, the endogenous *Drosophila* Plk4 protein present in early embryos and determine its mobility and oligomerisation in the cytoplasm. These parameters are important steps towards understanding how Plk4 travels to the centrosome and what are the physiological Plk4 levels regulating canonical centriole biogenesis. My second objective was to establish an experimental system where centriole *de novo* biogenesis can be studied with high spatio-temporal resolution. The *D. melanogaster* egg extract is the ideal system to tackle the problem since it combines the diversity of available transgenic lines with the ease of performing biochemical perturbations. Finally, I used this *ex vivo* assay to understand the general principles of *de novo* centriole biogenesis. The system was validated by characterising some of the centriolar and PCM components that are incorporated during biogenesis by spinning disk confocal microscopy and using super-resolution microscopy and EM. The spatial and temporal characterisation of *de novo* biogenesis was performed for the first birth events and compared to random predictions from stochastic models. Finally, we looked at how Plk4 concentration impacts the centriole assembly process, in terms of its temporal kinetics and centrosome number formation.

Chapter 2

Determination of endogenous Plk4 properties in the early *Drosophila* *melanogaster* embryo

2.1 Author Contribution

All experiments were planned by myself and my supervisors Mónica Bettencourt-Dias and Ivo Telley in collaboration with Dr. Satyajit Mayor and Thomas van Zanten, a Post-Doc fellow at Mayor's lab at the National Centre for Biological Sciences (NCBS) in Bangalore, India. I produced the dmPlk4 CRISPR fly lines, acquired and analysed the live imaging data in blastoderm embryos. Fluorescence correlation spectroscopy (FCS) measurements were collected by me and Thomas van Zanten, and the data analysis was performed by Thomas van Zanten. The size-exclusion chromatography and subsequent protein concentration was done at Instituto de Biologia Experimental e Tecnológica (IBET) in the lab of Tiago Bandejas.

2.2 Summary

Polo-like kinase 4 (Plk4) is a central player in centriole biogenesis. Nonetheless, its endogenous concentration, cell-cycle dynamics and mode of transport remain largely unknown. In this Chapter, I created flies that express endogenous Plk4 labelled with fluorescent reporters and characterised Plk4 localisation at the centrosome by live imaging throughout the cell-cycle, in developing embryos. Plk4 levels oscillate at the centrosome during nuclear cycles 10 to 13, peaking in S-phase when centrioles duplicate, becoming almost undetectable throughout mitosis and increasing again in telophase. We then determined several physical parameters of Plk4 in the cytosol by single-molecule quantification using Fluorescence correlation spectroscopy (FCS). Two Plk4 fractions

with very different diffusion coefficients were identified: one moving rapidly and another very slowly, probably associating to quasi-immobile structures. We also determined the average Plk4 cytosolic concentration, confirming that its endogenous levels are very low. Finally, we provide evidences that Plk4 forms low-order oligomers, which possibly interact with cytoplasmic microtubules.

Our findings raise interesting hypotheses regarding the mechanisms regulating Plk4 centrosomal localisation and activity, and I discuss how these are important for the spatio-temporal and numerical regulation of centriole biogenesis.

2.3 Introduction

Centrioles are microtubule(MT)-based structures that assemble centrosomes and cilia in eukaryotic cells. The animal centrosome is composed of two cylindrical centrioles, surrounded by a multi-layered protein network called pericentriolar material (PCM). The PCM is responsible for anchoring and nucleating MTs, conferring to the centrosome its capacity to remodel the cytoskeleton, establish cell polarity and organise the spindle poles in mitosis. Centrioles can also anchor to the cell membrane (and are then called basal bodies) and nucleate motile and immotile cilia. Cilia play multiple functions in different cell types, such as signalling, sensing environmental cues, cell motility and fluid flow.

Defects in basal bodies and/or in the ciliary apparatus cause a broad range of human diseases, generically called ciliopathies (Bettencourt-Dias et al., 2011; Hildebrandt et al., 2011). Genetic mutations in centriolar proteins such as Plk4, Stil/Ana2 or Sas6 cause problems in brain development which often result in microcephaly and dwarfism (Khan et al., 2014; Kumar et al., 2008;

Martin et al., 2014; Shaheen et al., 2014). Additionally, numerical and structural centriolar abnormalities are a hallmark of genomic instability and cancer (Ganem et al., 2009; Godinho and Pellman, 2014; Levine et al., 2018; Marteil et al., 2018; Silkworth et al., 2009).

In proliferating cells, centriole number is tightly regulated during the cell-cycle. Centrioles duplicate only once at G1/S transition, forming one procentriole adjacent to each of the two mother centrioles. From S-phase to mitosis, the daughter centrioles elongate and by late mitosis, they undergo centriole-to-centrosome conversion through the recruitment of Cep135/Bld10, Ana1 and Cep152/Asl, becoming competent for duplication in the next cell-cycle (Fu et al., 2016). After mitosis, each daughter cell inherits exactly one pair of centrioles.

In the fast nuclear cycles of the syncytial *Drosophila melanogaster* embryo, the centrosome cycle is modified accordingly. The two centrosomes separate at the beginning of S-phase, before centriole duplication, and attach to the nuclear envelope, organising the MT network around the nucleus. Throughout S-phase, centrioles duplicate and the centrosomes migrate towards opposite poles while still attached to the nucleus through a fibrogranular connection. By late S-phase, the two centrosomes, each containing two centrioles, are positioned at the poles of the nucleus and are no longer attached to the nuclear membrane. During prophase, after the nuclear envelope partially breaks down, the centrosomes start organising the mitotic spindle. In anaphase the centrioles disengage and by telophase the centrosomes separate (Callaini and Riparbelli, 1990; Debec et al., 1999; González et al., 1998). Centriole duplication and DNA replication are usually coupled in the early fly embryo, but these cycles can be decoupled by blocking DNA synthesis with aphidicolin, while centrosomes continue to divide (Raff and Glover, 1989).

Centriole duplication does not depend on nuclear division either. This is evident in embryos from mothers homozygous for the maternal effect lethal mutation *gnu* that undergo repeated rounds of DNA and centrosome duplication without chromosome segregation (Freeman et al., 1986). The centrosomes are critical for MT organisation throughout these rapid nuclear cycles in the embryo (Megraw et al., 1999; Rodrigues-Martins et al., 2008). The first nuclear divisions occur deep inside the cell but, between cycles 7 to 9, the nuclei and centrosomes migrate towards the cortex, and by cycle 10 they dock to the cellular membrane, forming the blastoderm (Foe and Alberts, 1983). At the cortex, the nuclei undergo another four mitotic rounds before cellularisation takes place (Farrell and O'Farrell, 2014; Foe and Alberts, 1983). When DNA synthesis is inhibited or chromosomes segregate abnormally, the nuclei are internalised (nuclear "fall-out"), while their centrosomes remain at the cortex (Gonzalez et al., 1990; Sullivan et al., 1993; Takada et al., 2003).

The early steps of centriole assembly are initiated by a conserved protein module composed of Plk4 (Zyg1 in *C. elegans*), Stil/Ana2 (Sas5 in *C. elegans*) and Sas6. Plk4, the master driver of centriole biogenesis (Bettencourt-Dias et al., 2005; Habedanck et al., 2005; Kleylein-Sohn et al., 2007), is recruited to the mother centrioles by Cep192, Cep152 and Cep53 in human cells. In *Drosophila*, Plk4 or Sak is recruited by Asl, whereas in *C. elegans* Spd2 recruits Zyg1. Mechanistically, it is not known how exactly those proteins recruit Plk4 and how the kinase moves in the cell and localises to the centrosome. One hypothesis is that Plk4 is transported to the centrosome with its recruiting molecules or alternatively, these recruiters sequester Plk4 once it reaches the centrosome. Plk4 mobility in the cytoplasm may be accomplished

solely by diffusion, by cytoskeleton-mediated transport or by a combination of mechanisms. Since *Xenopus* Plk4 binds and stabilizes MTs (Montenegro Gouveia et al., 2018), one possibility is that *Drosophila* Plk4 travels along the MTs to the centrosomes, where it generates a positive feedback loop promoting its own MT-dependent recruitment. An alternative hypothesis is that Plk4 associates with large molecular components or transiently binds and unbinds MTs in the cytosol.

In late mitosis/G1, before procentriole formation, Plk4 is recruited and localises around the mother centriole in a ring-shape manner. Stil/Ana2 is phosphorylated at its N-terminus by Plk4 and loads onto a single site on the mother (Dzhindzhev et al., 2017; Mclamarrah et al., 2018). The interaction between Plk4 and Stil stabilizes Plk4, preventing its degradation (Ohta et al., 2018). Plk4 triggers its auto-destruction asymmetrically, restricting its localisation to the single, Stil-enriched spot (Dzhindzhev et al., 2017; Ohta et al., 2018). Disruption of Plk4 degradation gives rise to stable Plk4 rings that recruit multiple Stil foci. Finally, Plk4 phosphorylates Stil on its STAN motif promoting binding and recruitment of Sas6 to the procentriole assembly site (Dzhindzhev et al., 2017; Kratz et al., 2015; Mclamarrah et al., 2018; Moyer et al., 2015). Sas6 and its binding partner Cep135/Bld10 assemble the nine-fold symmetrical cartwheel, around which the MT walls of the new procentriole attach (Breugel et al., 2011; Kitagawa et al., 2011; Nakazawa et al., 2007). Overexpression of Plk4, and to a lesser extent of Stil and Sas6, drive the formation of several daughter centrioles around the mother, therefore their levels must be well-regulated in cells to accurately control the number of procentrioles formed each cell-cycle.

Quantitative analysis of the intracellular levels of centrosomal proteins by Mass-Spectrometry has provided estimations of protein

copy number in asynchronous human cells (Bauer et al., 2016). This study has detected between 1200- 5000 copies of Plk4 per cell, from which 70 molecules are loaded at the centrosome. Together with Stil and Sas6, these are some of the least abundant proteins in the human centrosome proteome (Bauer et al., 2016). Protein levels are regulated by transcriptional and translational processes and by protein degradation. The transcriptional regulation of Plk4 is still not fully understood but several studies have clarified how the protein suffers turnover. Plk4 degradation relies on its homodimerisation and autophosphorylation in multiple residues; first in two sites within the conserved downstream regulatory element (degron) and secondly within a phospho-cluster flanking the degron. Together, these phosphorylations recruit the binding of the SCF Slimb/ β TrCP-E3 ubiquitin ligase complex, triggering rapid protein degradation via the 26S proteasome (Cunha-Ferreira et al., 2009; Cunha-Ferreira et al., 2013; Guderian et al., 2010; Holland et al., 2012a; Klebba et al., 2013; Rogers et al., 2009).

The combination between low expression levels and fast degradation, render endogenous Plk4 detection, either by Western blot or using fluorescent reporters, extremely difficult and, so far, it has not been reported in flies. It is not known how Plk4 movement occurs within cells and how it impacts Plk4 localisation, and ultimately, its activity at the centrosome and centriole biogenesis. Here, we have characterised the centriolar dynamics of endogenous *D. melanogaster* Plk4 throughout the cell-cycle and determined its physical properties in the cytoplasm of the syncytial embryo. First, we tagged the endogenous Plk4 alleles with the brightest fluorescent reporters currently available. Next, we characterised the bulk Plk4 centrosomal turnover in the fly embryo during nuclear cycles 10-13. Finally, we determined Plk4 concentration, oligomeric state and

diffusion coefficient in the cytoplasm by Fluorescence Correlation Spectroscopy (FCS). FCS is a measurement technique with single-molecule sensitivity, therefore ideal for quantification of low abundance proteins, present at nanomolar to picomolar concentrations in cells. In fact, this technique has been used to determine the oligomerisation state of another centriolar protein, Sas6, in human U2OS cells (Keller et al., 2014). Moreover, Plk1, another member of the Polo-like kinase family, has been studied by FCS in human RPE1 cells (Mahen et al., 2011). The FCS measurements allowed distinguishing distinct diffusion coefficients for Plk1 in the cytoplasm, which correlated with its kinase activity during different cell-cycle stages (Mahen et al., 2011).

FCS experiments measure fluctuations in fluorescence intensity as fluorescent molecules go through the observational focal volume. These fluctuations are correlated over time allowing one to draw an autocorrelation function (ACF). The starting value of the autocorrelation function, or the y-offset, is inversely proportional to the exact number of particles in the detection volume (Jameson et al., 2009). Knowing the exact particle number, their brightness (counts per molecule - CPM) and the focal volume, allows calculating the concentration of a particle and its oligomerisation state. Determining Plk4 oligomerisation in the cytoplasm is essential since self-interaction regulates not only Plk4 turnover but also its activity. Plk4 becomes fully activated by *trans*-auto-phosphorylation in the T-loop, within its kinase domain (Lopes et al., 2015). Consequently, we hypothesise that Plk4 oligomerisation should be a well-regulated process, preferentially taking place at the centrosome.

Finally, the average residence time of a particle within the FCS observation volume allows estimating its diffusion coefficient and determine how Plk4 moves inside the cell; if it is mostly by

diffusion; if it is transported e.g. through the cytoskeleton, or if it is spatially confined, i.e. by transiently binding to organelles or other molecules. All these critical parameters allow understanding how Plk4 localises at the centrosome and provide a quantitative perspective on how Plk4 molecules spatially and temporally regulate centriole duplication.

2.4 Material and Methods

2.4.1 Fly strains and fly husbandry

All flies were reared according to standard procedures and maintained at 25 °C, avoiding overcrowding. Fly stocks were grown on medium containing molasses, beet syrup, cornmeal, yeast, soy flour, agar and water. The fly stock pUb-RFP:: β 2Tubulin/CyO (Kitazawa et al., 2014) was a gift from Prof. Yoshihiro Inoue, Kyoto Institute of Technology, Japan. Transgenic endogenous mEGFP::dmPlk4 and mNeonGreen::dmPlk4 flies were generated in-house by CRISPR/Cas9-mediated gene editing. 3-4 days before an experiment, w^{1118} ; pUb-RFP::2Tubulin/CyO; mEGFP::dmPlk4 or w^{1118} ; pUb-RFP:: β 2Tubulin/CyO; mNeonGreen::dmPlk4 adult flies were transferred to a cage coupled to an apple juice agar plate supplemented with fresh yeast paste. The cage was maintained at 25°C, under 50-60% humidity. The plates of the cage were changed every 3 to 4 hours.

2.4.2 Glass coverslips preparation

Glass coverslips were cleaned to remove autofluorescent residues from their surface. They were sonicated once in 3M sodium

hydroxide for 10 minutes, followed by 3-4 dip-and-drain washes in milliQ water. Next, they were sonicated in “Piranha” solution (H_2SO_4 and H_2O_2 (30% concentrated) mixed at 3:2 ratio) for 15 minutes, followed by two washes in milliQ water, once in 96% ethanol and twice again in milliQ water for 5 minutes each. Coverslips were spin-dried and stored in a clean and dry rack.

2.4.3 Embryo collection and sample preparation

On the day of the experiment, the plate of the cage was regularly replaced. For both time-lapse imaging and FCS experiments 1-hour embryo collections were performed. The embryos were removed from the agar plate using a fine paintbrush and transferred to a small basket sieve immersed in milliQ water. Next, the embryos were dechorionated in 7% bleach solution (Sigma-Aldrich) for 20-30 seconds and washed twice in milliQ water inside the basket. The dechorionated embryos were aligned side-by-side on an agar block and transferred to a thin line of heptane glue drawn on a clean coverglass. The sample was then covered in halocarbon oil (Votalef oil 10S from VWR) and placed on a coverslip holder fitting the microscope stage.

2.4.4 Time-lapse imaging on a spinning disk confocal microscope and image data analysis of whole embryos

Time-lapse movies of blastoderm embryos were acquired at 20°C on a Nikon Eclipse Ti-E microscope equipped with a Yokogawa CSU-X1 Spinning Disk confocal scanner. Images were recorded with a Photometrics electron-multiplying CCD (EMCCD) camera.

Images shown in the results section are Maximum-intensity projections (MIPs) of 0.4 μm optical sections acquired with a Plan Fluor 40x 1.3 NA oil immersion objective using a piezoelectric stage (Physik Instrumente) with 220 μm travel range. Embryo staging and selection was done based on the detection of the fluorescent reporter RFP::2-Tubulin, indicating that embryos were beyond nuclear cycle 8. Accurate developmental staging was challenging in these embryos because nuclear distribution is more irregular than in the wild-type as several nuclei undergo internalisation. Nonetheless, nuclear density was compared in all embryos to time-align the acquisitions and confidently determine developmental progression (according to (Foe and Alberts, 1983)). Dual-colour (491 nm and 561 nm excitation lasers) time-lapses were recorded using Metamorph image acquisition software.

Postacquisition image processing was performed using Fiji (National Institutes of Health - NIH (Schindelin et al., 2012)). All time-lapses movies were first bleach-corrected with Fiji's exponential fit algorithm. Next, maximum-intensity projections (MIPs) were produced from the image stacks and centrosome analysis was performed semi-automatically, using a custom-made macro. Briefly, a copy of the original bleach-corrected mNeonGreen-Plk4 MIP was processed in order to enhance edges and allow threshold-based detection of the centrosomes. First, a median intensity projection was subtracted from the MIP to eliminate most of the diffuse background fluorescence. Next, a Gaussian Blur filter with Sigma = 0.7 (Radius) was applied to the images, followed by a background subtraction with a rolling ball radius of 20 pixels. A histogram-based automatic threshold (*'RenyEntropy'*) was then applied to the images, these were converted into a binary mask and submitted to particle detection using the "Analyze Particles" plugin. The Regions

of Interest (ROIs) were chosen according to their size (area: 2-12 pixels) and circularity (0.8-1.00), taking into consideration that centrosomes are diffraction limited spot-like signals. Finally, the ROIs selection was used to measure the signal intensity of the centrosomal Plk4 spots on the MIP from the original bleach-corrected images. The measurements were exported to MS Excel and further analysed. All mNeonGreen-Plk4 (NG-Plk4) quantifications were normalised to background fluorescence measured in five independent ROIs throughout the time-lapse, except in the case of Figure 2.2C where the NG-Plk4 intensities were normalised to the minimum intensity value detected in each oscillatory curve, hence aligning all curves at the x-axis and facilitating their visualization. Statistical analysis and graphic representations of centrosomal Plk4 intensity were performed using Prism 7 (GraphPad Software). All the details regarding sample size, statistical tests and descriptive statistics are indicated in the respective figure legends and main text. Selected stills from the time-lapse acquisitions were processed with Photoshop CS6 (Adobe). Final figures were produced using Illustrator CS6 (Adobe).

2.4.5 Fluorescence Correlation Spectroscopy acquisition and data analysis

All FCS measurements were performed on a point-scanning confocal microscope (Zeiss LSM780 Confocor3) equipped with a UV-VIS-IR C Achromat 40X 1.2 NA water-immersion objective and a gallium arsenide detector array wavelength selected between 491-561nm. The system was aligned and calibrated each day before the experiment using the known diffusion coefficient of rhodamine 6G ($410 \mu\text{m}^2/\text{s}$). This allowed us to determine the lateral beam waist (w_{xy})

= 232 nm) and the structure factor ($S = 5.77$) of the focused laser (Point Spread Function, PSF). The resultant volume of illumination is calculated through:

$$V_{\text{eff}} = \pi^{(3/2)} \cdot w_{xy} \cdot w_z = \pi^{(3/2)} \cdot w_{xy} \cdot S \cdot w_{xy}$$

The values for w_{xy} and S were used as constants in the subsequent model-based fittings of the autocorrelation functions (ACF) and the volume was used to calculate the concentration (see below).

To quantitatively assess both fluorescent tags mEGFP and mNeonGreen, these were first measured in a cytoplasm-compatible buffer. Fluorescence intensity in time ($I(t)$) was recorded as 6 iterations of 10s. Each 10s trace was autocorrelated into an ACF, $G(\tau)$, using the Zeiss onboard autocorrelator which calculates the self-similarity through:

$$G(\tau) = \langle \Delta I(t) \cdot \Delta I(t + \tau) \rangle \cdot \langle I(t) \rangle^{-2}$$

Here $\langle \rangle$ denotes the time-average, $\Delta I(t) = I(t) - \langle I(t) \rangle$ and τ is called the timelag. The resulting $G(\tau)$ curves of the fluorophores in buffer were readily fitted using a regular 3D diffusion model:

$$G(\tau) = 1/N \cdot GT(\tau) \cdot GD(\tau)$$

N reflects the number of moving particles in the confocal volume and $GT(\tau)$ is the correlation function associated to blinking/triplet kinetics:

$$GT(\tau) = (1+T)/(1-T) \cdot \exp^{-(\tau/\tau_T)}$$

Where T is the fraction of molecules in the dark state and τ_T the lifetime of the darkstate. $GD(\tau)$ is the correlation function associated to diffusion which in this case is simple Brownian diffusion in 3D:

$$GD(\tau) = 1/(1 + \tau/\tau_D) \cdot 1/\sqrt{1 + S^2 \cdot \tau / \tau_D}$$

These fittings allowed us to measure the number of molecules in the confocal volume and therefore their brightness ($\langle I(t) \rangle / N$) together with the characteristic diffusion times (τ_D).

The above model fit is based on the assumption that there are only two characteristic timescales generating the ACF. In order to get a model free estimate of the number of timescales involved we used a Maximum Entropy Method based fitting (MEMfit) of the combined and normalised ACFs of each experiment. MEMfit analyses the FCS autocorrelation data in terms of a quasicontinuous distribution of diffusing components making it an ideal model to examine the ACF of a highly heterogeneous system without prior knowledge of the amount of diffusing species.

To be able to quantify the brightness of individual fluorescent tags in an embryo the purified mEGFP or mNeonGreen was injected into dechorionated embryos. An anomalous coefficient had to be included to fit the resultant ACF:

$$GD(\tau) = 1/(1 + (\tau/\tau_D)^a) \cdot 1/\sqrt{1 + S^{-2} \cdot (\tau / \tau_D)^a}$$

For simple Brownian diffusion $a = 1$ and the fit function is identical to the one used to fit the fluorophores in buffer. However, for fluorophores injected into the cytosol of embryos the fitting algorithm gave an anomalous coefficient of $a = 0.8$. An anomalous coefficient smaller than 1 indicates constrained diffusion and could be caused by the more crowded environment in the yolk. In addition, the large amount of (uncorrelated) autofluorescence generated by the yolk required a background correction factor which leads to an underestimation of the brightness. The background values were determined per excitation power from embryos lacking the Plk4 reporter. If the background itself does not autocorrelate it has no

influence on the obtained timescales in the data. Nevertheless, the background will impact the absolute number, N , and consequently also on the calculated brightness. To background correct all the data for the N was corrected as:

$$N_{\text{corr}} = N \cdot ((\langle I(t) \rangle - \text{BG}) / \langle I(t) \rangle)^2$$

Where BG is the measured background from embryos lacking the reporter fluorophore. Consequently the corrected brightness was calculated as:

$$BN_{\text{corr}} = (\langle I(t) \rangle - \text{BG}) / N_{\text{corr}}$$

Finally, any 1 millisecond-binned intensity trace that contained changes in average intensity (most likely arising from yolk spheres moving through the confocal spot during the measurement) were discarded from the analysis.

For the measurements of mNeonGreen-Plk4, embryo staging was done based on the RFP::Beta2Tubulin reporter. We chose embryos at blastoderm stage, in division cycles 10 or 11. Before each FCS acquisition series, a large field-of-view image of the embryo was acquired. Six different, 10 seconds long intensity traces were measured at the inter-nuclear cytoplasmic space of the syncytium. The 10s measurement was long enough to obtain sufficient passage events and short enough to avoid each trace to be contaminated by events that do not arise from NeonGreen-Plk4 diffusing in the cytosol.

From these measurements, the MEMfit method on the normalised ACF indicates three timescales for the tagged-Plk4 molecules. A first timescale of 5-50 μs corresponding to the triplet state dynamics that were similarly found in both the buffer as well as

from fluorophores injected in the embryo. A second timescale of about 0.8ms, most likely coming from simple diffusion (see similarity to mNeonGreen monomer in cytosol). And a third timescale of diffusion that is much slower, 9ms. In order to fit the ACFs the diffusional part of the fit function was associated with two components:

$$GD(\tau) = f \cdot GD1(\tau) + (1-f) \cdot GD2(\tau) = f \cdot [1/(1 + \tau/\tau D1) \cdot 1/\sqrt{1 + S^{-2} \cdot \tau / \tau D1}] + (1-f) \cdot [1/(1 + \tau/\tau D2) \cdot 1/\sqrt{1 + S^{-2} \cdot \tau / \tau D2}]$$

The fraction f corresponds to the fast diffusing Plk4. The Diffusion Coefficient of each of the components can be calculated from the diffusion timescales τD via:

$$D = w_{xy}^2 / 4 \cdot \tau D$$

If the molecules mNeonGreen and mNeonGreen-Plk4 are assumed to be globular (i.e. spherical) and their diffusion the result of simple Brownian motion in solution, it is possible to estimate both their hydrodynamic radius as well as the viscosity of the fluid via the Stokes-Einstein equation:

$$D = k_B \cdot T / (6 \cdot \pi \cdot \eta \cdot r_h)$$

where k_B is the Boltzmann constant, T is temperature, η is the viscosity and r_h is the hydrodynamic radius. Even when not all the constants are known one can use comparative experimental situations to estimate the parameter of choice. For example, the viscosity of the embryo cytosol (η_2) can be estimated by using the same molecule and measure its Diffusion Coefficient (D_2) and compare it to the Diffusion Coefficient (D_1) of that same molecule in a solution of known viscosity (η_1).

$$D_1 / D_2 = \eta_2 / \eta_1$$

The same holds true for an estimation of a hydrodynamic radius but here viscosity should remain identical and the diffusion coefficient of

the molecule of choice must be compared with the diffusion coefficient of a molecule with known hydrodynamic radius.

2.4.6 mNeonGreen and mEGFP protein purification

The mEGFP and the mNeonGreen coding sequences were cloned with an N-terminus Streptavidin-Binding Peptide (SBP)-Tag and a flexible linker, into the pETMz expression vector (from the EMBL, Germany), between *NcoI* and *BamHI* restriction sites. The 6xHis::Z-tag::TEV::SBP::linker::mEGFP/mNeonGreen proteins were expressed in BL21 (Rosetta) Competent *E. coli* at 25°C for 5 hours. The grown liquid cultures were harvested and centrifuged at 4000 rpm for 25 minutes, at 4°C. The pellets were flash-frozen in liquid nitrogen and stored at -80°C.

The pellets were resuspended in ice-cold lysis buffer containing 50 mM K-Hepes (pH 7.5), 250 mM KCl, 1mM MgCl₂, 1 mM DTT, 7 mM of Imidazole, 1x DNaseI and 1x Protease inhibitors. Each sample was applied to a pre-chilled French-press, equilibrated with Lysis buffer, and run twice at a constant pressure (around 12kPa). The cell lysate was collected in a flask on ice and ultracentrifuged at 4°C for 25 min at 50000 rpm using a Ti-70 rotor (Beckman). The protein purification was done through affinity chromatography on a Ni-column (HiTrap chelating HP column 1 ml, GE HealthCare). The column was loaded with a filtered solution of 100 mM nickel chloride, washed extensively with milliQ water and equilibrated with wash buffer (50 mM K-Hepes (pH 7.5), 250 mM KCl, 1mM MgCl₂, 1 mM DTT, 7 mM of Imidazole). The clarified lysate was applied to the column (at 1.5 ml/min), followed by 200 ml wash buffer. The protein was eluted at 1.5 ml/min with elution buffer: 50 mM K-Hepes (pH 7.5), 250 mM KCl, 1mM MgCl₂, 1 mM DTT, 400

mM of Imidazole. 1 ml sample fractions were collected and kept at 4°C. The most concentrated samples were pooled together (final concentration: 20 mg/ml) and their N-terminus 6xHis::Z-tag was cleaved with TEV protease overnight at 4°C by treating with 150U TEV/mg of protein. The following day, the cleaved protein was passed through a column for size-exclusion chromatography to remove contaminants, the cleaved tag and the TEV protease (with Tiago Bandeiras at IBET, Oeiras, Portugal). Additionally, the elution buffer was exchanged to a storage buffer: 50 mM K-Hepes (pH 7.8), 100 mM KCl, 2 mM MgCl₂, 1 mM DTT, 1 mM EGTA. The HiLoad Superdex 75 16/60 (GE HealthCare) gel filtration column was equilibrated with storage buffer for 1 hour. The sample was spun at 15000 rpm for 15 min at 4°C and the clear fraction was applied to the gel filtration column coupled to an AKTA device at 1 ml/min. The cleaved mEGFP and mNeonGreen proteins were concentrated approximately 5 times using Amicon 10K Centrifugal filters. Pure glycerol was added at 5% v/v to the concentrated proteins and small aliquots were snap-frozen in liquid nitrogen and stored at -80°C.

2.5 Results

2.5.1 Targeting the endogenous *Drosophila melanogaster* Plk4 locus

Measuring Plk4 physiological properties first required producing transgenic flies by knocking-in a fluorescent reporter into the endogenous Plk4 locus by CRISPR/Cas9-mediated homologous recombination (Port et al., 2014). Twenty base-pairs guide RNAs (gRNA) targeting the N-terminal region of dmPlk4, with 5' *BbsI*-compatible overhangs, were ordered from Sigma-Aldrich as single-stranded oligonucleotides (Table 1). gRNA off-target potential was

assessed using online CRISPR target finders:
<http://www.flyrnai.org/crispr/>
<http://tools.flycrispr.molbio.wisc.edu/targetFinder/>.

The complementary oligonucleotides were annealed, phosphorylated and cloned into *BbsI*-digested pCFD3-dU6:3gRNA expression plasmid (from Simon Bullock, MRC, Cambridge, UK). The gRNA constructs were confirmed by Sanger sequencing using the primer U6-3_seq_F2 (Table 3). Plasmid DNA donor templates were designed for homologous recombination-mediated integration of the green fluorescent reporters mNeonGreen (Shaner et al., 2013) and mEGFP (gift from Thomas Surrey, Crick Institute, UK) between the 5'UTR and the first coding exon of dmPlk4. 1-kbp long 5' and 3' homology arms were PCR-amplified from genomic DNA isolated from *y1,M{nos-Cas9.P}ZH-2A,w** flies (Table 2) ((Port et al., 2014), Stock BL#54591, acquired from Bloomington). The mEGFP and mNeonGreen coding sequences were PCR amplified from plasmids (Table 2). All fragments were sub-cloned into the pUC19 plasmid (Stratagene) using restriction enzymes: 5' Homology Arm - *NdeI* and *EcoRI*; Fluorescent tag + linker - *EcoRI* and *KpnI*; 3' Homology Arm *KpnI* and *XbaI*. Synonymous mutations were performed on the homology arms, removing the protospacer-adjacent motif (PAM) sequence from the donor plasmid to prevent re-targeting after integration. The final donor template for homologous recombination-mediated integration was composed of a fluorescent reporter and a short flexible linker (bold sequence in Table 2, and depicted in dark green in Figure 1A) flanked by 1-kbp homology arms from the dmPlk4 genomic locus (Figure 1A). The two circular plasmids pCFD3-Plk4_gRNA and mNeonGreen or mEGFP donor vector were co-injected, each at a concentration of 500ng/μL, into *y1,M{nos-Cas9.P}ZH-2A,w** flies, expressing the Hs-Cas9 endonuclease

under the *Drosophila* germline-specific promoter *nanos* (Port et al., 2014). Injected flies (F_0) were crossed to a balancer strain and single-fly crosses were established from their offspring (F_1). The resulting, genetically identical, F_2 generation was screened for positive integrations by PCR from genomic DNA using primers dmPLK4 5UTR 3 FW and dmPLK4 1exon Rev (Table 3). Insertion of the fluorescent tag into the Plk4 endogenous locus (HR Plk4) causes a migration shift of the PCR product in the agarose gel compared to the untagged locus (WT Plk4) (Figure 1B). Positive candidates were confirmed by Sanger sequencing using primers annealing upstream the dmPlk4 start codon and within the gene region (Figures 1A and 1B).

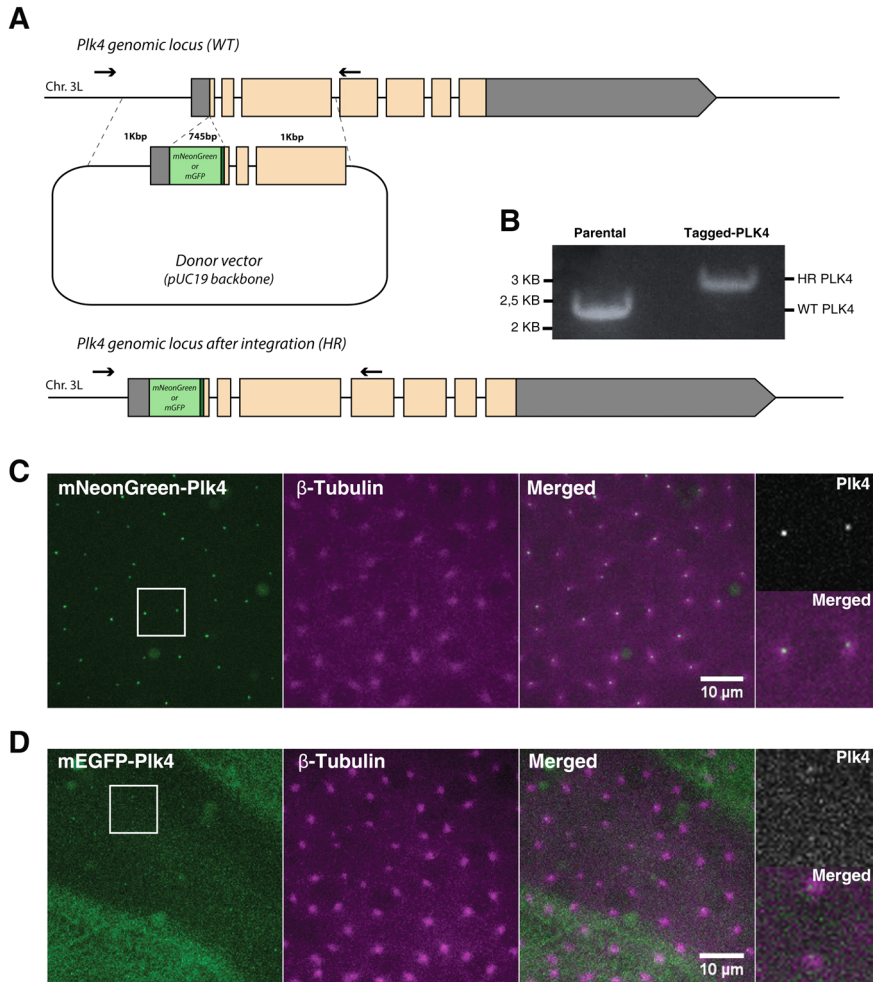


Figure 2.1 – Insertion of a fluorescent tag into *Drosophila* Plk4 endogenous locus. **A)** Schematic representation of the wild-type dmPlk4 locus (WT) and of the dmPlk4 locus after successful tag integration (HR). A donor plasmid carrying either the mEGFP or the mNeonGreen reporter and a small linker (dark green) flanked by 1 Kbp homology arms was used for homologous recombination. The UTRs are shown in grey and the coding sequences are depicted in orange. The arrows indicate the position of the screening primers dmPLK4 5UTR 3 FW and dmPLK4 1exon Rev, which are located outside the homology arms. **B)** Integration of a fluorescent tag into Plk4 endogenous locus (HR Plk4) causes a migration shift of the PCR

product in the agarose gel compared to the untagged Plk4 locus (WT Plk4). **C** and **D**) Maximum intensity projections (MIPs) from time-lapse videos of developing *D. melanogaster* embryos expressing endogenous mNeonGreen-Plk4 (green) (**C**) or mEGFP-Plk4 (green) (**D**) and microtubule reporter RFP- β -tubulin (magenta). PLK4 localises at the centrosomes (high intensity tubulin spots) in interphase. Larger green dots result from yolk auto-fluorescence. Insets show in detail the co-localisation between the mNeonGreen/mEGFP-Plk4 spots and the tubulin foci. The acquisition settings and dynamic range of the images are different since mEGFP-Plk4 cannot be detected with the same settings as mNeonGreen-Plk4.

Table 1. List of guide RNAs used to target dmPLK4 N-terminus by CRISPR/Cas9.

| Name | sense (5'-3') | antisense (5'-3') |
|----------------|--------------------------|--------------------------|
| dmPLK4 gRNA 1* | GTCGGCTAGCTATGTTATCCAAT | AAACATTGGATAACATAGCTAGC |
| dmPLK4 gRNA 2 | GTCGTGTTTCTCCAACGCCCGAT | AAACATCGGGCGTTTGGAGAAACA |
| dmPLK4 gRNA 3 | GTCGTGTAGACTTACTGAGCCACT | AAACAGTGGCTCAGTAAGTCTACA |

* *dmPlk4 gRNA_1* gave the best targeting result.

Table 2. List of primers used to clone the donor vectors with the fluorescent reporters. The linker sequence is highlighted in bold.

| Name | Forward (5'-3') | Reverse (5'-3') |
|-------------------------------|---|--|
| 5' Homology Arm | CATATGCGAGGACACTTTCCAG CACTAC | GAATTCAGCTAGCCTTTTTTCTGT AGACTTACTGAGCCACTTCGAATG |
| 3' Homology Arm | GGTACCATGTTATCGAATCGAGC GTTTGGAGAAACAATTGAGG | GGATCCTAGAGTGAGATTCTACTA GC |
| mNeonGreen/ mEGFP + linker | GAATTCATGGTGAGCAAGGGCG AGGAG | GGT ACCGCCGGAGCCGCCGCCG CCGGAGCCGCCCTTGTACAGCTC GTCCATGC |

Table 3. Sequencing and screening primers.

| Name | Sequence (5'-3') | Purpose |
|----------------------|----------------------------|--|
| U6-3_seq_F2 | GCTCACCTGTGATTGCTCC | sequencing the gRNAs cloned into pCFD3 |
| dmPLK4 5UTR 1 REV | CATTAGTGAAGATCATTAGCCAGC | sequencing the 5'UTR region of dmPlk4 |
| dmPLK4 5UTR 1 FW | CAAATATATTGGTGATAGTGCAGCCC | sequencing the 5'UTR region of dmPlk4 |
| dmPLK4 5UTR 2 REV | CCGAAACAATGCCTAATGAGATATG | sequencing the 5'UTR region of dmPlk4 |
| dmPLK4 5UTR 2 FW | GGGCTCAGCTTATTGTGGGATCGG | sequencing the 5'UTR region of dmPlk4 |
| dmPLK4 5UTR 3 REV | GCTGGAAAGTGCCTCGAAAATCC | sequencing the 5'UTR region of dmPlk4 |
| dmPLK4 5UTR 3 FW | GGCGTAGAAGCTGATGGATAATTGC | Screening for positive insertions |
| dmPLK4 5UTR 4 REV | GCCGCAGTGTGCCGAACTTTTTCG | sequencing the 5'UTR region of dmPlk4 |
| dmPLK4 5UTR 4 FW | GACGCCGAAGATGCCCAGACTATC | sequencing the 5'UTR region of dmPlk4 |
| dmPLK4 5UTR 5 FW | CCCTCTTTATCGGGCTTGGCATCAAG | sequencing the 5'UTR region of dmPlk4 |
| dmPLK4 (155-177) REV | ACGCGGTTAGTGAGTCCAGTGC | sequencing within the dmPlk4 gene |
| dmPLK4 F 501-521 | TGAGCGCCATATGACCATGT | sequencing within the dmPlk4 gene |
| dmPLK4 (745-768) REV | GGCGGGCGTCCAACCAGCAGGGTG | sequencing within the dmPlk4 gene |
| dmPLK4 1exon Rev | GGAAGCACTTGTTGTGGTCCTGAG | Screening for positive insertions |
| dmPLK4 F 1000 | AATTGCCTTATGAACAGACAGGT | sequencing within the dmPlk4 gene |
| Sak 5 exon R | ATCTCGTAGGCCATCCAATCTCTG | sequencing within the dmPlk4 gene |
| dmPLK4 F 1501-1521 | AAAGTCACATACTTCAGTAC | sequencing within the dmPlk4 gene |

Flies expressing mEGFP-Plk4 and mNeonGreen-Plk4 (from hereon called NG-Plk4) alleles are homozygous-viable and fertile, indicating that both fusion proteins support the rapid cycles of centriole duplication essential during early embryonic development (Rodrigues-Martins et al., 2008). Both endogenous Plk4 fusions localise at the centrosomes of the developing syncytium in a cell-cycle-dependent manner, with highest intensity during S-phase (Figures 2.1 C and D). However, the mEGFP-Plk4 signal is much dimmer and harder to detect than the NG-Plk4. This likely results

from the different photophysical characteristics of the two fluorophores: mNeonGreen is around 2.7 times brighter than mEGFP, due to its higher extinction coefficient (116 vs. 56 mM⁻¹ cm⁻¹) and quantum yield (0.8 vs. 0.6) (Shaner et al., 2013). Since the cytoplasm of the *Drosophila* embryo is filled with autofluorescent particles emitting in the green wavelength range, such as large yolk spheres visible in Figures 2.1 C and D and smaller lipid granules, the overall brightness of the reporter is a critical property in this system, especially when the goal is to image low abundance proteins, such as dmPlk4. We did not find any other differences between the two fly lines and, therefore, we carried on our thorough quantitative characterisation of Plk4 centrosomal dynamics using only the brightest NG-Plk4 line.

2.5.2 Plk4 levels at the centrosome fluctuate in sync with the cell-cycle in early fly development

At the beginning of my thesis, little was known about the regulation of Plk4 localisation at the centrosome along the cell-cycle in the fly embryo. I observed that the levels of dmPlk4 at the centrosome are cell-cycle dependent: the lowest at metaphase, increasing during late mitosis and early S-phase, reaching a peak by mid-S-phase and then declining until nuclear envelope breakdown (Figures 2.2 A –C; see supplementary Video 1; also reported in (Aydogan et al., 2018) with a GFP-Plk4 rescue allele in the Plk4 null mutant background). In fact, NG-Plk4 centrosomal levels show an oscillatory behaviour throughout the nuclear cycles 10-13 in bleach-corrected time-lapses movies, as shown for seven embryos time-aligned at metaphase of nuclear cycle 10 (Figure 2.2 C). Moreover,

the maximum Plk4 intensity in S-phase (i.e., the inflection point in the intensity curves) is not different in cycles 11 to 13 within each embryo (Figures 2.2 B and C - Kruskal-Wallis test, p-value=0.96) suggesting that a similar amount of NG-Plk4 is incorporated at the centrosome each cycle. Even though the genetically identical NG-Plk4 CRISPR fly line has the reporter inserted at the endogenous locus, each embryo expresses slightly different Plk4 levels and has distinct cell-cycle progression. In Figure 2.2 C the curves have different intensity amplitudes and quickly become out-of-phase. Since Plk4 intensity at the centrosome peaks in S-phase and the valleys correspond to mitotic levels, the cell-cycle duration is different between embryos (Figure 2.2 C) and positively correlated with Plk4 centrosomal intensity (Figure 2.2 D - Spearman's rank correlation).

We speculated whether the differences in cell-cycle duration and Plk4 levels at the centrosome are associated with centriole over-duplication, since the later can cause problems in establishing bipolar mitotic spindles and delay mitotic progression (Yang et al., 2008). We observed mitotic defects, mostly tripolar divisions, in all homozygous NG-Plk4 embryos (Figure 2.2 E) and these were less prevalent in heterozygous flies, carrying one wild-type Plk4 copy (data not shown). Such multipolar divisions are likely due to an abnormal (higher) centrosome number, since NG-Plk4 signal is often detected at the poles of the tripolar spindles in early mitosis. However, we did not find any positive correlation between Plk4 intensity at the centrosome and mitotic defects. In fact, the embryos with the highest Plk4 intensity (embryos A and B) show the lowest percentage of mitotic defects in mitosis 10 to 13 (Figure 2.2 E). It is possible that embryos taking longer to cycle have the least mitotic defects because they have enough time to correct them (for e.g.

clustering supernumerary centrosomes into a bipolar spindle), before anaphase onset.

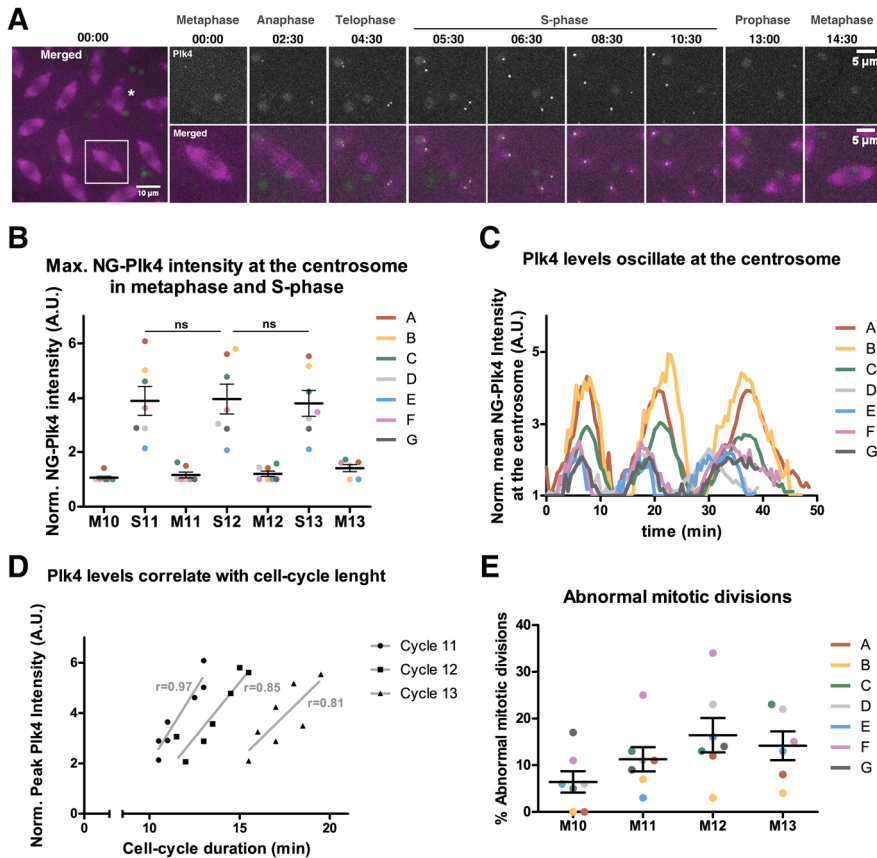


Figure 2.2 – Plk4 levels at the centrosome are cell-cycle dependent. A)

MIPs taken from a time-lapse movie of an early *D. melanogaster* embryo expressing endogenous mNeonGreen-Plk4 (green) and RFP- β -tubulin (magenta). At timepoint $t=0:00$ the embryo is in metaphase of nuclear cycle 11. The insets show the progression of a single nucleus and its daughters, throughout one cell-cycle. The cell-cycle stage is indicated above each image. Time is reported as min:sec. The asterisk indicates an abnormal mitotic spindle. **B)** Maximum mean intensity of NG-Plk4 at the centrosomes recorded during S-phase (“S”) and metaphase (“M”), at nuclear cycles 10 to 13 for seven cycling embryos (A to G). The data is represented as mean

± SEM. The mean maximum intensity of NG-Plk4 recorded in S-phase from cycles 11 to 13 is not statistically different (Kruskal-Wallis non-parametric test, p-value=0.96). **C)** Mean integrated intensity of centrosomal NG-Plk4 from seven cycling embryos undergoing nuclear cycles 10 to 13. At t=0 min all embryos are time-aligned at metaphase of nuclear cycle 10. **D)** Maximum Plk4 intensity at the centrosome positively correlates with cell-cycle duration, determined from the RFP- β -tubulin reporter, in embryos undergoing nuclear cycles 11 to 13 (Spearman's rank correlation coefficient r). In Figures **B** to **E**, for seven homozygous NG-Plk4 embryos (colour-coded A to G) an average of 53, 106 and 198 centrosomes were measured per embryo in S-phase of cycles 11, 12 and 13, respectively. A.U., arbitrary units. **E)** Percentage of abnormal mitotic divisions recorded in mitosis ("M") 10 to 13.

2.5.3 Plk4 single-molecule quantification and cytoplasmic diffusion in syncytial embryos

Having characterised the bulk Plk4 dynamics at the centrosome, we wanted to determine its diffusion and oligomerisation in the cytoplasm. Conventional imaging by spinning-disk confocal microscopy is not sensitive enough for such analysis, so we performed single-molecule Plk4 quantifications in the cytoplasm, using Fluorescent Correlation Spectroscopy (FCS). FCS measures fluctuations in fluorescence intensity caused by particles moving in and out of the focal volume (Figure 2.3 A). It relies on a sensitive detector capable of counting single photons and determining their arrival times (Figure 2.3 B), from which the intensity fluctuations are autocorrelated in time (Figure 2.3 C). Fitting the autocorrelation function (ACF) to a diffusion model allows determining the average number of fluorescent particles (N_0), and how long they take to pass through the observation volume, known

as the characteristic diffusion time τ_D (Figure 2.3 C). If the measurement setup is well calibrated, it is possible to calculate the concentration (Concentration = $N_0/\text{focal volume}$) and oligomeric state of a molecule, based on its brightness (mean intensity per particle = mean trace intensity value/ N_0). Therefore, the ACF represents the time-dependent decay in fluorescence caused by molecules traveling into and out of the observation volume. The travelling time is not only determined by random diffusion but additionally by potential transient interactions with organelles, other molecules, oligomerisation, directionality and volume exclusion. Although the observed diffusion time is characteristic of a given molecule, other intensity fluctuations due to the photo-physical properties of the fluorescent probe bound to it play a role. Different reporters have distinct characteristics such as the on and off rate of blinking, whereby a molecule transits between the bright and dark states (triplet state); photo-stability (some fluorophores bleach faster than others); and brightness, i.e. how many photons they emit per unit time. These properties are unavoidable during FCS measurements and determine the apparent diffusion rate of a labelled molecule. Fast decays in the ACF ($< 10^{-4}$ s) are typically due to photophysical properties of the fluorophore, namely triplet state transitions. Slower decays in the ACF ($> 10^{-4}$ s, usually in the ms range) are typically associated to molecules diffusing in and out of the PSF (**Figure 2.3 C**).

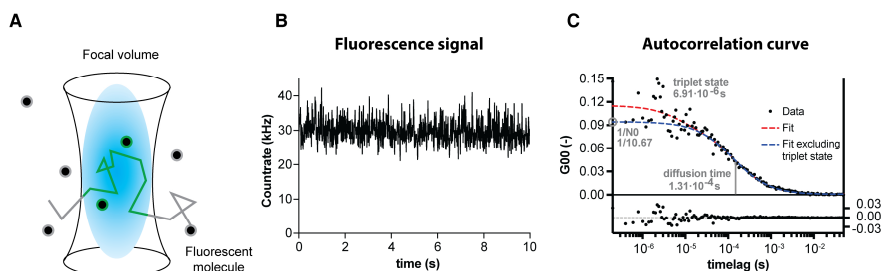


Figure 2.3 – General schematic representation of FCS data acquisition. **A)** Fluorescent particles passing through the focal volume cause fluctuations in fluorescence intensity recorded over time **(B)** and autocorrelated **(C)**, plotted as a function $G(t)$ of the observed timelag τ (in seconds), the ACF. The ACF is fitted to a 3D diffusion model from which the characteristic diffusion time τ_D is calculated and the average number of particles N_0 , the inverse of the y-axis intercept, is estimated. The red curve represents the fit to a diffusion model that includes the triplet state of the fluorophore, resulting in a fast decay in the ACF (6.91×10^{-6} s), followed by a diffusional timescale (1.31×10^{-4} s). The blue curve is the fit to a pure diffusion model (i.e. excluding the triplet state).

Given that FCS had never been performed inside the syncytial fly embryo, our first aim was assessing the ideal conditions - laser excitation power and depth within the sample - to collect the FCS data. We started out by determining the brightness and diffusion of the fluorophores alone, which helped us optimising the conditions to acquire FCS measurements in the whole fly embryo. We conducted FCS measurements with purified monomeric NeonGreen and EGFP in a cytoplasm-compatible buffer (pH=7.8) (Figures 2.4 A - C) and in the cytosol after injection into the syncytial fly embryo (Figures 2.4 D - E). Below 20 μW , both fluorophores in buffer increase their brightness linearly with laser power. However, at higher laser power, their emission saturates and starts deviating from linearity (Figures

2.4 A and B). At even higher laser powers a decrease in the diffusion time indicates that the molecules are bleached before they leave the focal volume (Figures 2.4 A and B). For the fluorophores injected into syncytial fly embryos there was a 2-3 fold loss in fluorophore brightness, even after correcting for the increase in background emission from embryo autofluorescence. This intensity dependent background correction was determined from flies without a Plk4 reporter in the green channel and applied to all subsequent measurements. The high background in the embryos also meant that a minimum 20 μ W excitation was required to properly detect the fluorescence fluctuations in the intensity traces. This probably results from a combination of the excitation light being absorbed as it is focused through the vitelline and cell membranes into the cytosol as well as a similar reduction in emission light caused by diffusing background molecules partly absorbing the fluorescent light on its way back to the objective.

In the cytosol, mEGFP is dimmer than mNeonGreen and, contrary to its behaviour in solution, it barely responds to increasing laser power (Figure 2.4 D). As for mNeonGreen, it increases its brightness with laser power but quickly saturates. Both diffusion times and brightness are maximal at about 50 μ W laser power, but drop at higher power most likely as a result of greater bleaching (Figure 2.4 E). Since mEGFP was much harder to detect, we chose the mNeonGreen as our main reporter.

The ACF determined for mNeonGreen in solution were best fitted with a single component diffusion and while mNeonGreen in the cytosol also only contained a single diffusional component, the ACF was best fitted including an anomaly coefficient. To have a more unbiased determination of the number of timescales, the data was fitted with the Maximum Entropy Method (MEM), which offers a

high-degree freedom in the distribution of diffusing components. The log-normal peaks from the MEMfit (Figures 2.4 C and F – continuous red distributions) describe the probability distribution of timescales in the ACF. The characteristic or most probable timescale were determined from the peak positions. The MEM results were consistent with a single component diffusion both in buffer and in the cytosol (Figure 2.4 C and F), indicating two different timescales, a fast timescale corresponding to the triplet state of mNeonGreen; 9.48×10^{-6} s in solution and shifted to 22×10^{-6} s in the cytoplasm as a results of the larger uncertainty in the ACF fitting; and a slower timescale corresponding to the 3D diffusion of mNeonGreen; measured at 1.59×10^{-4} s in solution and slowed down to 6.54×10^{-4} s in the cytoplasm (Figures 2.4 C and F). The decrease in diffusion is likely caused by greater viscosity in the cytosol. Based on the fact that diffusion scales inversely with viscosity, we can conclude a four-fold increase in viscosity of the cytosol compared to solution, for single mNeonGreen fluorophores freely diffusing.

We also performed measurements of mNeonGreen in the embryo at constant laser power to determine the ideal depth for further FCS experiments (data not shown). Again, we looked for indications of changes in the PSF, i.e. reduction in brightness and diffusion times, as we measured further into the sample. We observed that beyond 5 μ m, the FCS measurements were affected by light scattering and light absorption from the background and, as a consequence, all quantifications were performed at a depth of approximately 5 μ m into the embryo.

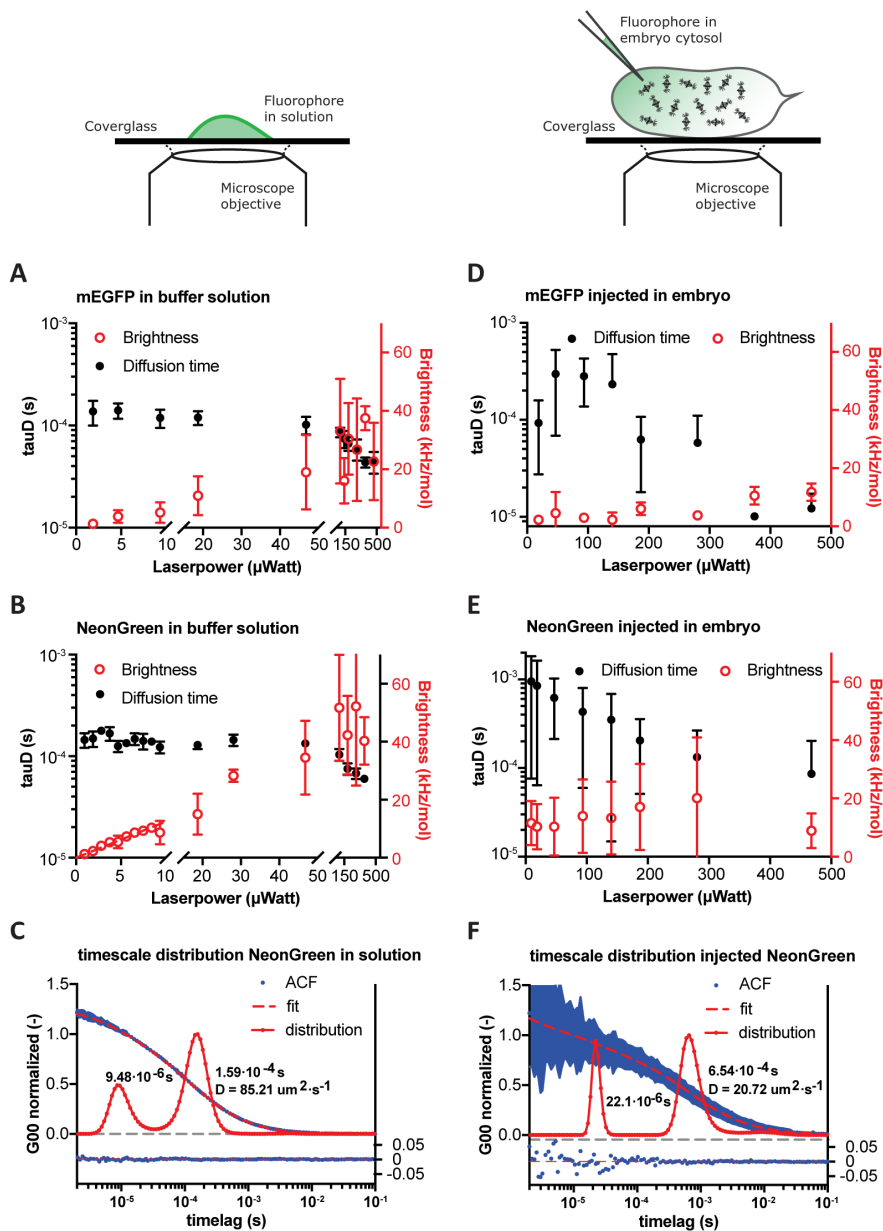


Figure 2.4 – FCS measurements of monomeric fluorophores in solution and in the cytoplasm. A - E) Normalised brightness (red) and diffusion time (black) measured at different excitation powers for mNeonGreen and mEGFP in a cytoplasm-compatible buffer (**A, B**) and injected into the cytosol of the syncytial fly embryo (**D, E**) (mean \pm SD). **C, F)**

F) Normalised fitted Autocorrelation Functions (ACF, blue dots), with standard deviation (shaded area) and Maximum Entropy Method (MEM) fit (red dashed line) and corresponding distributions (red dots and line) for mNeonGreen in solution (**C**) and injected into the cytoplasm (**F**), respectively. The timelags (diffusion times) determined with the two fitting methods agree and are depicted next to the MEM-fit curves. The fast timescale peak corresponds to the triplet state of the fluorophore (9.48×10^{-6} s in solution; 22×10^{-6} s in the cytoplasm), whereas the second slower timescale peak corresponds to the 3D diffusion of mNeonGreen, from which its diffusion coefficient D , was calculated (1.59×10^{-4} s, $D=85.21 \mu\text{m}^2/\text{s}$ in solution; 6.54×10^{-4} s, $D=20.72 \mu\text{m}^2/\text{s}$ in the cytoplasm). The residuals from the fitted data are shown below the graphs.

Since there were no reference studies published at the time, these pilot experiments with mNeonGreen were critical to determine the optimum conditions for FCS acquisition in the whole fly embryo. Using the previously optimised conditions, we analysed the behaviour of homozygous NG-Plk4 in the cytosol. Despite the very low abundance of Plk4 in cells, we could detect bursts of NG-Plk4 fluorescence above the background, measured in RFP::Tubulin flies (Figure 2.5 A). More importantly the NG-Plk4 traces generated clear ACF, whereas the background fluorescence measured in RFP::Tubulin flies did not autocorrelate (Figure 2.5 B). For NG-Plk4, the normalised ACF were best fitted, with minimal residuals, to a two-component diffusion model, which was corroborated by the MEM fit distribution (Figure 2.5 C). The fast triplet state was measured at 7.85×10^{-6} s and two fractions of diffusing NG-Plk4 were detected in the cytoplasm: one faster, diffusing at $17.17 \mu\text{m}^2/\text{s}$ (close to the fluorophore alone) and another slower, diffusing at $1.49 \mu\text{m}^2/\text{s}$. Based on the increase of hydrodynamic radius (R_h) alone, the

diffusion coefficient of NG-Plk4 in the cytosol should scale with molecular weight (MW) as $\sim MW^{1/3}$. With the molecular weight of mNeonGreen being 26.6 kDa and Plk4 around 86 kDa, NG-Plk4 monomers should have a diffusion coefficient of about $12 \mu\text{m}^2/\text{s}$. Assuming a similar relationship for the slower diffusion coefficient of $1.49 \mu\text{m}^2/\text{s}$, a self-oligomerisation in the order of 530 molecules would have to occur to explain the measurements. This is not supported by the intensity traces which never show bursts of that amplitude (Figure 2.5 A, note that there are no intensity bursts several orders of magnitude higher than others). While this implies the absence of self-oligomers in the order of hundreds, the timescales can still be suggestive of Plk4 assembling in large scale structures. On the other hand, it can also be evidence of Plk4 undergoing restrictive mobility due to its binding to a quasi-immobile substrate. Such immobile structure cannot be the centrosome since this would produce a massive disruption in the intensity count-rates while going through the focal volume and, as a consequence, it would not give rise to a proper ACF.

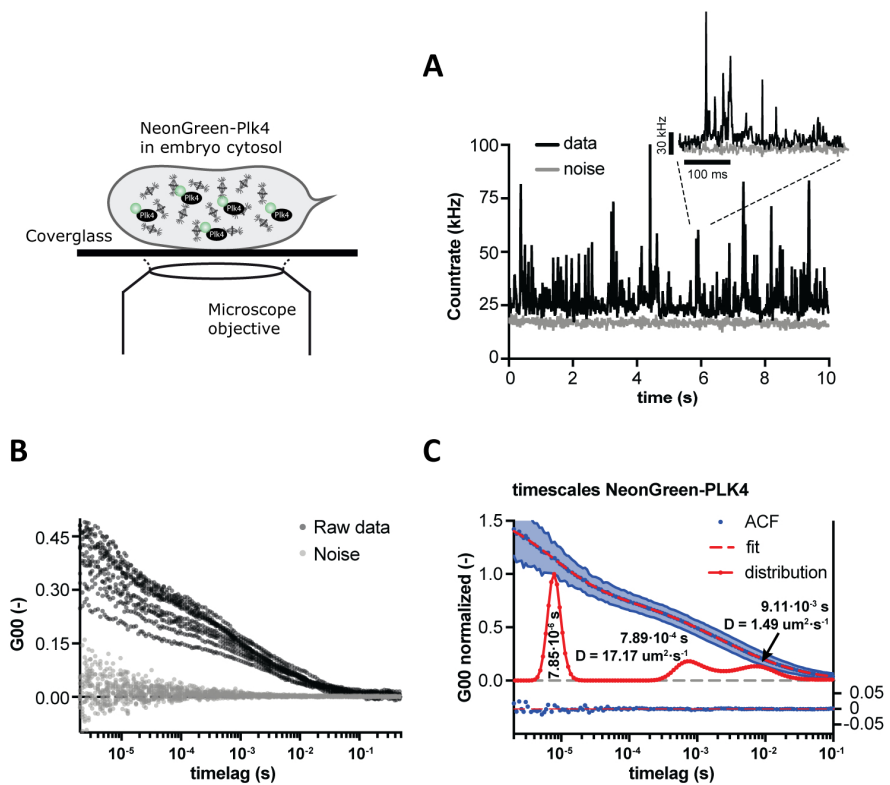


Figure 2.5 – Single-molecule mNeonGreen-Plk4 quantifications in the cytosol of the syncytial fly embryo. A) NG-Plk4 and background (noise) intensity traces and **B)** raw ACFs from multiple independent FCS measurements. **C)** Normalised fitted ACF, with standard deviation (“fit” – red dashed line) and MEM distributions (“distribution” – red line) for NG-Plk4 in the cytoplasm. Based on the two fitting methods, three timescales were determined: the fastest timescale peak corresponds to the triplet state of the fluorophore ($7.85 \times 10^{-6} \text{ s}$); whereas the second and third slower timescales correspond to distinct 3D diffusional mobility of NG-Plk4 in the cytoplasm, from which the Diffusion coefficients (D) were calculated (fastest fraction: $7.89 \times 10^{-4} \text{ s}$, $D = 17.2 \text{ } \mu\text{m}^2/\text{s}$; slower fraction: $9.11 \times 10^{-3} \text{ s}$, $D = 1.49 \text{ } \mu\text{m}^2/\text{s}$). The residuals from the fitted data (“fit”) are shown below the graphs.

We confirmed that the presence of two diffusing Plk4 fractions was not an artefact caused by the fluorophore by analysing mEGFP-Plk4 mobility. Despite the poor signal/noise of mEGFP in the cytosol, we could also detect a second (4.49×10^{-4} s) and a third (7.55×10^{-3} s) timescale corresponding to two distinct diffusing mEGFP-Plk4 pools (Figure 2.6).

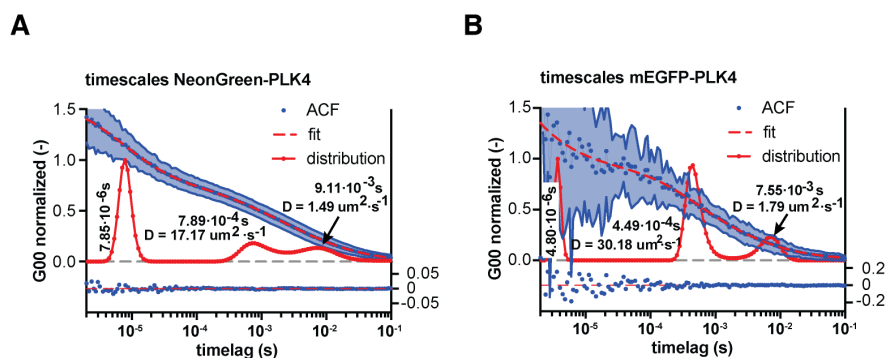


Figure 2.6 – Single-molecule mNeonGreen-Plk4 and mEGFP-Plk4 quantifications demonstrate that two different Plk4 fractions move in the cytosol of the syncytial fly embryo. Normalised fitted ACF (blue dots), with standard deviation (shaded area) and MEM fit (red dashed line) and distributions (red dot-line) for NG-Plk4 (**A**) and for mEGFP-Plk4 (**B**) in the cytoplasm. Based on the two fitting methods, three timescales were determined for Plk4 tagged with the two different green reporters: the fastest timescale peak corresponds to the triplet state of the fluorophore (7.85×10^{-6} s for mNeonGreen, 4.80×10^{-6} s for mEGFP); whereas the second and third slower timescales correspond to distinct 3D diffusional mobility of Plk4 in the cytoplasm, from which the Diffusion coefficients (D) were calculated. The fastest pool shows a timescale of 7.89×10^{-4} s and $D = 17.2 \mu\text{m}^2/\text{s}$, when coupled to mNeonGreen; and 4.49×10^{-4} s and $D = 30.2 \mu\text{m}^2/\text{s}$; when labelled with mEGFP. The slower pool has a timescale of 9.11×10^{-3} s and $D = 1.49 \mu\text{m}^2/\text{s}$ tagged with mNeonGreen; and 7.55×10^{-3} s and $D = 1.79$

$\mu\text{m}^2/\text{s}$ tagged with mEGFP. The residuals from the fitted data (“fit”) are shown below the graphs.

Next, we calculated the total concentration of NG-Plk4 in the cytosol and determined its oligomeric state using the brightness of the injected NeonGreen monomer as a reference. Plk4 concentration in the cytosol is about 7.55 nM (which coincidentally matched the final concentration of injected fluorophore) and moves in the cytosol as an oligomer (mean brightness of 16.51kHz per NG-Plk4 particle compared to 8.75kHz per mNeonGreen monomer). Nevertheless, even though FCS is a single-molecule technique that allows determining the brightness per molecule, these calculations are derived from traces of 10 s duration. In other words, the resultant brightness per molecule is in fact the average brightness of all the molecules that travelled through the focal volume during the 10 s long measurement. This suggests that, on average, Plk4 is detected self-associated into low-order oligomers, forming dimers to tetramers at most although the exact distribution is still unclear (Figure 2.7).

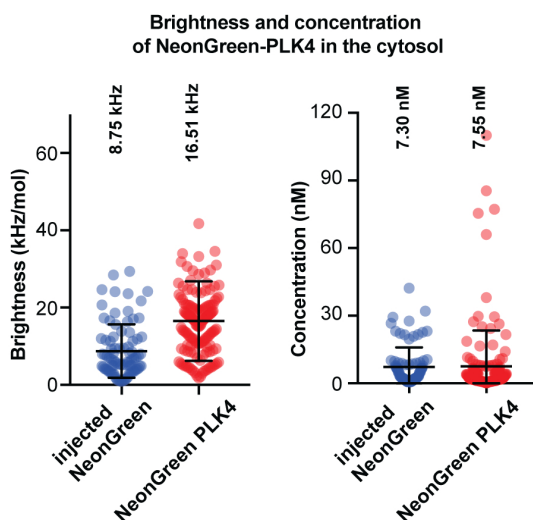


Figure 2.7 – Plk4 oligomerises in the cytosol of the *Drosophila* blastoderm embryo. Normalised NG-Plk4 brightness (intensity per particle) in the cytosol is higher than the single mNeonGreen monomer injected into the cytosol (mean \pm SD), even though they were measured at a similar concentration, indicating that Plk4 is not only present as a monomer but it also associates into low-order oligomers (from dimers to tetramers).

Finally, we wanted to investigate the dual mobility of Plk4 in the cytosol and understand the origin of the second fraction, diffusing at about $1.49 \mu\text{m}^2/\text{s}$. Knowing that *Xenopus* Plk4 interacts with the microtubules (MTs) (Montenegro Gouveia et al., 2018) and that perhaps these can be involved in Plk4 transport to the centrosome, we performed microtubule depolymerisation experiments by injecting Nocodazole into the NG-Plk4 embryos. Both DMSO (control) and Nocodazole treated embryos display two diffusing pools, present at similar fractions as the untreated NG-Plk4 (Table 4). The two pools in DMSO-treated embryos diffuse at similar speeds as in the untreated embryos (Figure 2.8 A, Table 4). In the Nocodazole perturbation both diffusion timescales are about three-fold slower, at $6.10 \mu\text{m}^2/\text{s}$ and $0.48 \mu\text{m}^2/\text{s}$, respectively (Figure 2.8 B; for easier comparison see Table 4). The brightness (intensity per particle) of NG-Plk4 decreases upon Nocodazole treatment, analogous to the injected fluorophore with regards to intensity (Figure 2.7), suggesting that MT depolymerisation causes Plk4 to dissociate into monomers. The concomitant increase in the concentration of Plk4 from 7.55 nM to 18.49 nM can be a result of Plk4 oligomer dissociation and/or due to the dissociation of Plk4 from MT filaments. The increase in concentration, nevertheless, discards the hypothesis that the decrease in brightness is a result of NG-Plk4 dilution upon volume increase caused by the injection of the drug. It

is possible that both Plk4 fractions bind to MTs but the fast diffusing pool binds more transiently, whereas the slower pool establishes stable interactions, hence becoming almost immobile. Upon MT depolymerisation, both fractions unbind MTs and self-dissociate, moving slower and increasing the overall Plk4 cytoplasmic concentration. More experiments are required to confirm this hypothesis. We cannot exclude the possibility that MT depolymerisation changes cytosol viscosity by increasing the concentration of free tubulin, thereby slowing down the mobility of all components diffusing in the cytoplasm.

Despite the bulk cell-cycle oscillations in Plk4 centrosomal localisation observed by live-imaging (supplementary Video 1), such S-phase-mitosis-S-phase transitions were not detected by FCS in the cytosol when comparing FCS measurements acquired during S-phase vs. mitosis (data not shown). This may be explained by the fraction of Plk4 molecules that localise at the centrosome being too low to impact the overall Plk4 concentration in the embryo's cytoplasm. It would also be indicative that the Plk4 concentration at the onset of embryogenesis is sufficient to drive multiple rounds of centriole biogenesis.

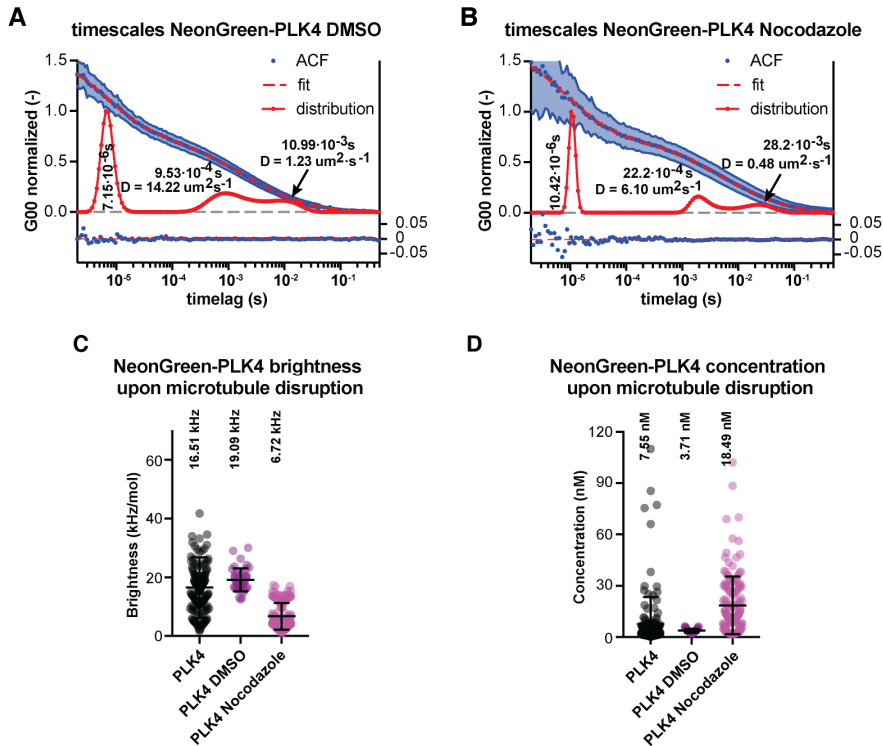


Figure 2.8 – Microtubule depolymerisation slows down the diffusion of both mNeonGreen-Plk4 fractions in the cytosol. ACF (blue dots) with standard deviation (shaded area) and MEM fit (red dashed line) and distributions (red dot-line) for NG-Plk4 in DMSO treated embryos (control) **(A)** and in embryos where microtubules were depolymerised with Nocodazole **(B)**. **A)** Three different timescales were observed, the fast one corresponding to the triplet state of mNeonGreen and two diffusing NG-Plk4 pools (fastest fraction: 9.53×10^{-4} s, $D=14.2 \mu\text{m}^2/\text{s}$; slower fraction: 11×10^{-3} s, $D=1.23 \mu\text{m}^2/\text{s}$) having similar diffusion as the untreated embryos shown in Figure 2.5. **B)** In embryos treated with Nocodazole, three different timescales are also determined but the two diffusing NG-Plk4 components are slower (fastest fraction: 22.2×10^{-4} s, $D=6.10 \mu\text{m}^2/\text{s}$; slower fraction: 28.2×10^{-3} s, $D=0.48 \mu\text{m}^2/\text{s}$). The residuals from the fitted data (“fit”) are shown below the graphs. **C)** Normalised mNeonGreen-Plk4 brightness (intensity per particle) in the cytosol decreases upon Nocodazole treatment, suggesting it dissociates becoming mostly a monomer (similar brightness as the

injected fluorophore in Figure 2.7). **D)** The monomerising effect of Nocodazole on Plk4 is accompanied by an increase in its overall concentration in the cytosol from 7.55 nM in untreated to 18.5 nM in the presence of the drug.

Table 4. Parameters determined from the model-based fittings. Total number of measurements and embryos analysed and diffusion model applied to each experimental condition. According to the model, either one or two diffusion components were determined and their characteristic timescales and diffusion coefficients calculated. The fraction of each diffusing pool is presented as a percentage.

| | # of measurements/ # of embryos | Diffusion model | timescale 1 (ms) | Diffusion coeff 1 ($\mu\text{m}^2/\text{s}$) | Fraction of D1 (%) | timescale 2 (ms) | Diffusion coeff 2 ($\mu\text{m}^2/\text{s}$) | Fraction of D2 (%) |
|--------------------------------|------------------------------------|--------------------------|---------------------|---|--------------------|---------------------|---|--------------------|
| mNeonGreen in solution | 24 | 1 component 3D | 0.15 | 85.2 | 100 | | | |
| mNeonGreen in the cytosol | 85 / 9 | 1 component anomalous 3D | 0.65 | 20.7 | 100 | | | |
| mNeonGreen-Plk4 in the cytosol | 147 / 11 | 2 component 3D | 0.79 | 17.2 | 52.3 | 9.11 | 1.49 | 47.7 |
| mNeonGreen-Plk4 + DMSO | 41 / 4 | 2 component 3D | 0.95 | 14.2 | 58 | 11 | 1.23 | 42 |
| mNeonGreen-Plk4 + Nocodazole | 146 / 6 | 2 component 3D | 2.22 | 6.1 | 58.6 | 28.2 | 0.48 | 41.4 |

2.6 Discussion and Conclusions

Plk4 plays a central role in centriole biogenesis and yet, due to its very low concentration in cells (Bauer et al., 2016), neither the localisation, nor the levels, nor in *in vivo* dynamics of the endogenous protein have been reported in *Drosophila melanogaster*. Here, we labelled the endogenous *Drosophila* Plk4 and characterised its localisation at the centrosome throughout the cell-cycle. We provide the first estimations of its concentration in the cytosol and present evidence that it forms low-order oligomers, which possibly associate with cytoplasmic microtubules (MTs). We discuss the implications

that our findings may have regarding Plk4 centrosomal localisation and activity and, most importantly, for the regulation of centriole biogenesis.

In this study, we have produced fly lines in which the endogenous Plk4 is labelled with fluorescent reporters at its N-terminus, between the 5'UTR and the first coding exon. Experiments with the endogenous Plk4 are challenging, not only because this is a low abundance protein, but also because its oligomerisation regulates both kinase activation and protein turnover (Cunha-Ferreira et al., 2013; Guderian et al., 2010; Holland et al., 2012b; Klebba et al., 2013; Lopes et al., 2015). These properties of Plk4 conditioned our choice of reporter; we selected the fluorophores with superior photophysical properties (brightest and more photostable) that, importantly, had undergone thorough monomerising enhancements. Flies with mEGFP or mNeonGreen (Myatt et al., 2017; Shaner et al., 2013) inserted at Plk4 endogenous locus are homozygous-viable but nevertheless show some mitotic defects during early development, which may be caused by centrosome amplification and establishment of multipolar mitotic spindles (Figure 2.2 E). We speculate that these defects result from either imposed steric hindrance or residual dimerisation of the fluorescent tags, despite their monomerising mutations. For most proteins in the cell, a low oligomerisation tendency does not necessarily give rise to a detectable phenotype. However, in the case of Plk4, numerous evidences indicate that this protein is extremely sensitive to any structural alterations, affecting its physiology and in our case probably triggering mild centriole overduplication. An alternative explanation for the centrosome amplification is that Plk4 expression is slightly altered in these flies upon the insertion of the fluorophore coding sequence between Plk4 5'UTR and the first exon. There are

evidences suggesting that the length of the 5'UTR region flanking the beginning of Plk4 coding sequence affects the levels of protein expression in the cell (Holland 2017, personal communication).

Despite our efforts, mEGFP-Plk4 is barely detectable both at the centrosome, by time-lapse imaging and in the cytosol, using FCS (Figure 2.1, Figure 2.4 D, Figure 2.6 B). It seems that, in a system with high autofluorescence emission in the green channel such as the embryo, any improvement in brightness has a large impact on protein detection (mNeonGreen is reportedly 2.7 times brighter than mEGFP (Shaner et al., 2013)). Plk4 localisation at the centrosome undergoes cell-cycle dependent oscillations (also reported in (Aydogan et al., 2018) with a rescue GFP-Plk4 construct under the endogenous promoter in the Plk4 null mutant background), reaching higher levels in S-phase, when centrioles duplicate and lower, often undetectable, levels during mitosis. Interestingly, the total centrosomal Plk4 amount incorporated in S-phase is similar every nuclear cycle for each embryo, suggesting that its centrosomal loading is well-regulated, which might be critical for the numerical and spatial control of pro-centriole assembly. Aydogan et al. 2018 proposed a role for Plk4 in centriole elongation in *Drosophila* embryos, so it is possible that the regulation of Plk4 centrosomal levels is relevant in two ways: to form only one pro-centriole per mother and to ensure that these grow to a constant size every embryonic division. Plk4 centrosomal loading is detected already in telophase (Figure 2.2 A), possibly priming centrioles for duplication in the next cycle, similar to what has been suggested in human cells (Zitouni et al., 2016). In the fly embryo, the centrosome cycle is different from somatic cells: centrosomes separate before pro-centriole formation, which may relate to Plk4 levels peaking at a different cell-cycle stage, i.e., not in mitosis like it has been observed

in murine and *Drosophila* S2 cells (Cunha-Ferreira et al., 2009; Fode et al., 1996; Rogers et al., 2009; Winkles and Alberts, 2005).

The peak in Plk4 centrosomal intensity is followed by a sharp decrease in its fluorescence, which perhaps results from the molecules being hyper-phosphorylated after their concentration and activation at the centrosome, hence triggering Plk4 degradation, possibly even at the centrosome. Centrosomal-localised protein degradation has been proposed for Cyclin B (Clute and Pines, 1999; Huang and Raff, 1999) and Nek2 (Hames et al., 2005), via the 26S proteasome, which also participates in Plk4 degradation (Cunha-Ferreira et al., 2009; Fode et al., 1996). The 26S proteasome and several of its activating regulators localise at the centrosome (Fabunmi et al., 2000; Wigley et al., 1999), where they potentially provide a local balance between protein enrichment and their timely degradation. For Plk4, this might offer an acute way of regulating its kinase activity in a cell-cycle that is extremely fast. However, Plk4 may also be de-localised from the centrosome due to a conformational change or loss of binding affinity with centrosomal molecules.

Finally, we observed that Plk4 expression levels are stochastic, despite the lines being genetically identical. Some embryos express more NG-Plk4 than others (Figure 2.2 B–D), which correlates with the duration of the cell-cycle (Figure 2.2 D), but not with the incidence of mitotic defects (Figure 2.2 E). This phenotypic variation is possibly due to epigenetic regulation or natural noise in transcription and translation and it has been moderately studied in other experimental models such as mice (Oey et al., 2015; Pritchard et al., 2006) and zebrafish (Román et al., 2018) but surprisingly has been poorly addressed in flies.

By means of FCS measurements, and using two independent data-fitting methods, we have found two distinct mobile species of fluorescently tagged Plk4 in the embryo cytosol with very different diffusion coefficients (Figure 2.5 C and Figure 2.6). A faster Plk4 pool diffuses at a speed closer to the mNeonGreen fluorophore alone, and a second pool diffuses much slower. This two-component diffusion was observed in two different Plk4 reporter lines, indicating that it is unlikely a consequence of the tag (Figure 2.6).

The fast Plk4 pool we detected is a lot faster than human Polo-like-kinase 1 (Plk1), measured by FCS in RPE1 cells. While NG-Plk4 diffuses at about $17.2 \mu\text{m}^2/\text{s}$, EGFP-Plk1, reportedly diffuses at about $6.6 \mu\text{m}^2/\text{s}$ in the cytosol (Mahen et al., 2011). EGFP-Plk1 mobility is proposed to be restricted, at least in the centrosome vicinity. Interestingly, MT depolymerisation decreases NG-Plk4 mobility down to $6.1 \mu\text{m}^2/\text{s}$, adopting a similar diffusive behaviour as Plk1 (Mahen et al., 2011).

The slowly diffusing Plk4 fraction is unlikely a consequence of oligomerisation because the measured timescale would imply Plk4 assembly into a very high-order oligomer (~530 molecules). This second fraction also moves slower in the presence of Nocodazole. Besides oligomerisation, what are the alternative explanations for the reduced mobility of NG-Plk4 upon Nocodazole treatment? NG-Plk4 could be slowed down due to alterations in the cytosolic material properties (for e.g. increase in viscosity) or because it establishes stable interactions with large scaffolds such as multiprotein complexes. The Nocodazole is dissolved in DMSO, a solvent that reportedly increases cytoplasmic viscosity (Yu and Quinn, 1994) and changes lipid stability in a concentration-dependent manner (Gurtovenko et al., 2007). We did observe a delay in NG-Plk4 mobility upon injection of pure DMSO but the

changes were much stronger in the presence of Nocodazole (Figure 2.8; Table 4), which indicates that MT depolymerisation itself causes an effect. We do not know how an overall MT depolymerisation impacts the physico-chemical properties of the cytoplasm so we cannot exclude that a bulk increase in free tubulin has an effect on Plk4 mobility. It would be important to conduct the Nocodazole experiment just with the injected fluorophore and assess if its diffusion also changes accordingly. Another alternative, is that perhaps the two types of mobility correspond to: 1) a fraction that moves rapidly along the MTs (at $17.2 \mu\text{m}^2/\text{s}$ and slowing down to $6.1 \mu\text{m}^2/\text{s}$ when MTs are depolymerised); and a 2) different pool that remains fairly static, perhaps confined, through the stable binding to cytoplasmic MT or large MT-interacting complexes (Figure 2.8). One last hypothesis is that the fast NG-Plk4 is monomeric, freely diffusing at similar speed as the mNeonGreen fluorophore alone. The second, slower pool is oligomeric and establishes long-lived interactions with MTs within large macromolecular complexes, continuously binding/unbinding MTs in the cytosol. From a more mechanistic perspective, the slow oligomeric pool may be clustered in a MT-dependent manner and primed to drive centriole formation, whereas the fast monomeric pool of Plk4 may be capable of easily supplying (inactive) molecules to an already active “seed”. We have not established whether MTs are involved in direct Plk4 recruitment to the centrioles. Moreover, Plk4 transport to the centrosome via MTs has to be confirmed with complementary measurements of NG-Plk4 intensity at the centrosome after MT-depolymerisation since, in most cell-types, cytoplasmic MTs are also nucleated and anchored at other organelles besides the centrosome (Wu and Akhmanova, 2017).

However, this is one of the outstanding questions in the field which deserves further investigation, particularly in the large fly embryo cell where MTs might facilitate Plk4 transport over longer distances into the vicinity of the centrosome.

We estimated Plk4 concentration in the cytosol to be 7.55 nM confirming that it is a very low abundance protein, as repeatedly mentioned in the literature. Our estimations agree with Plk4 concentration in human cells (around 4000 copies per cell; ~2 nM) measured by quantitative Mass-Spectrometry in whole-cell lysates (Bauer et al., 2016). For reference, Sas6 concentration, another low-abundance centrosomal protein, varies between 100 and 300 nM in human cells depending on the cell-cycle stage (Keller et al., 2014).

Comparing NG-Plk4 brightness (intensity per particle) in the cytosol to the injected NeonGreen monomer indicates that Plk4 forms low-order oligomers in the cytosol, in the order of dimers to tetramers (Figure 2.7). However, it is unlikely that the fast Plk4 fraction corresponds to monomers and the slower to oligomers, as the difference in the diffusion coefficient would require a much larger Plk4 oligomer to be assembled in the cytosol to explain a magnitude difference. This suggests that, at endogenous levels, Plk4 only assembles into large-scale scaffolds at the centrosome. Since Plk4 full activation depends on its *trans*-auto-phosphorylation and oligomerisation (Lopes et al., 2015), the low-order self-interaction in the cytosol might prevent Plk4 activation outside the centrosome and regulate the location of pro-centriole formation, restricting Plk4 activity to the centrosomal compartment.

Following this study, the next logical steps would be to do Fluorescence recovery after photobleaching (FRAP) analysis of Plk4 at the centrosome to further understand its kinetics of binding and unbinding to the centrioles, in combination with MT

depolymerisation. Finally, we would like to simultaneously analyse Plk4 diffusion in the cytoplasm and its centrosomal loading, by Raster Image Correlation Spectroscopy (RICS) to better understand which mechanism and what modulates Plk4 localisation at the centrosome throughout the cell-cycle.

2.7 Acknowledgements

We would like to thank the Central Imaging and Flow Cytometry Facility (CIFF) at the National Centre for Biological Sciences (NCBS) in Bangalore, where all FCS experiments were done.

We thank Tiago Bandeiras at Instituto de Biologia Experimental e Tecnológica (IBET), Oeiras, for the gel filtration chromatography conducted in his facility.

Chapter 3

**An ex vivo system to study de novo
centriole biogenesis in *Drosophila
melanogaster* eggs**

3.1 Author Contribution

This experimental system was originally developed by my supervisor Ivo Telley in Telley *et al.* 2013. In this Chapter, I describe how I tailored it to study centriole biogenesis with help from Jorge Carvalho, a Post-Doc fellow at Telley's Lab. The 3D-SIM acquisitions were done with David Pointu from OMX. I conducted the sample preparation for the Electron Microscopy (EM) validation with Sara Bonucci, from IGC's EM Facility led by Erin Tranfield, and Sara did the EM processing and image acquisition.

3.2 Summary

Centriole duplication is a highly regulated process that occurs once and only once per cell cycle. The synchronization between centriole duplication and segregation with the cell-cycle, ensures that cycling cells retain a normal centrosome number. However, centriole number and size vary among different organisms and cell-types. For instance, animal oocytes are devoid of centrioles and upon fertilisation the sperm centriole recruits pericentriolar material (PCM) components deposited by the mother, establishing a functional centrosome. Remarkably, centrosomes can also form *de novo* in eggs, either by spontaneous MTOC formation in species that develop parthenogenetically or artificially, upon cytoplasmic activation or overexpression of Polo-like kinase 4 (Plk4). The spatial and temporal dynamics of *de novo* centriole formation are poorly known, mostly because previous studies lacked the appropriate techniques to look into this process live.

Here we have developed a cell-free assay to investigate centriole biogenesis live by confocal microscopy, at high temporal

and spatial resolution. This system relies on the production of cytoplasmic explants from single *Drosophila melanogaster* eggs overexpressing Plk4. We chose the best suited fluorescent reporters available and optimized imaging conditions to accomplish a reliable centrosome detection in the cytoplasm. Finally, we validated the assay using other microscopy techniques and confirmed that the centrosomes that form in the explants bear centrioles at their core and undergo canonical duplication in these explants.

3.3 Introduction

Centrosomes are the main microtubule organising centres (MTOCs) in animal cells. Centrosomes usually comprise a pair of centrioles surrounded by a protein network called pericentriolar material (PCM). The PCM is indispensable for microtubule nucleation and centriole biogenesis. In proliferating cells, centrosomes duplicate only once per cell cycle, whereby a single daughter forms orthogonally to a mother centriole.

Loss of centrosomal MTOC activity and centriole elimination are hallmarks of cell specialization. For e.g., centrioles are eliminated in animal oocytes during oogenesis and in myoblasts during skeletal muscle differentiation (reviewed in (Cunha-Ferreira et al., 2009)). Interestingly, despite losing their centrioles, oocytes retain most pericentriolar proteins which, after fertilisation, complement the centriole from the sperm giving rise to a functional MTOC. In some biological systems centrioles form *de novo*, without any centriole being previously present in the cell. This process occurs naturally in organisms that lack centrosomes during their life-cycles and only assemble centrioles to form cilia. That is the case of plants that produce ciliated sperm (Renzaglia and Garbary, 2001),

planarians that only assemble centrioles in terminally differentiated ciliated cells (Azimzadeh et al., 2012), amoebae species such as *Naegleria gruberi* undergoing amoeboid to flagellate transition (Dingle and Fulton, 1966; Fritz-Laylin et al., 2016; Fulton and Dingle, 1971) or even several species of motile parasitic alveolates (Francia et al., 2016; Grimes, 1973a; Grimes, 1973b; Sinden et al., 1976; Sinden et al., 1978); reviewed in (Nabais et al., 2018)).

Interestingly, *de novo* centrosome formation can also trigger parthenogenetic development in some insect species that develop without male contribution. In the wasps *Nasonia vitripennis* and *Muscidifurax uniraptor* (Riparbelli et al., 1998; Tram and Sullivan, 2000) and in the fly *Drosophila mercatorum* (Riparbelli and Callaini, 2003), unfertilised eggs form multiple centrosomes spontaneously at the cortex of the egg at late stages of meiosis. When two of these asters interact with the female pronucleus they initiate normal egg development to adulthood.

Centrioles can also form *de novo* after artificial perturbations. Vertebrate cells are capable of assembling centrioles after their centrosomes have been physically removed or laser ablated. Eggs from sea urchin and surf clam can form multiple centrosomes *de novo* when artificially activated (Dirksen, 1961; Kato and Sugiyama, 1971; Kuriyama et al., 1986; Miki-Noumura, 1977; Palazzo et al., 1992; Schatten et al., 1985). Finally, Plk4 upregulation drives *de novo* centriole biogenesis in unfertilised *Drosophila* eggs (Rodrigues-Martins et al., 2007) and *de novo* assembly of MTOC structures in *Xenopus* egg extracts (Eckerdt et al., 2011; Montenegro Gouveia et al., 2018). The spatial and temporal dynamics underlying *de novo* centriole assembly have never been characterized *in vivo* due to the lack of an appropriate system to study this process. For many species, their genome is not properly annotated and have very

limited genetic tools, making it difficult to dissect the molecular mechanisms governing cellular processes. Additionally, large volume samples, such as animal eggs, cannot be easily visualized by live cell imaging due to optical constraints. As a consequence, the mechanisms have been mostly inferred by looking at fixed samples, which lack adequate information on the dynamical changes happening throughout centriole formation *in vivo*.

Here, we have established a novel assay to visualize and study centriole *de novo* biogenesis live, based on genetic constructs previously made by Rodrigues-Martins et al. 2007 and other genetically encoded tools, readily available for *Drosophila melanogaster*. We take an *ex vivo* approach that allows isolating and live imaging small cytosolic volumes from a single unfertilised fly egg overexpressing PLK4 specifically in the germline. The volume reduction herein obtained allows comparatively fast time-lapse imaging together with diffraction-limited spatial resolution. Moreover, being a cell-free system without cellular boundaries, this experimental approach is most suitable for drug perturbations, protein titration and mixing cytosol from different genetic backgrounds.

Although this assay has previously been described (Telley et al., 2013), we have optimised it to study centriole biogenesis. Additionally, this protocol had only been applied to fertilised fly embryos, so we first had to test if it would also work with cytosol extracted from unfertilised eggs. Next, we had to define a strategy to drive centriole *de novo* biogenesis, either by adding recombinant *Drosophila* Plk4 to the cytosol or overexpressing Plk4 genetically. Finally, we tested centriolar and centrosomal markers as MTOC reporters and optimised the imaging conditions for the best centrosome detection in 4D, providing a proof-of-concept that this

system can be applied to answer a variety of questions regarding centriole assembly.

3.4 Materials

3.4.1 Fly strains and fly husbandry

This procedure required optimised practices of fly husbandry to ensure that during the course of the experiments, virgin females laid a good amount of unfertilised eggs. Fly stocks were reared according to standard procedures and maintained at 25 °C. Germline-specific Plk4 overexpression was accomplished using the Gal4-UASp system. This system is based on the yeast transcriptional activator Gal4 and the Gal4 responsive Upstream Activating Sequence (UAS), and allows the expression of proteins in specific tissues or cell types by crossing transgenic flies carrying a gene of interest under a UAS promoter with flies expressing a Gal4 driver under a tissue specific promoter. Flies carrying the pUASp-Plk4 (Upstream Activation Sequence promoter) construct, previously cloned in the lab and injected at BestGene Inc., were crossed with V32-Gal4 (*w**; *P{maternal-atubulin4-GAL::VP16}V2H*) flies (kindly provided by Dr. Daniel St Johnston) driving dmPLK4 overexpression in the female germline (Rørth, 1998). Two different combinations of genetic reporters were tested to select the most robust one for centrosome visualization: i) pUb-Spd2::GFP (Homemade, BestGene Inc.) in combination with endogenous-Jupiter::mCherry, as a reporter for centrosomal microtubule activity (gift from Daniel St Johnston, (Lowe et al., 2014)); and ii) pUASp-endogenous-promoter-Ana1::tdTomato (gift from Tomer Avidor-Reiss, (Blachon et al., 2008)) with endogenous-Jupiter::mGFP (*P{PTT-GA}JupiterG00147*, (Morin et al., 2001)). Around a hundred virgin females, overexpressing Plk4

and a combination of centrosomal fluorescent reporters in the germline, were transferred to a cage coupled to an apple juice agar plate supplemented with fresh yeast-paste. Several cages were maintained at 25°C, under 50-60% humidity, and the plates were changed every 3 to 4 hours. While fertilised females typically reach their optimal egg laying peak within the first week after their eclosure, we realised that virgin females lay very few eggs during the first week but increase this number during the second week. Thus, the experiments were performed with mature females.

3.4.2 Glass coverslips and capillaries preparation

Glass coverslips and capillaries (0.75mm inner diameter, 1 mm outer diameter, Sutter Instrument) were cleaned following the protocol described in 2.4.2. Capillaries were washed individually by passing ethanol and water through their opening, using a wash bottle. Clean coverslips were functionalized with Poly-L-lysine solution 0.01 % (PLL, Sigma-Aldrich) for 20 minutes, followed by multiple dip-drain-washes in milliQ water. The coverslips were spin-dried and stored in a clean and dry rack. The PLL treatment is stable for up to 2 weeks, after which the glass surface becomes too hydrophilic for extract deposition. Clean capillaries were forged into glass needles by pulling them on a vertical pipette puller (Narishige PC-10), using a one-step pulling protocol, at 55% heating power. Using a sharp scalpel, the tip of the capillary was cut into a 25-35 μm diameter pointed aperture (Telley et al., 2013).

3.4.3 Embryo collection and sample preparation

On the day of the experiment, the plate of the cage was regularly replaced. Freshly laid unfertilised eggs (20 minutes collections) were recovered from virgin females and dechorionated according to the protocol in section 2.4.3. For these experiments, eggs were aligned side-by-side in the same anterior-posterior orientation so that, once installed on the microscope, the posterior side of all eggs point at the extraction pipette. The eggs were immobilised on the coverslip slightly off-centred, leaving the centre clean for extract deposition and imaging, and they were covered in halocarbon oil (Voltalef oil 10S from VWR).

3.5 Methodology

3.5.1 Extract preparation

Once set up on the microscope, the eggs were inspected using the 20x objective in transmission light mode. Freshly laid eggs were chosen based on the presence of wide perivitelline gaps at the anterior and posterior poles, which is caused by cytoplasm retraction in very early embryos and eggs (Campos-Ortega and Hartenstein, 1997). A desired egg and a sharp glass needle were positioned at the same focal plane and, with a swift pipette movement, the egg was punctured through the vitelline membrane at its posterior end. The cytoplasm with its components was immediately aspirated, carefully controlling the flow rate using a microfluidics syringe pump. The extraction was completed by inverting the pump direction and inverting the pressure in the syringe until the flow in the pipette completely stopped. The pipette was withdrawn from the egg and

the microscope stage moved so the field of view showed a clean area on the glass coverslip. Then, small droplets of cytoplasm were deposited on the PLL-functionalized glass surface by gently pressing the micropipette against the surface and regulating the flow rate in the syringe pump. By operating the micromanipulator up and down the Z-axis and moving the stage in XY, multiple droplets were deposited on the glass surface, forming explants under halocarbon oil, which prevents dehydration of the cytoplasm (see Figure 3.1A). A step-by-step detailed protocol was originally published in (Telley et al., 2013) and, more recently, in (de-Carvalho et al., 2018). The size of the droplets was empirically decided and manually controlled by operating the syringe pump. The goal was to produce droplets between 40 to 80 μm in diameter, fitting the confocal field of view at 60x magnification, allowing high-resolution time-lapse imaging of the entire volume. The complete procedure from extraction to deposition takes less than two minutes.

3.5.2 Time-lapse explant imaging on the spinning disk confocal microscope

After extract deposition, the droplets were inspected in confocal fluorescence mode to detect the presence of centrosomes. At this stage, the aim was to find an explant that lacked any detectable signal from both fluorescence reporters and, thus, was initially devoid of centrosomes. Only one such explant per egg extraction was selected and monitored by time-lapse imaging. Over time, multiple centrosomes formed *de novo*, filling the droplet and allowing us to visualize the very early steps of centriole assembly.

The acquisition settings were optimised to collect images at high spatio-temporal resolution while avoiding excessive bleaching and phototoxicity. Phototoxicity is particularly striking in these explants because the cytoplasmic volumes are small, rapidly accumulating reactive oxygen ions produced during exposure to light. Laser intensity and camera exposure were lowered to the minimum while allowing image acquisition of the full volume of the explant and robust MTOC detection. Time-lapse acquisition of individual droplets was done on a Plan Apo VC 60x 1.2 NA water objective with an Andor iXon3 888 EMCCD camera. To circumvent the problem of water evaporation over an extended time course, we used Cargille Laser liquid oil immersion media, which has the same refractive index as water. Optical sections of 0.45 μm were acquired on a Yokogawa CSU-W1 Spinning Disk confocal scanner using a piezoelectric Z-stage (PI 737.2SL), installed on a Nikon Eclipse Ti-E microscope. Dual-colour (488 nm and 561 nm excitation laser lines), 15 seconds time-lapses were recorded in Andor IQ3 software. Multi-stack, time-lapse calibrated images were deconvolved with Huygens (Scientific Volume Imaging, The Netherlands) using a Point Spread Function (PSF) automatically calculated from the data set and run in batch mode, for each channel separately. 32-bit deconvolved images were converted to 16-bit and processed using Fiji (NIH (Schindelin et al., 2012)). Fluorescence intensity quantifications were conducted in Maximum intensity projections (MIPs) and graphic representations were performed using Prism 7 (GraphPad Software). Selected stills from the time-lapse acquisitions were processed with Photoshop CS6 (Adobe). Final schemes were produced using Illustrator CS6 (Adobe).

3.5.3 3D-Structured Illumination Microscopy

Cytoplasmic droplets were imaged with a Plan Apo 60x NA 1.42 oil objective on a GE HealthCare Deltavision OMX system, equipped with two PCO Edge 5.5 sCMOS cameras and 488 nm and 568 nm laserlines. Spherical aberrations were minimised by matching the refractive index of the immersion oil to that of the cytosol, providing the most symmetrical point spread function. 15 seconds, multi-stack time-lapses were acquired, with 0.125 μm Z-steps and 15 frames (three angles and five phases per angle) per Z-section. Images were reconstructed in Applied Precision's softWorx software and processed using Fiji (NIH, (Schindelin et al., 2012)). Selected stills were assembled into final figures with Photoshop CS6 (Adobe).

3.5.4 Correlative Light Electron Microscopy

The day before processing, 1.5mm MatTek glass gridded bottom dishes were coated with 2% 3-Aminopropyl-Trimethoxysilane (APES), diluted in acetone, to improve the attachment of the sample to the dish. The dishes were incubated with 2% APES for 15 minutes and then rinsed thoroughly under running tap water for 5 minutes. They were left at 37°C overnight to dry out. For the light microscopy analysis, four to five unfertilised eggs overexpressing Plk4 and expressing centrosomal markers were placed in the middle of a MatTek dish and burst with a fine tungsten needle. The membranes were pushed aside and the cytosol was immediately covered in 2.5 μL of 4% Formaldehyde in 0.1M Phosphate Buffer to start the pre-fixation. The samples were quickly examined at the spinning-disk confocal microscopy to check the quality of the cytosol (evidence of dehydration) and for the

presence of the fluorescent centrosomal reporters. Good samples were carefully fixed, adding another 20 μL of 4% Formaldehyde in 0.1M Phosphate Buffer and incubating for 1 hour at RT. After the pre-fixation, the samples were incubated at 37°C for another 30 minutes, and carefully washed twice with 150 μL of 0.1M Phosphate Buffer, making sure the cytosol did not detach from the glass. Next, the samples were imaged at the confocal microscope for a final quality control and determining the positions of interest within the sample, using the alphanumeric pattern printed on the MatTek dish. The samples were then fixed with 2.5% Glutaraldehyde in 0.1M Phosphate Buffer, for 20 minutes at RT and processed for transmission electron microscopy analysis. After fixation, the samples were washed twice in 0.1M Phosphate Buffer. Post-fixation was done with 1% Osmium Tetroxide and 0.8% Potassium Ferrocyanide in 0.1M Phosphate Buffer, for 30 minutes, on ice, followed by washes in 0.1M Phosphate Buffer and distilled water. Samples were then stained with 0.5% Uranyl Acetate in distilled water, for 1 hour, at RT, in the dark, followed by a graded series of ethanol. At this point, using a small needle, the glass was detached from the dish and flipped on top of a BEEM capsule with 100% EPON. Polymerization was done at 60°C, overnight.

Correlation between the two techniques was done prior the sectioning. 100 nm sections were taken using a diamond knife, on a Leica Ultramicrotome, and post-stained with Uranyl Acetate and Lead Citrate. Image acquisition was done in a 120kV Hitachi H-7650 Transmission Electron Microscope. Images were processed using Fiji (NIH, (Schindelin et al., 2012)).

3.6 Results and Discussion

Over recent years, a tremendous progress in the optical microscopy field has pushed the boundaries of biological imaging towards higher spatial resolution and the observation of cellular processes *live*. Yet, for most optical techniques, imaging within axial depth is limited, making it impossible to observe events that take place deep inside large volume samples as in the case of the fruit-fly embryo. Here, we have described a cell-free assay that solves this limitation by generating cell cortex-free micro-scale explants that can be fully visualized and that retain the native characteristics of the cytoplasm *in vivo* (Figure 3.1).

A major challenge in this study is centriole size, which is very close to the resolution limit caused by the diffraction of visible light, rendering centrioles hard to detect and distinguish from background fluorescence by optical microscopy. After testing more than one protein reporter and tinkering the image acquisition parameters, we were capable of observing *live* the onset of centriole assembly in the cytoplasm and follow centrosome dynamics over time.

As an open system, the extract system facilitates chemical manipulation by mixing of components dissolved in a cytoplasm-compatible buffer. Initially, our plan was to add recombinant *Drosophila* Plk4 to the extract of wild-type unfertilised eggs and record centriole biogenesis. However, we were unsuccessful at purifying highly concentrated and active protein. Consequently, we resorted to a different strategy to upregulate Plk4 in eggs: using the same inducible pUASp-Plk4 genetic construct created in Rodrigues-Martins et al. 2007, we accomplished a strong protein expression in the female germline. We confirmed that this construct was functional by driving its expression with the V32-Gal4 and checking female

fertility: fertilised embryos laid by V32-Gal4/pUASp-Plk4 females did not develop, indicating that the Plk4 genetic construct is being properly overexpressed (Rodrigues-Martins et al., 2007). The *Drosophila* egg is ideal to study centriole assembly since all the proteins necessary to make 2¹³ centrosomes are maternally inherited and, in the absence of fertilisation, centrioles are not present in the cell. These aspects motivated us to conduct our experiments in unfertilised eggs, whereby any centrosomes observed would inevitably result from *de novo* formation and not from centriole amplification of the paternally inherited centrioles. Next, we proceeded to analyse centrosome behaviour by confocal optical microscopy using Ana1::tdTomato; Jupiter::mGFP or Spd2::GFP; Jupiter::mCherry genetic reporters. We performed cytoplasmic extractions from single unfertilised eggs overexpressing Plk4 and deposited small explants on the glass surface (Figure 3.1 A). Then, we recorded centrosome biogenesis within individual droplets by fast time-lapse acquisitions (one droplet per egg) (Figure 3.1 B).

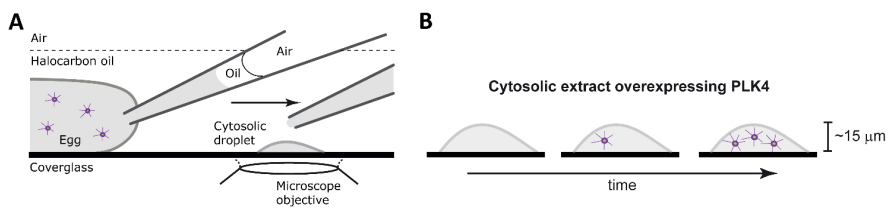
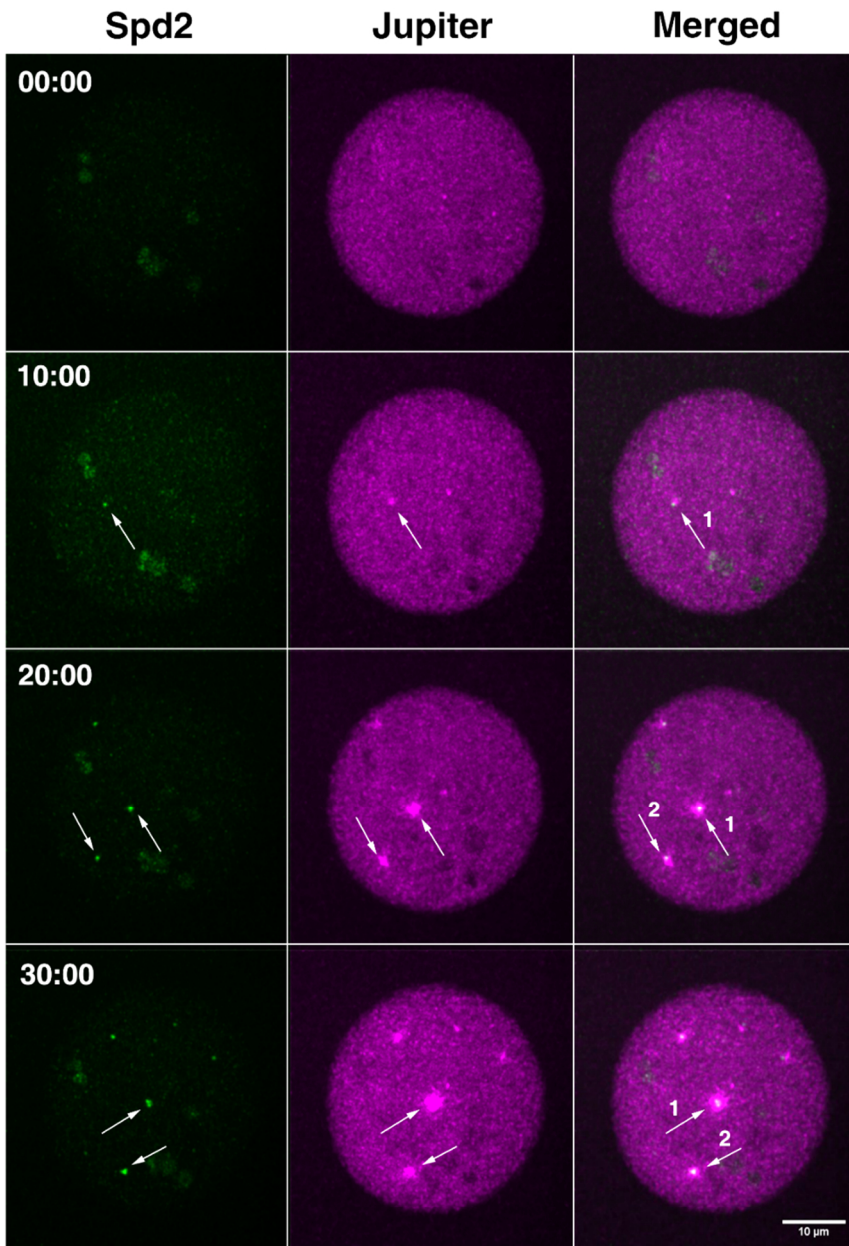


Figure 3.1 – Schematic representation of the extraction procedure and time-lapse acquisition. A) After rupturing the cell membrane with a sharp micropipette, the egg cytoplasm is carefully aspirated. Flow direction is inverted to deposit small cytosolic droplets on the functionalized coverglass. The entire procedure is conducted under halocarbon oil so that the cytoplasm does not come in contact with air. **B)** Schematic time-lapse of an explant isolated from a *Drosophila* egg overexpressing PLK4.

Centrosomes are absent in the first time point and form *de novo* throughout the experiment.

Ideally, we would have preferred working with a centriolar marker (Ana1) instead of a PCM component (Spd2) but the choice of reporter was conditioned by signal intensity and its consistency (stable across samples). By comparing time-lapse acquisitions from different egg samples (Figures 3.3 and 3.4), we found that the intensity of the Ana1 signal is variable between eggs and impossible to detect in some acquisitions. We speculate that this might be a consequence of some genetic interaction of the maternal Gal4 with the UAS sequence present in the Ana1::tdTomato transgene. In addition, the signal intensity is dimmer for Ana1::tdTomato than for the Spd2::GFP reporter. Normalised intensity quantifications for the two first centrosomes formed *de novo* in the explant reported by Ana1::tdTomato or by Spd2::GFP revealed that both signals increase over time but Ana1 intensity is considerably lower than Spd2 (compare fold-change to background in graphs from Figures 3.2 and 3.3). As centrosomes mature in explants, they incorporate more centrosomal markers (Ana1 and Spd2) and recruit more PCM, increasing their MTOC capacity, as reported by the Jupiter signal (Figures 3.2, 3.3 and 3.4). All centrosomes formed in these explants are stable, they are not eliminated (at least within the first hour of the process) and are capable of duplicating (notice centrosome insets 1 and 2 in Figure 3.2 and inset 1 in Figure 3.3 and supplementary Video 1).



10:00 20:00 30:00

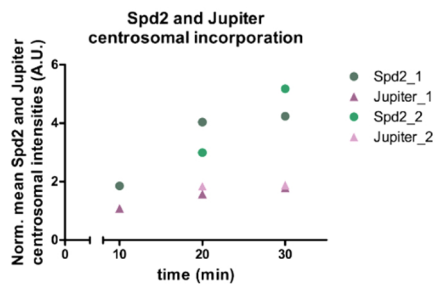
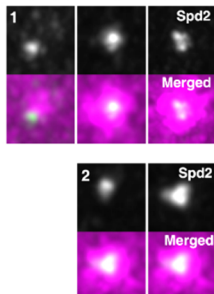


Figure 3.2 – Visualization of centrosome biogenesis in a *Drosophila* egg extract, reported by Sdp2::GFP and Jupiter::mCherry. Maximum intensity projections (MIPs) from a time-lapse video following *de novo* centrosome biogenesis in an explant overexpressing Plk4. Arrows depict the first and second centrosomes formed *de novo*, for which normalized mean centrosomal intensities are plotted as fold-change increase over time. Time is reported as min:sec.

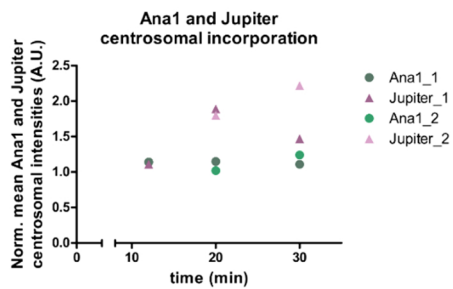
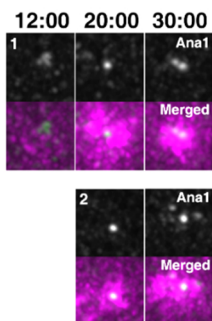
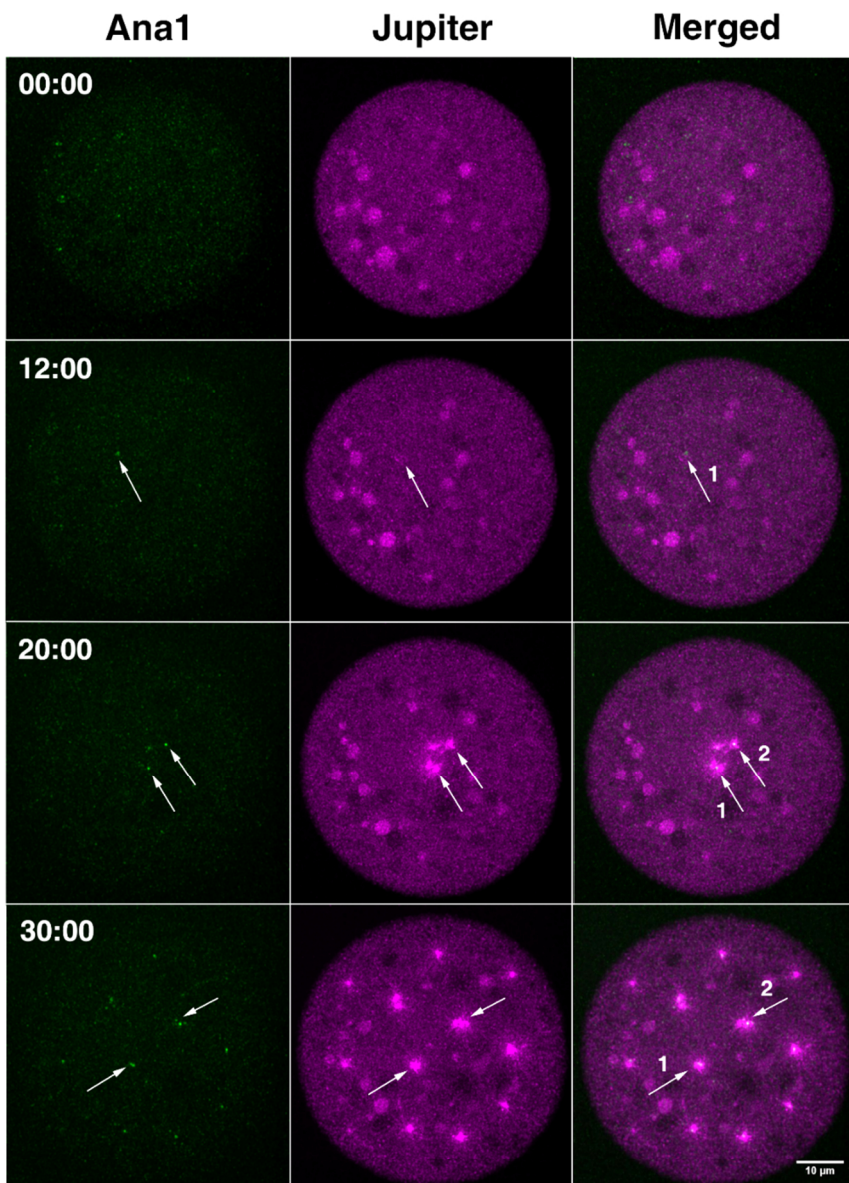


Figure 3.3 – Visualization of centrosome biogenesis in a *Drosophila* egg extract, reported by Ana1::tdTomato and Jupiter::GFP. MIPs from a time-lapse video following *de novo* centrosome biogenesis in an explant overexpressing Plk4. In this acquisition, the Ana1::tdTomato fluorescence signal is detectable. Arrows depict the first and second centrosomes formed *de novo*, for which normalized mean centrosomal intensities are plotted as fold-change increase over time. Time is reported as min:sec.

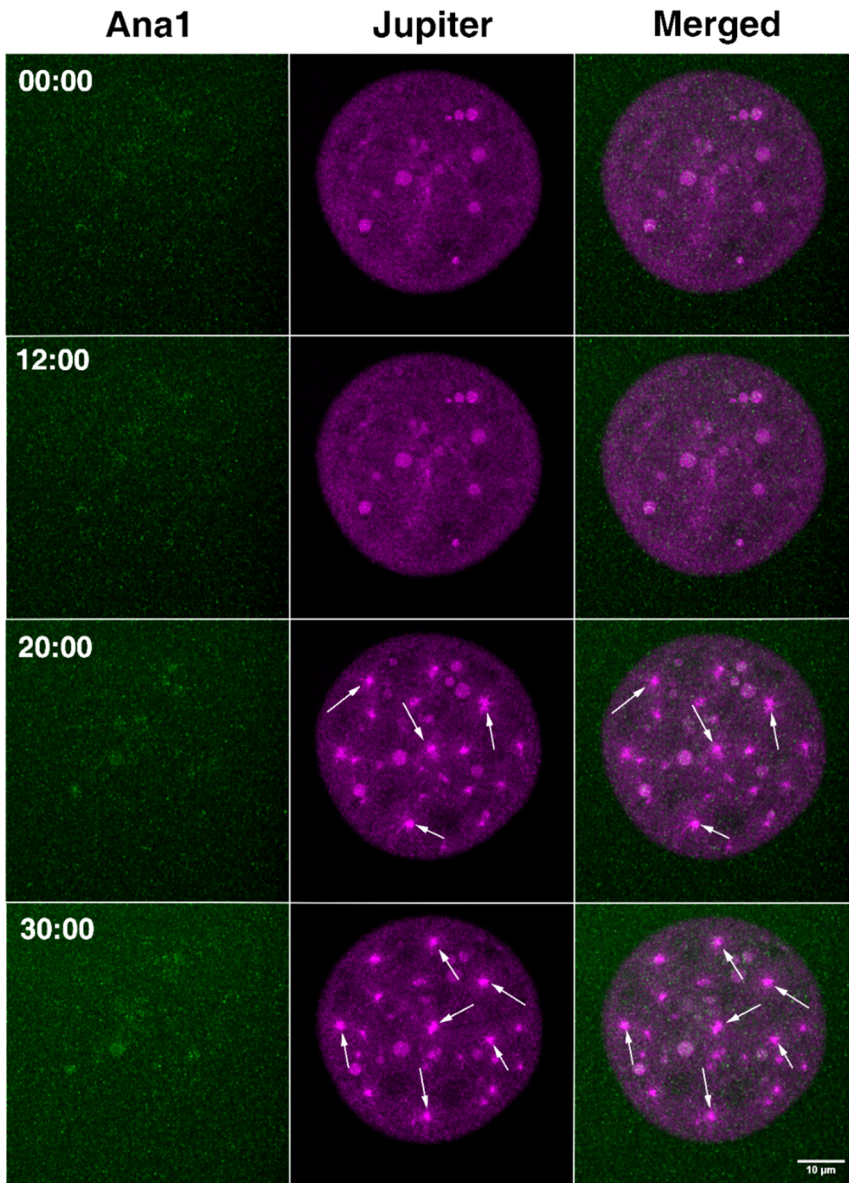


Figure 3.4 – Visualization of centrosome biogenesis in a *Drosophila* egg extract, reported by Ana1::tdTomato and Jupiter::GFP. MIPs from a time-lapse video following *de novo* centrosome biogenesis (arrows) in an explant overexpressing Plk4. In this acquisition, the Ana1::tdTomato fluorescence signal is undetectable. Time is reported as min:sec.

Since the Spd2::GFP signal is brighter and more photostable, we chose it as our routine centrosomal reporter and proceeded to validate centriole formation by 3D-Structured Illumination Microscopy (SIM), which has approximately twice the spatial resolution of conventional confocal microscopy. Spd2::GFP visualised by 3D-SIM forms a ring at the centre of the MT asters, with an inner diameter of about 230-320 nm in longitudinal sections (Figure 3.5, Insets). Spd2 also forms toroids at the centrosome in *Drosophila* syncytial embryos, whereby Spd2 projections extend from a central hollow, which presumably contains a centriole (Conduit et al., 2014).

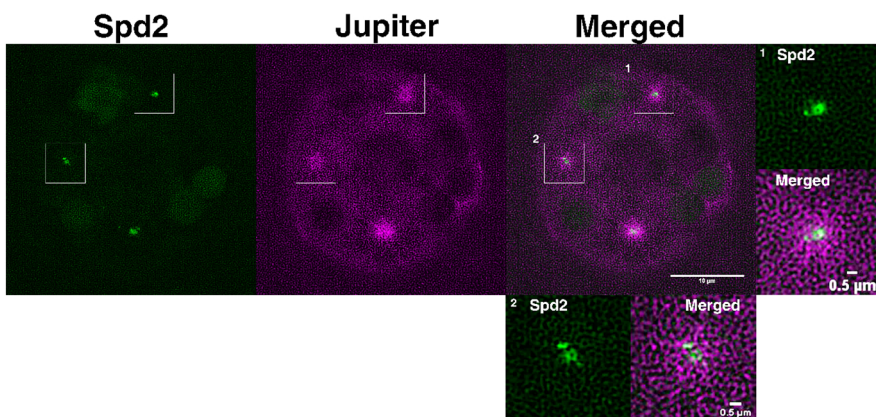


Figure 3.5 – Visualization of centrosome biogenesis in a *Drosophila* egg extract by 3D-SIM. MIPs from a time-lapse following *de novo* centrosome biogenesis in an explant overexpressing Plk4. Centrioles (insets) are detected as barrel-shaped structures surrounded by the PCM component Spd2. These centrioles can duplicate multiple times.

Validation by Electron Microscopy (EM) had previously been performed in intact eggs overexpressing Plk4, confirming the assembly of structurally normal centrioles (Rodrigues-Martins et al.,

2007). In our case, EM validation was not possible to conduct in the droplets since the explants are imbedded in mineral oil, which is not compatible with sample processing. Instead we fixed and processed the whole cytoplasm from eggs ruptured in 0.1M Phosphate Buffer with 4% Formaldehyde to pre-fix the cytosol.

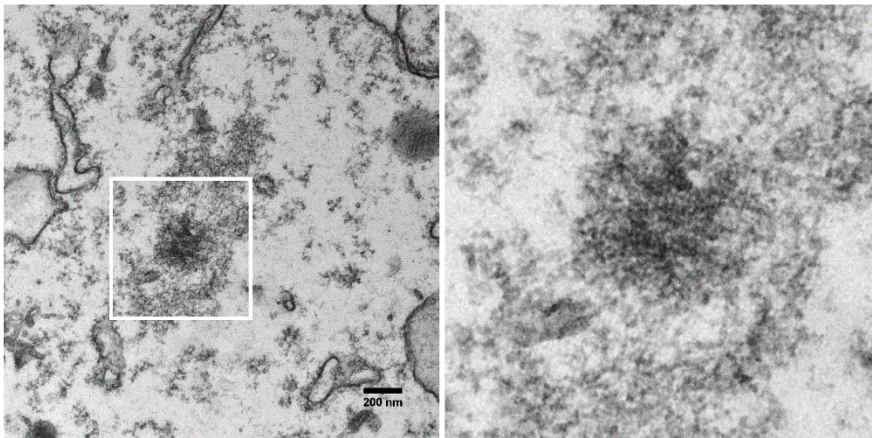


Figure 3.6 – The MTOCs formed *de novo* in the cytoplasm seem to contain centrioles. *De novo* formed centrosomes contain centriolar-like structures, as assessed by transmission electron microscopy. The right-hand side panel is a higher magnification of the left image inset.

We validated by 3D-SIM (Figure 3.5) and transmission EM (Figure 3.6) that the centrosomes detected by optical microscopy appear to contain centrioles at their core, establishing this single egg extract system as a successful method to understand the principles underlying centrosome *de novo* biogenesis. Moreover, 3D-SIM imaging confirmed that smaller daughter centrioles form adjacently to older centrioles that first formed *de novo*, indicating that centriole duplication also occurs in this system (Figure 3.5 insets).

Cellular extracts have been widely used to answer fundamental questions in cell biology, revealing emergent biological properties that cannot be well-understood from *in vitro* reconstitutions. At the same time, they provide a reductionist approach, removing the constraints brought by a selective cell membrane cortex and the large volume of the fly egg/embryo. The generation of multiple explants from a single fly egg provides the ideal experimental scenario for perturbations, as some explants serve as internal controls, originated from the same egg/cytoplasmic source.

Having this system fully working allows us to test different hypotheses concerning centrosome biology. How is *de novo* biogenesis spatially and temporally regulated? What is the role of the cytoskeleton? What are the critical Plk4 levels to drive centriole biogenesis? What is the interplay between canonical duplication and *de novo* biogenesis? What spatial cues do centrosomes respond to? These and other questions can be answered by biochemical manipulations adding drugs or recombinant proteins, by mechanical perturbations via physical boundaries and manipulation with cantilevers, in combination with optical perturbations such as laser ablation and optical activation/inactivation of protein kinases, phosphatases, molecular motors and drugs (Bergeijk et al., 2016; Van Bergeijk et al., 2015; Zhou et al., 2017).

3.7 Acknowledgements

We would like to thank the technical support of IGC's Advanced Imaging Facility (AIF-UIC), which is supported by the national Portuguese funding ref# PPBI-POCI-01-0145-FEDER-

022122, co-financed by Lisboa Regional Operational Programme (Lisboa 2020), under the Portugal 2020 Partnership Agreement, through the European Regional Development Fund (FEDER) and Fundação para a Ciência e a Tecnologia (FCT; Portugal).

We acknowledge S. Bonucci and E.M. Tranfield from the Electron Microscopy Facility at the Instituto Gulbenkian de Ciência for sample processing and imaging. We acknowledge Tomer Avidor-Reiss and Daniel St Johnston for sharing with us the *Ana1::tdTomato* and the *w**; *maternal- α tubulin4-GAL::VP16* fly lines, respectively.

Chapter 4

Spatial and Temporal kinetics of de novo centriole assembly in unfertilised eggs

4.1 Author Contribution

All experiments were planned and executed by myself, supervised by Mónica Bettencourt-Dias and Ivo Telley, and in collaboration with Dr. Jorge Carneiro at Instituto Gulbenkian de Ciência in Oeiras, Portugal. I was helped by Jorge Carvalho while conducting complex experiments at the microscope. Delphine Pessoa, a PhD student supervised by Jorge Carneiro, did the statistical analyses and modelling from the experimental data.

4.2 Summary

In cycling cells, centrosome formation via canonical duplication is spatially, temporally and numerically regulated by the presence of mature centrioles in the cell. However, in several eukaryotic cell-types, centrioles assemble *de novo*, yet very little is known regarding the regulation of this process. Overexpression of Polo-like kinase 4 (Plk4) triggers *de novo* assembly of multiple centrioles in the cytosol of unfertilised *Drosophila* eggs. We took advantage of this to establish an *ex vivo* assay in which we produce small cytosolic explants suitable for live-imaging, allowing us to dissect the factors underlying centriole *de novo* assembly and investigate how it is spatially and temporally regulated. Surprisingly, we found that both canonical duplication and *de novo* pathways happen in parallel within the same cytoplasmic explant, at their own temporal kinetics suggesting that, under the conditions we tested, each process does not inhibit the other. We followed centriole *de novo* biogenesis over time and determined where and when these formed in the droplets. Comparing our observations to stochastic models demonstrated that recently formed centrioles do not impact the location where new centrioles assemble *de novo*, at high levels of Plk4 overexpression.

Based on the time lag between centriole birth, Asl incorporation and their duplication, we hypothesise that the spatial independency may result from centrioles being immature and initially lacking the right amount of components. We have observed that after an initial temporal delay, centrosomes assemble at a rapid rate that accelerates over time. This burst in biogenesis is not explained by a cell-cycle dependent mechanism but, instead, Plk4 concentration and probably its activation, seems to be the main driving force regulating the process. Diluting Plk4 concentration causes a longer delay in the birth of the first centrosome but it does not strongly impact the spatio-temporal assembly of the following events, indicating that the apparent acceleration in centriole assembly is likely a consequence of local Plk4 concentration and auto-activation, driving centriole biogenesis in several places independently. Altogether, these results show that Plk4 levels are critical in controlling the onset of centriole *de novo* formation and its temporal kinetics.

4.3 Introduction

Centrioles and Basal Bodies (CBBs) are microtubule-based structures that assemble centrosomes and cilia. These organelles play multiple functions in cells, from sensing environmental cues to cell motility, cytoskeleton remodelling, establishing cell polarity and division. The centrosome is the major microtubule organising centre (MTOC) in most animal cells. Each centrosome has two cylindrical centrioles, surrounded by a non-membrane-bound compartment containing hundreds of proteins organised in layers - the pericentriolar material (PCM). The PCM is responsible for anchoring

and nucleating microtubules. CBBs also nucleate motile and immotile cilia.

Cells regulate CBBs biogenesis to ensure they assemble at the right place, time and number. Failure in regulating this process can cause problems in cell division and produce cellular defects associated to several human diseases. CBBs form via different pathways, of which the best characterised is centriole duplication, also called canonical biogenesis. Following this pathway, centrioles assemble in G1 to S transition of the cell-cycle, whereby a single procentriole forms at the proximal side of each of the two mother centrioles (reviewed in (Breslow and Holland, 2019; Nigg and Holland, 2018)). This process entails that the location, timing and number of procentrioles assembled are determined by existing centrioles ((Banterle and Gönczy, 2017; Breslow and Holland, 2019)). The two daughter centrioles elongate throughout S and G2 phases and, in late G2, centrioles undergo centriole-to-centrosome conversion; i.e. they lose the cartwheel (in vertebrate cells), recruit more PCM components and become competent for duplication in the next cycle (Fu et al., 2016; Izquierdo et al., 2014; Wang et al., 2011). After mitosis, one centrosome is segregated to each daughter cell.

Canonical biogenesis is coupled to the cell-cycle, ensuring that CBBs form only once and cells maintain a correct centriole number while proliferating. However, centriole biogenesis can occur through non-canonical pathways, for example, in multiciliated cells that undergo massive centriole amplification in the presence of resident centrioles (deuterosome-mediated biogenesis) or *de novo* centriole formation, where centrioles assemble in the absence of centrioles in the cell/organism (reviewed in (Nabais et al., 2018)). Even though these modes of biogenesis are widespread in eukaryotic organisms, little is known in terms of their regulation and evolutionary origin.

De novo CBB biogenesis is a naturally occurring process in amoebae species undergoing amoebae to flagellated life transition (best studied in *Naegleria gruberi*) (Dingle and Fulton, 1966; Fritz-Laylin et al., 2016; Fulton and Dingle, 1971); in some land plants that produce flagellated sperm (Renzaglia and Garbary, 2001), in protists that also alternate between centriolar and acentriolar (cysts) life-cycle phases (Grimes, 1973a; Grimes, 1973b) and in parthenogenic insects that develop without fertilisation (Riparbelli and Callaini, 2003; Riparbelli et al., 1998; Tram and Sullivan, 2000). In most animals, centrioles are lost during female oogenesis and are brought by the sperm upon egg fertilisation. However, in some hymenoptera and diptera species that develop parthenogenetically, centrioles form *de novo* in the egg without sperm contribution (Riparbelli and Callaini, 2003; Riparbelli et al., 1998; Tram and Sullivan, 2000).

Previous studies have proposed that the *de novo* assembly pathway is generally inhibited in cells when centrioles are present. *Chlamydomonas reinhardtii* carrying a mutated copy of the centrin gene, have defects in centriole segregation giving rise to progeny without centrioles that, within one or two generations, reacquires centrioles *de novo* (Marshall et al., 2001). The fast rate at which centrioles form *de novo* suggested that when present, centrioles negatively regulate the *de novo* pathway and play a dominant role in biogenesis, whereas in their absence centrioles readily form *de novo* (Marshall et al., 2001). In acentriolar somatic human cells, centrioles also assemble *de novo* efficiently within few cell-cycles (La Terra et al., 2005; Lambrus et al., 2015; Uetake et al., 2007) and the presence of a single centriole appears to be enough to suppress further *de novo* biogenesis (La Terra et al., 2005; Lambrus et al., 2015). These studies in *Chlamydomonas* and human cultured cells suggest that existing centrioles sequester activating molecules that

drive centriole biogenesis, thus directly or indirectly inhibiting the activity of those components in the cytosol and suppressing *de novo* centriole assembly (Lambrus et al., 2015; Marshall et al., 2001).

Is there any temporal, spatial and numerical regulation behind *de novo* centriole biogenesis? Do existing centrioles antagonise the *de novo* pathway and if so, how do they accomplish that? Tackling these questions requires generating centrioles *de novo* in a controlled system, suitable for spatial and temporal characterisation of the process and experimental perturbations, such as the *ex vivo* assay described in Chapter 3.

Polo-like kinase 4 (Plk4) is a master regulator of centriole biogenesis. Levels of active Plk4 in the cell must be tightly regulated to maintain a correct centriole number and a normal cell-cycle. Plk4 overexpression is sufficient to drive both centriole overduplication close to existing centrioles and *de novo* biogenesis in the cytosol, when centrioles are absent in the cell or when its concentration is very high (Lopes et al., 2015; Peel et al., 2007; Rodrigues-Martins et al., 2007). This suggests that Plk4 operates in terms of non-linear thresholds: there is a critical threshold for the formation of a single centriole but if Plk4 concentration is high, it surpasses the threshold for multiple procentriole initiation. Plk4 activity is controlled by *trans*-autophosphorylation of a conserved residue in the catalytic domain that triggers a positive feedback loop for kinase activation, while *trans*-auto-phosphorylation of a degron motif and adjacent residues activates a negative feedback loop leading to Plk4 degradation (Cunha-Ferreira et al., 2009; Cunha-Ferreira et al., 2013; Guderian et al., 2010; Lopes et al., 2015). In cells containing centrosomes, recruitment of Plk4 to the centrioles disfavours its accumulation and autoactivation in the cytoplasm. However, in the absence of centrioles, Plk4 remains in the cytoplasm, becoming more

concentrated than in cells where centrosomes are normally present. This likely increases the chances of stochastic stable Plk4 interactions leading to *de novo* centriole assembly if the levels are high enough. It is not known how Plk4 concentration modulates the spatio-temporal kinetics of *de novo* biogenesis.

The first evidences of *de novo* centrosome biogenesis in *Drosophila melanogaster* were published by Rodrigues-Martins et al. and Peel et al. in 2007. Rodrigues-Martins et al. (2007) showed that genetic upregulation of Plk4, induces *de novo* centriole formation in unfertilised eggs and centrosome amplification in embryos. Interestingly, they observed that biogenesis is dependent on both cell-cycle and developmental stages, since Plk4 overexpression triggers centrosome amplification only after meiotic resumption but not during oogenesis. Additionally, in embryos, amplification is first detected at anaphase or telophase of the first mitotic division, whereas in eggs centrosomes were reported to be present 30 minutes after egg laying. Limited by the techniques available, this characterisation was based on time-point analysis of fixed samples, which does not reflect the complete kinetics of the process. Rodrigues-Martins and colleagues observed that centrosome biogenesis starts earlier in embryos than in unfertilised egg, suggesting that *de novo* centriole formation is a slower process than centriole duplication or that the cytoplasmic state of embryos is biochemically more permissive than the egg's cytosol. Peel and colleagues (2007) also described that Plk4 overexpression drives *de novo* biogenesis in unfertilised eggs and centriole amplification in the fly brain and, more recently, a similar phenotype was observed in spermatocytes (Lopes et al., 2015).

Conversely, it was also shown that centrosomes are not essential in most *Drosophila* cells but are crucial during the rapid

nuclear cycles in early development and during spermatogenesis (Rodrigues-martins et al., 2008). The egg has all the components necessary for the first fast mitotic cycles previously deposited by the mother, which might explain why numerous centrosomes can readily be assembled in the case of a perturbation (such as Plk4 upregulation in *D. melanogaster*) or in parthenogenesis (Schatten, 1994). Previous studies lacked the appropriate approach to characterise the kinetics of *de novo* biogenesis with good temporal and spatial resolution.

Here, we aim at understanding how Plk4 concentration drives centriole assembly, towards finding its critical threshold for centriole formation. We also want to assess the role of resident centrioles in the biogenesis of new ones by looking for signatures of either activating or inhibitory effects. We take advantage of the established assay previously described in Chapter 3, to investigate the rules of *de novo* biogenesis, based on similar genetic tools previously used by Rodrigues-Martins et al. 2007. Our *ex vivo* approach allows isolating and live imaging small volumes of cytosol from single unfertilised egg overexpressing Plk4 in the germline. Through the volume reduction herein obtained we can, for the first time, conduct fast live-imaging of centriole *de novo* assembly with good spatial resolution. We present a combination of experimental results and mathematical modelling which prompts to better understand how this biological process is behaving and to test different hypotheses. Moreover, the accessibility of the extract facilitates biochemical manipulations; from drug perturbations to mixing cytosolic extracts from different genetic backgrounds, these approaches are valuable towards dissecting the process. We provide new perspectives into centriole formation in the absence of a mature mother centriole.

4.4 Material and Methods

4.4.1 Fly strains and fly husbandry

All flies were reared according to standard procedures and maintained at 25 °C. Germline-specific Plk4 overexpression was accomplished using the Gal4-UASp system. Flies carrying the pUASp-Plk4 (Upstream Activation Sequence promoter) construct, previously cloned in the lab and injected at BestGene Inc., were crossed with V32-Gal4 (*w*^{*}; P{*maternal-atubulin4*-GAL::VP16}V2H) flies, provided by Dr Daniel St Johnston, driving dmPLK4 overexpression in the female germline (Rørth, 1998). Centrosomes were detected using several centriolar/centrosomal reporters: *i*) pUb-Spd2::GFP (Homemade, BestGene Inc.); *ii*) pUASp-endogenous-promoter-Ana1::tdTomato (gift from Tomer Avidor-Reiss, (Blachon et al., 2008)); *iii*) pUASp-GFP::Plk4 (Homemade, BestGene Inc.); *iv*) pUASp-endogenous-promoter-Sas6::GFP (gift from Tomer Avidor-Reiss, (Blachon et al., 2008)); *v*) pUASp-endogenous-promoter-Asl::mCherry (gift from Jordan Raff, (Conduit et al., 2015)), in combination with either endogenous-Jupiter::mGFP (Morin et al., 2001) or endogenous-Jupiter::mCherry, as reporters for centrosomal MT activity (gift from Daniel St Johnston, (Lowe et al., 2014)). Around a hundred virgin females, overexpressing Plk4 in the background of a centrosomal/centriolar reporter and endogenously labelled Jupiter, were transferred to a cage coupled to an apple juice agar plate supplemented with fresh yeast-paste. The cages were maintained at 25°C, under 50-60% humidity, and the plates were changed every 3 to 4 hours.

4.4.2 Sample preparation and extraction

On the day of the experiment, the plate of the cage was regularly replaced. Freshly laid unfertilised eggs (20 minutes collections) were recovered from virgin females and dechorionated according to the protocol in section 2.4.3. The eggs were aligned and mounted on a clean, PLL-functionalized coverslip using embryo glue and covered in halocarbon oil. The preparation of the glass material and extraction procedure is described in Sections 3.4 and 3.5.

4.4.3 Time-lapse explant imaging on the spinning disk confocal microscope

Single *Drosophila* egg extract was produced according to the protocol in Section 3.5. After extract deposition, the explants were inspected in fluorescence mode to detect the presence of centrosomes. Explants were selected based on absence of both fluorescence reporters. Centrosome formation was followed by time-lapse imaging in droplets initially devoid of centrosomes. Acquisitions were done on a Plan Apo VC 60x 1.2 NA water objective with an Andor iXon3 888 EMCCD camera. To circumvent the problem of water evaporation over a long time course imaging, we used Cargille Laser liquid oil immersion media, which has the same refractive index as water. 0.45 μm optical sections were acquired on a Yokogawa CSU-W1 Spinning Disk confocal scanner using a piezoelectric stage (PI 737.2SL), installed on a Nikon Eclipse Ti-E microscope. Unless stated differently, dual-colour (488 nm and 561 nm excitation laser lines), 15 seconds time-lapses of the explant volume were recorded in IQ software.

4.4.4 Biochemical perturbations

The accessibility of the explant system facilitates biochemical and mechanical manipulations. Biochemical perturbations were performed by mixing into the Plk4 overexpressing extract, the peptide coding for human p27, which inhibits Cdk2 and Cdk1 ((Besson et al., 2008; Pagano, 2004; Russo et al., 1996) gift from Raquel Oliveira, IGC), diluted in a cytoplasm-compatible buffer. This buffer is routinely used in the lab and consists of 50 mM K-Hepes, 50 mM KCl and 1 mM MgCl₂, pH adjusted to 7.8 with KOH. The inhibitor in aqueous solution was directly added to cytosolic explants deposited on the coverslip, using an oil-driven hydraulic microinjector.

Plk4 dilution was accomplished by mixing cytoplasm from flies with different genetic backgrounds. Unfertilised eggs collected from females overexpressing Plk4 in the germline (genotype: V32-Gal4/ pUb-Spd2::GFP; endogenous-Jupiter::mCherry/pUASp-GFP::Plk4) were homogenised in unfertilised eggs from females without the transgenic pUASp element (genotype: V32-Gal4/ pUb-Spd2::GFP; endogenous-Jupiter::mCherry/pUASp-GFP::Plk4), where all components are at wild-type levels, specifically diluting Plk4 final concentration in the cytoplasm. Small droplets were made from 1:5 overexpression:wild-type egg dilutions and images were acquired for 40 minutes. All time-lapse acquisitions in these perturbation experiments were acquired at 1 minute time-interval with 0.45 µm optical sections, using a Plan Apo VC 60x 1.2 NA water objective.

4.4.5 Data analysis

Multi-stack, time-lapse calibrated images were deconvolved with Huygens (Scientific Volume Imaging, The Netherlands) using a Point Spread Function (PSF) automatically calculated from the data

set and run in batch mode, for each channel separately. 32-bit, deconvolved images were converted to 16-bit and processed using FIJI (NIH, (Schindelin et al., 2012)). Centrosomes were tracked using *TrackMate v3.5.1* plugin (Jaqaman et al., 2008). *TrackMate* operates in a modular manner, by which the user navigates through several steps in the tracking process – particle detection, particle visualisation, particle linking, lineage tracing, analysis - and can perform each task independently and in an automated, semi-automated or manual way. Centrosomes were identified by the Spd2::GFP localisation at the centre of mass (i.e. the most intense pixels) of the microtubule aster. Relying on this co-localisation criteria, we performed the *TrackMate* analysis sequentially, starting with the Jupiter::mCherry channel. First, we applied a *3D Gaussian Blur* filter to the images, facilitating the particle detection on *TrackMate* using the Laplacian of Gaussian algorithm. The microtubule asters were automatically detected inside spheres of approximately 0.7 μm in radius, adjusting the threshold value for each time-lapse video independently. Next, the first four *de novo* formed asters were manually linked/tracked from the list of detected particles. A corrected XYZT coordinate matrix of the first *de novo* events was saved for each video and imported to MatLab R2016b (The MathWorks, Inc.). MatLab was used to build a 3D binary mask with spheres of radius r (where $r \geq$ microtubule aster size), centred at the detected coordinate points. This was motivated by the large number of auto-fluorescent yolk particles of intermediate signal intensity, which needed to be excluded from the results of the automated particle tracking. The resulting 3D masks were concatenated into 4D hyperstacks, using the *Bio-Formats importer* plugin in FIJI. The Spd2::GFP images were multiplied by the corresponding 4D binary masks, resulting in a 4D image retaining

the pixel intensity values solely within the Jupiter::mCherry ROIs. Next, we used *TrackMate* to detect centrioles within spheres of 0.3 μm radius, combining sub-pixel localisation and a *Median* filter. After detection, the particles were manually tracked. The final centrosome tracks were exported as an Excel MS spreadsheet. Selected stills from the time-lapse acquisitions were processed with Photoshop CS6 (Adobe). Graphic representations were performed using Prism 7 (GraphPad Software) and the final figures were assembled in Illustrator CS6 (Adobe).

4.4.6 Statistics and modelling

Centrosome tracking data was imported in R version 3.4.1 for further analysis and modelling. The data was analysed in two ways: one aiming at identifying possible spatial constraints in the positioning of the centrioles relative to each other within the droplet at the time a centrosome is formed (neglecting time), while the other aimed at understanding temporal constraints (neglecting space). The data was analysed statistically, and simulations were performed in an effort to understand the underlying principles. The details regarding sample size, statistical tests and descriptive statistics are indicated in the respective figure legends and in the main text.

The experimental data was compared to simulated data by calculating the empirical cumulative distributions of each dataset (one experimental and 100 simulated – each consisting of 68 droplets) using the function *ecdf* from the *stats* package; and overlapping the median and 95% confidence interval (from the quantiles 0.025 to 0.975) of the simulated datasets' cumulative distributions with the corresponding empirical distribution from the experimental dataset. Random numbers were generated using the function *runif* from the *stats* library.

For the spatial analysis, each time a new centriole appeared, the 3D pairwise distances between centrioles was calculated and labelled according to appearance relative to prior centrosomes in the droplet. This allowed keeping track of event order and, if any spatial effect of existing centrosomes on the appearance of a new centrosome was present, we would be able to detect a difference in their pairwise distances. To test this, the function *kruskal.test* of the *stats* library was used to perform the Kruskal-Wallis rank sum test on the pair-wise distances and labels. To complement this analysis, we decided to compare the distributions of pairwise distances with those expected by a spatially null model whereby centrosomes appear randomly across the available space in the droplet. To simulate this null model, sets of random points were simulated in sections of semi-spheres of similar geometry as each of the experimental droplets, characterised by height h and diameter d . To this effect, a height z was generated which satisfied $q_1 = \frac{z(d^2(6h - 3z) + 4hz(3hz(2z)))}{3d^2h^2 + 4h^4}$ – where q_1 was a random number between 0 and 1 – by applying the *optim* function from the *stats* library with the “Brent” method, starting with $z = 0$. This ensured that the z coordinate was selected proportionally to the area of the circle it specifies. The two extremes, $z = 0$ and $z = 1$, correspond to the lowest and highest point of the droplet, respectively. Subsequently, the coordinates x and y were generated, within the respective circle at height z , by generating a random angle θ between 0 and 2π , and a random number q_2 between 0 and 1, resulting in $x = r \cos(\theta)$ and $y = r \sin(\theta)$, where $r = a\sqrt{q_2}$, $a = 2\sqrt{(h - z)(2R - (h - z))}$ and $R = \frac{d^2 + 4h^2}{8h}$. The pairwise distances between simulated points were calculated in the same way as for the experimental data, and the respective empirical cumulative distributions were computed and

compared to the experimental empirical distribution, as described above.

For the temporal analysis, the waiting times between centrosome births were calculated from the data and labelled according to which centrosome had just formed. Accounting for a possible change of centrosome birth rate as a function of the number of existing centrosomes, centrosome birth rates were estimated from each of the observed distributions of waiting times by Maximum Likelihood using the *fitdistr* function from the *MASS* library. The experimental data was then compared with a temporal null model whereby centrosomes form at a constant rate in time, irrespective of the existence of other centrosomes and of the volume of the droplet. To this effect, random samples of Poisson distributed waiting times were generated using the *rexp* function of the *stats* library, using the rate estimated from the waiting times between the appearance of the first and second centrosomes. The empirical cumulative distributions of these waiting times were compared to those from experimental data, as described above.

4.5 Results

4.5.1 Centrosomes assembled *de novo* recruit centriolar and centrosomal components

Plk4 overexpression triggers the stochastic formation of multiple centrioles in the cytosolic explants. Our time-lapse recordings revealed that several centriolar and centrosomal proteins are incorporated at these newly formed centrosomes and enriched over time (Figure 4.1).

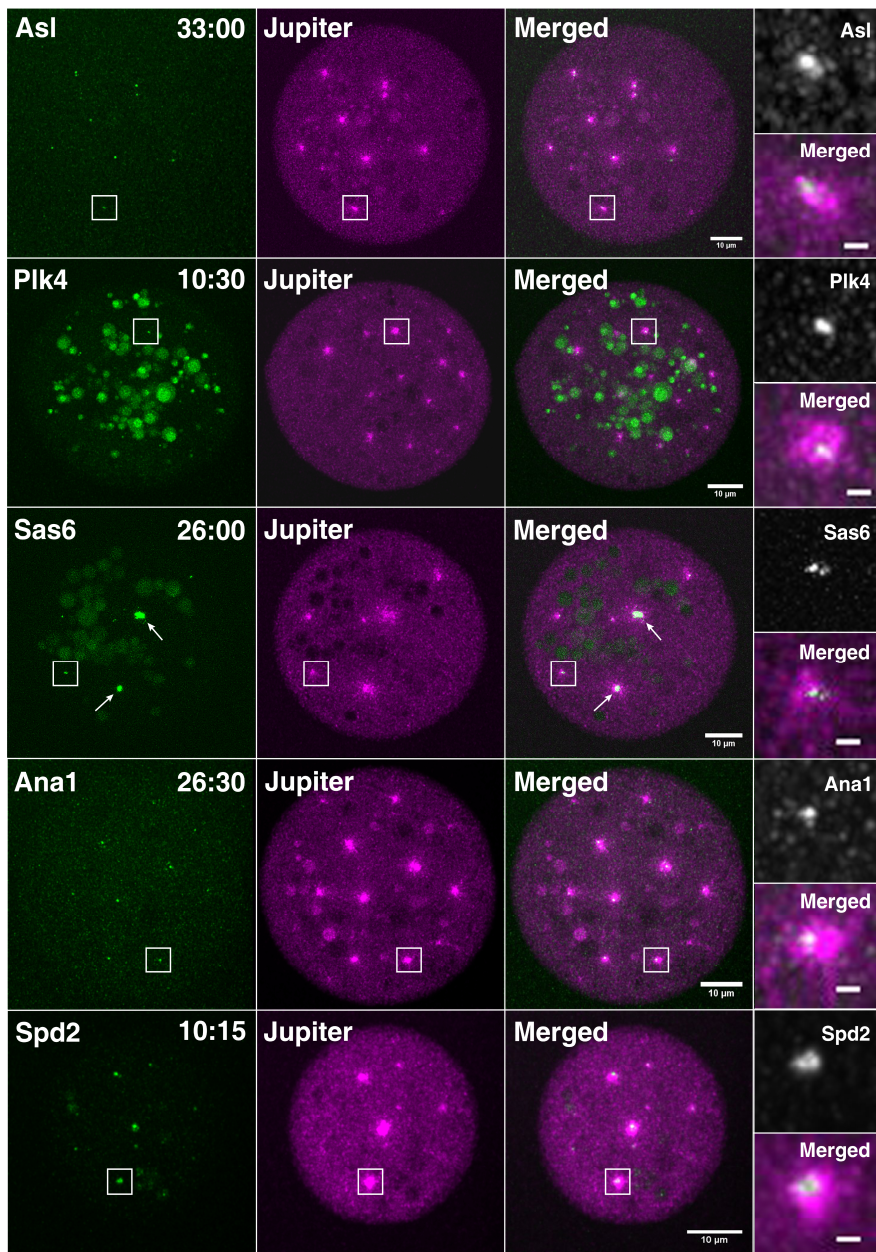


Figure 4.1 – Centrosomes formed *de novo* in explants from unfertilised fly eggs overexpressing Plk4 incorporate centriolar and centrosomal components. Maximum intensity projections (MIPs) from time-lapse videos following *de novo* centrosome biogenesis in different

explants overexpressing Plk4. Newly assembled centrosomes can load Asl, Plk4, Sas6, Ana1 and Spd2, and nucleate microtubules (reported by the microtubule-associated protein Jupiter), shown in more detail in the insets with each marker combination. Notice, in the insets, that the centrioles formed *de novo* also duplicate. The larger green blobs result from yolk auto-fluorescence, highly noticeable in the Plk4 panel. Arrows indicate large Sas6 aggregates. Time is reported as min:sec.

We confirmed that the same molecules that are required, at distinct steps, for building new centrosomes through canonical biogenesis are common to the *de novo* pathway. Asl, the Plk4 and PCM recruiter, localises at the centrosomes formed *de novo* possibly priming them for duplication. Plk4, the trigger for biogenesis, is also incorporated into the *de novo* assembled MTOCs and into duplicated centrioles, as it is also seen for Ana1. Sas6, the main cartwheel component, is a good reporter of pro-centriole assembly but, additionally, it forms large aggregates in this system, which initially do not nucleate microtubules but over time acquire MTOC ability and split into many Sas6-positive particles that spread in the cytoplasm (Figure 4.1 - arrows). Spd2 reports PCM accumulation, which notoriously increases over time (Figure 4.1, supplementary Video 2).

With these live-imaging experiments we have observed that centriole formation can in fact be much faster than previously hypothesised (Rodrigues-Martins et al., 2007) and, more importantly, centrioles form simultaneously by canonical duplication and *de novo* biogenesis within the same explant, indicating that “older” centrioles and their duplication do not prevent *de novo* centriole assembly (supplementary Video 2 and documented in more detail below in Figure 4.6).

Having conducted a molecular validation of the centrosomes assembled in our experimental assay, we set out to determine which factors influence the location and timing of centrosome biogenesis. Though a variety of processes may regulate *de novo* centriole birth, here we have focused on three potential mechanisms: the role of pre-assembled (older) centrioles, the activity of cell-cycle components and the concentration of rate-limiting molecules. Testing these hypotheses required driving an initial symmetry-breaking event, i.e., starting the process of *de novo* assembly, which was accomplished by increasing the levels of the Plk4 activator. After the first centrosome had formed, we could finally test if older centrioles affect the biogenesis of others, e.g. by promoting (activating effect) or repressing (inhibitory effect) the birth of new ones. Next, we speculated whether the cell-cycle machinery alters the permissiveness of the cytoplasm regarding centriole assembly and, finally, we tested how Plk4 concentration impacts biogenesis.

4.5.2 Spatial organization of centriole *de novo* assembly

We focused our analysis on the first four events of *de novo* “birth”, scoring 3D inter-event distance and time, determining the spatial distribution and temporal kinetics of *de novo* biogenesis (Figures 4.2 A and 4.3 A). Statistics on the observed pairwise inter-event distance did not reveal a significant difference between them (Kruskal-Wallis mean rank test). However, we noticed that new centrosomes form, on average, more than 10 μm away from previous ones, regardless of centriole rank and droplet size (Figures 4.2 B and C). This observation made us wonder if the process we are studying is purely random or if we are, in fact, uncovering some

kind of spatial regulation (e.g. a short-distance inhibitory effect) imposed by pre-formed centrioles on the birth of their neighbours. To test this hypothesis we collaborated with theoreticians and designed stochastic models with similar constraints as in our experimental system, allowing us to compare observed and simulated data. From modelling the inter-event distance between four random events within 3D droplets of similar dimensions we found, within the measurement accuracy, that our observations do not deviate from random predictions (Figure 4.2 D). These results suggest that the place where new centrosomes assemble is not determined by their neighbours and, therefore, under these experimental conditions, and contrary to what has been proposed (La Terra et al., 2005; Lambrus et al., 2015; Marshall et al., 2001), existing centrosomes behave as passive entities in the initial stages of centriole *de novo* assembly. Being this the case, we also expected that centrosomes would not bias in time the formation of new ones.

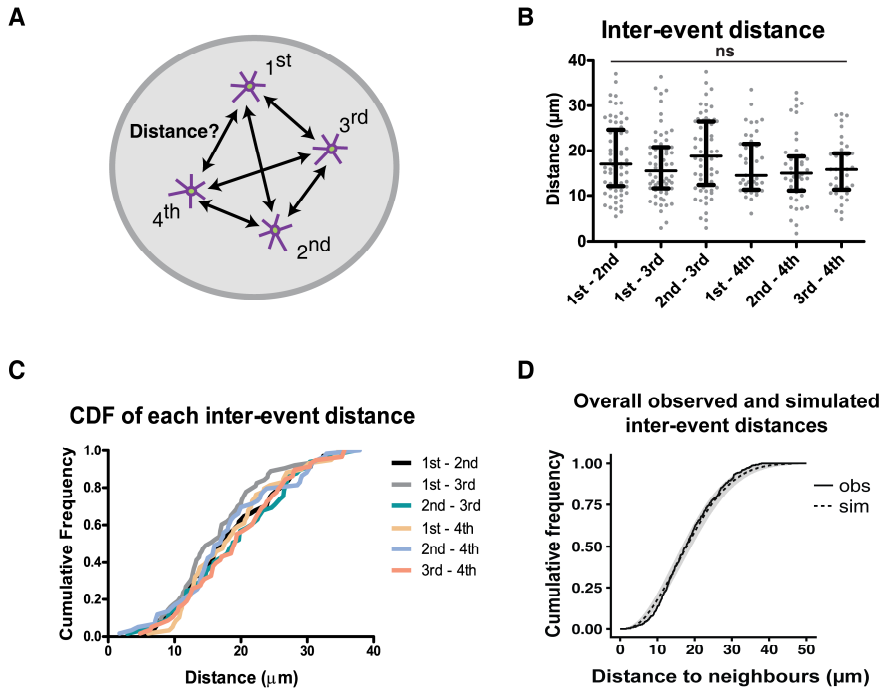


Figure 4.2 – Centrosome *de novo* biogenesis in space. **A)** Schematic representation of the experimental data analysis. The first four centrosomes formed *de novo* in the explants were tracked in 3D using the intensity signal from the Jupiter (MT reporter) channel (first tracking round) and Spd2 (centrosomal reporter) channel (second tracking round) combined. For each of the *de novo* birth events, an XYZT coordinate matrix was retrieved, from which the inter-event distances were calculated. Experimental N=68 droplets/eggs. **B and C)** Observed inter-event distance between all pairwise combinations of the first four *de novo* biogenesis events. **B)** Median inter-event distance with interquartile range. No statistical difference is detected between pairwise distances (Kruskal-Wallis mean rank test). **C)** Cumulative distribution function (CDF), i.e., the sum of probabilities of the random variable *Distance* up to a given value, for each inter-event distance calculated. The CDF allows testing statistical differences between probability distributions. **D)** *In silico* simulations were performed to test if the observed experimental data deviates from a theoretical scenario where all four birth events form at random positions

within droplets with similar geometry as in the experiments. Four random events were obtained in 100 simulations of 68 droplets. The graph depicts the median CDF of all experimentally observed (*obs*, continuous line) and all simulated (*sim*, dashed line) inter-events distances, while the grey envelope indicates the 95% Confidence Interval (from quantile 2.5% to 97.5%) for the simulated data. The experimental observations do not deviate from random simulations, suggesting that neighbour centrosomes do not influence the site where new centrosomes assemble *de novo*.

4.5.3 Temporal kinetics of centriole *de novo* biogenesis

Next, we analysed the temporal kinetics of centriole assembly by measuring the waiting times between birth events. The rate of centriole biogenesis in the droplets is fast, within a few minutes or less, following a rare-event (Poisson-like) statistics. We observed a long lag-phase until the birth of the first *de novo* event, after which the process seemingly accelerates (Figures 4.3 B and C). This suggests that at these levels of overexpression, Plk4 (and the other centrosomal components) are not rate-limiting, otherwise we would expect the rate of biogenesis to slow down as the components are consumed and depleted from the cytosol. Since we observed quite the opposite, we set to determine by modelling if the rate of biogenesis was indeed changing with each centriole formed *de novo*, which may indicate the presence of a positive feedforward molecular mechanism, possibly as a consequence of Plk4 activation.

Theoretical simulations assuming a constant rate of biogenesis predict that all waiting times should follow a similar distribution. Observed and simulated waiting time distributions do not overlap, but differ more as centriole number increases (Figure 4.3 D). Estimations of experimental birth rates using maximum likelihood fitting also indicate that the biogenesis rates increase as

more centrioles form (Figure 4.3 E). Altogether, the *in silico* simulations demonstrate that the rate of *de novo* biogenesis accelerates after one centriole is formed. These results raise the question of what underlies the changing rate in centriole *de novo* biogenesis. One hypothesis is that centrioles cause the acceleration, for instance by catalysing the biogenesis of new ones by pre-activating critical molecules. Alternatively, the changing rate we observe is centriole-independent and due to: i) a cell-cycle-like transition, yet undescribed in *Drosophila* eggs; ii) fluctuations in Plk4 concentration and local kinase activation in the cytosol, which triggers positive feedback cascades that culminate into centriole biogenesis at multiple sites. I proceeded to test these latter two hypotheses.

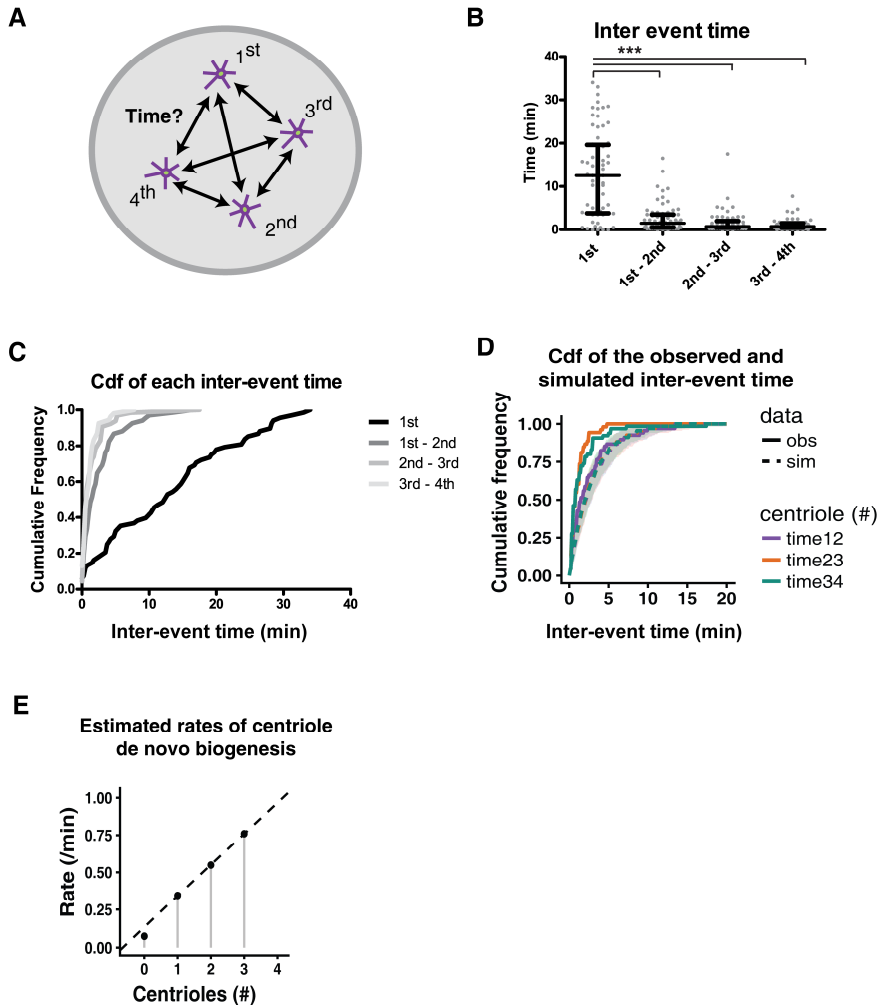


Figure 4.3 – Centrosome *de novo* biogenesis in time. **A)** Schematic representation of the experimental data analysis. The first four centrosomes formed *de novo* in the explants were tracked in 3D using the intensity signal from the Jupiter (MT reporter) channel and Spd2 channel. For each of the *de novo* birth events, an XYZT coordinate matrix was retrieved, from which the inter-event time were calculated. Experimental N=68 droplets/eggs. **B & C)** Observed inter-event time between the first four *de novo* biogenesis events. **B)** Median inter-event time with interquartile range. Note that, on average, the first *de novo* centrosome takes more than 10 min to form but subsequent *de novo* events assemble faster. The mean waiting times to the

first, and between the first to the second and the second to the third events are statistically different (Kruskal-Wallis mean rank test). **C)** Cumulative distribution function (CDF), i.e., the sum of probabilities of the random variable *Waiting time* up to a given value, for each inter-event time calculated. The CDF allows testing statistical differences between probability distributions. **D)** *In silico* simulations were performed to test if the observed experimental data deviates from a theoretical scenario where all four birth events form at a constant rate within an explant with similar geometry as in the experiments. Four random events were obtained in 100 simulations of 68 droplets. Due to the high uncertainty associated with the time of birth of the first event (i.e. it is not an absolute measurement since the initial time reference is arbitrary), the rate of birth used in the modelling was approximated to the inter-event time between the first and second events. The graph depicts the median CDF of the experimentally observed (*obs*, continuous line) and simulated (*sim*, dashed line) waiting times between the first and second, second and third and third and fourth events, while the grey envelope indicates the 95% Confidence Interval (from quantile 2.5% to 97.5%) for the simulations. The observed and simulated waiting time distributions do not overlap, and differ more as centriole number increases, suggesting that the rate of biogenesis is increasing over time. **E)** Estimation of the experimental birth rates using Maximum Likelihood (ML) fitting. An exponential distribution with rate $\lambda > 0$ was fitted by ML to the CDF of each observed waiting times. The estimated rate per min is represented in the graph as a function of the number of centrioles previously/already present in the volume. The rates of biogenesis seem to increase as more centrioles form.

We went on to test whether a cell cycle-like transition was causing the burst in centriole biogenesis observed after the initial temporal delay. In *Xenopus*, Cdk1 (and Cyclin B) activity is high in unfertilised eggs, as they are arrested in Meiosis II (MII). At this stage, Cdk1/Cyclin B binds to Stil, the substrate of Plk4, preventing Plk4 from triggering centriole biogenesis. Cdk1/Cyclin B is

inactivated after fertilisation, allowing Plk4 to bind and phosphorylate Stil and recruit Sas6 (Zitouni et al., 2016). In Rodrigues et al. 2007, the authors have demonstrated that, in the *Drosophila* embryo, Plk4-driven centriole overduplication only takes place in telophase of the first mitotic division, after Cdk1 inactivation. Moreover, centrioles do not form *de novo* before meiotic completion in eggs overexpressing Plk4 (Rodrigues-Martins et al., 2007). In *Xenopus* MII extracts, microtubule asters are promptly formed upon concomitant addition of Plk4 and RO-3306, a chemical Cdk1 inhibitor that drives the cytoplasm into interphase (Zitouni et al., 2016).

In species that develop parthenogenetically, centrosomes form *de novo* in their eggs only upon meiotic resumption. Egg activation and meiotic completion are accompanied by profound translational and proteomic changes, whereby key molecules involved in development are upregulated or downregulated, driving what is called egg-to-embryo transition. In *Drosophila*, several of those changes are orchestrated by the Ser/Thr Pan Gu (PNG) kinase, which regulates hundreds of maternal mRNAs, and is required for the onset of mitotic divisions in the fly embryo (Fenger et al., 2000; Lee et al., 2003; Shamanski and Orr-Weaver, 1991). The PNG promotes translation of Cyclin B and the formation of an active Cdk1/Cyclin B complex that drives entry into the first embryonic mitotic division (Vardy and Orr-Weaver, 2007). It is unclear whether Cdk1/Cyclin B is active in unfertilised eggs, but Cyclin B levels appear to be high in asynchronous unfertilised egg collected after 2 hours (Horner et al., 2006; Vardy and Orr-Weaver, 2007).

We asked whether inhibition of Cdk1 would allow Plk4 to induce centriole biogenesis earlier and thus reduce the observed lag-phase preceding the birth of the first centrosomes in the

explants. We performed Cdk1 inhibition by mixing a biochemical inhibitor, the peptide p27 with the egg extract overexpressing Plk4. This inhibitor was shown to trigger mitotic exit within 2-3 minutes in metaphase-arrested fly embryos (Oliveira et al., 2010), so we injected p27 into wild-type cycling embryos as a positive control for the activity of the peptide (Figure 4.4 A).

Since our hypothesis was that Cdk1 inhibition might anticipate centriole biogenesis in the explants with p27 compared to untreated explants, we measured the temporal kinetics of biogenesis after introducing the perturbation by counting how many explants formed centrosomes 10 minutes after the perturbation (Figure 4.4 B and C).

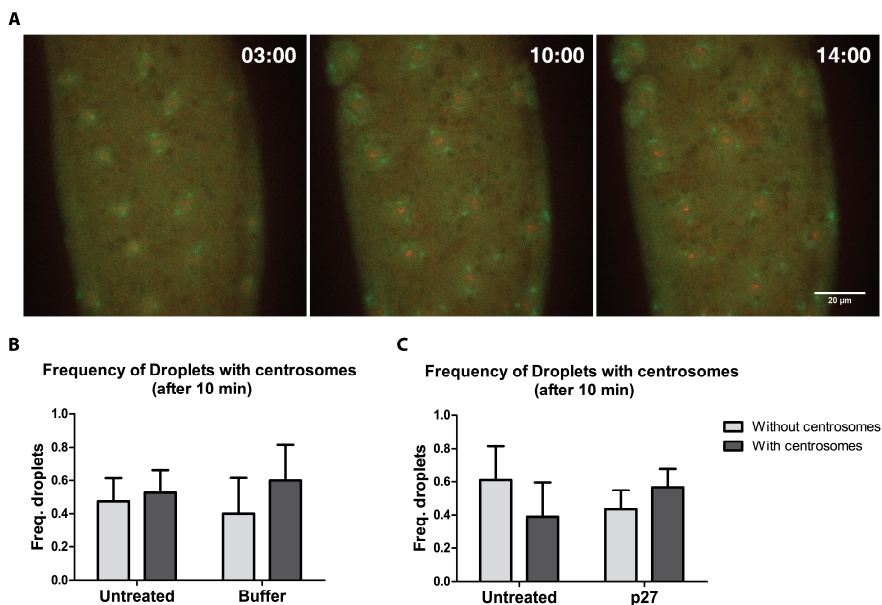


Figure 4.4 – Cdk1 inhibition in *Drosophila* embryos and unfertilised eggs. A) Cycling embryos arrest at mitotic onset upon Cdk1 inhibition with p27. The chromosomes (red, reported by Histone2Av) in the nuclei start condensing and MT nucleation (green, reported by Jupiter) from the centrosomes increases but the embryos do not progress through mitosis. Time after injection is reported as min:sec. **B & C)** Cdk1 inhibition in

explants from unfertilised eggs overexpressing Plk4. Mean (\pm SEM) frequency of explants with and without centrosomes, ten minutes after mixing only buffer **(B)** or p27 inhibitor **(C)**. **B)** Due to the characteristics of our assay and to avoid performing multiple micromanipulations at the same time, the buffer where p27 was purified in was first tested and compared to untreated explants. Four independent experiments (5-6 explants each). **C)** The effect of p27 was compared to untreated explants in five independent experiments (5-6 explants each).

While the p27 inhibitor appeared to be functional in embryos, producing the expected arrest phenotype (Figure 4.4 A), in the unfertilised explants overexpressing Plk4, the onset of centriole biogenesis was not faster in the presence of p27 than in buffer or untreated controls (Figure 4.4 B and C) suggesting that, in this system, Cdk1 inhibition does not cause a large impact on the temporal dynamics of centriole formation. It is possible that in unfertilised eggs, Cdk1 is already inactivated as they have exited MII, since in flies this process is independent of fertilisation. Therefore, the limiting factor for centriole biogenesis at this stage may be different.

Next, we tested our second hypothesis, i.e. that different Plk4 levels modulate centriole biogenesis. Plk4 is a limiting factor for centriole assembly and, consequently, the burst in biogenesis possibly results from local (stochastic) Plk4 accumulation and its activation. We do not expect that Plk4 cytosolic concentration alone is the driver of biogenesis, since it already accumulates during oogenesis and meiosis in the overexpression background, yet no centrosomes are formed then. Instead, we reason that Plk4 activation and phosphorylation of downstream targets are the critical

steps and, accordingly, we expect than at higher concentrations, Plk4 molecules will *trans*-auto-phosphorylate faster and presumably cross a critical threshold of activity earlier, thus accelerating the onset of centriole biogenesis.

Since, so far, we were unable to purify highly concentrated recombinant *D. melanogaster* Plk4 in the appropriate buffer to use in fly extracts, we resorted to a different approach whereby we mix cytosolic extracts from genetically different eggs to change the levels of Plk4 upregulation. Wild-type eggs have all components at similar concentrations as Plk4 overexpressing eggs, except for Plk4 itself. Consequently, mixing these two egg extracts dilutes only Plk4. Serial cytosolic dilutions would then allow us to titrate Plk4 concentration and determine the effect of those dilutions in the kinetics of centriole biogenesis.

A 1:5 Plk4 extract dilution in wild-type eggs causes a longer delay in the birth of the first *de novo* event, delaying the average waiting time from 7 minutes in the untreated overexpression (OE) to 25 minutes in the dilution (Figures 4.5 A and B). We recorded centrosome formation in the explants by quantifying the number of droplets that assembled centrosomes throughout the experiment, starting from an initial condition $t=0$ min when all droplets lacked centrosomes (Figure 4.5 C). After 10 minutes, 90% of the undiluted overexpression had centrosomes in the explants whereas only 3% of the diluted extract droplets had centrosomes present. After 40 minutes, about 40% of 1:5 diluted extract had assemble centrosomes whereas the overexpression control had centrosomes in all droplets (Figure 4.5 C). Our results indicate that at a 1:5 Plk4 dilution we are approaching the critical threshold in Plk4 concentration required to form centrosomes *de novo*. The temporal delay in centrosome formation observed in the dilution experiments

goes against the hypothesis of a fixed temporal mechanism, cell-cycle related, playing a major role for the onset of centriole biogenesis. Finally, we also measured the inter-event distances between the first three *de novo* events at different Plk4 concentrations and only found a difference at the medium range distances (Figure 4.5 D).

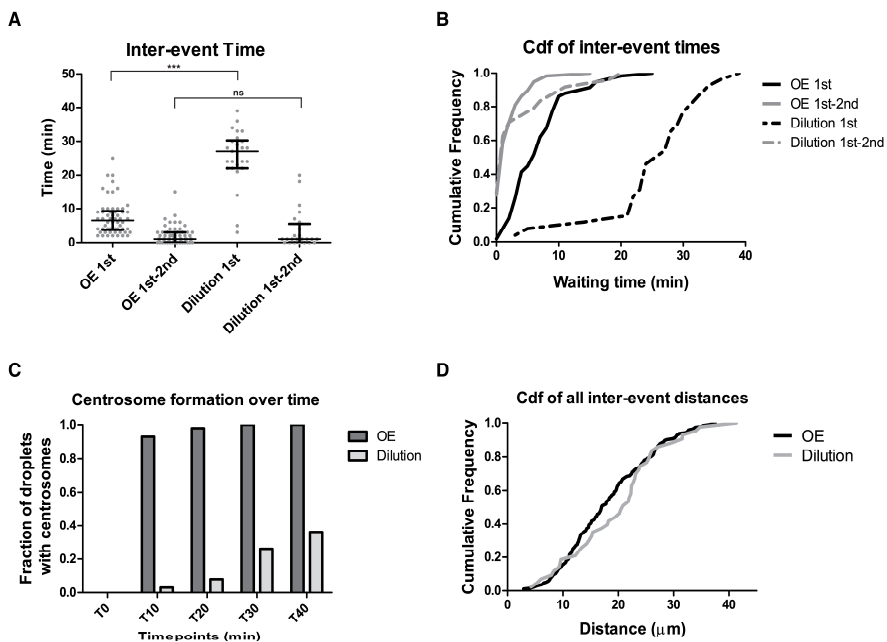


Figure 4.5 – Temporal dynamics of *de novo* centrosome biogenesis upon dilution of Plk4 concentration in the cytoplasm. A & B Time to the first event and inter-event time between the first and second centrosomes formed *de novo* in undiluted Plk4 overexpression extract (OE) [N=58 droplets] and 1:5 Plk4 extract diluted in wild-type (Dilution) [N=26 droplets]. The waiting time for the first event is significantly changed with Plk4 1:5 dilution. Median waiting time with interquartile range. **C**) Fraction of droplets with centrosomes at five timepoints (0, 10, 20, 30 and 40 minutes) throughout the experiment. After 40 minutes, only 40% of the explants with Plk4 dilution (Dilution) had centrosomes whereas in the

control overexpression (OE), all explants were filled with centrosomes. **D)** CDF of inter-event distances between the first three centrosomes formed *de novo* in control overexpression and dilution experiments.

Neither a cell-cycle mechanism based on Cdk1 activity, nor older centrosomes seem to have a critical role in the *de novo* biogenesis of the first centrosomes. Possibly, the onset of biogenesis relies solely on Plk4 activation in the cytosol. Nonetheless, it is surprising that apart from centriole duplication, centrosomes do not influence the *de novo* birth location of others. We asked whether this could be due to newly formed centrosomes being immature and thus incapable of producing an effect on others.

4.5.4 Centriole maturation and duplication

Finally, we investigated the interplay between *de novo* and canonical biogenesis. We observed that centrioles that assemble *de novo* in the droplets duplicate several times, while in other regions of the cytosol, more centrioles assemble *de novo*, showing that both pathways happen concomitantly and do not inhibit each other (supplementary Video 2).

We visualised with different centrosomal reporters that, after centriole duplication, one centriole is usually brighter and/or larger than the other(s) (Figure 4.6 A), suggesting that centrioles undergo maturation in the droplets, and that this is likely required for their duplication. Asl is important for centriole maturation, enabling daughter centrioles to duplicate in the next cell cycle in the fly embryo (Fu 2016). We measured how long after having detected MT asters with Jupiter (i.e. when an MTOC was born), the Asl signal was

also detected at the centrosome, indicating the presence of a mature centriole (maturation time). After Asl incorporation, we calculated how long it takes to clearly see more than one Asl dot (duplication time) (Figure 4.6 B). Concurrently, we also measured Asl centrosomal intensity over time. We observed that two Asl dots (duplicated centrioles) are seen, on average, 3 minutes after a single Asl dot localises at the MTOC. This is accompanied by an increase in Asl centrosomal intensity, usually followed by a drop in intensity when duplicated centrioles move apart (square in Figure 4.6 B). We hypothesise that there is a threshold in Asl levels at which centrioles become competent for duplication, despite not having gone through mitosis and undergoing the normal changes in the cell-cycle usually required for centrioles to become mothers. Interestingly, the first centriole formed in the droplets takes a similar time to duplicate in the overexpression and Plk4 dilution experiments (Figure 4.6 C, Mann-Whitney test, p-value = 0.5878), suggesting that Plk4 is not a limiting factor at these concentrations and, moreover, that canonical biogenesis is not only spatially robust, but also temporally well-regulated, even in a system devoid of a typical cell-cycle “clock” (Figures 4.6 B and C).

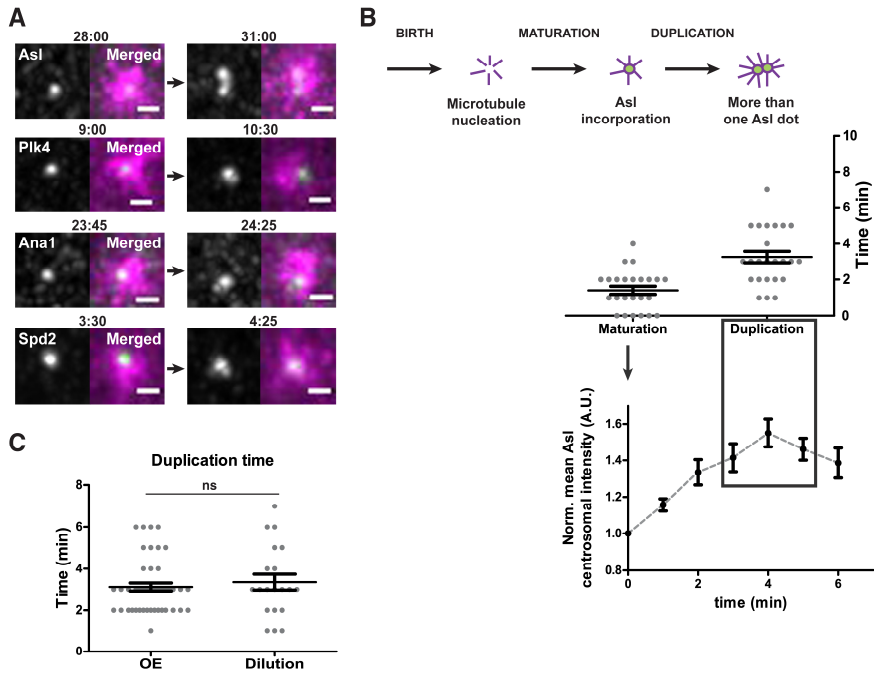


Figure 4.6 – Centrioles duplicate after forming *de novo* and incorporating Asl in the *Drosophila* egg extract overexpressing Plk4.

A) Insets taken from time-lapse videos depicting centrioles formed *de novo* before and after their duplication, in explants overexpressing Plk4 and different centrosomal reporters. Time is reported as min:sec. Scalebar = 1 μ m. **B)** Centrioles duplicate after Asl incorporation. Mean (\pm SEM) maturation and duplication time and normalised mean (\pm SEM) Asl centrosomal levels measured for 24 centrosomes assembled in the egg extracts. The square in the intensity graph highlights the time-window within which centrioles duplicate and often split and move away. **C)** Centrioles formed *de novo* duplicate, on average, 3 min after their biogenesis, both in the overexpression (OE, N=44 centrioles) and dilution (1:5 Plk4 Dilution, N=20 centrioles) experiments (Mean \pm SEM). The duplication time is not statistically different between the two conditions (Mann-Whitney test, p-value = 0.5878).

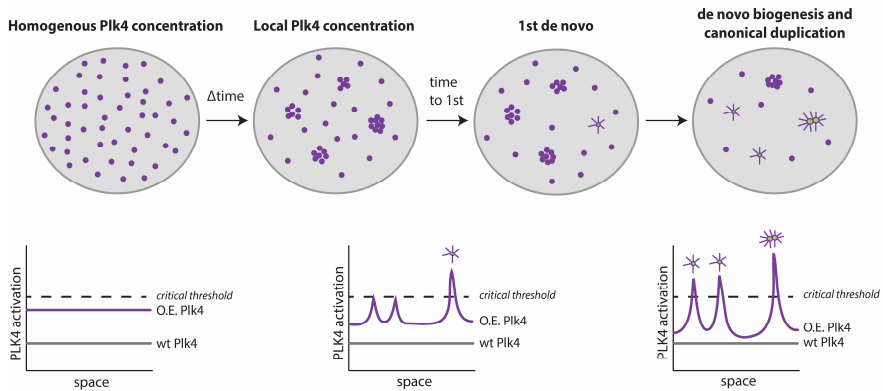


Figure 4.7 – Model proposing a mechanism for the regulation of centriole *de novo* biogenesis and duplication, based on Plk4 activity.

The starting condition in explants without centrosomes may be a scenario where Plk4 is homogeneously concentrated in the cytosol and its local activity is below the critical threshold required to trigger centriole formation. Over time, Plk4 molecules may randomly encounter and locally concentrate due to self-affinity. If Plk4 concentration is locally high enough, it will *trans*-auto-activate beyond a critical threshold for centriole biogenesis, giving rise to the birth of the first *de novo* event. Then, the process of centrosome biogenesis accelerates probably as a result of the time it takes to locally concentrate enough Plk4 for it to become active and drive biogenesis in multiple independent sites. When centrioles have formed, they recruit Plk4 and duplicate. Plk4 is depicted in purple. This model relies on self-affinity of centrosomal components and positive molecular feedforward loops, whereby Plk4 activation is non-linearly controlled by its local concentration.

4.6 Discussion and Conclusions

In this Chapter, our main aim was to understand how Plk4 levels regulate the onset and mode of centriole biogenesis in space and time. Centriole assembly via canonical duplication is spatially,

temporally and numerically controlled by the presence of mature centrioles in the cell. Here, we were interested in dissecting the factors that promote centriole *de novo* assembly and investigate what kind of regulation underlies this process. Previous studies have indicated that at very high Plk4 concentration both canonical and *de novo* biogenesis can occur, but it was not possible to study it by live-imaging (Lopes et al., 2015; Peel et al., 2007; Rodrigues-Martins et al., 2007).

We developed an assay where we can manipulate centriole *de novo* formation and acquire images of ongoing biogenesis at high spatio-temporal resolution. Unfertilised fly eggs do not have centrioles, but overexpression of the limiting component Plk4 triggers centriole biogenesis, allowing us to properly document their assembly in a limited volume of cytoplasm where all other components necessary to build these structures are naturally present. Multiple centrosomes form *de novo* at high Plk4 levels and incorporate distinct molecular components, such as Plk4 and its main centriolar recruiter in flies, Asl. Ana1 and the PCM component Spd2 are also loaded and all of these molecules become enriched over time, converting into brighter and/or larger foci that nucleate more MTs. These observations suggest that the centrioles assembled *de novo* in this system are stable (i.e. not degraded) and possibly undergo time-dependent maturation, even in the absence of a cell-cycle (Figure 4.1). Sas6, the main component of the cartwheel, is recruited to the MTOCs but it additionally forms large aggregates which likely correspond to the Sas6-Ana2 cytoplasmic particles called SAPs, described to occur upon overexpression of these two proteins in the fly spermatocytes (Stevens et al., 2010). We noticed that these particles have very specific dynamics; when cytosolic explants are made they lack MT activity but, over time, they

start nucleating MTs and split into many small Sas6-positive particles that diffuse to the cytoplasm, away from the large aggregate (arrows in Figure 4.1, video not shown).

We generally observed a temporal lag until the first centrosome was detected in the explants, after which centrosome assembly seemed to be much faster (Figure 4.3 B). Centriole distribution in the cytoplasm was difficult to interpret; while centrosomes formed *de novo*, concomitantly, they also duplicated. Altogether, these observations made us wonder about the dynamics of centrosome *de novo* formation and, more specifically, how the birth of one centrosome impacts the cytoplasm and regulates the birth of other centrioles. Tackling this problem required mathematical modelling to compare our observations to random predictions. The results we have obtained strongly indicate that the first *de novo* events are spatially independent, suggesting that recently formed centrioles do not bias the location where new ones assemble *de novo* in our system (Figure 4.2 D). This might be due to the fact that shortly after forming, centrosomes are still immature and might not have yet all the components at the right concentration that render them competent to affect biogenesis. We will discuss this further, when we address Asl loading and the co-occurrence of biogenesis pathways.

While the first centrosome takes longer to assemble *de novo*, the kinetics of biogenesis change after its birth and theoretical simulations indicate that the rate of centriole formation accelerates, with an increase in rate of biogenesis with every centriole born (Figures 4.3 D and E). This resembles a bimodal switch, in agreement with the non-linear kinetics of Plk4 activation as a function of its total concentration described by Lopes et al. 2015, suggesting that the transition from the initial lag phase to the burst in

biogenesis might be a consequence of Plk4 *trans*-autoactivation in the cytosol, which depends on their stochastic encounters.

Previous work has shown that high Plk4 overexpression can induce centriole assembly in *D. melanogaster* eggs only after meiotic exit (Rodrigues-Martins et al., 2007). Similarly, the MTOCs that assemble *de novo* in eggs of parthenogenetic species are only detected upon meiotic resumption. At this developmental stage, numerous alterations take place which drive the egg-to-embryo transition. Extensive translational and proteomic changes occur that lead to the upregulation or downregulation of key developmental molecules after egg activation. Many of those changes are operated by the PNG kinase, which regulates hundreds of maternal mRNAs, and is required for the onset of mitotic divisions in the fly embryo (Fenger et al., 2000; Hara et al., 2018; Shamanski and Orr-Weaver, 1991). One of its main targets is Cyclin B, promoting its mRNA translation and forming an active Cdk1/Cyclin B complex that drives entry into the first mitosis (Vardy and Orr-Weaver, 2007).

Very little is known about the cell-cycle profile in unfertilised fly eggs, except that asynchronous unfertilised egg collected after 2 hours show high Cyclin B levels by Western Blot, when compared to cycling embryos (Horner et al., 2006; Vardy and Orr-Weaver, 2007). Based on these published observations we were compelled to test if cell-cycle dependency was an additional factor contributing to the temporal onset of centriole assembly. It is known that Cdk1/Cyclin B levels need to be low for Plk4 to bind and phosphorylate Ana2, which then leads to Sas6 recruitment to the centrosome and centriole biogenesis (reviewed in Arquint and Nigg, 2016; Zitouni et al., 2016). In the experiments where we inhibited Cdk1, the main driver of mitotic progression in the fly embryo, the birth of the first centrosomes was not accelerated in the explants (Figure 4.4). This

suggests that the cell-cycle does not play a significant role in this system. Nonetheless, we need to be careful with our interpretation due to the low number of experiments performed. Interestingly, another putative substrate of the PNG complex is Slimb/Slimb, the E3 ubiquitin ligase that binds to hyperphosphorylated Plk4 and triggers its degradation. According to a wide transcriptome screening covering *Drosophila* egg activation, Slimb mRNA is translationally inhibited by PNG (Kronja et al., 2014). One hypothesis is that Slimb downregulation at egg-to-embryo transition impacts Plk4 stability, allowing Plk4 to stay active after meiotic resumption. However, this effect would only be seen after most (centrosomal) Slimb suffers turnover. Since Slimb has several targets, the best way to test this hypothesis is to conduct experiments with mutant non-degradable Plk4 (Cunha-Ferreira et al., 2009; Cunha-Ferreira et al., 2013; Rogers et al., 2009).

Interestingly, if the cell-cycle does not play a strong role in this system, the centrosomal enrichment of molecular components over time observed in our experiments must be a consequence of diffusion and strong affinity between centrosomal components. This agrees with recent literature highlighting the importance of self-assembly in driving biological reactions and, in particular, centriole formation. Sas6 self-assembly into homodimers is at the heart of the universal 9-fold symmetry (Breugel et al., 2011; Kitagawa et al., 2011; Nakazawa et al., 2007). Together with Bld10, these molecules can organise into a bona fide cartwheel structure *in vitro* (Guichard et al., 2017). Other centrosomal components spontaneously form condensates *in vitro*. At high local concentration the *C. elegans* master PCM recruiter Spd5 (Woodruff et al., 2017) and the *Xenopus* Plk4 (Montenegro Gouveia et al., 2018) form supramolecular scaffolds that bind other PCM proteins and recruit α - and β -tubulin,

organising MT asters. In addition, MTs likely play an active role in the centrosomal enrichment of some of those proteins. For some of the reporter combinations we have imaged, MT nucleation was detected before we could see the centrosomal component at the centre of the MTOC. This not only indicates that different components are loaded within different time-scales but it also suggests that the early steps of centriole assembly likely take place in a MT and PCM-rich environment, even in the case of *de novo* biogenesis. At this stage, when pro-centrioles are less stable and lack several core molecules, a combined effort between PCM molecules and radial aster nucleation may be important to create a biochemically distinct compartment and bring key components necessary for centriole assembly.

After excluding that neither older centrioles nor the cell-cycle are the main regulators of the *de novo* biogenesis we wanted to test the role of Plk4 concentration, and indirectly its activation, in biogenesis by changing Plk4 levels in the cytosol. We hypothesised that if Plk4 activation is the main driver of centriole biogenesis onset and this is dependent on Plk4 (local) accumulation, then Plk4 cytoplasmic dilution should lower the chances of molecules meeting and delay the kinetics of biogenesis. Accordingly, we observed a strong delay in the *de novo* birth of the first centrosomes upon 1:5 Plk4 dilution in wild-type extract (Figures 4.5 A and B). The spatial dynamics were not very different from the high Plk4 levels, except at the medium-range distances (Figure 4.5 D).

These experiments further support that the total amount of Plk4 in the system and its activation are a main driving force of centriole biogenesis. Concretely, we propose that time-dependent stochastic accumulation of Plk4 in multiple places in the cytoplasm drives the phenomenon of fast *de novo* centriole assembly (Figure

4.7). The apparent acceleration in biogenesis we measured is probably the outcome of the time it takes for Plk4 to form stable oligomers and to become active, which in turn depends on its concentration (Figure 4.7). The waiting time is variable between eggs at high Plk4 overexpression, since the inducible Gal4-UAS system drives variable levels of protein expression (Goentoro et al., 2006), which becomes more evident when a 1:5 Plk4 dilution is performed and compared to the unperturbed upregulation.

It has been suggested that once centrioles are formed *de novo* in a system previously lacking centrioles, any other events of biogenesis will be “templated”, i.e., follow the canonical pathway, since centrioles accumulate critical components (La Terra et al., 2005; Lambrus et al., 2015; Marshall et al., 2001; Uetake et al., 2007). This seems to be the case in *Naegleria gruberi*, where the first basal body assembles *de novo* but the second duplicates from the first (Fritz-Laylin et al., 2016). However, we clearly see that centrioles continue to form *de novo* after the first is born and undergoes duplication. Both biogenesis pathways, canonical duplication and *de novo*, happen in parallel within the same explant, indicating that “older” centrioles and their duplication does not prevent *de novo* centriole assembly, even at lower Plk4 overexpression. Perhaps centrioles that have just assembled *de novo* are too naïve to generate an inhibitory or activating signal. In cycling cells, newly born centrioles can neither duplicate nor nucleate MTs until they undergo centriole-to-centrosome conversion during mitosis (Izquierdo et al., 2014; Wang et al., 2011). This maturation entails that daughter centrioles sequentially load Bld10, Ana1 and Asl in *Drosophila* and human cells, allowing them to recruit PCM components and become mother centrioles in the following cell-cycle. Determination of centriole maturation time, assessed in

our experiments by the temporal gap between aster formation and Asl detection, has shown that centrioles take longer to duplicate than to recruit Asl (Figure 4.6 C). This suggests that, for centrioles to become mature and capable of duplicating, they need to load a certain amount of Asl (and possibly other critical components), perhaps explaining why they do not seem to affect the place of birth of others.

On the other hand, it is quite interesting that centrioles acquire duplication capacity without needing to go through mitosis to mature. We also observed that duplication time is quite consistent for the first centrosomes assembled *de novo* at high (undiluted) and lower (diluted) Plk4 levels, indicating that despite the absence of a typical cell-cycle “clock”, canonical biogenesis is both spatially and temporally robust. Hence we propose that different “running clocks” regulate *de novo* and canonical biogenesis.

In the Plk4 dilution experiments, we seem to be approaching the critical threshold for Plk4-driven centriole biogenesis, given that after 40 minutes, more than half the droplets do not assemble centrosomes (Figure 4.5 C). Diluting Plk4 even further might bring its concentration in the cytoplasm to levels at which one and only one centrosome can form *de novo*. If such outcome is possible to achieve, it should tell us the minimum amount of Plk4 (over the egg’s basal levels) necessary to drive the formation of a single centriole. In the future, it would be important to determine how much more Plk4 the overexpression line contains over the wild-type eggs.

Finally, we wonder if our findings in *D. melanogaster* resemble what happens in insect eggs that develop parthenogenetically. In the wasps *Nasonia vitripennis* and *Muscidifurax uniraptor* (Riparbelli et al., 1998; Tram and Sullivan, 2000) and in the fly *D. mercatorum* (Riparbelli and Callaini, 2003), multiple functional centrosomes form

spontaneously in the egg. Two of these asters interact with the female pronucleus, assembling the first mitotic spindle and triggering normal egg development to adulthood. In *D. mercatorum*, the centrosomes that assemble *de novo* can also duplicate and they do so in a cell-cycle dependent way. It would be very relevant to determine if the burst in centrosome assembly coincides with an increase in Plk4 concentration in the eggs from these species. Just like in our system, a highly variable number of MTOCs are assembled, suggesting the presence of a weak control mechanisms against *de novo* centriole formation in the germline, once the eggs have been activated. It would be interesting to document centrosome birth dynamics and their maturation in these natural systems to find more about the principles that govern centriole *de novo* formation and their evolutionary conservation.

Our results further support that Plk4 levels must be well-regulated in cells to form the right number of centrioles, since the presence of centrioles is not necessarily enough to ensure centrioles can only form in the vicinity of existing ones. We try to provide better insights on how centriole biogenesis depends on Plk4 concentration and, possibly, on centriole maturation.

4.7 Acknowledgements

We acknowledge the technical support of IGC's Advanced Imaging Facility (AIF-UIC), which is supported by the national Portuguese funding ref# PPBI-POCI-01-0145-FEDER-022122, co-financed by Lisboa Regional Operational Programme (Lisboa 2020), under the Portugal 2020 Partnership Agreement, through the

European Regional Development Fund (FEDER) and Fundação para a Ciência e a Tecnologia (FCT; Portugal).

We also acknowledge Tomer Avidor-Reiss for sharing the Ana1::tdTomato and pUASp-endogenous-promoter-Sas6::GFP fly lines, Daniel St Johnston for the *w**; *maternal- α tubulin4*-GAL::VP16 and endogenous-Jupiter::mCherry flies and Jordan Raff for sharing the pUASp-endogenous-promoter-Asl::mCherry transgenic line.

Chapter 5

Final Discussion

“(...) the problem which has interested cytologists and embryologists for many years, namely, whether an ordinarily self-duplicating body may, under certain conditions, seem to be created de novo.” - (Dirksen, 1961), On The presence of centrioles in artificially activated sea urchin eggs.

It was not long after their discovery in cells in the late 1890's (by Boveri and van Beneden), that scientists began proposing that centrioles were not always assembled through duplication (Harvey, 1936; Yatsu, 1905). The fascinating discovery that such an intricate structure can form without a template and yet be fully functional, raises a variety of questions regarding the regulation of organelle biogenesis which stays pertinent to this date. And while much scientific effort has contributed to our current understanding of the regulation of pro-centriole assembly next to an already present and mature mother structure (recently reviewed in (Breslow and Holland, 2019; Nigg and Holland, 2018)), much less is known regarding the “unguided” *de novo* centriole formation. Starting my PhD, I was captivated by the concept of studying centriole assembly at its very beginning, “starting from zero” as you may. In the course of this project, I quickly became aware of the frustrating caveats of my scientific endeavour, while exploring a less conventional question in a still very underdeveloped experimental system. Apart from that, what we arrived into is still an incomplete story. One can easily argue that is always the case, but the point is that, either due to experimental or conceptual gaps, the results chapters appear more fragmented than what they should. My aim in this final discussion is to revisit the most important results and discuss them under an integrative perspective as well as debate a few “loose ends”; what

they might suggest and how these could be experimentally addressed.

Endogenous Plk4 levels and the regulation of centriole duplication

Plk4 is undoubtedly a fundamental player in centriole biogenesis and numerous studies have contributed to our current body of knowledge; by revealing its centrosomal recruiters and several of its interactors, disclosing key features of its crystal structure, and clarifying how the kinase drives its own activation and degradation. From where we stand now, for fully understanding Plk4 biology (and centriole assembly), quantitative assessments of its behaviour in live cells are much needed. We must determine Plk4 levels at the centrosome and in the cytosol, find out how the balance between these compartments changes under different physiological conditions, measure Plk4 interactions with other cellular components, and assess the chemico-physical properties underlying its localisation within the cell.

In Chapter 2, we set to determine Plk4 endogenous localisation and levels during the cell-cycle, along with its mode of diffusion and oligomerisation in fly embryos. We have discussed how these measurements are important to build a quantitative framework relating the transition of Plk4 molecules from the cytosol to the centriolar compartment, which ultimately controls centriole duplication.

From a broad perspective, several quantitative approaches could have been used to tackle this problem, but since our motivation was to measure Plk4 in a defined place and time within the cell, during a known developmental stage, all label-free proteomic analysis were excluded upfront since these rely on large(r)-scale

production of protein extracts without any spatial information and often limited temporal resolution. Accordingly, we opted for FCS, a fluorescence technique with single-molecule sensitivity, particularly suited for detecting live molecules present at low concentration in cells. Invariably, one of the weaknesses of this approach, is that it relies on the coupling of a probe to Plk4. The very low concentration of this protein and its high sensitivity to genetic and structural modifications, render its labelling challenging and imposed a first methodological compromise. We made fly lines with state-of-the-art fluorophores inserted at the endogenous Plk4 genomic locus and, for the first time, we were able to visualise endogenous Plk4 *live*, one of the lowest-abundance proteins in the centrosome proteome. However, one particular caveat needs to be taken in account: both constructs introduced a small, yet obvious phenotype in embryos, which might result from mild centrosome amplification, nonetheless much lower than what we observed upon Plk4 overexpression, also presented in this thesis.

The analysis of post-processed time-lapse images revealed Plk4 centrosomal dynamics through multiple nuclear cycles in the fly syncytium. The profile of Plk4 intensity oscillations, more specifically, the increase in the period of these oscillations (full width at half maximum amplitude), concomitantly with longer cell-cycle progression, as well as the constant maximum amount of Plk4 localised per centrosome per cycle, suggest that the centrosomal incorporation and decay is being directly or indirectly regulated by the cell-cycle. While Plk4 molecules possibly undergo continuous turnover (on/off at the centrosome), we unveiled two distinct phases, one where loading is favourable and another, where loading is less favourable and the system is biased towards Plk4 loss from the centrosome, starting even before pro-centrioles are fully formed

(also observed in (Aydogan et al., 2018)). Plk4 loading might be mostly due to random centrosome encountering (hence, being a pressing matter to find how Plk4 moves in the cell!) and anchoring, the decay implies some alteration once Plk4 has accumulated at the centrosome: either its phosphorylation causes a steric modification in protein conformation preventing its centrosomal binding; or its binding partner(s) are displaced from the centrosome, or Plk4 is degraded. Among these three hypotheses, the most interesting for me is that perhaps the hyperphosphorylated form of Plk4 undergoes rapid degradation at the centrosome. Since Slimb, E3 ubiquitin ligase that mediates Plk4 interaction is present at the centrioles through the cell-cycle in S2 cells (Rogers 2009), we speculate that the shift towards Plk4 loss might be caused by its proteasomal degradation at the centrosome. To further test this hypothesis it would be important to conduct Fluorescence recovery after photobleaching (FRAP) experiments on the Plk4 centrosomal fraction and combine these with proteasome perturbation. Very recently, it was proposed that Plk4 recruitment and its dissociation from centrioles in the fly embryo is governed by changes in binding affinity with its main recruiter Asl (Aydogan et al., 2019). The model presented in this study suggests that Asl phosphorylation by Plk4 (Boese et al., 2018), reduces Asl-Plk4 binding affinity, so that Plk4 is displaced from the centrioles in a time and phosphorylation-dependent manner (Aydogan et al., 2019).

As demonstrated in other *Drosophila* studies and in different species, we also confirmed that Plk4 is not fully enriched at the centrosome over the time-window of centriole duplication, and yet pro-centrioles still assemble properly (Aydogan et al., 2018; Cunha-Ferreira et al., 2009; Rogers et al., 2009; Zitouni et al., 2016). This is likely because its main kinase activity is actually required earlier in

the cell-cycle, upon the interaction with Stil in late mitosis/early interphase (Dzhindzhev et al., 2017; Mclamarrah et al., 2018; Ohta et al., 2018; Zitouni et al., 2016), and what we detect in S-phase is a peak in intensity of hyperphosphorylated and inactive Plk4 protein, waiting to be processed.

Higher bulk Plk4 centrosomal levels correlate positively with cell-cycle duration, suggesting an interaction between Plk4 and cell-cycle progression. Since cell-cycle progression is heterogeneous in wild-type embryos due to several factors, among which variation in the levels of molecules regulating cell-cycle progression (for instance differences in levels of maternal Cyclin B significantly alter S-phase duration (Crest et al., 2007)) and changes in temperature, one possible explanation is that longer interphases allow Plk4 to accumulate at the centrosome for longer, becoming more enriched in the embryos that cycle slower. An alternative hypothesis is that Plk4 affects the cell-cycle somehow acting upon the DNA replication checkpoint, which becomes active as the fly embryo transits from preblastoderm to blastoderm (Crest et al., 2007; Farrell and O'Farrell, 2014). Higher Plk4 levels might delay entry into mitosis by preventing the activity of Cdc25 phosphatases required to dephosphorylate and activate the Cdk1-Cyclin B complex. Unfortunately, it is very hard to image the preblastoderm stages without resorting to light-sheet microscopy and any manipulation of the checkpoint is hardly a clean experiment, so ultimately, we would have to resort to live sensors monitoring the activity of the checkpoint in embryos expressing different NG-Plk4 levels, to tackle this question.

Absolute Plk4 cytosolic quantifications by FCS required planning and developing good internal references. We purified each fluorophore and collected only their monomeric fractions from gel

filtration. The major challenge we faced when we started the FCS experiments was the lack of studies in whole fly embryos, which implied a few weeks of experimental optimisation using the monomeric fluorophores to ensure we had the right conditions to collect the data. Here, we must highlight how important it was to have injected the fluorophores into the cytosol and not having to rely on their measurements in solution. While for diffusion calculations, a solution of fluorophore with a known diffusion coefficient is usually enough, determining molecule oligomerisation and concentration needs a calibration with similar photophysical characteristics within the same environment. Again, we had to sacrifice some goals, namely collecting data at several depths since the quality of the signal is highly compromised deeper within the embryo cytoplasm due to autofluorescence, photobleaching, and light-scattering. It would be important to sample NG-Plk4 at different depths to understand if the protein is homogeneously distributed in the cytosol or if it is compartmentalised, for e.g. having a distinct concentration in the vicinity of nuclei (and associated centrosomes) vs. elsewhere in the cytoplasm. Some of the optical problems previously mentioned may be overcome by using two-photon excitation, which allows for a deeper penetration into the sample.

Our FCS measurements detected two fractions of mNeonGreen-Plk4 diffusing in the peri-nuclear cytosol using two different methods to analyse the data. The faster Plk4 pool diffuses at $17.17 \mu\text{m}^2/\text{s}$, whereas the slower, diffuses at $1.49 \mu\text{m}^2/\text{s}$, and both fractions diffuse slower upon MT depolymerisation with Nocodazole. It is tempting to speculate that since Plk4 is capable of binding MTs in other species (Montenegro Gouveia et al., 2018), perhaps *Drosophila* Plk4 also binds cytoplasmic MTs, moving along them over large distances in the embryo and localising closer to the

centrosomes. The speed at which motor proteins move along MTs has mostly been determined *in vitro* and it is rather variable between different MAPs: while some motors like kinesin 14 are fast (0.7 $\mu\text{m/s}$), others like kinesin-5 are slow (0.04 $\mu\text{m/s}$), depending on their directionality, activity and processivity (White et al., 2015). A cool experiment would be injecting photoswitchable MT depolymerising drugs (Photostatins) (Borowiak et al., 2015), to reversibly switch MT dynamics on and off *in vivo* and test how MT depolymerisation impacts endogenous Plk4 centrosomal localisation in the embryo. If MTs have a role in transporting Plk4 and contributing for its centrosomal localisation we should detect a decrease in Plk4 levels at the centrosome upon MT depolymerisation and a rescue in its recruitment upon light-mediated inactivation of the drug.

Even though the hypothesis that *Drosophila* Plk4 binds MTs or large-MT interacting complexes is quite exciting, we cannot exclude the possibility that the effect on Plk4 diffusion in Nocodazole-treated embryos is due to an increase in the viscosity of the cytoplasm, consequently slowing down the diffusion of all molecules and therefore perturbing the mobility of both *Drosophila* Plk4 pools, as we have observed. Further experiments are required to test how MT depolymerisation in the *Drosophila* embryo changes the diffusion coefficient of other molecules with known MT binding activity.

Finally, we have determined the endogenous Plk4 concentration driving centriole duplication in the fly embryo (~7.55 nM). Alongside, we also found that Plk4 forms low-order oligomers but not large scaffolds in the cytosol, indicating that multi-Plk4 complexes are only assembled at the centrosome under normal levels. In agreement, though some centrioles overduplicate in the mNeonGreen-Plk4 embryos, we have never observed centriole formation elsewhere in the cytosol (i.e. “unguided/*de novo*”

assembly), convincing us that our measurements are not far from unlabelled Plk4 physiological concentration.

High Plk4 levels and the regulation of the onset and mode of centriole biogenesis

Having established some ground-level quantifications for endogenous Plk4 concentration is helpful for understanding systems where Plk4 is more concentrated and drives other modes of centriole formation. Many studies have described centriole *de novo* assembly across eukaryotic species but no other has yet visualised live the process while aiming at understanding its spatio-temporal regulation. Tackling this problem required an experimental system, which we validated in Chapter 3, whereby a microfluidics approach enables the production of small cytoplasmic explants suitable for quantitative fluorescence microscopy at high spatio-temporal resolution. Despite the obvious advantages of our experimental system, there are still aspects we do not fully master and the resolution is diffraction-limited so our analysis is insightful but restricted to clearly visible centrosomes. We still do not know how centriolar precursors and the intermediate steps in centriole *de novo* assembly look like in this system, but learning this would probably require doing *on-the-fly* Correlative Light Electron Microscopy in the droplets.

In Chapter 4 we further demonstrated that high Plk4 concentration drives the assembly of multiple centrosomes in the cytosolic explants without any apparent number regulation. We show, by live cell imaging, that these centrosomes incorporate multiple components over time. While the first centrosome takes longer to assemble, the subsequent “birth” events are faster,

accelerating with every centrosome formed *de novo*. In this system, where few centrioles have just assembled, the location where they form *de novo* is independent of each other and no particular spatial pattern is observed. Taking these conclusions, however simple they might seem, required modelling a system similar to the experimental one and testing if the experimental observations deviated from the stochastic predictions determined *in silico*, before jumping into any further experiments.

Finding that centriole biogenesis accelerates and that centriole location does not seem to impact the *de novo* location of subsequent ones was surprising and unexpected. For once, it has been proposed that the *de novo* assembly pathway is usually inhibited when centrioles are present (La Terra et al., 2005; Lambrus et al., 2015; Marshall et al., 2001; Uetake et al., 2007), so we would predict centrioles to assemble *de novo* far away from the previous ones and, moreover, we would expect most centrioles to form via canonical duplication. Centrioles accumulate critical components, such as Plk4 and many other proteins (as we have shown in our assays) so, we would expect most birth events to happen by duplication within the same, biochemically inducing environment (Marshall et al., 2001). This was definitely not the case, as centrioles duplicated while concomitantly, new centrosomes formed *de novo* in the cytosol at random distances. Additionally, the faster temporal kinetics we observed hints that a molecular feedforward loop may underlie the process of biogenesis, therefore we did not find evidences of an inhibitory effect between centrosomes formed *de novo*.

While a clear temporal signature underlying a faster kinetics in biogenesis was found, we could not easily conclude from modelling if the acceleration in birth rate is dependent or independent of centrioles, in order to determine the mechanism

behind the sudden burst and acceleration in centriole biogenesis. Non-exclusive possibilities might explain the onset of centriole assembly; a cell-cycle-like transition changing the overall permissiveness of the cytoplasm; and/or Plk4 molecules stochastically concentrating in the cytoplasm, establishing stable and higher-order scaffolds that recruit other components, therefore driving biogenesis.

It is not known whether and how the cell-cycle is regulated in unfertilised fly eggs. Unfertilised eggs have been activated to complete meiosis II as they crossed the oviduct, before being laid by their mothers (Heifetz et al., 2001). The literature indicates that eggs collected within 2 hours post-laying have high Cyclin B levels, but it is not known whether it forms active Cdk1-Cyclin B complexes (Horner et al., 2006; Vardy and Orr-Weaver, 2007). Moreover, we know that downregulation of Cdk1-Cyclin B activity is critical for Plk4 to bind and phosphorylate Ana2 and recruit Sas6, together giving rise to pro-centriole formation (reviewed in Arquint and Nigg, 2016; Zitouni et al., 2016). Our Cdk1 inhibition experiments did not provide a clear evidence of a cell-cycle dependent regulation in this system. Perhaps it would be worth conducting the opposite experiment by which we supplement the extract with a constitutively active Cdk1 and determine if it completely abolishes centriole biogenesis in the presence of high Plk4 levels. Alternatively, unfertilised *Drosophila* eggs are insensitive to the activity of this kinase and remain so until fertilisation occurs and nuclear mitotic divisions begin.

Although it would be exciting to find a cell-cycle-like transition in fly eggs, similarly to what occurs in *Xenopus* egg extracts, cell-cycle progression alone, without the upregulation of a limiting component like Plk4, does not drive MTOC assembly. Diluting Plk4 concentration in the cytosol changes the kinetics of centriole

biogenesis, delaying the *de novo* birth of the first centrosome and to a much smaller extent, the birth of subsequent events. This experiment strongly indicates that Plk4 concentration is a main driver of the onset of centriole assembly in this system. Time-dependent, stochastic accumulation of Plk4 in the cytoplasm drives multiple *de novo* centriole assembly. The apparent acceleration in biogenesis we have measured might be the outcome of the time it takes for Plk4 to form stable, higher-order oligomers in multiple sites in the cytosol, which is dependent on its concentration, which then results in Plk4 becoming active and driving centriole assembly in several locations almost at the same time. The most elegant way to test this hypothesis would be to overexpress a Plk4 allele coupled to a light-responsive element and force Plk4 to associate, hopefully while preserving its activity. Using light-pulses, we would be able to induce Plk4 local concentration and test if this is enough to trigger centriole assembly in the extracts at any desired moment.

Even in the absence of a typical cell-cycle in the eggs, I observed that centrioles undergo time-dependent maturation and they become capable of duplication within 3-4 minutes after they form *de novo*. This is remarkable since a body of studies propose that cell-cycle progression and the centriolar modifications associated with it, are required for centrioles to mature and become competent mothers (Fu et al., 2016; Wang et al., 2011).

It has been proposed that when centrioles are present in the cell (even if they have formed *de novo*), biogenesis would mostly be “templated” from these (Lambrus et al., 2015; Marshall et al., 2001). However, we have confirmed that while several daughter centrioles assemble over time, centrioles continue forming *de novo*, showing that both pathways are not necessarily mutually exclusive and that centrioles alone are not sufficient to inhibit the *de novo* pathway.

The fact that in most cells centrioles only duplicate is probably a consequence of several mechanisms favouring this process, rather than active inhibition of *de novo* biogenesis. The low levels of limiting components, the cell-cycle dependent protein synthesis and degradation and consequently differential centrosomal enrichment of molecules, strong affinity between centrosomal molecules, favourable biochemical environment within the centrosome “phase” that favours the activation of molecules and their interaction with their partners, may be amongst the leading causes. Taking Plk4 as a case-study, our FCS experiments support some of these hypotheses, namely that it is normally present at low concentration in the cytosol; it moves rapidly, perhaps even in a targeted way (via MTs); it undergoes cell-cycle dependent regulation and it forms low order oligomers outside the centrosome. Another rate-limiting centrosomal component, Sas6, was shown to have a similar behaviour in the cytosol in human cells (Keller et al., 2014). Apart from its slower diffusion coefficient compared to Plk4, Sas6 is present in the cytosol mainly as a homodimer, suggesting that its oligomerisation into a ninefold symmetrical structure, occurs mostly at the centrosomes (Keller et al., 2014).

More experiments are required for further understanding how Plk4 levels modulate centriole biogenesis. First, we need to quantify the difference in Plk4 amount between the Gal4-UAS overexpression and endogenous eggs, to bring our 1:5 dilution experiment into a quantitative context. Our aim is accomplishing these quantifications by Western Blot, either using an antibody against Plk4 which we recently purified (not shown) or taking advantage of our CRISPR targeted flies and use a commercially available antibody against mNeonGreen or mEGFP. Secondly, we can conduct new dilution experiments and determine how these

impact the kinetics and mode of centriole biogenesis. At 1:5 dilution both *de novo* and duplication pathways co-occur in the droplets, but we hypothesise that at higher dilution we might only observe single centrioles forming *de novo* which perhaps undergo duplication at most, after an exceptionally long waiting time but no further *de novo* assembly takes place, thus uncoupling the two modes of biogenesis. Finally, expressing different Plk4 mutants in the droplets, such as non-degradable or constitutively active forms (Cunha-Ferreira et al., 2009; Lopes et al., 2015), or even developing mutants that cannot self-oligomerise, may provide interesting insights regarding Plk4 activity and centriole biogenesis.

In conclusion, our work has brought the field some important steps towards a quantitative understanding of Plk4 properties *in vivo* and how these may be important in the regulation of centriole formation. The measurements conducted in the early developing embryo were relevant to learn and establish some ground-rules, before investigating the *de novo* biogenesis driven by high Plk4 levels. Working at the interface of molecular biology and biophysics allowed us to determine properties of centriole *de novo* assembly and probe the role of older centrioles in the biogenesis of others without the burden of a large cell structure that cannot be fully visualised or manipulated. We have raised new hypotheses regarding centriole formation, whereby most can be tested in the experimental system we described and validated herein. Future work ought to address the link between Plk4 concentration, its activity and centriole number control. One major ambition is to be able to precisely manipulate Plk4 concentration in the explants using recombinant protein and determine how it modulates centriole number and the pathways of biogenesis. Moreover, it would be extremely valuable to develop a FRET-based biosensor for Plk4

activity, which could be easily added to the explants and report Plk4 activation in a setup where its concentration is known.

References

- Adon, A. M., Zeng, X., Harrison, M. K., Sannem, S., Kiyokawa, H., Kaldis, P. and Saavedra, H. I.** (2010). Cdk2 and Cdk4 Regulate the Centrosome Cycle and Are Critical Mediators of Centrosome Amplification in p53-Null Cells. *Mol. Cell. Biol.* **30**, 694–710.
- Agircan, F. G., Schiebel, E. and Mardin, B. R.** (2014). Separate to operate: control of centrosome positioning and separation. *Philos. Trans. R. Soc. Lond. B. Biol. Sci.* **369**,.
- Al Jord, A., Lemaître, A.I., Delgehr, N., Faucourt, M., Spassky, N. and Meunier, A.** (2014). Centriole amplification by mother and daughter centrioles differs in multiciliated cells. *Nature* **516**, 104–107.
- Alushin, G. M., Lander, G. C., Kellogg, E. H., Zhang, R., Baker, D. and Nogales, E.** (2014). High resolution microtubule structures reveal the structural transitions in $\alpha\beta$ -tubulin upon GTP hydrolysis. *Cell* **157**, 1117–1129.
- Alvarez-Rodrigo, I., Conduit, P. T., Baumbach, J., Novak, Z. A., Aydogan, M. G., Wainman, A. and Raff, J. W.** (2018). A positive feedback loop drives centrosome maturation in flies. *bioRxiv*.
- Anderson, R. G. W. and Brenner, R. M.** (1971). The formation of basal bodies (Centrioles) in the Rhesus Monkey oviduct. *J. Cell Biol.* **50**, 10–34.
- Arbi, M., Pefani, D.-E., Taraviras, S. and Lygerou, Z.** (2017). Controlling centriole numbers: Geminin family members as master regulators of centriole amplification and multiciliogenesis. *Chromosoma* DOI:10.1007/s00412-017-0652-7.
- Archambault, V. and Glover, D. M.** (2009). Polo-like kinases: conservation and divergence in their functions and regulation. *Nat. Rev. Mol. Cell Biol.* **10**, 265–275.
- Arquint, C. and Nigg, E. A.** (2014). STIL microcephaly mutations interfere with APC/C-mediated degradation and cause centriole amplification. *Curr. Biol.* **24**, 351–360.
- Arquint, C. and Nigg, E. A.** (2016). The PLK4–STIL–SAS-6 module at the core of centriole duplication. *Biochem. Soc. Trans.* **44**, 1253–1263.
- Arquint, C., Gabryjonczyk, A. M., Imseng, S., Böhm, R., Sauer, E., Hiller, S., Nigg, E. A. and Maier, T.** (2015). STIL binding to Polo-box 3 of PLK4 regulates centriole duplication. *Elife* **4**,.
- Avidor-Reiss, T.** (2018). Rapid Evolution of Sperm Produces Diverse Centriole Structures that Reveal the Most Rudimentary. *Cells* **7**,.
- Ayaz, P., Munyoki, S., Geyer, E. A., Piedra, F. A., Vu, E. S., Bromberg, R., Otwinowski, Z., Grishin, N. V., Brautigam, C. A. and Rice, L.**

- M. (2014). A tethered delivery mechanism explains the catalytic action of a microtubule polymerase. *Elife* **3**, 1–19.
- Aydogan, M. G., Wainman, A., Saurya, S., Steinacker, T. L., Caballe, A., Novak, Z. A., Baumbach, J., Muschalik, N. and Raff, J. W.** (2018). A homeostatic clock sets daughter centriole size in flies. *J. Cell Biol.* **217**, 1233–1248.
- Aydogan, M. G., Steinacker, T. L., Mofatteh, M., Gartenmann, L., Wainman, A., Saurya, S., Conduit, P. T., Zhou, F. Y., Boemo, M. A. and Raff, J. W.** (2019). A free-running oscillator times and executes centriole biogenesis. *bioRxiv*.
- Azimzadeh, J.** (2014b). Exploring the evolutionary history of centrosomes. *Philos. Trans. R. Soc. Lond. B. Biol. Sci.* **369**, 20130453.
- Azimzadeh, J., Hergert, P., Delouvé, A., Euteneuer, U., Formstecher, E., Khodjakov, A. and Bornens, M.** (2009). hPOC5 is a centrin-binding protein required for assembly of full-length centrioles. *J. Cell Biol.* **185**, 101–114.
- Azimzadeh, J., Wong, M. L., Downhour, D. M., Alvarado, A. S. and Marshall, W. F.** (2012). Centrosome loss in the evolution of planarians. *Science*. **335**, 461–463.
- Baccetyi, B. and Dallai, R.** (1978). The spermatozoon of Arthropoda. XXX. The multiflagellate spermatozoon in the termite *Mastotermes darwiniensis*. *J. Cell Biol.* **76**, 569–576.
- Bahtz, R., Seidler, J., Arnold, M., Haselmann-Weiss, U., Antony, C., Lehmann, W. D. and Hoffmann, I.** (2012). GCP6 is a substrate of Plk4 and required for centriole duplication. *J. Cell Sci.* **125**, 486–496.
- Banterle, N. and Gönczy, P.** (2017). Centriole Biogenesis: From Identifying the Characters to Understanding the Plot. *Annu. Rev. Cell Dev Biol.* **33**, 23–49.
- Barisic, M., Silva, R., Tripathy, S. K., Magiera, M. M., Zaytsev, A. V., Pereira, A. L., Janke, C., Grishchuk, E. L. and Maiato, H.** (2015). Microtubule detyrosination guides chromosomes during mitosis. *Science*. **348**, 799–803.
- Barnum, K. J. and O’Connell, M. J.** (2014). Cell Cycle Regulation by Checkpoints. *Methods Mol. Biol.* **1170**, 29–40.
- Basto, R., Lau, J., Vinogradova, T., Gardiol, A., Woods, C. G., Khodjakov, A. and Raff, J. W.** (2006). Flies without Centrioles. *Cell* **125**, 1375–1386.
- Basto, R., Brunk, K., Vinadogrova, T., Peel, N., Franz, A., Khodjakov, A. and Raff, J. W.** (2008). Centrosome Amplification Can Initiate Tumorigenesis in Flies. *Cell* **133**, 1032–1042.
- Bauer, M., Cubizolles, F., Schmidt, A. and Nigg, E. A.** (2016).

Quantitative analysis of human centrosome architecture by targeted proteomics and fluorescence imaging. *EMBO J.* **35**, 2152–2166.

- Bazzi, H. and Anderson, K. V.** (2014). Acentriolar mitosis activates a p53-dependent apoptosis pathway in the mouse embryo. *Proc. Natl. Acad. Sci.* **111**, E1491–E1500.
- Benoit, M. P. M. H., Asenjo, A. B. and Sosa, H.** (2018). Cryo-EM reveals the structural basis of microtubule depolymerization by kinesin-13s. *Nat. Commun.* **9**, 1–13.
- Bergeijk, P. Van, Hoogenraad, C. C. and Kapitein, L. C.** (2016). Right Time, Right Place: Probing the Functions of Organelle Positioning. *Trends Cell Biol.* **26**, 121–134.
- Besson, A., Dowdy, S. F. and Roberts, J. M.** (2008). Review CDK Inhibitors: Cell Cycle Regulators and Beyond. *Dev. Cell* **14**, 159–169.
- Bettencourt-Dias, M., Rodrigues-Martins, A., Carpenter, L., Riparbelli, M., Lehmann, L., Gatt, M. K., Carmo, N., Balloux, F., Callaini, G. and Glover, D. M.** (2005). SAK/PLK4 is required for centriole duplication and flagella development. *Curr. Biol.* **15**, 2199–2207.
- Bettencourt-Dias, M., Hildebrandt, F., Pellman, D., Woods, G. and Godinho, S. A.** (2011). Centrosomes and cilia in human disease. *Trends Genet.* **27**, 307–15.
- Blachon, S., Gopalakrishnan, J., Omori, Y., Polyanovsky, A., Church, A., Nicastro, D., Malicki, J. and Avidor-Reiss, T.** (2008). Drosophila asterless and vertebrate Cep152 Are orthologs essential for centriole duplication. *Genetics* **180**, 2081–94.
- Blachon, S., Cai, X., Roberts, K. A., Yang, K., Polyanovsky, A., Church, A. and Avidor-Reiss, T.** (2009). A proximal centriole-like structure is present in Drosophila spermatids and can serve as a model to study centriole duplication. *Genetics* **182**, 133–144.
- Blackwell, R., Sweezy-schindler, O., Edelmaier, C., Gergely, Z. R., Flynn, P. J., Montes, S., Crapo, A., Doostan, A., Mcintosh, J. R., Glaser, M. A., et al.** (2017). Contributions of Microtubule Dynamic Instability and Rotational Diffusion to Kinetochores Capture. *Biophys. J.* **112**, 552–563.
- Blow, J. J.** (1993). Preventing Re-replication of DNA in a Single Cell Cycle: Evidence for a Replication Licensing Factor. *J. Cell Biol.* **122**, 993–1002.
- Blow, J. J. and Laskey, R. A.** (1986). Initiation of DNA Replication in Nuclei and Purified DNA by a Cell-Free Extract of Xenopus Eggs. *Cell* **47**, 577–587.
- Bobinnec, Y., Khodjakov, A., Mir, L. M., Rieder, C. L., Eddé, B. and Bornens, M.** (1998). Centriole disassembly in vivo and its effect on

- centrosome structure and function in vertebrate cells. *J. Cell Biol.* **143**, 1575–1589.
- Boese, C. J., Nye, J., Buster, D. W., Mclamarrah, T. A., Byrnes, A. E., Slep, K. C., Rusan, N. M. and Rogers, G. C.** (2018). Asterless is a Polo-like kinase 4 substrate that both activates and inhibits kinase activity depending on its phosphorylation state. *Mol. Biol. Cell* **29**, 2874–2886.
- Bornens, M.** (2002). Centrosome composition and microtubule anchoring mechanisms. *Curr. Opin. Cell Biol.* **14**, 25–34.
- Bornens, M.** (2008). Organelle positioning and cell polarity. *Nat. Rev. Mol. Cell Biol.* **9**, 874–886.
- Borowiak, M., Nahaboo, W., Reynders, M., Nekolla, K., Jalinot, P., Hasserodt, J., Rehberg, M., Delattre, M., Zahler, S., Vollmar, A., et al.** (2015). Photoswitchable Inhibitors of Microtubule Dynamics Optically Control Mitosis and Cell Death. *Cell* **162**, 403–411.
- Borrego-Pinto, J., Somogyi, K., Karreman, M., König, J., Müller-Reichert, T., Bettencourt-Dias, M., Gönczy, P., Schwab, Y. and Lénart, P.** (2016). Distinct mechanisms eliminate mother and daughter centrioles in meiosis of starfish oocytes. *J. Cell Biol.* **212**, 815–827.
- Breslow, D. K. and Holland, A. J.** (2019). Mechanism and Regulation of Centriole and Cilium Biogenesis. *Annu. Rev. Biochem.* **88**, 11.1-11.34.
- Breugel, M. Van, Hirono, M., Andreeva, A., Yanagisawa, H., Yamaguchi, S., Nakazawa, Y., Morgner, N., Petrovich, M., Robinson, C. V, Johnson, C. M., et al.** (2011). Structures of Sas-6 Suggest Its Centriolar. *Science*. **331**, 1196–1199.
- Brilot, A. F. and Agard, D. A.** (2018). The Atomic Structure of the Microtubule-Nucleating γ -Tubulin Small Complex and its Implications for Regulation. *bioRxiv*.
- Brouhard, G. J. and Rice, L. M.** (2018). Microtubule dynamics: an interplay of biochemistry and mechanics. *Nat. Rev. Mol. Cell Biol.* **19**, 451–463.
- Brown, N. J., Marjanovic, M., Luders, J., Stracker, T. H. and Costanzo, V.** (2013). Cep63 and Cep152 Cooperate to Ensure Centriole Duplication. *PLoS One* **8**,.
- Brownlee, C. W., Klebba, J. E., Buster, D. W. and Rogers, G. C.** (2011). The Protein Phosphatase 2A regulatory subunit Twins stabilizes Plk4 to induce centriole amplification. *J. Cell Biol.* **195**, 231–243.
- Bruinsma, W., Macůrek, L., Freire, R., Lindqvist, A. and Medema, R. H.** (2014). Bora and Aurora-A continue to activate Plk1 in mitosis. *J. Cell Sci.* **127**, 801–811.

- Burkard, M. E., Maciejowski, J., Rodriguez-Bravo, V., Repka, M., Lowery, D. M., Clauser, K. R., Zhang, C., Shokat, K. M., Carr, S. A., Yaffe, M. B., et al.** (2009). Plk1 self-organization and priming phosphorylation of HsCYK-4 at the spindle midzone regulate the onset of division in human cells. *PLoS Biol.* **7**, 1–16.
- Bury, L., Coelho, P. A., Simeone, A., Ferries, S., Eyers, C. E., Eyers, P. A., Zernicka-Goetz, M. and Glover, D. M.** (2017). Plk4 and Aurora A cooperate in the initiation of acentriolar spindle assembly in mammalian oocytes. *J. Cell Biol.* **216**, 3571–3590.
- Cabral, G., Sans, S. S., Cowan, C. R. and Dammermann, A.** (2013). Multiple mechanisms contribute to centriole separation in *C. elegans*. *Curr. Biol.* **23**, 1380–1387.
- Callaini, G. and Riparbelli, M. G.** (1990). Centriole and centrosome cycle in the early *Drosophila* embryo. *J. Cell Sci.* **97**, 539–544.
- Callaini, G., Whitfield, W. G. F. and Riparbelli, M. G.** (1997). Centriole and Centrosome Dynamics during the Embryonic Cell Cycles That Follow the Formation of the Cellular Blastoderm in *Drosophila*. *Exp. Cell Res.* **234**, 183–190.
- Campos-Ortega, Iose A. and Hartenstein, V.** (1997). *The Embryonic Development of Drosophila melanogaster*.
- Carvalho-Santos, Z., Azimzadeh, J., Pereira-Leal, J. B. and Bettencourt-Dias, M.** (2011). Tracing the origins of centrioles, cilia, and flagella. *J. Cell Biol.* **194**, 165–75.
- Carvalho-Santos, Z., Machado, P., Alvarez-Martins, I., Gouveia, S. M., Jana, S. C., Duarte, P., Amado, T., Branco, P., Freitas, M. C., Silva, S. T. N., et al.** (2012). BLD10/CEP135 Is a Microtubule-Associated Protein that Controls the Formation of the Flagellum Central Microtubule Pair. *Dev. Cell* **23**, 412–424.
- Caudron, N., Arnal, I., Buhler, E., Job, D. and Valiron, O.** (2002). Microtubule nucleation from stable tubulin oligomers. *J. Biol. Chem.* **277**, 50973–50979.
- Cavalier-Smith, T.** (2002). The phagotrophic origin of eukaryotes and phylogenetic classification on protozoa. *Int. J. Syst. Evol. Microbiol.* **52**, 297–354.
- Cavanaugh, A. M. and Jaspersen, S. L.** (2017). Big Lessons from Little Yeast: Budding and Fission Yeast Centrosome Structure, Duplication, and Function. *Annu. Rev. Genet.* **51**, 361–383.
- Chakraborti, S., Natarajan, K., Curiel, J., Janke, C. and Liu, J.** (2016). The Emerging Role of the Tubulin Code: From the Tubulin Molecule to Neuronal Function and Disease. *Cytoskeleton* **73**, 521–550.
- Chang, C., Hsu, W., Tsai, J., Tang, C. C. and Tang, T. K.** (2016). CEP295

- interacts with microtubules and is required for centriole elongation. *J. Cell Sci.* **129**, 2501–2513.
- Chen, J. V., Kao, L. R., Jana, S. C., Loukianova, E. S., Mendonça, S., Cabrera, O. A., Singh, P., Cabernard, C., Eberl, D. F., Dias, M. B., et al.** (2015). Rootletin organizes the ciliary rootlet to achieve neuron sensory function in *Drosophila*. *J. Cell Biol.* **211**, 435–453.
- Chen, J. V., Buchwalter, R. A., Kao, L. and Megraw, T. L.** (2017). A Splice Variant of Centrosomin Converts Mitochondria to Microtubule-Organizing Centers. *Curr. Biol.* **27**, 1928–1940.
- Cizmecioglu, O., Arnold, M., Bahtz, R., Settele, F., Ehret, L., Haselmann-Weiss, U., Antony, C. and Hoffmann, I.** (2010). Cep152 acts as a scaffold for recruitment of Plk4 and CPAP to the centrosome. *J. Cell Biol.* **191**, 731–9.
- Clute, P. and Pines, J.** (1999). Temporal and spatial control of cyclin B1 destruction in metaphase. *Nat. Cell Biol.* **1**, 82–87.
- Coelho, P. A., Bury, L., Sharif, B., Riparbelli, M. G., Fu, J., Callaini, G. and Glover, D. M.** (2013). Spindle Formation in the Mouse Embryo Requires Plk4 in the Absence of Centrioles. *Dev. Cell* **27**, 586–597.
- Conduit, P. T., Brunk, K., Dobbelaere, J., Dix, C. I., Lucas, E. P. and Raff, J. W.** (2010). Centrioles Regulate Centrosome Size by Controlling the Rate of Cnn Incorporation into the PCM. *Curr. Biol.* **20**, 2178–2186.
- Conduit, P. T., Richens, J. H., Wainman, A., Holder, J., Vicente, C. C., Pratt, M. B., Dix, C. I., Novak, Z. a, Dobbie, I. M., Schermelleh, L., et al.** (2014a). A molecular mechanism of mitotic centrosome assembly in *Drosophila*. *Elife* **3**,.
- Conduit, P. T., Feng, Z., Richens, J. H., Baumbach, J., Wainman, A., Bakshi, S. D., Dobbelaere, J., Johnson, S., Lea, S. M. and Raff, J. W.** (2014b). The centrosome-specific phosphorylation of Cnn by Polo/Plk1 drives Cnn scaffold assembly and centrosome maturation. *Dev. Cell* **28**, 659–69.
- Conduit, P. T., Wainman, A., Novak, Z. A., Weil, T. T. and Raff, J. W.** (2015). Re-examining the role of *Drosophila* Sas-4 in centrosome assembly using two-colour-3D-SIM FRAP. *Elife* **4**,.
- Cottee, M. A., Muschalik, N., Johnson, S., Leveson, J., Raff, J. W. and Susan, L. M.** (2015). The homo-oligomerisation of both Sas-6 and Ana2 is required for efficient centriole assembly in flies. *Elife*.
- Courtois, A., Schuh, M., Ellenberg, J. and Hiiragi, T.** (2012). The transition from meiotic to mitotic spindle assembly is gradual during early mammalian development. *J. Cell Biol.* **198**, 357–370.

- Crest, J., Oxnard, N., Ji, J. and Schubiger, G.** (2007). Onset of the DNA Replication Checkpoint in the Early *Drosophila* Embryo. *Genetics* **175**, 567–584.
- Cunha-Ferreira, I., Rodrigues-Martins, A., Bento, I., Riparbelli, M., Zhang, W., Laue, E., Callaini, G., Glover, D. M. and Bettencourt-Dias, M.** (2009a). The SCF/Slimb Ubiquitin Ligase Limits Centrosome Amplification through Degradation of SAK/PLK4. *Curr. Biol.* **19**, 43–49.
- Cunha-Ferreira, I., Bento, I. and Bettencourt-Dias, M.** (2009b). From zero to many: control of centriole number in development and disease. *Traffic* **10**, 482–98.
- Cunha-Ferreira, I., Bento, I., Pimenta-Marques, A., Jana, S. C., Lince-Faria, M., Duarte, P., Borrego-Pinto, J., Gilberto, S., Amado, T., Brito, D., et al.** (2013). Regulation of Autophosphorylation Controls PLK4 Self-Destruction and Centriole Number. *Curr. Biol.* **23**, 2245–2254.
- Dammermann, A., Müller-Reichert, T., Pelletier, L., Habermann, B., Desai, A. and Oegema, K.** (2004). Centriole assembly requires both centriolar and pericentriolar material proteins. *Dev. Cell* **7**, 815–829.
- Dammermann, A., Maddox, P. S., Desai, A. and Oegema, K.** (2008). SAS-4 is recruited to a dynamic structure in newly forming centrioles that is stabilized by the gamma-tubulin-mediated addition of centriolar microtubules. *J. Cell Biol.* **180**, 771–785.
- de-Carvalho, J., Deshpande, O., Nabais, C. and Telley, I. A.** (2018). *A cell-free system of Drosophila egg explants supporting native mitotic cycles*. 1st ed. Elsevier Inc.
- de Cárcer, G., Escobar, B., Higuero, A. M., García, L., Ansón, A., Pérez, G., Mollejo, M., Manning, G., Meléndez, B., Abad-Rodríguez, J., et al.** (2011). Plk5, a polo box domain-only protein with specific roles in neuron differentiation and glioblastoma suppression. *Mol. Cell. Biol.* **31**, 1225–1239.
- Debec, A., Marcaillou, C., Bobinnec, Y. and Borot, C.** (1999). The centrosome cycle in syncytial *Drosophila* embryos analyzed by energy filtering transmission electron microscopy. *Biol. Cell* **91**, 379–391.
- Delattre, M., Canard, C. and Gönczy, P.** (2006). Sequential protein recruitment in *C. elegans* centriole formation. *Curr. Biol.* **16**, 1844–9.
- Delgehyr, N., Mao, G., Tom, B., Riparbelli, M. G., Callaini, G. and Glover, D. M.** (2012). Klp10A, a Microtubule-Depolymerizing Kinesin-13, Cooperates with CP110 to Control *Drosophila* Centriole Length. *Curr. Biol.* **22**, 502–509.
- Deneke, V. E., Melbinger, A., Vergassola, M. and Talia, S. Di** (2016).

Waves of Cdk1 activity in S-phase synchronize the cell cycle in *Drosophila* embryos. *Dev. Cell* **38**, 399–412.

- Denu, R. A., Zasadil, L. M., Kanugh, C., Laffin, J., Weaver, B. A. and Burkard, M. E.** (2016). Centrosome amplification induces high grade features and is prognostic of worse outcomes in breast cancer. *BMC Cancer* **16**,.
- Denu, R. A., Shabbir, M., Nihal, M., Singh, C. K., Longley, B. J., Burkard, M. E. and Ahmad, N.** (2018). Centriole Overduplication is the Predominant Mechanism Leading to Centrosome Amplification in Melanoma. *Mol. Cancer Res.*
- Desai, A. and Mitchison, T. J.** (1997). Microtubule polymerization dynamics. *Annu. Rev. Cell Dev. Biol.* **13**, 83–117.
- Dingle, A. D. and Fulton, C.** (1966). Development of the flagellar apparatus of *Naegleria*. *J. Cell Biol.* **31**, 43–54.
- Dirksen, E. R.** (1961). The presence of centrioles in artificially activated sea urchin eggs. *J. Cell Biol.* **11**, 244–247.
- Dirksen, E. R.** (1971). Centriole morphogenesis in developing ciliated epithelium of the mouse oviduct. *J. Cell Biol.* **51**, 286–302.
- Dix, C. I. and Raff, J. W.** (2007). *Drosophila* Spd-2 Recruits PCM to the Sperm Centriole, but Is Dispensable for Centriole Duplication. *Curr. Biol.* **17**, 1759–1764.
- Dobbelaere, J., Josué, F., Suijkerbuijk, S., Baum, B., Tapon, N. and Raff, J.** (2008). A genome-wide RNAi screen to dissect centriole duplication and centrosome maturation in *Drosophila*. *PLoS Biol.* **6**, 1975–1990.
- Doonan, J. H., Lloyd, C. W. and Duckett, J. G.** (1986). Anti-tubulin antibodies locate the blepharoplast during spermatogenesis in the fern *Platyzoma microphyllum* R.Br.: a correlated immunofluorescence and electron-microscopic study. *J. Cell Sci.* **81**, 243–265.
- Driver, J. W., Geyer, E. A., Bailey, M. E., Rice, L. M. and Asbury, C. L.** (2017). Direct measurement of conformational strain energy in protofilaments curling outward from disassembling microtubule tips. *Elife* **6**, 1–18.
- Duensing, A., Liu, Y., Tseng, M., Malumbres, M., Barbacid, M. and Duensing, S.** (2006). Cyclin-dependent kinase 2 is dispensable for normal centrosome duplication but required for oncogene-induced centrosome overduplication. *Oncogene* **25**, 2943–2949.
- Dzhindzhev, N. S., Yu, Q. D., Weiskopf, K., Tzolovsky, G., Cunha-Ferreira, I., Riparbelli, M., Rodrigues-Martins, A., Bettencourt-Dias, M., Callaini, G. and Glover, D. M.** (2010). Asterless is a scaffold for the onset of centriole assembly. *Nature* **467**, 714–8.

- Dzhindzhev, N. S., Tzolovsky, G., Lipinski, Z., Schneider, S., Lattao, R., Fu, J., Debski, J., Dadlez, M. and Glover, D. M.** (2014). Plk4 Phosphorylates Ana2 to Trigger Sas6 Recruitment and Procentriole Formation. *Curr. Biol.* **24**, 2526–2532.
- Dzhindzhev, N. S., Tzolovsky, G., Lipinski, Z., Abdelaziz, M., Debski, J., Dadlez, M. and Glover, D. M.** (2017). Two-step phosphorylation of Ana2 by Plk4 is required for the sequential loading of Ana2 and Sas6 to initiate procentriole formation. *Open Biol.* **7**,.
- Eckerdt, F., Yamamoto, T. M., Lewellyn, A. L. and Maller, J. L.** (2011). Identification of a polo-like kinase 4-dependent pathway for de novo centriole formation. *Curr. Biol.* **21**, 428–32.
- Edgar, B. A. and Schubiger, G.** (1986). Parameters Controlling Transcriptional Activation during Early Drosophila Development. *Cell* **44**, 871–877.
- Edgar, B. A., Sprenger, F., Duronio, R. J., Leopold, P. and Farrell, P. H. O.** (1994). Distinct molecular mechanisms regulate cell cycle timing at successive stages of Drosophila embryogenesis. *Genes Dev.* **8**, 440–452.
- Elia, A. E., Cantley, L. C. and Yaffe, M. B.** (2003a). Proteomic Screen Finds pSer-pThr-Binding Domain Localizing Plk1 to Mitotic Substrates. *Science.* **299**, 1228–1231.
- Elia, A. E. H., Rellos, P., Haire, L. F., Chao, J. W., Ivins, F. J., Hoepker, K., Mohammad, D., Cantley, L. C., Smerdon, S. J. and Yaffe, M. B.** (2003b). The molecular basis for phosphodependent substrate targeting and regulation of Plks by the Polo-box domain. *Cell* **115**, 83–95.
- Evans, T., Rosenthal, E. T., Youngblom, J., Distel, D. and Hunt, T.** (1983). Cyclin: A Protein Specified by Maternal mRNA in Sea Urchin Eggs That Is Destroyed at Each Cleavage Division. *Cell* **33**, 389–396.
- Fabunmi, R. P., Wigley, W. C., Thomas, P. J. and Demartino, G. N.** (2000). Activity and Regulation of the Centrosome-associated Proteasome. *J. Biol. Chem.* **275**, 409–413.
- Farache, D., Emorine, L., Haren, L. and Merdes, A.** (2018). Assembly and regulation of gamma-tubulin complexes. *Open Biol.* **8**,.
- Farrell, J. A. and O'Farrell, P. H.** (2014). From egg to gastrula: How the cell cycle is remodeled during the Drosophila mid-blastula transition. *Annu. Rev. Genet.* **48**, 269–294.
- Feldman, J. L. and Priess, J. R.** (2012). A role for the centrosome and PAR-3 in the hand-off of MTOC function during epithelial polarization. *Curr. Biol.* **22**, 575–582.
- Fenger, D. D., Carminati, J. L., Burney-Sigman, D. L., Kashevsky, H.,**

- Dines, J. L., Elfring, L. K. and Orr-Weaver, T. L.** (2000). PAN GU: a protein kinase that inhibits S-phase and promotes mitosis in early *Drosophila* development. *Development* **127**, 4763–4774.
- Findeisen, M., El-denary, M., Kapitza, T., Graf, R. and Strausfeld, U.** (1999). Cyclin A-dependent kinase activity affects chromatin binding of ORC, Cdc6, and MCM in egg extracts of *Xenopus laevis*. *Eur J Biochem* **264**, 415–426.
- Findeisen, P., Mühlhausen, S., Dempewolf, S., Hertzog, J., Zietlow, A., Carlomagno, T. and Kollmar, M.** (2014). Six subgroups and extensive recent duplications characterize the evolution of the eukaryotic tubulin protein family. *Genome Biol. Evol.* **6**, 2274–2288.
- Fischer, M., Quaas, M., Wintsche, A., Müller, G. A. and Engeland, K.** (2014). Polo-like kinase 4 transcription is activated via CRE and NRF1 elements, repressed by DREAM through CDE/CHR sites and deregulated by HPV E7 protein. *Nucleic Acids Res.* **42**, 163–180.
- Flemming, W.** (1965). Contributions to the Knowledge of the Cell. *J. Cell Biol.* **25**,.
- Fletcher, D. A. and Mullins, R. D.** (2010). Cell mechanics and the cytoskeleton. *Nature* **463**, 485–492.
- Fode, C., Motro, B., Yousefi, S., Heffernan, M. and Dennis, J. W.** (1994). Sak, a murine protein-serine/threonine kinase that is related to the *Drosophila* polo kinase and involved in cell proliferation. *Proc. Natl. Acad. Sci. U. S. A.* **91**, 6388–6392.
- Fode, C., Binkert, C. and Dennis, J.** (1996). Constitutive Expression of Murine Sak-a Suppresses Cell Growth and Induces Multinucleation. *Mol. Cell. Biol.* **16**, 4665–4672.
- Foe, V. E. and Alberts, B. M.** (1983). Studies of nuclear and cytoplasmic behaviour during the five mitotic cycles that precede gastrulation in *Drosophila* embryogenesis. *J. Cell Sci.* **61**, 31–70.
- Fong, K.-W., Choi, Y.-K., Rattner, J. B., Qi and Z., R.** (2008). CDK5RAP2 Is a Pericentriolar Protein That Functions in Centrosomal Attachment of the gamma-Tubulin Ring Complex. *Mol. Biol. Cell* **19**, 115–125.
- Fontela, Y. C., Kadavath, H., Biernat, J., Riedel, D., Mandelkow, E. and Zweckstetter, M.** (2017). Multivalent cross-linking of actin filaments and microtubules through the microtubule-associated protein Tau. *Nat. Commun.* **8**,.
- Francia, M. E., Dubremetz, J. F. and Morrissette, N. S.** (2016). Basal body structure and composition in the apicomplexans *Toxoplasma* and *Plasmodium*. *Cilia* **5**, DOI: 10.1186/s13630-016-0025-5.
- Franz, A., Roque, H., Saurya, S., Dobbelaere, J. and Raff, J. W.** (2013). CP110 exhibits novel regulatory activities during centriole assembly

- in *Drosophila*. *J. Cell Biol.* **203**, 785–99.
- Freeman, M., Nüsslein-Volhard, C. and Glover, D. M.** (1986). The dissociation of Nuclear and Centrosomal Division in *gnu*, a Mutation causing Giant Nuclei in *Drosophila*. *Cell* **46**, 457–468.
- Fritz-Laylin, L. K. and Fulton, C.** (2016). Naegleria: a classic model for de novo basal body assembly. *Cilia* **5**, DOI: 10.1186/s13630-016-0032-6.
- Fritz-Laylin, L. K., Assaf, Z. J., Chen, S. and Cande, W. Z.** (2010). Naegleria gruberi de novo basal body assembly occurs via stepwise incorporation of conserved proteins. *Eukaryot. Cell* **9**, 860–865.
- Fritz-Laylin, L. K., Levy, Y. Y., Levitan, E., Chen, S., Cande, W. Z., Lai, E. Y. and Fulton, C.** (2016). Rapid centriole assembly in Naegleria reveals conserved roles for both de novo and mentored assembly. *Cytoskeleton* **73**, 109–116.
- Fry, A. M., Sampson, J., Shak, C. and Shackleton, S.** (2017). Recent advances in pericentriolar material organization: ordered layers and scaffolding gels. *F1000Research* **6**,.
- Fu, J. and Glover, D. M.** (2012). Structured illumination of the interface between centriole and peri-centriolar material. *Open Biol.* **2**,.
- Fu, J., Lipinszki, Z., Rangone, H., Min, M., Mykura, C., Chao-chu, J., Schneider, S., Dzhindzhev, N. S., Gottardo, M., Riparbelli, G., et al.** (2016). Conserved Molecular Interactions in Centriole-to-Centrosome Conversion. *Nat. Cell Biol.* **18**, 87–99.
- Fulton, C. and Dingle, A. D.** (1971). Basal bodies, but not centrioles, in naegleria. *J. Cell Biol.* **51**, 826–835.
- Gall, J. G.** (1961). Centriole replication. A study of spermatogenesis in the snail *Viviparus*. *J Biophys Biochem Cytol* **10**, 163–193.
- Galletta, B. J., Fagerstrom, C. J., Schoborg, T. A., Mclamarrah, T. A., Ryniawec, J. M., Buster, D. W., Slep, K. C., Rogers, G. C. and Rusan, N. M.** (2016). A centrosome interactome provides insight into organelle assembly and reveals a non-duplication role for PLK4. *Nat. Commun.* **7**,.
- Ganem, N. J., Godinho, S. a and Pellman, D.** (2009). A Mechanism Linking Extra Centrosomes to Chromosomal Instability. *Nature* **460**, 278–282.
- Gao, Y., Anthony, S. M., Yu, Y., Yi, Y. and Yu, Y.** (2018). Cargos Rotate at Microtubule Intersections during Intracellular Trafficking. *Biophys. J.* **114**, 2900–2909.
- Gardner, M. K., Charlebois, B. D., Jánosi, I. M., Howard, J., Hunt, A. J. and Odde, D. J.** (2011). Rapid microtubule self-assembly kinetics. *Cell* **146**, 582–592.

- Giansanti, M. G., Bucciarelli, E., Bonaccorsi, S. and Gatti, M.** (2008). *Drosophila* SPD-2 Is an Essential Centriole Component Required for PCM Recruitment and Astral-Microtubule Nucleation. *Curr. Biol.* **18**, 303–309.
- Gifford, E. M. and Larson, S.** (1980). Developmental Features of the Spermatogenous Cell in *Ginkgo biloba*. *Am. J. Bot.* **67**, 119–124.
- Gimpel, P., Lee, Y. L., Sobota, R. M., Calvi, A., Koullourou, V., Patel, R., Mamchaoui, K., Nédélec, F., Shackleton, S., Schmoranz, J., et al.** (2017). Nesprin-1 α -Dependent Microtubule Nucleation from the Nuclear Envelope via Akap450 Is Necessary for Nuclear Positioning in Muscle Cells. *Curr. Biol.* **27**, 1–11.
- Godfrey, M., Touati, S. A., Kataria, M., Jones, A., Snijders, A. P. and Uhlmann, F.** (2017). PP2ACdc55 Phosphatase Imposes Ordered Cell-Cycle Phosphorylation by Opposing Threonine Phosphorylation. *Mol. Cell* **65**, 393–402.
- Godinho, S. A. and Pellman, D.** (2014). Causes and consequences of centrosome abnormalities in cancer. *Philos. Trans. R. Soc. B Biol. Sci.* **369**, .
- Godinho, S. A., Picone, R., Burute, M., Dagher, R., Su, Y., Leung, C. T., Polyak, K., Brugge, J. S., Thery, M. and Pellman, D.** (2014). Oncogene-like induction of cellular invasion from centrosome amplification. *Nature* **510**, 167–171.
- Goenczy, P., Echeverri, C., Oegema, K., Coulson, A., Jones, S. J. M., Copley, R. R., Duperon, J., Oegema, J., Brehm, M., Cassin, E., et al.** (2000). Functional genomic analysis of cell division in *C. elegans* using RNAi of genes on chromosome III. *Nature* **408**, 331–336.
- Goentoro, L. A., Yakoby, N., Goodhouse, J., Schupbach, T. and Shvartsman, S. Y.** (2006). Quantitative Analysis of the GAL4/UAS System in *Drosophila* Oogenesis. *Genesis* **44**, 66–74.
- Gomez-Ferrera, M. A., Rath, U., Buster, D. W., Chanda, S. K., Caldwell, J. S., Rines, D. R. and Sharp, D. J.** (2007). Human Cep192 Is Required for Mitotic Centrosome and Spindle Assembly. *Curr. Biol.* **17**, 1960–1966.
- González-Reyes, A., Elliot, H. and St Johnston, D.** (1995). Polarization of both major body axes in *Drosophila* by gurken-torpedo signalling. *Nature* **375**, 654–658.
- Gonzalez, C., Saunders, R. D., Casal, J., Molina, I., Carmena, M., Ripoll, P. and Glover, D. M.** (1990). Mutations at the *asp* locus of *Drosophila* lead to multiple free centrosomes in syncytial embryos, but restrict centrosome duplication in larval neuroblasts. *J. Cell Sci.* **96 (Pt 4)**, 605–616.
- González, C., Tavosanis, G. and Mollinari, C.** (1998). Centrosomes and

- microtubule organisation during *Drosophila* development. *J. Cell Sci.* **111**, 2697–2706.
- Goodson, H. V and Jonasson, E. M.** (2018). Microtubules and Microtubule-Associated Proteins. *Cold Spring Harb Perspect Biol.*
- Gopalakrishnan, J., Mennella, V., Blachon, S., Zhai, B., Smith, A. H., Megraw, T. L., Nicastro, D., Gygi, S. P., Agard, D. a and Avidor-Reiss, T.** (2011). Sas-4 provides a scaffold for cytoplasmic complexes and tethers them in a centrosome. *Nat. Commun.* **2**,.
- Goshima, G., Wollman, R., Goodwin, S. S., Zhang, N., M, J., Vale, R. D. and Stuurman, N.** (2007). Genes required for mitotic spindle assembly in *Drosophila* S2 cells. *Science.* **316**, 417–421.
- Goshima, G., Mayer, M., Zhang, N., Stuurman, N. and Vale, R. D.** (2008). Augmin: a protein complex required for centrosome-independent microtubule generation within the spindle. *J. Cell Biol.* **181**, 421–429.
- Gottardo, M., Callaini, G. and Riparbelli, M. G.** (2015). The *Drosophila* centriole conversion of doublets into triplets within the stem cell niche. *J. Cell Sci.* **128**, 2437–2442.
- Gräf, R., Batsios, P. and Meyer, I.** (2015). Evolution of centrosomes and the nuclear lamina: Amoebozoan assets. *Eur. J. Cell Biol.* **94**, 249–256.
- Grau, M. B., Curto, G. G., Rocha, C., Magiera, M. M., Sousa, P. M., Giordano, T., Spassky, N. and Janke, C.** (2013). Tubulin glycosylases and glutamylases have distinct functions in stabilization and motility of ependymal cilia. *J. Cell Biol.* **202**, 441–451.
- Greenan, G., Keszthelyi, B., Vale, R. D. and Agard, D. A.** (2018). Insights into centriole biogenesis and evolution revealed by cryoTomography of doublet and triplet centrioles. *Elife* **7**,.
- Grimes, G. W.** (1973a). Origin and development of kinetosomes in *Oxytricha fallax*. *J. Cell Sci.* **13**, 43–53.
- Grimes, G. W.** (1973b). Morphological discontinuity of kinetosomes during the life cycle of *Oxytricha fallax*. *J. Cell Biol.* **57**, 229–232.
- Guardavaccaro, D., Kudo, Y., Boulaire, J., Barchi, M., Busino, L., Donzelli, M., Margottin-Goguet, F., Jackson, P. K., Yamasaki, L. and Pagano, M.** (2003). Control of Meiotic and Mitotic Progression by the F box Protein Beta-Trcp1 in vivo. *Dev. Cell* **4**, 799–812.
- Guderian, G., Westendorf, J., Uldschmid, A. and Nigg, E. a** (2010). Plk4 trans-autophosphorylation regulates centriole number by controlling betaTrCP-mediated degradation. *J. Cell Sci.* **123**, 2163–2169.
- Gudi, R., Haycraft, C. J., Bell, P. D., Li, Z. and Vasu, C.** (2015). Centrobin-mediated regulation of CPAP level limits centriole length during elongation stage. *J. Biol. Chem.* **290**, 6890–6902.

- Gueth-Hallonet, C., Antony, C., Aghion, J., Santa-Maria, A., Lajoie-Mazenc, I., Wright, M. and Maro, B.** (1993). gamma-Tubulin is present in acentriolar MTOCs during early mouse development. *J. Cell Sci.* **105**, 157–166.
- Guichard, P., Chrétien, D., Marco, S. and Tassin, A.-M.** (2010). Procentriole assembly revealed by cryo-electron tomography. *EMBO J.* **29**, 1565–1572.
- Guichard, P., Hamel, V., Guennec, M. Le, Banterle, N., Iacovache, I., Nemcikova, V., Fluckiger, I., Goldie, K. N., Stahlberg, H., Levy, D., et al.** (2017). Cell-free reconstitution reveals centriole cartwheel assembly mechanisms. *Nat. Commun.* **8**,.
- Guichet, A., Peri, F. and Roth, S.** (2001). Stable anterior anchoring of the oocyte nucleus is required to establish dorsoventral polarity of the drosophila egg. *Dev. Biol.* **237**, 93–106.
- Gurtovenko, A. A., Anwar, J. and Yorkshire, W.** (2007). Modulating the Structure and Properties of Cell Membranes: The Molecular Mechanism of Action of Dimethyl Sulfoxide. *J. Phys Chem* 10453–10460.
- Guse, A., Carroll, C. W., Moree, B., Fuller, C. J. and Straight, A. F.** (2012). In vitro centromere and kinetochore assembly on defined chromatin templates. *Nature* **477**, 354–358.
- Gutierrez-Escribano, P. and Nurse, P.** (2015). A single cyclin–CDK complex is sufficient for both mitotic and meiotic progression in fission yeast. *Nat. Commun.* **6**,.
- Habedanck, R., Stierhof, Y.-D., Wilkinson, C. J. and Nigg, E. A.** (2005). The Polo kinase PLK4 functions in centriole duplication. *Nat. Cell Biol.* **7**, 1140–1146.
- Hagiwara, H., Ohwada, N. and Takata, K.** (2004). Cell Biology of Normal and Abnormal Ciliogenesis in the Ciliated Epithelium. *Int. Rev. Cytol.* **234**, 101–141.
- Hales, K. G., Korey, C. A., Larracuenta, A. M. and Roberts, D. M.** (2015). Genetics on the Fly: A Primer on the Drosophila Model System. *Genetics* **201**, 815–842.
- Hamada, T.** (2014). Microtubule Organization and Microtubule-Associated Proteins in Plant Cells. *Int. Rev. Cell Mol. Biol.* **312**, 1–52.
- Hames, R. S., Crookes, R. E., Straatman, K. R., Merdes, A., Hayes, M. J., Faragher, A. J. and Fry, A. M.** (2005). Dynamic Recruitment of Nek2 Kinase to the Centrosome Involves Microtubules, PCM-1, and Localized Proteasomal Degradation. *Mol. Biol. Cell* **16**, 1711–1724.
- Hannak, E., Kirkham, M., Hyman, A. A. and Oegema, K.** (2001). Aurora-A kinase is required for centrosome maturation in *Caenorhabditis*

- elegans*. *J. Cell Biol.* **155**, 1109–1115.
- Hannak, E., Oegema, K., Kirkham, M., Gönczy, P., Habermann, B. and Hyman, A. A.** (2002). The kinetically dominant assembly pathway for centrosomal asters in *Caenorhabditis elegans* is gamma-tubulin dependent. *J. Cell Biol.* **157**, 591–602.
- Hara, M., Lourido, S., Petrova, B., Lou, H. J., Von Stetina, J. R., Kashevsky, H., Turk, B. E. and Orr-Weaver, T. L.** (2018). Identification of PNG kinase substrates uncovers interactions with the translational repressor TRAL in the oocyte-to-embryo transition. *Elife* **7**, 1–19.
- Hartwell, L. H. and Weinert, T. A.** (1989). Checkpoints: Controls That Ensure the Order of Cell Cycle Events. *Science*. **246**,.
- Hartwell, L. H., Culotti, J., Pringle, J. R. and Reid, B. J.** (1974). Genetic Control of the Cell Division Cycle in Yeast. *Science*. **183**, 46–51.
- Harvey, E. B.** (1936). Parthenogenetic Merogony or Cleavage without Nuclei in *Arbacia punctulata*. *Mar. Biol. Lab.* **71**, 101–121.
- Hatch, E. M., Kulukian, A., Holland, A. J., Cleveland, D. W. and Stearns, T.** (2010). Cep152 interacts with Plk4 and is required for centriole duplication. *J. Cell Biol.* **191**, 721–729.
- Heald, R., Tournebize, R., Blank, T., Sandatzopoulos, R., Becker, P., Hyman, A. and Karsenti, E.** (1996). Self organisation of microtubules into bipolar spindles around artificial chromosomes in *Xenopus* egg extracts. *Nature* **382**, 420–425.
- Heifetz, Y., Yu, J. and Wolfner, M. F.** (2001). Ovulation Triggers Activation of *Drosophila* Oocytes. *Dev. Biol.* **234**, 416–424.
- Hepler, P. K.** (1976). The blepharoplast of *Marsilea*: its de novo formation and spindle association. *J. Cell Sci.* **21**, 361–90.
- Hertig, A. T. and Adams, E. C.** (1967). Studies on the human oocyte and its follicle. *J. Cell Biol.* **34**, 647–75.
- Hildebrandt, F., Benzing, T. and Katsanis, N.** (2011). Ciliopathies. *N. Engl J. Med* **364**, 1533–1543.
- Hinchcliffe, E. H., Li, C., Thompson, E. A., Maller, J. L. and Sluder, G.** (1999). Requirement of Cdk2-cyclin E activity for repeated centrosome reproduction in *Xenopus* egg extracts. *Science*. **283**, 851–854.
- Hirono, M.** (2014). Cartwheel assembly. *Phil. Trans. R. Soc. B* **369**,.
- Hochegger, H., Takeda, S. and Hunt, T.** (2008). Cyclin-dependent kinases and cell-cycle transitions: does one fit all? *Nat. Rev. Mol. Cell Biol.* **9**, 910–916.

- Hodges, M. E., Scheumann, N., Wickstead, B., Langdale, J. A. and Gull, K.** (2010). Reconstructing the evolutionary history of the centriole from protein components. *J. Cell Sci.* **123**, 1407–1413.
- Hodges, M. E., Wickstead, B., Gull, K. and Langdale, J. A.** (2012). The evolution of land plant cilia. *New Phytol.* **195**, 526–540.
- Hoffman, J. C. and Vaughn, K. C.** (1995). Using the Developing Spermatogenous Cells of Ceratopteris to Unlock the Mysteries of the Plant Cytoskeleton. *Int. J. Plant Sci.* **156**, 346–358.
- Hoffman, J. C., Vaughn, K. C. and Joshi, H. C.** (1994). Structural and immunocytochemical characterization of microtubule organizing centers in pteridophyte spermatogenous cells. *Protoplasma* **179**, 46–60.
- Hoh, R. A., Stowe, T. R., Turk, E. and Stearns, T.** (2012). Transcriptional Program of Ciliated Epithelial Cells Reveals New Cilium and Centrosome Components and Links to Human Disease. *PLoS One* **7**, e52166.
- Holland, A. J., Lan, W., Niessen, S., Hoover, H. and Cleveland, D. W.** (2010). Polo-like kinase 4 kinase activity limits centrosome overduplication by autoregulating its own stability. *J. Cell Biol.* **188**, 191–8.
- Holland, A. J., Fachinetti, D., Da Cruz, S., Zhu, Q., Vitre, B., Lince-Faria, M., Chen, D., Parish, N., Verma, I. M., Bettencourt-Dias, M., et al.** (2012a). Polo-like kinase 4 controls centriole duplication but does not directly regulate cytokinesis. *Mol. Biol. Cell* **23**, 1838–1845.
- Holland, A. J., Fachinetti, D., Zhu, Q., Bauer, M., Verma, I. M., Nigg, E. a and Cleveland, D. W.** (2012b). The autoregulated instability of Polo-like kinase 4 limits centrosome duplication to once per cell cycle. *Genes Dev.* **26**, 2684–9.
- Holy, T. E. and Leibler, S.** (1994). Dynamic instability of microtubules as an efficient way to search in space. *Proc. Natl. Acad. Sci.* **91**, 5682–5685.
- Horner, V. L., Czank, A., Jang, J. K., Singh, N., Williams, B. C., Puro, J., Kubli, E., Hanes, S. D., McKim, K. S., Wolfner, M. F., et al.** (2006). The Drosophila Calcipressin Sarah Is Required for Several Aspects of Egg Activation. *Curr. Biol.* **16**, 1441–1446.
- Howard, J. and Hyman, A. A.** (2009). Growth, fluctuation and switching at microtubule plus ends. *Nat. Rev. Mol. Cell Biol.* **10**, 569–574.
- Hoyer-fender, S.** (2012). Centrosomes in fertilization , early embryonic development, stem cell division, and cancer. *Atlas Genet Cytogenet Oncol Haematol.*
- Huang, J. and Raff, J. W.** (1999). The disappearance of cyclin B at the end

- of mitosis is regulated spatially in *Drosophila* cells. *EMBO J.* **18**, 2184–2195.
- Huber, F., Schnauß, J., Rönicke, S., Rauch, P., Müller, K., Fütterer, C. and Käs, J.** (2013). Emergent complexity of the cytoskeleton: from single filaments to tissue. *Adv. Phys.* **62**, 1–112.
- Hunter, A. W., Caplow, M., Coy, D. L., Hancock, W. O., Diez, S., Wordeman, L. and Howard, J.** (2003). The kinesin-related protein MCAK is a microtubule depolymerase that forms an ATP-hydrolyzing complex at microtubule ends. *Mol. Cell* **11**, 445–457.
- Hyman, A. and Karsenti, E.** (1998). The role of nucleation in patterning microtubule networks. *J. Cell Sci.* **111**, 2077–2083.
- Hyman, A. A., Chretien, D., Arnal, I. and Wade, R. H.** (1995). Structural Changes Accompanying GTP Hydrolysis in Microtubules: Information from a Slowly Hydrolyzable Analogue Guanylyl-(alpha/beta)-Methylene-Diphosphonate. *J. Cell Biol.* **128**, 117–125.
- Hyman, A. A., Weber, C. A. and Julicher, F.** (2014). Liquid-liquid Phase Separation in Biology. *Annu Rev Cell Dev Biol.* **30**, 39–58.
- Ikegami, K., Sato, S., Nakamura, K., Ostrowski, L. E. and Setou, M.** (2010). Tubulin polyglutamylation is essential for airway ciliary function through the regulation of beating asymmetry. *Proc. Natl. Acad. Sci.* **107**, 10490–10495.
- Ito, D. and Bettencourt-Dias, M.** (2018). Centrosome Remodelling in Evolution. *Cells* **7**,.
- Izquierdo, D., Wang, W.-J., Uryu, K. and Tsou, M.-F. B.** (2014). Stabilization of cartwheel-less centrioles for duplication requires CEP295-mediated centriole to centrosome conversion. *Cell. Rep.* **8**, 957–965.
- Jameson, D. M., Ross, J. A. and Albanesi, J. P.** (2009). Fluorescence fluctuation spectroscopy: Ushering in a new age of enlightenment for cellular dynamics. *Biophys. Rev.* **1**, 105–118.
- Jana, S. C., Bazan, J. F. and Bettencourt-Dias, M.** (2012). Polo boxes come out of the crypt: a new view of PLK function and evolution. *Structure* **20**, 1801–4.
- Jana, S. C., Mendonça, S., Machado, P., Werner, S., Rocha, J., Pereira, A., Maiato, H. and Bettencourt-Dias, M.** (2018). Differential regulation of transition zone and centriole proteins contributes to ciliary base diversity. *Nat. Cell Biol.* **20**, 928–941.
- Janke, C. and Montagnac, G.** (2017). Causes and Consequences of Microtubule Acetylation. *Curr. Biol.* **27**, R1287–R1292.
- Jaqaman, K., Loerke, D., Mettlen, M., Kuwata, H., Grinstein, S., Schmid, S. L. and Danuser, G.** (2008). Robust single-particle tracking in live-

cell time-lapse sequences. *Nat. Methods* **5**, 695–702.

- Jeske, M., Meyer, S., Temme, C., Freudenreich, D. and Wahle, E.** (2006). Rapid ATP-dependent Deadenylation of nanos mRNA in a Cell-free System from *Drosophila* Embryos. *J. Biol. Chem.* **281**, 25124–25133.
- Johnson, E. F., Stewart, K. D., Woods, K. W., Giranda, V. L. and Luo, Y.** (2007). Pharmacological and functional comparison of the polo-like kinase family: insight into inhibitor and substrate specificity. *Biochemistry* **46**, 9551–9563.
- Joshi, H. C.** (1993). Gamma-Tubulin: The Hub of Cellular Microtubule Assemblies. *BioEssays* **15**, 637–643.
- Kalnins, V. I. and Porter, K. R.** (1969). Centriole Replication During Ciliogenesis in the Chick Tracheal Epithelium. *Z Zellforsch* **100**, 1–30.
- Kato, K. H. and Sugiyama, M.** (1971). On the de novo formation of the centriole in the activated sea urchin egg. *Dev. Growth Differ.* **13**, 359–366.
- Kazazian, K., Go, C., Wu, H., Brashavitskaya, O., Xu, R., Dennis, J. W., Gingras, A. and Swallow, C. J.** (2017). Plk4 Promotes Cancer Invasion and Metastasis through Arp2/3 Complex Regulation of the Actin Cytoskeleton. *Cancer Res.* **77**,.
- Keller, D., Orpinell, M., Olivier, N., Wachsmuth, M., Mahen, R., Wyss, R., Hachet, V., Ellenberg, J., Manley, S. and Gönczy, P.** (2014). Mechanisms of HsSAS-6 assembly promoting centriole formation in human cells. *J. Cell Biol.* **204**, 697–712.
- Kemp, C. A., Kopish, K. R., Zipperlen, P., Ahringer, J. and Connell, K. F. O.** (2004). Centrosome Maturation and Duplication in *C. elegans* Require the Coiled-Coil Protein SPD-2. *Dev. Cell* **6**, 511–523.
- Khan, M. A., Rupp, V. M., Orpinell, M., Hussain, M. S., Altmüller, J., Steinmetz, M. O., Enzinger, C., Thiele, H., Höhne, W., Nürnberg, G., et al.** (2014). A missense mutation in the PISA domain of HsSAS-6 causes autosomal recessive primary microcephaly in a large consanguineous pakistani family. *Hum. Mol. Genet.* **23**, 5940–5949.
- Khanal, I., Elbediwy, A., Diaz de la Loza, M. del C., Fletcher, G. C. and Thompson, B. J.** (2016). Shot and Patronin polarise microtubules to direct membrane traffic and biogenesis of microvilli in epithelia. *J. Cell Sci.* **129**, 2651–2659.
- Khire, A., Vizue, A. A., Davila, E. and Avidor-Reiss, T.** (2015). Asterless Reduction During Spermiogenesis is Regulated by Plk4 and is Essential for Zygote Development in *Drosophila*. *Curr. Biol.* **25**, 2956–2963.
- Khire, A., Jo, K. H., Kong, D., Akhshi, T., Blachon, S., Cekic, A. R.,**

- Hynek, S., Ha, A., Loncarek, J., Mennella, V., et al.** (2016). Centriole Remodeling during Spermiogenesis in Report Centriole Remodeling during Spermiogenesis in *Drosophila*. *Curr. Biol.* **26**, 3183–3189.
- Khodjakov, A., Rieder, C. L., Sluder, G., Cassels, G., Sibon, O. and Wang, C.-L.** (2002). De novo formation of centrosomes in vertebrate cells arrested during S phase. *J. Cell Biol.* **158**, 1171–1181.
- Kim, H.-K., Kang, J.-G., Yumura, S., Walsh, C. J., Jin, W. C. and Lee, J.** (2005). De novo formation of basal bodies in *Naegleria gruberi*: Regulation by phosphorylation. *J. Cell Biol.* **169**, 719–724.
- Kim, T.-S., Park, J.-E., Shukla, A., Choi, S., Murugan, R. N., Lee, J. H., Ahn, M., Rhee, K., Bang, J. K., Kim, B. Y., et al.** (2013). Hierarchical recruitment of Plk4 and regulation of centriole biogenesis by two centrosomal scaffolds, Cep192 and Cep152. *Proc. Natl. Acad. Sci. U. S. A.* **110**, E4849-57.
- Kitagawa, D., Busso, C., Flückiger, I. and Gönczy, P.** (2009). Phosphorylation of SAS-6 by ZYG-1 is critical for centriole formation in *C. elegans* embryos. *Dev. Cell* **17**, 900–7.
- Kitagawa, D., Vakonakis, I., Olieric, N., Hilbert, M., Keller, D., Olieric, V., Bortfeld, M., Erat, M. C., Flückiger, I., Gönczy, P., et al.** (2011). Structural basis of the 9-fold symmetry of centrioles. *Cell* **144**, 364–375.
- Kitazawa, D., Matsuo, T., Kaizuka, K., Miyauchi, C., Hayashi, D. and Inoue, Y. H.** (2014). Orbit/CLASP is required for myosin accumulation at the cleavage furrow in *Drosophila* male meiosis. *PLoS One* **9**.
- Klebba, J. E., Buster, D. W., Nguyen, A. L., Swatkoski, S., Gucek, M., Rusan, N. M. and Rogers, G. C.** (2013). Polo-like Kinase 4 Autodeconstructs by Generating Its Slimb-Binding Phosphodegron. *Curr. Biol.* **23**, 2255–61.
- Klebba, J. E., Galletta, B. J., Nye, J., Plevock, K. M., Buster, D. W., Hollingsworth, N. a., Slep, K. C., Rusan, N. M. and Rogers, G. C.** (2015a). Two Polo-like kinase 4 binding domains in Asterless perform distinct roles in regulating kinase stability. *J. Cell Biol.* **208**, 401–414.
- Klebba, J. E., Buster, D. W., McLamarrah, T. A., Rusan, N. M. and Rogers, G. C.** (2015b). Autoinhibition and relief mechanism for Polo-like kinase 4. *Proc. Natl. Acad. Sci.* **112**, E657–E666.
- Kleylein-Sohn, J., Westendorf, J., Le Clech, M., Habedanck, R., Stierhof, Y.-D. and Nigg, E. a** (2007). Plk4-induced centriole biogenesis in human cells. *Dev. Cell* **13**, 190–202.
- Klink, V. P. and Wolniak, S. M.** (2001). Centrin is necessary for the formation of the motile apparatus in spermatids of *Marsilea*. *Mol. Biol. Cell* **12**, 761–776.

- Klos Dehring, D. A., Vldar, E. K., Werner, M. E., Mitchell, J. W., Hwang, P. and Mitchell, B. J.** (2013). Deuterosome Mediated Centriole Biogenesis. *Dev. Cell* **27**, 103–112.
- Ko, M. A., Rosario, C. O., Hudson, J. W., Kulkarni, S., Pollett, A., Dennis, J. W. and Swallow, C. J.** (2005). Plk4 haploinsufficiency causes mitotic infidelity and carcinogenesis. *Nat. Genet.* **37**, 883–888.
- Kohlmaier, G., Loncarek, J., Meng, X., Mcewen, B. F., Spektor, A., Dynlacht, B. D., Khodjakov, A. and Gönczy, P.** (2009). Overly long centrioles and defective cell division upon excess of the SAS-4-related protein CPAP. *Curr. Biol.* **19**, 1012–1018.
- Kollman, J. M., Greenberg, C. H., Li, S., Moritz, M., Zelter, A., Fong, K. K., Fernandez, J., Sali, A., Kilmartin, J., Trisha, N., et al.** (2015). Ring closure activates yeast γ TuRC for species-specific microtubule nucleation. *Nat. Struct. Mol. Biol.* **22**, 132–137.
- Kong, D., Farmer, V., Shukla, A., James, J., Gruskin, R., Kiriyama, S. and Loncarek, J.** (2014). Centriole maturation requires regulated Plk1 activity during two consecutive cell cycles. *J. Cell Biol.* **206**, 855–865.
- Kratz, A., Ba, F., Richter, K. T. and Hoffmann, I.** (2015). Plk4-dependent phosphorylation of STIL is required for centriole duplication. *Biol. Open* **4**, 370–377.
- Kronja, I., Yuan, B., Eichhorn, S. W., Dzeyk, K., Krijgsveld, J., Bartel, D. P. and Orr-Weaver, T. L.** (2014). Widespread changes in the posttranscriptional landscape at the Drosophila oocyte-to-embryo transition. *Cell Rep.* **7**, 1495–1508.
- Kumar, A., Girimaji, S. C., Duvvari, M. R. and Blanton, S. H.** (2008). Mutations in STIL, encoding a pericentriolar and centrosomal protein, cause primary microcephaly. *Am. J. Hum. Genet.* **84**, 286–290.
- Kuriyama, R. and Borisy, G. G.** (1981). Centriole Cycle in Chinese Hamster Ovary Cells as Determined by Whole-mount Electron Microscopy. *J. Cell Biol.* **91**, 814–821.
- Kuriyama, R., Borisy, G. G. and Masui, Y.** (1986). Microtubule cycles in oocytes of the surf clam, *Spisula solidissima*: An immunofluorescence study. *Dev. Biol.* **114**, 151–160.
- Kuriyama, R., Terada, Y., Lee, K. S. and Wang, C. L. C.** (2007). Centrosome replication in hydroxyurea-arrested CHO cells expressing GFP-tagged centrin2. *J. Cell Sci.* **120**, 2444–2453.
- La Terra, S., English, C. N., Hergert, P., McEwen, B. F., Sluder, G. and Khodjakov, A.** (2005). The de novo centriole assembly pathway in HeLa cells: Cell cycle progression and centriole assembly/maturation. *J. Cell Biol.* **168**, 713–722.

- Lacey, K. R., Jackson, P. and Stearns, T.** (1999). Cyclin-dependent kinase control of centrosome duplication. *Proc. Natl. Acad. Sci. USA* **96**, 2817–2822.
- Lai, D., Visser-grieve, S. and Yang, X.** (2012). Tumour suppressor genes in chemotherapeutic drug response. *Biosci Rep* **32**, 361–374.
- Lambrus, B., Clutario, K. M., Daggubati, V., Snyder, M., Sluder, G. and Holland, A.** (2015). p53 protects against genome instability following centriole duplication failure. *J. Cell Biol.* **210**, 63–77.
- Lawo, S., Bashkurov, M., Mullin, M., Ferreria, M. G., Kittler, R., Habermann, B., Tagliaferro, A., Poser, I., Hutchins, J. R. A., Pinchev, D., et al.** (2009). Article HAUS , the 8-Subunit Human Augmin Complex , Regulates Centrosome and Spindle Integrity. *Curr. Biol.* **19**, 816–826.
- Lawo, S., Hasegan, M., Gupta, G. D. and Pelletier, L.** (2012). Subdiffraction imaging of centrosomes reveals higher-order organizational features of pericentriolar material. *Nat. Cell Biol.* **14**, 1148–1158.
- Lee, K. and Rhee, K.** (2011). PLK1 phosphorylation of pericentrin initiates centrosome maturation at the onset of mitosis. *J. Cell Biol.* **195**, 1093–1101.
- Lee, K. S., Grenfell, T. Z., Yarm, F. R. and Erikson, R. L.** (1998). Mutation of the polo-box disrupts localization and mitotic functions of the mammalian polo kinase Plk. *Proc. Natl. Acad. Sci. U. S. A.* **95**, 9301–9306.
- Lee, L. A., Hoewyk, D. van and Orr-Weaver, T. L.** (2003). The Drosophila cell cycle kinase PAN GU forms an active complex with PLUTONIUM and GNU to regulate embryonic divisions. *Genes Dev.* **17**, 2979–2991.
- Lee, K. S., Park, J. E., Kang, Y. H., Zimmerman, W., Soung, N. K., Seong, Y. S., Kwak, S. J. and Erikson, R. L.** (2008). Mechanisms of mammalian polo-like kinase 1 (Plk1) localization: Self- versus non-self-priming. *Cell Cycle* **7**, 141–145.
- Lee, J., Kang, S., Choi, Y. S. eok, Kim, H.-K., Yeo, C.-Y., Lee, Y., Roth, J. and Lee, J.** (2015). Identification of a cell cycle-dependent duplicating complex that assembles basal bodies de novo in Naegleria. *Protist* **166**, 1–13.
- Lee, I., Kim, G. S., Bae, J. S., Kim, J., Rhee, K. and Hwang, D. S.** (2017a). The DNA replication protein Cdc6 inhibits the microtubule-organizing activity of the centrosome. *J. Biol. Chem.* **292**, 16267–16276.
- Lee, M., Seo, M. Y., Chang, J., Hwang, D. S. and Rhee, K.** (2017b). PLK4 phosphorylation of CP110 is required for efficient centriole assembly. *Cell Cycle* **16**, 1225–1234.

- Leidel, S., Delattre, M., Cerutti, L., Baumer, K. and Gönczy, P.** (2005). SAS-6 defines a protein family required for centrosome duplication in *C. elegans* and in human cells. *Nat. Cell Biol.* **7**, 115–125.
- Lessard, D. V., Zinder, O. J., Hotta, T., Verhey, K. J., Ohi, R. and Berger, C. L.** (2018). Regulation of KIF1A motility via polyglutamylolation of tubulin C-terminal tails. *bioRxiv*.
- Leung, G. C., Hudson, J. W., Kozarova, A., Davidson, A., Dennis, J. W. and Sicheri, F.** (2002). The Sak polo-box comprises a structural domain sufficient for mitotic subcellular localization. *Nat. Struct. Biol.* **9**, 719–24.
- Levine, M. S. and Holland, A. J.** (2014). Previews Polo-like Kinase 4 Shapes Up. *Structure* **22**, 1071–1073.
- Levine, M. S., Bakker, B., Boeckx, B., Moyett, J., Lu, J., Spierings, D. C., Lansdorp, P. M., Cleveland, D. W., Foijer, F. and Holland, A. J.** (2018). Centrosome amplification is sufficient to promote spontaneous tumorigenesis in mammals. *Dev. Cell* **40**, 313–322.
- Li, C., Vassilev, A. and Depamphilis, M. L.** (2004). Role for Cdk1 (Cdc2)/Cyclin A in Preventing the Mammalian Origin Recognition Complex 's Largest Subunit (Orc1) from Binding to Chromatin during Mitosis. *Mol. Cell. Biol.* **24**, 5875–5886.
- Liao, Z., Zhang, H., Fan, P., Huang, Q., Dong, K., Qi, Y., Song, J., Chen, L., Liang, H., Chen, X., et al.** (2019). High PLK4 expression promotes tumor progression and induces epithelial-mesenchymal transition by regulating the Wnt/betacatenin signaling pathway in colorectal cancer. *Int. J. Oncol.* **54**, 479–490.
- Lin, Y., Chang, C., Hsu, W., Tang, C. C., Lin, Y., Chou, E., Wu, C. and Tang, T. K.** (2013). Human microcephaly protein CEP135 binds to hSAS-6 and CPAP, and is required for centriole assembly. *EMBO J.* **32**, 1141–1154.
- Lin, T. C., Neuner, A., Schlosser, Y., Scharf, A., Weber, L. and Schiebel, E.** (2014). Cell-cycle dependent phosphorylation of yeast pericentrin regulates γ -TUSC-mediated microtubule nucleation. *Elife* **3**,.
- Lin, T., Neuner, A. and Schiebel, E.** (2015). Targeting of gamma-tubulin complexes to microtubule organizing center: conservation and divergence. *Trends Cell Biol.* **25**, 296–307.
- Lingle, W. L., Barrett, S. L., Negron, V. C., D'Assoro, A. B., Boeneman, K., Liu, W., Whitehead, C. M., Reynolds, C. and Salisbury, J. L.** (2002). Centrosome amplification drives chromosomal instability in breast tumor development. *Proc. Natl. Acad. Sci.* **99**, 1978–1983.
- Liu, T., Tian, J., Wang, G., Yu, Y., Wang, C., Ma, Y., Zhang, X., Xia, G., Liu, B. and Kong, Z.** (2014). Report Augmin Triggers Microtubule-Dependent Microtubule Nucleation in Interphase Plant Cells. *Curr.*

Biol. **24**, 2708–2713.

- Liu, Y., Gupta, G. D., Barnabas, D. D., Agircan, F. G., Mehmood, S., Wu, D., Coyaud, E., Johnson, C. M., Mclaughlin, S. H., Andreeva, A., et al.** (2018). Direct binding of CEP85 to STIL ensures robust PLK4 activation and efficient centriole assembly. *Nat. Commun.* **9**.
- Lohka, M. J. and Masui, Y.** (1983). Formation in vitro of Sperm Pronuclei and Mitotic Chromosomes Induced by Amphibian Ooplasmic Components. *Science*. **220**, 719–721.
- Lohka, M. J. and Masui, Y.** (1984). Effects of Ca⁺ Ions on the Formation of Metaphase Chromosomes and Sperm Pronuclei in Cell-free Preparations from Unactivated *Rana pipiens* Eggs. *Dev. Biol.* **103**, 434–442.
- Loncarek, J; Hergert, P; Khodjakov, A.** (2010). Centriole reduplication during prolonged interphase requires procentriole maturation governed by Plk1. *Curr. Biol.* **20**, 1277–1282.
- Loncarek, J. and Bettencourt-Dias, M.** (2018). Building the right centriole for each cell type. *J. Cell Biol.*
- Lopes, C. A. M., Jana, S. C., Cunha-Ferreira, I., Zitouni, S., Bento, I., Duarte, P., Gilberto, S., Freixo, F., Guerrero, A., Francia, M., et al.** (2015). PLK4 trans-Autoactivation Controls Centriole Biogenesis in Space. *Dev. Cell* **35**, 222–235.
- Lopes, C. A. M., Mesquita, M., Cunha, A. I., Cardoso, J., Carapeta, S., Laranjeira, C., Pinto, A. E., Pereira-Leal, J. B., Dias-Pereira, A., Bettencourt-Dias, M., et al.** (2018). Centrosome amplification arises before neoplasia and increases upon p53 loss in tumorigenesis. *J. Cell Biol.* **217**, 2353–2363.
- Lott, S. E., Villalta, J. E., Schroth, G. P., Luo, S., Tonkin, L. A. and Michael, B.** (2011). Noncanonical Compensation of Zygotic X Transcription in Early *Drosophila melanogaster* Development Revealed through Single-Embryo RNA-Seq. *PLoS Biol.* **9**.
- Lowe, N., Rees, J. S., Roote, J., Ryder, E., Armean, I. M., Johnson, G., Drummond, E., Spriggs, H., Drummond, J., Magbanua, J. P., et al.** (2014). Analysis of the expression patterns, subcellular localisations and interaction partners of *Drosophila* proteins using a pigP protein trap library. *Development* **141**, 3994–4005.
- Luders, J. and Stearns, T.** (2007). Microtubule-organizing centres: a re-evaluation. *Nat. Rev. Mol. Cell Biol.* **8**, 161–167.
- Lyon, A. S., Morin, G., Moritz, M., Yabut, K. C. B., Vojnar, T., Zelter, A., Muller, E., Davis, T. N. and Agard, D. A.** (2016). Higher-order oligomerization of Spc110p drives gamma-tubulin ring complex assembly. *Mol. Biol. Cell* **27**, 2245–2258.

- Macûrek, L., Lindqvist, A., Lim, D., Lampson, M. A., Klompaker, R., Freire, R., Clouin, C., Taylor, S. S., Yaffe, M. B. and Medema, R. H.** (2008). Polo-like kinase-1 is activated by aurora A to promote checkpoint recovery. *Nature* **455**, 119–123.
- Maddox, P., Straight, A., Coughlin, P., Mitchison, T. J. and Salmon, E. D.** (2003). Direct observation of microtubule dynamics at kinetochores in *Xenopus* extract spindles: implications for spindle mechanics. *J. Cell Biol.* **162**, 377–382.
- Magiera, M. M., Singh, P., Gadadhar, S. and Janke, C.** (2018). Tubulin Posttranslational Modifications and Emerging Links to Human Disease. *Cell* **173**, 1323–1327.
- Mahen, R., Jeyasekharan, A. D., Barry, N. P. and Venkitaraman, A. R.** (2011). Continuous polo-like kinase 1 activity regulates diffusion to maintain centrosome self-organization during mitosis. *Proc. Natl. Acad. Sci.* **108**, 9310–9315.
- Mahowald, A. P. and Strassheim, J. M.** (1970). Intercellular Migration of Centrioles in the Germarium of *Drosophila melanogaster*. An Electron Microscopic Study. *J. Cell Biol.* **45**, 306–320.
- Malumbres, M. and Barbacid, M.** (2005). Mammalian cyclin-dependent kinases. *Trends Biochem. Sci.* **30**, 630–641.
- Malumbres, M. and Barbacid, M.** (2009). Cell cycle, CDKs and cancer: a changing paradigm. *Nat. Rev. Cancer* **9**, 153–166.
- Manandhar, G., Sutovsky, P., Joshi, H. C., Stearns, T. and Schatten, G.** (1998). Centrosome reduction during mouse spermiogenesis. *Dev. Biol.* **203**, 424–434.
- Manandhar, G., Schatten, H. and Sutovsky, P.** (2005). Centrosome Reduction During Gametogenesis and Its Significance. *Biol. Reprod.* **72**, 2–13.
- Maniswami, R. R., Prashanth, S., Karanth, A. V., Koushik, S., Govindaraj, H., Mullangi, R., Rajagopal, S. and Jegatheesan, S. K.** (2018). PLK4: a link between centriole biogenesis and cancer. *Expert Opin. Ther. Targets* **22**, 59–73.
- Manka, S. W. and Moores, C. A.** (2018). The role of tubulin–tubulin lattice contacts in the mechanism of microtubule dynamic instability. *Nat. Struct. Mol. Biol.* **1**,.
- Mantel, C., Braun, S. E., Reid, S., Henegariu, O., Liu, L., Hangoc, G. and Broxmeyer, H. E.** (1999). P21(Cip-1/Waf-1) Deficiency Causes Deformed Nuclear Architecture, Centriole Overduplication, Polyploidy, and Relaxed Microtubule Damage Checkpoints in Human Hematopoietic Cells. *Blood* **93**, 1390–8.
- Marina, M. and Saavedra, H. I.** (2014). Nek2 and Plk4: prognostic markers,

- drivers of breast tumorigenesis and drug resistance. *Front. Biosci.* **19**, 352–365.
- Marshall, W. F., Vucica, Y. and Rosenbaum, J. L.** (2001). Kinetics and regulation of de novo centriole assembly: Implications for the mechanism of centriole duplication. *Curr. Biol.* **11**, 308–17.
- Marteil, G. and Bettencourt-Dias, M.** (2017). Centrosome Cycle. *eLS John Wiley Sons*.
- Marteil, G., Guerrero, A., Vieira, A. F., De Almeida, B. P., Machado, P., Mendonça, S., Mesquita, M., Villarreal, B., Fonseca, I., Francia, M. E., et al.** (2018). Over-elongation of centrioles in cancer promotes centriole amplification and chromosome missegregation. *Nat. Commun.* **9**,.
- Martin, C., Ahmad, I., Klingseisen, A., Sajid, M., Bicknell, L. S., Leitch, A., Nürnberg, G., Reza, M., Murray, J. E., Hunt, D., et al.** (2014). Mutations in PLK4, encoding a master regulator of centriole biogenesis, cause microcephaly, growth failure and retinopathy. *Nat. Genet.* **46**, 1283–1292.
- Massagué, J.** (2004). G1 cell-cycle control and cancer. *Nature* **432**, 298–306.
- Masui, Y. and Wang, P.** (1998). Cell cycle transition in early embryonic development of *Xenopus laevis*. *Biol. Cell* **90**, 537–548.
- Maurer, S. P., Fourniol, F. J., Bohner, G., Moores, C. A. and Surrey, T.** (2012). EBs Recognize a Nucleotide- Dependent Structural Cap at Growing Microtubule Ends. *Cell* **149**, 371–382.
- Mazzarello, P.** (1999). A unifying concept: the history of cell theory. *Nat. Cell Biol.* **1**, 13–15.
- McIntosh, J. and Hays, T.** (2016). A Brief History of Research on Mitotic Mechanisms. *Biology (Basel)*. **5**,.
- Mclamarrh, T. A., Buster, D. W., Galletta, B. J., Boese, C. J., Ryniawec, J. M., Hollingsworth, N. A., Byrnes, A. E., Brownlee, C. W., Slep, K. C., Rusan, N. M., et al.** (2018). An ordered pattern of Ana2 phosphorylation by Plk4 is required for centriole assembly. *J. Cell Biol.* **217**, 1217–1231.
- Megraw, T. L., Li, K., Kao, L. and Kaufman, T. C.** (1999). The Centrosomin protein is required for centrosome assembly and function during cleavage in *Drosophila*. *Development* **126**, 2829–2839.
- Meitinger, F., Anzola, J. V., Kaulich, M., Richardson, A., Stender, J. D., Benner, C., Glass, C. K., Dowdy, S. F., Desai, A., Shiau, A. K., et al.** (2016). 53BP1 and USP28 mediate p53 activation and G1 arrest after centrosome loss or extended mitotic duration. *J. Cell Biol.* **214**,

155–166.

- Mennella, V., Keszthelyi, B., McDonald, K. L., Chhun, B., Kan, F., Rogers, G. C., Huang, B. and Agard, D. A.** (2012). Sub-diffraction-resolution fluorescence microscopy reveals a domain of the centrosome critical for pericentriolar material organization. *Nat. Cell Biol.* **14**, 1159–1168.
- Meraldi, P., Lukas, J., Fry, A., Bartek, J. and Nigg, E.** (1999). Centrosome duplication in mammalian somatic cells requires E2F and Cdk2-cyclin A. *Nat. Cell Biol.* **1**, 88–93.
- Metzger, T., Gache, V., Xu, M., Cadot, B., Folker, E. S., Richardson, B. E., Gomes, E. R. and Baylies, M. K.** (2012). MAP and kinesin-dependent nuclear positioning is required for skeletal muscle function. *Nature* **484**, 120–124.
- Meunier, A. and Azimzadeh, J.** (2016). Multiciliated cells in animals. *Cold Spring Harb. Perspect. Biol.* **8**, a028233.
- Mikeladze-Dvali, T., von Tobel, L., Strnad, P., Knott, G., Leonhardt, H., Schermelleh, L. and Gonczy, P.** (2012). Analysis of centriole elimination during *C. elegans* oogenesis. *Development* **139**, 1670–1679.
- Miki-Noumura, T.** (1977). Studies on the de novo formation of centrioles: aster formation in the activated eggs of sea urchin. *J. Cell Sci.* **24**, 203–216.
- Minami, A., Murai, T., Nakanishi, A., Kitagishi, Y., Ichimura, M. and Matsuda, S.** (2017). Cell Cycle Regulation via the p53, PTEN, and BRCA1 Tumor Suppressors. *IntechOpen* 53–66.
- Mirkovic, M., Hutter, L. H., Novák, B. and Oliveira, R. A.** (2015). Premature Sister Chromatid Separation Is Poorly Detected by the Spindle Assembly Checkpoint as a Result of System-Level Feedback. *Cell Rep.* **13**, 469–478.
- Mirvis, M., Stearns, T. and James Nelson, W.** (2018). Cilium structure, assembly, and disassembly regulated by the cytoskeleton. *Biochem. J.* **475**, 2329–2353.
- Mitchison, T. and Kirschner, M.** (1984). Dynamic instability of microtubule growth. *Nature* **312**, 237–242.
- Mizukami, I. and Gall, J.** (1966). Centriole replication. II. Sperm formation in the fern, *Marsilea*, and the cycad, *Zamia*. *J. Cell Biol.* **29**, 97–111.
- Moir, D. and Botstein, D.** (1982). Determination of the order of gene function in the yeast nuclear division pathway using *cs* and *ts* mutants. *Genetics* 565–577.
- Monroy, B. Y., Sawyer, D. L., Ackermann, B. E., Borden, M. M., Tan, T. C. and Ori-mckenney, K. M.** (2018). Competition between

microtubule-associated proteins directs motor transport. *Nat. Commun.* **9**, 1–12.

Montenegro Gouveia, S., Zitouni, S., Kong, D., Duarte, P., Ferreira Gomes, B., Sousa, A. L., Tranfield, E. M., Hyman, A., Loncarek, J. and Bettencourt-Dias, M. (2018). PLK4 is a microtubule-associated protein that self-assembles promoting de novo MTOC formation. *J. Cell Sci.* **132**,.

Morgan, D. O. (2007). *The Cell Cycle - Principles of Control*.

Mori, M., Hazan, R., Danielian, P. S., Mahoney, J. E., Li, H., Lu, J., Miller, E. S., Zhu, X., Lees, J. A. and Cardoso, W. V. (2017). Cytoplasmic E2f4 forms organizing centres for initiation of centriole amplification during multiciliogenesis. *Nat. Commun.* **8**, 15857.

Morin, X., Daneman, R., Zavortink, M. and Chia, W. (2001). A protein trap strategy to detect GFP-tagged proteins expressed from their endogenous loci in *Drosophila*. *Proc. Natl. Acad. Sci. U. S. A.* **98**, 15050–15055.

Moritz, M., Braunfeld, M. B., Sedat, J. W., Alberts, B. and Agard, D. A. (1995). Microtubule nucleation by gamma-tubulin containing rings in the centrosome. *Nature* **378**, 638–640.

Moser, J. W. and Kreitner, G. L. (1970). Centrosome Structure in *Anthoceros laevis* and *Marchantia polymorpha*. *J. Cell Biol.* **44**, 454–458.

Moyer, T. C., Clutario, K. M., Lambrus, B. G., Daggubati, V. and Holland, A. J. (2015). Binding of STIL to Plk4 activates kinase activity to promote centriole assembly. *J. Cell Biol.* **209**, 863–878.

Muroyama, A. and Lechler, T. (2017). Microtubule organization, dynamics and functions in differentiated cells. *Development* **144**, 3012–3021.

Muroyama, A., Seldin, L. and Lechler, T. (2016). Divergent regulation of functionally distinct γ -tubulin complexes during differentiation. *J. Cell Biol.* **213**, 679–692.

Murray, A. W., Desai, A. B. and Salmon, E. D. (1996). Real time observation of anaphase in vitro. *Proc. Natl. Acad. Sci.* **93**, 12327–12332.

Musacchio, A. and Salmon, E. D. (2007). The spindle-assembly checkpoint in space and time. *Nat. Rev. Mol. Cell Biol.* **8**, 379–393.

Myatt, D. P., Hatter, L., Rogers, S. E., Terry, A. E. and Clifton, L. A. (2017). Monomeric green fluorescent protein as a protein standard for small angle scattering. *Biomed. Spectrosc. Imaging* **6**, 123–134.

Nabais, C., Pereira, S. G. and Bettencourt-Dias, M. (2018). Noncanonical Biogenesis of Centrioles and Basal Bodies. *Cold Spring Harb. Symp. Quant. Biol.* **82**, 123–135.

- Nakazawa, Y., Hiraki, M., Kamiya, R. and Hirono, M.** (2007). SAS-6 is a Cartwheel Protein that Establishes the 9-Fold Symmetry of the Centriole. *Curr. Biol.* **17**, 2169–2174.
- Nashchekin, D., Fernandes, A. R. and St Johnston, D.** (2016). Patronin/Shot Cortical Foci Assemble the Noncentrosomal Microtubule Array that Specifies the Drosophila Anterior-Posterior Axis. *Dev. Cell* **38**, 61–72.
- Nigg, E. A. and Holland, A. J.** (2018). Once and only once: mechanisms of centriole duplication and their deregulation in disease. *Nat. Rev. Mol. Cell Biol.*
- Nishitani, H. and Lygerou, Z.** (2004). DNA Replication Licensing. *Front. Biosci.* **9**, 2115–2132.
- Nithianantham, S., Cook, B. D., Beans, M., Guo, F., Chang, F. and Al-Bassam, J.** (2018). Structural basis of tubulin recruitment and assembly by microtubule polymerases with tumor overexpressed gene (TOG) domain arrays. *Elife* **7**, 1–33.
- Nogales, E., Wolf, S. G. and Downing, K. H.** (1998). Structure of the alpha beta tubulin dimer by electron crystallography. *Nature* **391**, 199–204.
- Norstog, K. J.** (1986). The blepharoplast of *Zamia pumila* L. *Bot. Gazette* **147**, 40–46.
- Novak, Z. A., Conduit, P. T., Wainman, A. and Raff, J. W.** (2014). Asterless Licenses Daughter Centrioles to Duplicate for the First Time in Drosophila Embryos. *Curr. Biol.* **24**, 1276–1282.
- Novak, Z. A., Wainman, A., Gartenmann, L. and Raff, J. W.** (2016). Cdk1 Phosphorylates Drosophila Sas-4 to Recruit Polo to Daughter Centrioles and Convert Them to Centrosomes. *Dev. Cell* **37**, 545–557.
- Nurse, P.** (2000). A Long Twentieth Century of the Cell Cycle and Beyond. *Cell* **100**, 71–78.
- Nurse, P. and Thuriaux, P.** (1980). Regulatory genes controlling mitosis in the fission yeast *Schizosaccharomyces pombe*. *Genetics* **96**, 627–637.
- O'Connell, K. F., Caron, C., Kopish, K. R., Hurd, D. D., Kempfues, K. J., Li, Y. and White, J. G.** (2001). The *C. elegans* zyg-1 gene encodes a regulator of centrosome duplication with distinct maternal and paternal roles in the embryo. *Cell* **105**, 547–558.
- Oakley, B. R., Paolillo, V. and Zheng, Y.** (2015). γ -Tubulin complexes in microtubule nucleation and beyond. *Mol. Biol. Cell* **26**, 2957–2962.
- Oey, H., Isbel, L., Hickey, P., Ebaid, B. and Whitelaw, E.** (2015). Genetic and epigenetic variation among inbred mouse littermates: identification of inter-individual differentially methylated regions.

- Ohta, M., Ashikawa, T., Nozaki, Y., Kozuka-Hata, H., Goto, H., Inagaki, M., Oyama, M. and Kitagawa, D.** (2014). Direct interaction of Plk4 with STIL ensures formation of a single procentriole per parental centriole. *Nat. Commun.* **5**.
- Ohta, M., Watanabe, K., Ashikawa, T., Nozaki, Y., Yoshida, S. and Kimura, A.** (2018). Bimodal Binding of STIL to Plk4 Controls Proper Centriole Copy Number. *Cell Rep.* **23**, 3160–3169.
- Oliveira, R. A., Hamilton, R. S., Pauli, A., Davis, I. and Nasmyth, K.** (2010). Cohesin cleavage and Cdk inhibition trigger formation of daughter nuclei. *Nat. Cell Biol.* **12**, 185–192.
- Ori-McKenney, K. M., Jan, L. Y. and Jan, Y.-N.** (2012). Golgi outposts shape dendrite morphology by functioning as sites of acentrosomal microtubule nucleation in neurons. *Neuron* **76**, 921–930.
- Pagano, M.** (2004). Control of DNA Synthesis and Mitosis by the Skp2-p27-Cdk1/2 Axis. *Mol. Cell* 414–416.
- Paintrand, M., Moudjou, M., Delacroix, H. and Bornens, M.** (1992). Centrosome Organization Their Sensitivity and Centriole Architecture: to Divalent Cations. *J. Struct. Biol.* **108**, 107–128.
- Palazzo, R. E., Vaisberg, E., Cole, R. W. and Rieder, C. L.** (1992). Centriole Duplication in Lysates of *Spisula solidissima* Oocytes. *Science.* **256**, 219–221.
- Park, J.-E., Sung, N.-K., Johmura, Y., Kang, Y. H., Liao, C., Lee, K. H., Park, C. H., Nicklaus, M. C. and Lee, K. S.** (2010). Polo-box domain: a versatile mediator of polo-like kinase function. *Cell. Mol. life Sci.* **67**, 1957–70.
- Peel, N., Stevens, N. R., Basto, R. and Raff, J. W.** (2007). Overexpressing Centriole-Replication Proteins In Vivo Induces Centriole Overduplication and De Novo Formation. *Curr. Biol.* **17**, 834–843.
- Peel, N., Dougherty, M., Goeres, J., Liu, Y. and O’Connell, K. F.** (2012). The *C. elegans* F-box proteins LIN-23 and SEL-10 antagonize centrosome duplication by regulating ZYG-1 levels. *J. Cell Sci.* **125**, 3535–44.
- Peet, D. R., Burroughs, N. J. and Cross, R. A.** (2018). Kinesin expands and stabilises the GDP-microtubule lattice Daniel. *Nat. Nanotechnol.* **13**, 386–391.
- Pelletier, L., Nurhan, O., Hannak, E., Cowan, C., Habermann, B., Ruer, M., Mu, T. and Hyman, A. A.** (2004). The *Caenorhabditis elegans* Centrosomal Protein SPD-2 Is Required for both Pericentriolar Material Recruitment and Centriole Duplication. *Curr. Biol.* **14**, 863–873.

- Pelletier, L., Toole, E. O., Schwager, A., Hyman, A. A. and Muller-Reichert, T.** (2006). Centriole assembly in *Caenorhabditis elegans*. *Nature* **444**, 619–623.
- Perkins, F. O.** (1970). Formation of Centriole and Centriole- Like Structures During Meiosis and Mitosis in *Labyrinthula* Sp. (Rhizopodea, Labyrinthulida). An electron-microscope study. *J. Cell Sci.* **6**, 629–653.
- Peset, I. and Vernos, I.** (2008). The TACC proteins: TACC-ling microtubule dynamics and centrosome function. *Trends Cell Biol.* **18**, 379–388.
- Pickett Heaps, J. D.** (1969). The evolution of the mitotic apparatus an attempt at comparative ultrastructural cytology in dividing plant cells. *Cytobios* **1**, 257–280.
- Pimenta-Marques, A., Bento, I., Lopes, C. A. M., Duarte, P., Jana, S. C. and Bettencourt-Dias, M.** (2016). A mechanism for the elimination of the female gamete centrosome in *Drosophila melanogaster*. *Science*. **353**, aaf4866.
- Pollard, T. D.** (2017). *Cell Biology, 3rd edition*.
- Pollard, T. D. and Goldman, R. D.** (2017). Overview of the Cytoskeleton from an Evolutionary Perspective. In *The Cytoskeleton*, p. Cold Spring Harbor Laboratory Press.
- Port, F., Chen, H.-M., Lee, T. and Bullock, S. L.** (2014). Optimized CRISPR/Cas tools for efficient germline and somatic genome engineering in *Drosophila*. *Proc. Natl. Acad. Sci. U. S. A.*
- Pritchard, C., Coil, D., Hawley, S., Hsu, L. and Nelson, P. S.** (2006). The contributions of normal variation and genetic background to mammalian gene expression. *Genome Biol.* **7**, 1–11.
- Puklowski, A., Homsy, Y., Keller, D., May, M., Chauhan, S., Kossatz, U., Grünwald, V., Kubicka, S., Pich, A., Manns, M. P., et al.** (2011). The SCF-FBXW5 E3-ubiquitin ligase is regulated by PLK4 and targets HsSAS-6 to control centrosome duplication. *Nat. Cell Biol.* **13**, 1004–9.
- Radford, S. J., Go, A. M. M. and McKim, K. S.** (2017). Cooperation Between Kinesin Motors Promotes Spindle Symmetry and Chromosome Organization in Oocytes. *Genetics* **205**, 517–527.
- Raff, J. W. and Glover, D. M.** (1988). Nuclear and cytoplasmic mitotic cycles continue in *Drosophila* embryos in which DNA synthesis is inhibited with aphidicolin. *J. Cell Biol.* **107**, 2009–2019.
- Raff, J. W. and Glover, D. M.** (1989). Centrosomes, and not nuclei, initiate pole cell formation in *Drosophila* embryos. *Cell* **57**, 611–619.
- Ramani, A., Mariappan, A., Gottardo, M., Debec, A., Feederle, R. and Gopalakrishnan, J.** (2018). Plk1/Polo Phosphorylates Sas-4 at the

Onset of Mitosis for an Efficient Recruitment of Pericentriolar Material to Centrosomes. *Cell Rep.* **25**, 3618–3630.

- Rattner, J. B. and Phillips, S. G.** (1973). Independence of centriole formation and DNA synthesis. *J. Cell Biol.* **57**, 359–372.
- Raybin, D. and Flavin, M.** (1975). An enzyme tyrosylating alpha-tubulin and its role in microtubule assembly. *Biochem. Biophys. Res. Commun.* **65**, 1081–1087.
- Raynaud-messina, B., Mazzolini, L., Moisand, A., Cirinesi, A. and Wright, M.** (2004). Elongation of centriolar microtubule triplets contributes to the formation of the mitotic spindle in γ -tubulin-depleted cells. *J. Cell Biol.* **117**, 5497–5507.
- Renzaglia, K. S. and Duckett, J. G.** (1987). Spermatogenesis in *Blasia pusilla*: From Young Antheridium through Mature Spermatozoid. *Bryologist* **90**, 419–449.
- Renzaglia, K. S. and Garbary, D. J.** (2001). Motile Gametes of Land Plants: Diversity, Development, and Evolution. *CRC Crit. Rev. Plant Sci.* **20**, 107–213.
- Renzaglia, K. S. and Maden, A. R.** (2000). Microtubule organizing centers and the origin of centrioles during spermatogenesis in the pteridophyte *Phylloglossum*. *Microsc. Res. Tech.* **49**, 496–505.
- Rice, L. M., Montabana, E. A. and Agard, D. A.** (2008). The lattice as allosteric effector: Structural studies of alpha beta- and gamma-tubulin clarify the role of GTP in microtubule assembly. *Proc. Natl. Acad. Sci.* **105**, 5378–5383.
- Riparbelli, M. G. and Callaini, G.** (2003). *Drosophila* parthenogenesis: A model for de novo centrosome assembly. *Dev. Biol.* **260**, 298–313.
- Riparbelli, M. G. and Callaini, G.** (2005). The meiotic spindle of the *Drosophila* oocyte: the role of Centrosomin and the central aster. *J. Cell Sci.* **118**, 2827–2836.
- Riparbelli, M. G., Whitfield, W. G. F., Dallai, R. and Callaini, G.** (1997). Assembly of the zygotic centrosome in the fertilized *Drosophila* egg. *Mech. Dev.* **65**, 135–144.
- Riparbelli, M. G., Stouthamer, R., Dallai, R. and Callaini, G.** (1998). Microtubule Organization during the Early Development of the Parthenogenetic Egg of the Hymenopteran *Muscidifurax uniraptor*. *Dev. Biol.* **195**, 89–99.
- Riparbelli, M. G., Callaini, G., Glover, D. M. and Avides, C.** (2002). A requirement for the Abnormal Spindle protein to organise microtubules of the central spindle for cytokinesis in *Drosophila*. *J. Cell Sci.* **115**, 913–922.
- Riparbelli, M. G., Callaini, G., Mercati, D., Hertel, H. and Dallai, R.**

- (2009). Centrioles to basal bodies in the spermiogenesis of *Mastotermes darwiniensis* (Insecta, Isoptera). *Cell Motil. Cytoskeleton* **66**, 248–259.
- Riparbelli, M. G., Cabrera, O. A., Callaini, G. and Megraw, T. L.** (2013). Unique properties of *Drosophila* spermatocyte primary cilia. *Biol. Open* **2**, 1137–1147.
- Rivero, S., Cardenas, J., Bornens, M. and Rios, R. M.** (2009). Microtubule nucleation at the cis-side of the Golgi apparatus requires AKAP450 and GM130. *EMBO J.* **28**, 1016–1028.
- Robbins, R. R.** (1984). Origin and behavior of bicentriolar centrosomes in the bryophyte *Riella americana*. *Protoplasma* **121**, 114–119.
- Robbins, E., Jentzsch, G. and Micali, A.** (1968). The centriole cycle in synchronized HeLa cells. *J. Cell Biol.* **36**, 329–339.
- Rodrigues-martins, A., Riparbelli, M., Callaini, G., Glover, D. M. and Bettencourt-Dias, M.** (2008). From centriole biogenesis to cellular function: Centrioles are essential for cell division at critical developmental stages. *Cell Cycle* **7**, 11–16.
- Rodrigues-Martins, A., Riparbelli, M., Callaini, G., Glover, D. M. and Bettencourt-Dias, M.** (2007). Revisiting the role of the mother centriole in centriole biogenesis. *Science*. **316**, 1046–1050.
- Rodriguez, O. C., Schaefer, A. W., Mandato, C. A., Forscher, P., Bement, W. M. and Waterman-Storer, C. M.** (2003). Conserved microtubule–actin interactions in cell movement and morphogenesis. *Nat. Cell Biol.* **5**, 599–609.
- Rogers, G. C., Rusan, N. M., Peifer, M. and Rogers, S. L.** (2008). A Multicomponent Assembly Pathway Contributes to the Formation of Acentrosomal Microtubule Arrays in Interphase *Drosophila* Cells. *Mol. Biol. Cell* **19**, 3163–3178.
- Rogers, G. C., Rusan, N. M., Roberts, D. M., Peifer, M. and Rogers, S. L.** (2009). The SCF Slimb ubiquitin ligase regulates Plk4/Sak levels to block centriole reduplication. *J. Cell Biol.* **184**, 225–239.
- Román, A., Vicente-page, J., Pérez-escudero, A., Carvajal-gonzález, J. M., Fernández-salguero, P. M. and Polavieja, G. G. De** (2018). Histone H4 acetylation regulates behavioral inter-individual variability in zebrafish. *Genome Biol.* **19**,.
- Rørth, P.** (1998). Gal4 in the *Drosophila* female germline. *Mech. Dev.* **78**, 113–118.
- Rosette, C. and Karin, Mi.** (1995). Cytoskeletal Control of Gene Expression: Depolymerization of Microtubules Activates NF- κ B. *J. Cell Biol.* **128**, 1111–1119.
- Rouviere, C., Houliston, E., Carre, D. and Chang, P.** (1994).

- Characteristics of Pronuclear Migration in *Beroe ovata*. *Cell Motil. Cytoskeleton* **29**, 301–311.
- Russo, A. A., Jeffrey, P. D., Patten, A. K., Massagué, J. and Pavletich, N. P.** (1996). Crystal structure of the p27Kip1 cyclin-dependent-kinase inhibitor bound to the cyclinA-Cdk2 complex. *Nature* **382**, 325–331.
- Rüthnick, D. and Schiebel, E.** (2016). Duplication of the Yeast Spindle Pole Body Once per Cell Cycle. *Mol. Cell. Biol.* **36**, 1324–1331.
- Saldivar, J. C. and Cimprich, K. A.** (2018). A new mitotic activity comes into focus. *Science*. **359**, 30–31.
- Salmon, W. C., Adams, M. C. and Waterman-storer, C. M.** (2002). Dual-wavelength fluorescent speckle microscopy reveals coupling of microtubule and actin movements in migrating cells. *J. Cell Biol.* **158**, 31–37.
- Salogiannis, J. and Reck-Peterson, S. L.** (2017). Hitchhiking: A Non-Canonical Mode of Microtubule-Based Transport. *Trends Cell Biol.* **27**, 141–150.
- Sánchez-Huertas, C., Freixo, F., Viais, R., Lacasa, C., Soriano, E. and Lüders, J.** (2016). Non-centrosomal nucleation mediated by augmin organizes microtubules in post-mitotic neurons and controls axonal microtubule polarity. *Nat. Commun.* **7**,.
- Sanchez, A. D. and Feldman, J. L.** (2017). Microtubule-organizing centers: from the centrosome to non-centrosomal sites. *Curr. Opin. Cell Biol.* **44**, 93–101.
- Sansregret, L., Dick, A. E., Smith, C. A., Mcainsh, A. D., Gerlich, D. W. and Petronczki, M.** (2014). Cdk1 Inactivation Terminates Mitotic Checkpoint Surveillance and Stabilizes Kinetochore Attachments in Anaphase. *Curr. Biol.* **24**, 638–645.
- Saurya, S., Roque, H., Novak, Z. A., Wainman, A., Aydogan, M. G., Volanakis, A., Sieber, B., Pinto, D. M. S. and Raff, J. W.** (2016). *Drosophila* Ana1 is required for centrosome assembly and centriole elongation. *J. Cell Sci.* **129**, 2514–2525.
- Schatten, G.** (1994). The centrosome and its mode of inheritance: the reduction of the centrosome during gametogenesis and its restoration during fertilization. *Dev. Biol.* **165**, 299–335.
- Schatten, G. and Stearns, T.** (2015). Sperm Centrosomes: Kiss Your Asterless Goodbye , for Fertility's Sake. *Curr. Biol.* **25**, R1178–R1181.
- Schatten, G., Simerly, C. and Schatten, H.** (1985). Microtubule configurations during fertilization, mitosis, and early development in the mouse and the requirement for egg microtubule-mediated motility during mammalian fertilization. *Proc. Natl. Acad. Sci. USA* **82**, 4152–4156.

- Schindelin, J., Arganda-Carreras, I., Frise, E., Kaynig, V., Longair, M., Pietzsch, T., Preibisch, S., Rueden, C., Saalfeld, S., Schmid, B., et al.** (2012). Fiji - an Open Source platform for biological image analysis Johannes. *Nat. Methods* **9**.
- Schmidt, T. I., Kleylein-Sohn, J., Westendorf, J., Le Clech, M., Lavoie, S. B., Stierhof, Y.-D. and Nigg, E. a** (2009). Control of centriole length by CPAP and CP110. *Curr. Biol.* **19**, 1005–11.
- Schnackenberg, B. J., Marzluff, W. F. and Sluder, G.** (2008). Cyclin E in Centrosome Duplication and Reduplication in Sea Urchin Zygotes. *J. Cell Physiol.* **217**, 626–631.
- Schöckel, L., Möckel, M., Mayer, B., Boos, D. and Stemmann, O.** (2011). Cleavage of cohesin rings coordinates the separation of centrioles and chromatids. *Nat. Cell Biol.* **13**, 966–972.
- Schulze, E. and Kirschner, M.** (1986). Microtubule Dynamics in Interphase Cells. *J. Cell Biol.* **102**, 1020–1031.
- Shaheen, R., Al Tala, S., Almoisheer, A. and Alkuraya, F. S.** (2014). Mutation in PLK4, encoding a master regulator of centriole formation, defines a novel locus for primordial dwarfism. *J. Med. Genet.* **51**, 814–816.
- Shamanski, F. L. and Orr-Weaver, T. L.** (1991). The *Drosophila* plutonium and pan gu genes regulate entry into S phase at fertilization. *Cell* **66**, 1289–1300.
- Shaner, N. C., Lambert, G. G., Chammas, A., Ni, Y., Cranfill, P. J., Baird, M. a, Sell, B. R., Allen, J. R., Day, R. N., Israelsson, M., et al.** (2013). A bright monomeric green fluorescent protein derived from *Branchiostoma lanceolatum*. *Nat. Methods* **10**, 407–414.
- Sharp, D. J. and Ross, J. L.** (2012). Microtubule-severing enzymes at the cutting edge. *J. Cell Sci.* **125**, 2561–2569.
- Shigematsu, H., Imasaki, T., Doki, C., Sumi, T., Aoki, M., Uchikubo-Kamo, T., Sakamoto, A., Tokuraku, K., Shirouzu, M. and Nitta, R.** (2018). Structural insight into microtubule stabilization and kinesin inhibition by Tau family MAPs. *J. Cell Biol.*
- Shimamura, M., Brown, R. C., Lemmon, B. E., Akashi, T., Mizuno, K., Nishihara, N., Tomizawa, K.-I., Yoshimoto, K., Deguchi, H., Hosoya, H., et al.** (2004). γ -Tubulin in Basal Land Plants: Characterization, Localization, and Implication in the Evolution of Acentriolar Microtubule Organizing Centers. *Plant Cell* **16**, 45–59.
- Shimanovskaya, E., Viscardi, V., Lesigang, J., Lettman, M. M., Qiao, R., Svergun, D. I., Round, A., Oegema, K. and Dong, G.** (2014). Structure of the *C. elegans* ZYG-1 Cryptic Polo Box Suggests a Conserved Mechanism for Centriolar Docking of Plk4 Kinases. *Structure* **22**, 1090–1104.

- Shintomi, K., Inoue, F., Watanabe, H., Ohsumi, K., Ohsugi, M. and Hirano, T.** (2017). Mitotic chromosome assembly despite nucleosome depletion in *Xenopus* egg extracts. *Science*. **356**, 1284–1287.
- Shukla, A., Kong, D., Sharma, M., Magidson, V. and Loncarek, J.** (2015). Plk1 relieves centriole block to reduplication by promoting daughter centriole maturation. *Nat. Commun.* **6**, 1–13.
- Siefert, J. C., Clowdusa, E. A. and Sansam, C. L.** (2015). Cell Cycle Control in the Early Embryonic Development of Aquatic Animal Species. *Comp Biochem Physiol C Toxicol Pharmacol.* **2015** **178**, 8–15.
- Silkworth, W. T., Nardi, I. K., Scholl, L. M. and Cimini, D.** (2009). Multipolar spindle pole coalescence is a major source of kinetochore mis-attachment and chromosome mis-segregation in cancer cells. *PLoS One* **4**,.
- Sillibourne, J. E. and Bornens, M.** (2010). Polo-like kinase 4: the odd one out of the family. *Cell Div.* **5**,.
- Sillibourne, J. E., Tack, F., Vloemans, N., Boeckx, A., Thambirajah, S., Bonnet, P., Ramaekers, F. C. S., Bornens, M. and Grand-Perret, T.** (2010). Autophosphorylation of Polo-like Kinase 4 and Its Role in Centriole Duplication. *Mol. Biol. Cell* **21**, 547–561.
- Sinden, R. E., Canning, E. U. and Spain, B.** (1976). Gametogenesis and fertilization in *Plasmodium yoelii nigeriensis*: a transmission electron microscope study. *Proc. R. Soc. B. Biol. Sci.* **193**, 55–76.
- Sinden, R. E., Canning, E. U., Bray, R. S. and Smalley, M. E.** (1978). Gametocyte and gamete development in *Plasmodium falciparum*. *Proc. R. Soc. B. Biol. Sci.* **201**, 375–399.
- Sirajuddin, M., Rice, L. M. and Vale, R. D.** (2014). Regulation of microtubule motors by tubulin isoforms and posttranslational modifications Minhajuddin. *Nat. Cell Biol.* **16**, 335–344.
- Sköld, H. N., Komma, D. J. and Endow, S. A.** (2015). Assembly pathway of the anastral *Drosophila* oocyte meiosis I spindle. *J. Cell Sci.* **118**, 1745–1755.
- Slevin, L. K., Nye, J., Pinkerton, D. C., Buster, D. W., Rogers, G. C. and Slep, K. C.** (2012). The structure of the plk4 cryptic polo box reveals two tandem polo boxes required for centriole duplication. *Structure* **20**, 1905–17.
- Song, M. H., Liu, Y., Anderson, D. E., Jahng, W. J. and O’Connell, K. F.** (2011). Protein Phosphatase 2A-SUR-6/B55 Regulates Centriole Duplication in *C. elegans* by Controlling the Levels of Centriole Assembly Factors. *Dev. Cell* **20**, 563–571.
- Sonnen, K. F., Schermelleh, L., Leonhardt, H. and Nigg, E. A.** (2012).

3D-structured illumination microscopy provides novel insight into architecture of human centrosomes. *Biol. Open* **1**, 965–976.

- Sonnen, K. F., Gabryjonczyk, A.-M., Anselm, E., Stierhof, Y.-D. and Nigg, E. a** (2013). Human Cep192 and Cep152 cooperate in Plk4 recruitment and centriole duplication. *J. Cell Sci.* **126**, 3223–33.
- Sorokin, S. P.** (1968). Reconstructions of centriole formation and ciliogenesis in mammalian lungs. *J. Cell Sci.* **3**, 207–230.
- Stearns, T. and Kirschner, M.** (1994). In Vitro Reconstitution of Centrosome Assembly and Function: The Central Role of γ -Tubulin. *Cell* **76**, 623–637.
- Stearns, T., Evans, L. and Kirschner, M.** (1991). Gamma-Tubulin Is a Highly Conserved Component of the Centrosome. *Cell* **65**, 625–636.
- Steinman, R. M.** (1968). An electron microscopic study of ciliogenesis in developing epidermis and trachea in the embryo of *Xenopus laevis*. *Am. J. Anat.* **122**, 19–55.
- Stevens, N. R., Roque, H. and Raff, J. W.** (2010). DSas-6 and Ana2 Coassemble into Tubules to Promote Centriole Duplication and Engagement. *Dev. Cell* **19**, 913–919.
- Su, T. T., Sprenger, F., Digregorio, P. J., Campbell, S. D. and Farrell, P. H. O.** (1998). Exit from mitosis in *Drosophila* syncytial embryos requires proteolysis and cyclin degradation, and is associated with localized dephosphorylation. *Genes Dev.* **12**, 1495–1503.
- Sugioka, K., Hamill, D. R., Lowry, J. B., Mcneely, M. E., Enrick, M., Richter, A. C., Kiebler, L. E., Priess, J. R. and Bowerman, B.** (2017). Centriolar SAS-7 acts upstream of SPD-2 to regulate centriole assembly and pericentriolar material formation. *Elife* **6:e20353**, 1–25.
- Suh, M. R., Han, J. W., No, Y. R. and Lee, J.** (2002). Transient concentration of a γ -tubulin-related protein with a pericentrin-related protein in the formation of basal bodies and flagella during the differentiation of *Naegleria gruberi*. *Cell Motil. Cytoskeleton* **52**, 66–81.
- Sulimenko, V., Hájková, Z., Klebanovych, A. and Dráber, P.** (2017). Regulation of microtubule nucleation mediated by γ -tubulin complexes. *Protoplasma*.
- Sullivan, M. and Morgan, D. O.** (2007). Finishing mitosis, one step at a time. *Nat. Rev. Mol. Cell Biol.* **8**, 894–903.
- Sullivan, W., Fogarty, P. and Theurkauf, W. E.** (1993). Mutations affecting the cytoskeletal organization of syncytial *Drosophila* embryos. *Development* **118**, 1245–1254.
- Surrey, T., Nedelec, F., Leibler, S. and Karsenti, E.** (2001). Physical properties determining self-organization of motors and microtubules.

Science. **292**, 1167–1171.

- Svitin, A. and Chesnokov, I.** (2010). Study of DNA replication in *Drosophila* using cell free in vitro system. *Cell Cycle* **9**, 815–819.
- Swaffer, M. P., Jones, A. W., Flynn, H. R., Snijders, A. P. and Nurse, P.** (2016). CDK Substrate Phosphorylation and Ordering the Cell Cycle. *Cell* **167**, 1750–1761.
- Swallow, C. J., Ko, M. a, Siddiqui, N. U., Hudson, J. W. and Dennis, J. W.** (2005). Sak/Plk4 and mitotic fidelity. *Oncogene* **24**, 306–12.
- Swift, H.** (1950). The constancy of desoxyribose nucleic acid in plant nuclei. *Proc. Natl. Acad. Sci.* **36**, 643–654.
- Sydor, A. M., Czymmek, K. J., Puchner, E. M. and Mennella, V.** (2015). Super-Resolution Microscopy: From Single Molecules to Supramolecular Assemblies. *Trends Cell Biol.* **25**, 730–748.
- Symeonidou, I., Taraviras, S. and Lygerou, Z.** (2012). Control over DNA replication in time and space. *FEBS Lett.* **586**, 2803–2812.
- Szyk, A., Deaconescu, A. M., Piszczek, G. and Mecak, and A. R.-** (2011). Tubulin tyrosine ligase structure reveals adaptation of an ancient fold to bind and modify tubulin. *Nat. Struct. Mol. Biol.* **18**, 1250–8.
- Takada, S., Kelkar, A. and Theurkauf, W. E.** (2003). *Drosophila* checkpoint kinase 2 couples centrosome function and spindle assembly to genomic integrity. *Cell* **113**, 87–99.
- Tang, C. C., Fu, R., Wu, K., Hsu, W. and Tang, T. K.** (2009). CPAP is a cell-cycle regulated protein that controls centriole length. *Nat. Cell Biol.* **11**, 825–831.
- Tavosanis, G., Llamazares, S., Goulielmos, G. and Gonzalez, C.** (1997). Essential role for γ -tubulin in the acentriolar female meiotic spindle of *Drosophila*. *EMBO J.* **16**, 1809–1819.
- Teixido-Travesa, N., Roig, J. and Luders, J.** (2012). The where, when and how of microtubule nucleation - one ring to rule them all. *J. Cell Sci.* **125**, 4445–4456.
- Telley, I. a, Gáspár, I., Ephrussi, A. and Surrey, T.** (2013). A single *Drosophila* embryo extract for the study of mitosis ex vivo. *Nat. Protoc.* **8**, 310–24.
- Terada, Y., Schatten, G., Hasegawa, H. and Yaegashi, N.** (2010). Essential Roles of the Sperm Centrosome in Human Fertilization: Developing the Therapy for Fertilization Failure due to Sperm Centrosomal Dysfunction. *Tohoku J. Exp. Med.* **220**, 247–258.
- Theurkauf, W. E., Alberts, B. M., Jan, Y. N. and Jongens, T. A.** (1993). A central role for microtubules in the differentiation of *Drosophila*

oocytes. *Development* **118**, 1169–1180.

- Tillery, M. M. L., Blake-Hedges, C., Zheng, Y., Buchwalter, R. A. and Megraw, T. L.** (2018). Centrosomal and Non-Centrosomal Microtubule-Organizing Centers (MTOCs) in *Drosophila melanogaster*. *Cells* **7**,.
- Tissot, N., Lepesant, J., Bernard, F., Legent, K., Bosveld, F., Martin, C. and Guichet, A.** (2017). Distinct molecular cues ensure a robust microtubule-dependent nuclear positioning in the *Drosophila* oocyte. *Nat. Commun.* **8**,.
- Tram, U. and Sullivan, W.** (2000). Reciprocal inheritance of centrosomes in the parthenogenetic Hymenopteran *Nasonia vitripennis*. *Curr. Biol.* **10**, 1413–1419.
- Tran, P. T., Walker, R. A. and Salmon, E. D.** (1997). A Metastable Intermediate State of Microtubule Dynamic Instability That Differs Significantly between Plus and Minus Ends. *J. Cell Biol.* **138**, 105–117.
- Tsaniras, S. C., Kanellakis, N., Symeonidou, I. E., Nikolopoulou, P., Lygerou, Z. and Taraviras, S.** (2014). Licensing of DNA replication, cancer, pluripotency and differentiation: An interlinked world? *Semin. Cell Dev. Biol.* **30**, 174–180.
- Tsou, M.-F. B. and Stearns, T.** (2006). Mechanism limiting centrosome duplication to once per cell cycle. *Nature* **442**, 947–951.
- Tsou, M.-F. B., Wang, W.-J., Yule, K. A., Uryu, K. and Jallepalli, P. V** (2009). Polo kinase and separase regulate the mitotic licensing of centriole duplication in human cells. *Dev. Cell* **17**, 344–354.
- Tsuchiya, Y., Yoshiba, S., Gupta, A., Watanabe, K. and Kitagawa, D.** (2016). Cep295 is a conserved scaffold protein required for generation of a bona fide mother centriole. *Nat. Commun.* **7**, 1–13.
- Tuschl, T., Zamore, P. D., Lehmann, R., Bartel, D. P. and Sharp, P. A.** (1999). Targeted mRNA degradation by double-stranded RNA in vitro. *Genes Dev.* **13**, 3191–3197.
- Uehara, R., Nozawa, R., Tomioka, A., Petry, S., Vale, R. D., Obuse, C. and Goshima, G.** (2009). The augmin complex plays a critical role in spindle microtubule generation for mitotic progression and cytokinesis in human cells. *Proc. Natl. Acad. Sci.* **106**, 6998–7003.
- Uetake, Y., Lončarek, J., Nordberg, J. J., English, C. N., La Terra, S., Khodjakov, A. and Sluder, G.** (2007a). Cell cycle progression and de novo centriole assembly after centrosomal removal in untransformed human cells. *J. Cell Biol.* **176**, 173–182.
- Uetake, Y., Loncarek, J., Nordberg, J. J., English, C. N., La Terra, S., Khodjakov, A. and Sluder, G.** (2007b). Cell cycle progression and

de novo centriole assembly after centrosomal removal in untransformed human cells. *J. Cell Biol.* **176**, 173–182.

- Van Bergeijk, P., Adrian, M., Hoogenraad, C. C. and Kapitein, L. C.** (2015). Optogenetic control of organelle transport and positioning. *Nature* **518**, 111–114.
- van Breugel, M., Hirono, M., Andreeva, A., Yanagisawa, H., Yamaguchi, S., Nakazawa, Y., Morgner, N., Petrovich, M., Ebong, I., Robinson, C. V, et al.** (2011). Structures of SAS-6 Suggest Its Organization in Centrioles. *Science*. **331**, 1196–1199.
- van de Weerd, B. C. M., Littler, D. R., Klompmaker, R., Huseinovic, A., Fish, A., Perrakis, A. and Medema, R. H.** (2008). Polo-box domains confer target specificity to the Polo-like kinase family. *Biochim. Biophys. Acta* **1783**, 1015–22.
- Vardy, L. and Orr-Weaver, T. L.** (2007). The Drosophila PNG Kinase Complex Regulates the Translation of Cyclin B. *Dev. Cell* **12**, 157–166.
- Varmark, H., Llamazares, S., Rebollo, E., Lange, B., Reina, J., Schwarz, H. and Gonzalez, C.** (2007). Asterless Is a Centriolar Protein Required for Centrosome Function and Embryo Development in Drosophila. *Curr. Biol.* **17**, 1735–1745.
- Vaughn, K. C. and Bowling, A. J.** (2008). Recovery of microtubules on the blepharoplast of Ceratopteris spermatogenous cells after oryzalin treatment. *Protoplasma* **233**, 231–240.
- Vaughn, K. C. and Renzaglia, K. S.** (2006). Structural and immunocytochemical characterization of the Ginkgo biloba L. sperm motility apparatus. *Protoplasma* **227**, 165–173.
- Velez, A. M. A., Howard, M. S., Kim, J. and Googe, P. B.** (2015). Markers for sebaceoma show a spectrum of cell cycle regulators, tumor suppressor genes, and oncogenes. *N. Am. J. Med. Sci.* **7**, 275–280.
- Vemu, A., Szczesna, E., Zehr, E. A., Spector, J. O., Grigorieff, N., Deaconescu, A. M. and Roll-Mecak, A.** (2018). Severing enzymes amplify microtubule arrays through lattice GTP-tubulin incorporation. *Science*. **361**,.
- Vinh, D. B. N., Kern, J. W., Hancock, W. O., Howard, J. and Davis, T. N.** (2002). Reconstitution and Characterization of Budding Yeast gamma-Tubulin Complex. *Mol. Biol. Cell* **13**, 1144–1157.
- Vladar, E. K. and Stearns, T.** (2007). Molecular characterization of centriole assembly in ciliated epithelial cells. *J. Cell Biol.* **178**, 31–42.
- Voelzmann, A., Liew, Y., Qu, Y., Hahn, I., Melero, C., Sánchez-soriano, N. and Prokop, A.** (2017). Drosophila Short stop as a paradigm for the role and regulation of spectraplakins. *Semin. Cell Dev. Biol.* **69**,

40–57.

- Vogt, N., Koch, I., Schwarz, H., Schnorrer, F. and Nüsslein-volhard, C.** (2006). The gammaTuRC components Grip75 and Grip128 have an essential microtubule-anchoring function in the *Drosophila* germline. *Development* **133**, 3963–3972.
- Wang, W., Soni, R. K., Uryu, K. and Tsou, M. B.** (2011). The conversion of centrioles to centrosomes: essential coupling of duplication with segregation. *J. Cell Biol.* **193**, 727–739.
- Wang, Z., Zhang, C. and Qi, R. Z.** (2014a). A newly identified myomegalin isoform functions in Golgi microtubule organization and ER-Golgi transport. *J. Cell Sci.* **127**, 4904–4917.
- Wang, G., Jiang, Q. and Zhang, C.** (2014b). The role of mitotic kinases in coupling the centrosome cycle with the assembly of the mitotic spindle. *J. Cell Sci.* **127**, 4111–4122.
- Wang, D., Nitta, R., Morikawa, M., Yajima, H., Inoue, S., Shigematsu, H., Kikkawa, M. and Hirokawa, N.** (2016). Motility and microtubule depolymerization mechanisms of the kinesin-8 motor, KIF19A. *Elife* **5**,.
- Waterman-storer, C., Duey, D. Y., Weber, K. L., Keech, J., Cheney, R. E., Salmon, E. D. and Bement, W. M.** (2000). Microtubules Remodel Actomyosin Networks in *Xenopus* Egg Extracts via Two Mechanisms of F-Actin Transport. *J. Cell Biol.* **150**, 361–376.
- Watson, J. D. and Crick, F. H.** (1953). Molecular Structure of Nucleic Acids. *Nature* **4356**, 305–311.
- White, D., Vries, G. De, Martin, J. and Dawes, A.** (2015). Microtubule patterning in the presence of moving motor proteins. *J. Theor. Biol.* **382**, 81–90.
- Wigley, W. C., Fabunmi, R. P., Lee, M. G., Marino, C. R., Muallem, S., Demartino, G. N. and Thomas, P. J.** (1999). Dynamic Association of Proteasomal Machinery with the Centrosome. *J. Cell Biol.* **145**, 481–490.
- Williams, B. C., Dernburg, A. F., Puro, J., Nokkala, S. and Goldberg, M. L.** (1997). The *Drosophila* kinesin-like protein KLP3A is required for proper behavior of male and female pronuclei at fertilization. *Development* **124**, 2365–2376.
- Winey, M. and Toole, E. O.** (2014). Centriole structure. *Phil. Trans. R. Soc. B* **369**,.
- Winkles, J. A. and Alberts, G. F.** (2005). Differential regulation of polo-like kinase 1, 2, 3, and 4 gene expression in mammalian cells and tissues. *Oncogene* **24**, 260–266.
- Wloga, D., Joachimiak, E., Louka, P. and Gaertig, J.** (2016).

Posttranslational Modifications of Tubulin and Cilia. *Cold Spring Harb. Perspect. Biol.*

- Wloga, D., Joachimiak, E. and Fabczak, H.** (2017). Tubulin Post-Translational Modifications and Microtubule Dynamics. *Int. J. Mol. Sci.* **18**,.
- Wong, C. and Stearns, T.** (2003). Centrosome number is controlled by a centrosome-intrinsic block to reduplication. *Nat. Cell Biol.* **5**, 539–44.
- Wong, Y. L., Anzola, J. V, Davis, R. L., Yoon, M., Motamedi, A., Kroll, A., Seo, C. P., Hsia, J. E., Kim, S. K., Mitchell, J. W., et al.** (2015). Reversible centriole depletion with an inhibitor of Polo-like kinase 4. *Science.* **348**, 1155–1160.
- Woodruff, J. B., Wueseke, O. and Hyman, A. A.** (2014). Pericentriolar material structure and dynamics. *Phil. Trans. R. Soc. B* **369**,.
- Woodruff, J. B., Ferreira Gomes, B., Widlund, P. O., Mahamid, J., Honigmann, A. and Hyman, A. A.** (2017). The Centrosome Is a Selective Condensate that Nucleates Microtubules by Concentrating Tubulin. *Cell* **169**, 1066–1077.
- Woolley, D. and Fawcett, D.** (1973). The degeneration and disappearance of the centrioles during the development of the rat spermatozoon. *Anat Rec* **177**, 289–301.
- Wu, J. and Akhmanova, A.** (2017). Microtubule-Organizing Centers. *Annu. Rev. Cell Dev. Biol.* **33**, 51–75.
- Xu, X., Huang, S., Zhang, B., Huang, F., Chi, W., Fu, J., Wang, G., Li, S., Jiang, Q. and Zhang, C.** (2017). DNA replication licensing factor Cdc6 and Plk4 kinase antagonistically regulate centrosome duplication via Sas-6. *Nat. Commun.* **8**,.
- Yamada, M. and Goshima, G.** (2017). Mitotic Spindle Assembly in Land Plants: Molecules and Mechanisms. *Biology (Basel)*. **6**,.
- Yamashita, Y., Kajigaya, S., Yoshida, K., Ueno, S., Ota, J., Ohmine, K., Ueda, M., Miyazato, A., Ohya, K. I., Kitamura, T., et al.** (2001). Sak Serine-Threonine Kinase Acts as an Effector of Tec Tyrosine Kinase. *J. Biol. Chem.* **276**, 39012–39020.
- Yang, Z., Lončarek, J., Khodjakov, A. and Rieder, C. L.** (2008). Extra centrosomes and/or chromosomes prolong mitosis in human cells. *Nat. Cell Biol.* **10**, 748–751.
- Yatsu, N.** (1905). The formation of centrosomes in enucleated egg-fragments. *J. Exp. Zool.* **2**,.
- Yu, Z. and Quinn, P. J.** (1994). Dimethyl Sulphoxide: A Review of Its Applications in Cell Biology. *Biosci. Rep.* **14**, 259–281.
- Yuan, K., Seller, C. A., Shermoen, A. W. and O’Farrell, P. H.** (2016).

Timing the *Drosophila* Mid-Blastula Transition: a cell cycle- centered view. *Trends Genet.* **32**, 496–507.

- Yuyu Song, Kirkpatrick, L. L., Schilling, A. B., Helseth, D. L., Chabot, N., Keillor, J. W., Johnson, G. V. W. and Brady, S. T.** (2013). Transglutaminase and Polyamination of Tubulin: Posttranslational Modification for Stabilizing Axonal Microtubules. *Neuron* **78**, 109–123.
- Zhang, X., Pei, Z., Ji, C., Zhang, X., Xu, J., Wang, J. and Additional** (2017). Novel Insights into the Role of the Cytoskeleton in Cancer. *IntechOpen*.
- Zhao, T., Graham, O. S., Raposo, A. and St Johnston, D.** (2012). Growing microtubules push the oocyte nucleus to polarize the *Drosophila* dorsal-ventral axis. *Science.* **336**, 999–1003.
- Zhao, H., Zhu, L., Zhu, Y., Cao, J., Li, S., Huang, Q., Xu, T., Huang, X., Yan, X. and Zhu, X.** (2013). The cep63 paralogue deup1 enables massive de novo centriole biogenesis for vertebrate multiciliogenesis. *Nat. Cell Biol.* **15**, 1434–1444.
- Zhou, X. X., Fan, L. Z., Li, P. and Lin, M. Z.** (2017). Optical control of cell signaling by single-chain photoswitchable kinases. *Science.* **355**, 836–842.
- Zhu, F., Lawo, S., Bird, A., Pinchev, D., Ralph, A., Richter, C., Müller-Reichert, T., Kittler, R., Hyman, A. A. and Pelletier, L.** (2008). The Mammalian SPD-2 Ortholog Cep192 Regulates Centrosome Biogenesis. *Curr. Biol.* **18**, 136–141.
- Zimmerman, W. C., Sillibourne, J., Rosa, J. and Doxsey, S. J.** (2004). Mitosis-specific Anchoring of gamma Tubulin Complexes by Pericentrin Controls Spindle Organization and Mitotic Entry. *Mol. Biol. Cell* **15**, 3642–3657.
- Zitouni, S., Nabais, C., Jana, S. C., Guerrero, A. and Bettencourt-Dias, M.** (2014). Polo-like kinases: structural variations lead to multiple functions. *Nat. Rev. Mol. cell Biol.* **15**, 433–452.
- Zitouni, S., Francia, M. E., Leal, F., Gouveia, S. M., Nabais, C., Duarte, P., Gilberto, S., Brito, D., Moyer, T., Ohta, M., et al.** (2016). CDK1 prevents unscheduled PLK4-STIL complex assembly in centriole biogenesis. *Curr. Biol.* **26**, 1127–1137.

ITQB-UNL | Av. da República, 2780-157 Oeiras, Portugal
Tel (+351) 214 469 100 | Fax (+351) 214 411 277

www.itqb.unl.pt